

Development of a solution-based process for hydroxyapatite and functionalised hydroxyapatite



A thesis submitted to the School of Chemistry,

Trinity College Dublin, 2024

For the degree of Doctor of Philosophy

By **Bríd Murphy**

Year:

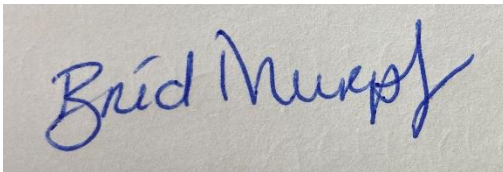
Supervisor: Prof. Michael A. Morris

Declaration

I declare that this thesis has not been submitted as an exercise for a degree at this or any other university and it is entirely my own work.

I agree to deposit this thesis in the University's open access institutional repository or allow the Library to do so on my behalf, subject to Irish Copyright Legislation and Trinity College Library conditions of use and acknowledgement.

I consent to the examiner retaining a copy of the thesis beyond the examining period, should they so wish (EU GDPR May 2018).



Name

Abstract

Hydroxyapatite coatings have long been established as a means of improving the osteointegration of metallic orthopaedic implants. Nonetheless there are both technical and commercial drawbacks associated with industrial coating techniques. Potential improvements such as adding therapeutic compounds highlight the need for new and innovative coating techniques. This thesis explores the use of metastable colloidal (particles between 1 and 1000nm in size) calcium and phosphate solutions that can lead to selective precipitation of insoluble hydroxyapatite mineral at a solution-surface interface. This process is intrinsically difficult to control and the introduction of careful process controls to all variables within this solution deposition system is needed to pave the way for industrial scale up of a novel laboratory-based system. Precise control and understanding of the process also allows for the investigation of the kinetics and mechanism of the deposition of hydroxyapatite on traditional and non-conventional surfaces.

There is always an ongoing need to improve the osteointegration of orthopaedic implants beyond what hydroxyapatite alone can offer so that rejection and revision surgery can be avoided. There is growing need for enhanced antimicrobial performance and drug delivery properties of biomedical surfaces to improve success rates of operations. This issue is addressed herein via design and testing of a polymer patterning method for the inclusion of additional active ions to a hydroxyapatite coating.

The work can be grouped into two core categories.

1. Understanding: this means that through experimentation, chemistry fundamentals, materials characterisation and data analysis an understanding of the molecular intricacies within a novel solution-deposition hydroxyapatite coating process is achieved. (Chapters 2, 3 & 4)
2. Functionalisation: investigation of the biological activity of a dopant and the design of experiments for a system which adds certain elements to an orthopaedic surface with a view to aiding patient outcomes. (Chapters 5 & 6)

Chapter 1 provides a background literature review of hydroxyapatite and its use as an orthopaedic coating. Detailed here are the limitations and challenges surrounding traditional coating techniques and their narrow focus on titanium based metallic parts. Opportunities regarding the doping of hydroxyapatite with novel materials on novel surfaces are identified and analytically compared.

Chapter 2 introduces the novel system of depositing hydroxyapatite using colloidal solutions of calcium and phosphates. The effect of solution concentration and deposition kinetics are explored and explained. A proposed chemical pathway for the nucleation and crystal growth of certain hydroxyapatite phases within solution is presented and confirmed to be accurate. Outlined are the optimum process settings of temperature, time, pH and concentration that produce repeatable hydroxyapatite films.

Chapter 3 leverages the findings and the novel system presented in Chapter 2 to deposit an 'ideal' hydroxyapatite film and investigate its attachment to bulk titanium parts. Detailed characterisation of the coating and the film's growth mechanism is provided.

Chapter 4 takes the findings of both Chapter 2 and Chapter 3 and applies the solution deposition process to non-bulk titanium parts such as silicon or silicon with 100 nm titanium films. Hydroxyapatite coating efficacy is shown to be dependent on substrate roughness, hydrophilicity and activation. Resulting data suggest that once hydroxyapatite seeds, it grows identically regardless of substrate.

Chapter 5 chapter represents a standalone study of gallium nano-coatings and introduces the field of block copolymer patterning with a view to overcoming some of the known challenges of doping hydroxyapatite. Block copolymer patterns are used to generate novel orthopaedic coatings of gallium oxide on silicon and titanium thin films. Extensive characterisation of gallium nanodot coating and biological assay tests show that controlled release of gallium ions from coating improves osteointegration. The osteogenesis and osteoclastogenesis tests were conducted by collaborators Mimma Maggio and Carolina Martens of the Hoey group.

Chapter 6 harnesses the findings of Chapter 5 and applies them to hydroxyapatite coatings formed using the parameters set out in Chapters 2 and 3. This groundbreaking work shows how a polymer pattern can be applied over a ceramic layer. Infiltration of the polymer layer with inorganic dopants of osteogenic and antimicrobial relevance acts as an innovative method of securing additive ions to hydroxyapatite. While elements such as gallium or zinc can be detected, it is fully proven to have no impact on the HA crystal structure or film properties.

Chapter 7 outlines the central findings of this work and highlights the major achievements which have contributed to the field of biomaterials research. A suggestion of future work is also presented which would further advance the conclusions of each chapter.

Acknowledgements

First, I must thank my supervisor Prof Mick A. Morris. Mick's enthusiasm for science is infectious and for the last four years he provided boundless support for new ideas. Mick was the ideal supervisor; never got in my business, always backed me when I needed it and never ever sweated the small stuff. With Mick as supervisor, you do not walk alone. Queen Niamh Cronly, project manager, budget adviser, guidance councillor, therapist and friend extraordinaire. Niamh made such an impact when she joined AMBER and I feel so lucky to have her on my team. Thank you for being so generous with your time Niamh, mostly enjoyed chatting to you about life not the project. A special mention for Lorraine Byrne whose advice in 2019 was a catalyst for this journey. Poor Lorraine, then I turned up at her place of work for the next four years! It was my pleasure to see her in action speaking at various events and I have loved knowing she is at the helm in AMBER.

Naturally, there are dozens of people to thank who work in the various technical teams in Trinity. Manueal Ruther for his help with every device in the Chemistry building. Raman Bekarevich for all his assistance with TEM. Clive Dowling, Cathal McCauley, Dermot Daly and Megan Canavan were always answering SOS calls from the SEM room or Unit 9 with humour and patience. Mark Kavanagh, David McCaffrey, Brendan Twamley, Peter Gleeson, Riley Gatensby – all of these have helped with various techniques. Joey Tilley and Seana Lynch have sorted out many a problematic PO and their contribution to AMBER cannot be understated. Thanks are due to the DePuy Synthes team especially Tim Crowley, Lucie Hankey and Aidan Cloonan, for their unfailing patience and support at each meeting and their very patient review of some disastrous documents. I learned so much from the three of you.

Thanks to the members of the Morris group. Ross, Tom and Andrew for getting me started. Nadia, Lipika and Sajjan for keeping me going through the bad days and cheering on the good days, friends for life, I hope. To the long-suffering Jhonattan Baez who endured more than his fair share of crazy Bríd. I will forever be thankful that Jhonattan was on the DePuy project with me, we have had so much fun even though Jhon's peak tends to be at 6:30am at Heuston station.

Jhon brought the wonderful Aislan into the fold, and I am told the three of us make up the 'DreamTeam.' I am very proud of the three of us and I am sure that our coffees, hikes and moral support led to our success.

To all my friends but particularly Grace Mc, Brónagh, Maevo and Grace M who listened to endless hours of imposter syndrome, doubts and rhetoric about gallium. Thanks so much for sticking by me and being ever ready with a voice note. My aunt Margaret who gave me a love of reading as a kid, this was invaluable. My aunt Eileen an OG woman in STEM and a massive advocate for those of us coming after her. My godfather Ger for painstakingly explaining the biological interactions to me. To my mom Pauline, who first had to suffer me doing engineering and not primary teaching, who then had to suffer me quitting a permanent job to do more engineering, thank you so much for always supporting me regardless. There were weeks I would not have gotten through without you, various financial support and more than one rescue mission to Dublin. To my dad James, another indelible enthusiast, this PhD was a shared dream we had. The pride you took in this project has been wonderful to experience and you can certainly still take some credit for the English of the published works. My brother Vincent, who drew and redrew, printed and reprinted schematics and parts for me. I am so grateful. I hope you know how much you facilitated this project, your work removed barriers at every stage, and it just would not have been completed without you. My other lovely siblings: John, Felicity and Hanna, my gorgeous in-laws: Sheila, David and Niall have always been there for me as I undertook this degree, and I am so grateful for them.

My best Pal Bruno! Your relentless pursuit of moving objects and small animals had me up early every morning and ensured I never spent too much time chained to my desk.

Lastly of course my hugest thanks to Colin 'Carlow' Kenny. This PhD has been a team effort and simply would not have happened without your love and support. We began this journey as cool kids in our 20s then ended it as a married couple with a house, a dog and a massive appreciation for well-engineered medical devices. Thank you so much for everything my love, maybe one day I will make you really proud by learning how to punctuate my own sentences.

Abbreviations

2D	Two Dimensional
3D	Three Dimensional
ACP	Amorphous Calcium Phosphate
AFM	Atomic Force Microscopy
ALP	Alkaline Phosphate
ARS	Alizarin Red Staining
BCP	Block Copolymer
BSA	Bovine Serum Albumin
Ca-P	Calcium phosphate
CDHA	Calcium Deficient Hydroxyapatite
cif	crystallographic information file
CM	Condition Media
DIW	Deionised Water
DLS	Dynamic Light Scattering
DMEM	Dulbecco's Modified Eagle Medium
DNA	Deoxyribonucleic Acid
DSC	Differential Scanning Calorimetry
EDX	Energy-Dispersive X-ray Spectroscopy
FBS	Foetal Bovine Serum
FDA	U.S. Food and Drug Administration
FFT	Fast Fourier Transform
FIB	Focussed Ion Beam
FTIR	Fourier Transform Infrared Spectroscopy
HA	Hydroxyapatite
HETCOR	Heteronuclear Correlation
hMSC	human Marrow Stem Cells
HRTEM	High Resolution Transmission Electron Microscope
IBTS	Irish Blood Transfusion Service
ICP	Inductively Coupled Plasma
ICP-OES	Inductively Coupled Plasma Optical Emission Spectroscopy
LSZ	Lysozyme
MSC	Mesenchymal Stem Cells
NMR	Nuclear Magnetic Resonance
OCP	Octacalcium Phosphate
P4VP	Poly(4-vinylpyridine)

P4VP-OH	hydroxyl terminated Poly(4-vinylpyridine)
PB	Polymer Brush
PBMC	Peripheral Blood Mononuclear Cells
PBS	Phosphate-buffered Saline
PEEK	Polyether Ether Ketone
PFA	Paraformaldehyde
pNPP	p-Nitrophenyl Phosphate
PS	Polystyrene
PS- <i>b</i> -P4VP	Polystyrene - <i>block</i> -Poly(4-vinylpyridine) Block Copolymer
QCM	Quartz Crystal Microbalance
Ra	Average roughness
RANKL	Receptor Activator of Nuclear factor Kappa-B Ligand
Rpv	Peak to Valley Roughness
SBF	Simulated Bodily Fluid
SEM	Scanning Electron Microscope
SEM-EDX	Scanning Electron Microscope with Energy-Dispersive X-ray Spectroscopy
TCP	Tricalcium Phosphate
TEM	Transmission Electron Microscope
TGA	Thermogravimetric Analysis
Ti-6AL-4V	Titanium Alloy: 90% titanium, 6% aluminium and 4% vanadium
TRAP	Tartrate-Resistant Acid Phosphatase
TRIS	Tris(hydroxymethyl)aminomethane
UV	Ultraviolet
WCA	Water Contact Angle
XPS	X-ray Photoelectron Spectroscopy
XRD	X-ray Diffraction
XRF	X-ray Fluorescence
α MEM	α -Minimum Essential Medium
α -TCP	Alpha - Tricalcium Phosphate
β -TCP	Beta- Tricalcium Phosphate

Notes on Publications

Parts of this project have been published in peer-reviewed journals prior to thesis submission.

Chapter 2 is published in full in the article “*Development of Hydroxyapatite Coatings for Orthopaedic Implants from Colloidal Solutions: Part 1—Effect of Solution Concentration and Deposition Kinetics*” co-authored by fellow PhD student Jhonattan Baez who worked with the same industry partner and our supervisor Mick A. Morris.

Chapter 3 follows on from Chapter 2 and is published in full in the article “*Development of Hydroxyapatite Coatings for Orthopaedic Implants from Colloidal Solutions: Part 2—Detailed Characterisation of the Coatings and Their Growth Mechanism*” again co-authored by J. Baez and M.A. Morris.

An extract of **Chapter 4** was published as a conference proceedings paper entitled “*Characterizing Hydroxyapatite Deposited from Solution onto Novel Substrates in Terms of Growth Mechanism and Physical Chemical Properties*”. Following on from this publication, the full **Chapter 4** was published as an extended version of the conference paper entitled “*Characterising Hydroxyapatite Deposited from Solution onto Novel Substrates: Growth Mechanism and Physical Properties.*” Both were co-authored by J. Baez and M.A. Morris.

Chapter 2, 3 and 4 were published in a special issue of the “*Nanomaterials*” journal following an invite from the editor after publication of the conference paper. The special issue these three papers belong to is “*Functional Coatings with Nanostructures: Synthesis, Characterizations and Applications.*”

Chapter 5 is published in full in the article “*Nano sized gallium oxide surface features for enhanced antimicrobial and osteo-integrative responses*” and co-authored by collaborative partners from Trinity Centre for Biomedical Engineering: C. Martins, M Maggio, and D.A. Hoey and of course M.A. Morris.

Chapter 6 has not been published for peer-review yet as it is submitted to the industry partner in an Invention Disclosure Form (IDF). Pending the decision of the IDF this chapter will potentially be drafted for a journal article.

Table of Contents

Declaration.....	i
Abstract.....	i
Acknowledgements.....	iv
Abbreviations.....	vi
Notes on Publications.....	viii
Table of Contents.....	ix
Chapter 1: Introduction.....	1
1.1 Overview and Motivation.....	1
1.2 Hydroxyapatite.....	2
1.3 Hydroxyapatite Coating.....	3
1.4 Bone Growth Process <i>in vivo</i>	4
1.5 Solution-Based Hydroxyapatite Formation and Phases.....	5
1.6 Porous Nature of Hydroxyapatite Coating.....	7
1.7 Bulk Titanium orthopaedic joint and alternative materials.....	8
1.8 Doping of Hydroxyapatite Coating.....	9
1.9 Gallium.....	10
1.10 Model Surfaces for Dopant Studies.....	12
1.11 Objective and Aims.....	12
1.12 References.....	14
Chapter 2: Development of hydroxyapatite coatings for orthopaedic implants from colloidal solutions, Part 1: effect of solution concentration and deposition kinetics.....	24
2.1 Introduction.....	24
2.2 Materials and Methods.....	27
2.3 Results.....	30
2.3.1 Kinetics of Process Solutions.....	30
2.3.2 Analysis of HA films formed from various process solutions.....	32
2.4. Conclusion.....	39
2.5 Appendix Chapter 2.....	40
Appendix 2.5.1. Molarity and Solubility of Chemicals Used.....	40
Appendix 2.5.2 Brief explanation behind allowing HA samples to Dry in ambient conditions.....	40
Appendix 2.5.3 Supplemental SEM Images.....	42
2.6 References.....	44

Chapter 3: Development of hydroxyapatite coatings for orthopaedic implants from colloidal solutions, Part 2: detailed characterisation of the coatings and their growth mechanism.....	49
3.1 Introduction.....	49
3.2. Materials and Methods	51
3.3 Results	54
3.3.1 Analysis of HA generated from within this process in powder form... 54	
3.3.2 Growth Mechanism of HA film on a titanium substrate.....	55
3.4 Conclusion	61
3.5 Appendix Chapter 3.....	62
Appendix 3.5.1 1D NMR Spectra	62
Appendix 3.5.2 TEM FFT fitting on Single Crystal	63
3.6 References.....	64
Chapter 4: Characterising Hydroxyapatite Deposited from Solution onto Novel Substrates: Growth Mechanism and Physical Properties	69
4.1. Introduction.....	70
4.2. Materials and Methods	73
4.3. Results	74
4.4. Conclusion.....	86
4.5 Appendix Chapter 4.....	87
Appendix 4.5.1 Water contact angle and Roughness data	87
Appendix 4.5.2 XPS Survey scans of Ti thin film samples	89
4.6 References.....	91
Chapter 5: Nano Sized Gallium Oxide Surface Features for Enhanced Antimicrobial and Osteo-Integrative Responses.....	96
5.1. Introduction.....	96
5.2. Experimental Methods.....	99
5.2.1 Block Copolymer Materials	99
5.2.2 Block Copolymer and Metal Infiltration Method	100
5.2.3 Characterisation of Gallium Nanodot Samples	100
5.3. Results and Discussion	100
5.3.1. Gallium Included into a Nanodot Array on a Surface	100
5.3.2 Nano Surfaces Facilitate a Controlled Release of Gallium.....	103
5.3.3 Nano Gallium Surfaces Demonstrate Excellent Sterility and Antimicrobial Activity.	105
5.4. Conclusion.....	105
5.5 Appendix Chapter 5.....	106
Appendix 5.5.1 Water Contact Angle Data.....	106

Appendix 5.5.2 Energy Dispersive X-ray Spectroscopy	107
Appendix 5.5.3 Antimicrobial Testing	109
Appendix 5.5.4 Biological Testing of Gallium Nanodot surfaces.....	110
Appendix 5.5.5 Effect of Silicon conditioned media on Human MSC and Monocyte viability	113
5.6 References	118
Chapter 6: Incorporating an additive layer over hydroxyapatite coating using polymeric patterns and inorganic infiltration.	124
6.1 Introduction	124
6.2 Materials and Methods.....	128
6.2.1 Polymer patterning and polymer brush film formation.....	128
6.2.2 Characterisation.....	129
6.3 Results.....	130
6.3.1 Formation of nano gallium coating cast via polymer template over HA films	130
6.3.2 Expansion of polymer brush templating to form zinc and gallium nanocoating on HA films.....	138
6.4 Conclusion	141
6.5 Appendix Chapter 6	142
Appendix 6.5.1 Block Copolymer Deposition Technique.	142
Appendix 6.5.2 Polymer Brush Deposition Technique.....	142
6.6 References	143
Chapter 7: Conclusions and Future Work	148
7.1 Perspective	148
7.2 Conclusions	148
7.3 Future Work.....	152
7.4 References	154
List of Publications	157
Journal Articles Published.....	157
Conferences	158

Chapter 1: Introduction

1.1 Overview and Motivation

The aim of this project is the development of a methodology for the deposition of hydroxyapatite and related layers on implant surfaces for osteointegration. It further explores the addition of inorganic compounds into these layers with a view of enhancing biocompatibility to aid joint replacement.

A global aging population and advancement in orthopaedic surgical possibilities drive the need for improvements in the materials used in implanted medical devices.[1], [2] In developed countries, bone and joint related degenerative diseases account for 50 % of all cases of chronic illness in people over 50 years of age, with that number predicted to grow.[3] The prevalence of total hip and knee replacement surgery in the population of the United States was around 1% in 2010 and has grown by 5% each year from 2020 onwards. [4]–[6] Improving the prognosis of these surgeries is therefore of major significance to world health.

Total hip or knee joint replacements are long established medical procedures but barriers remain which prevent the most favourable patient outcomes.[7] Osteointegration (sometimes osseointegration) is defined as the functional biological response of living bone tissue to the surface of a foreign load bearing implant and plays a major role in successful implant fixation.[8], [9] Successful implant fixation in the immediate timeframe post-joint replacement has a direct correlation to implant performance.[10]–[12] However, total joint replacement surgeries also have an associated risk of surgical infection leading to implant failure. [13]–[16] Therefore, a strategy to mitigate the risks associated with surgery, as well as to promote implant fixation, is worth exploring.

Synthetic hydroxyapatite (HA) is employed as a coating on metallic knee or hip implants to smooth the transition from surgery to healing for a patient by promoting osteointegration.[17] Ultimately, HA coating of implants aids patient healing because the body recognises HA as bone material and not as foreign tissue. The recognition of HA as such improves cell response and minimises rejection. This catalyses the process of osteointegration of an implant, meaning that bone in-growth in the area will ensure implant fixation. Improving

osteointegration through HA film optimisation and reducing microbial activity through HA doping is the motivation of this work.

The following review of literature is intended to give a broad overview of HA and a high-level introduction to existing HA coating processes. Optimising HA processes is addressed through the lens of biological HA growth. The requirement for titanium implants to be coated with HA for osteointegration is discussed, with the disadvantages of titanium implants also noted. A summary of inorganic compounds which could enhance HA's performance is provided as well as the means by which these dopants could be evaluated.

1.2 Hydroxyapatite

Hydroxyapatite (HA) or biological apatite is the main ceramic component of bones and teeth in the human body. HA consists of mineral calcium, phosphate and OH groups, generically denoted as $\text{Ca}_{10}(\text{PO}_4)_6(\text{OH})_2$. HA's rigidity and compressive strength is offset *in vivo* by collagen fibres that add elasticity to bones. [18], [19] The crystal structure of HA is hexagonal with the space group being $P6_3/m$. The hydroxyl ions lie at the corners of the planes, see **Figure 1.1**.

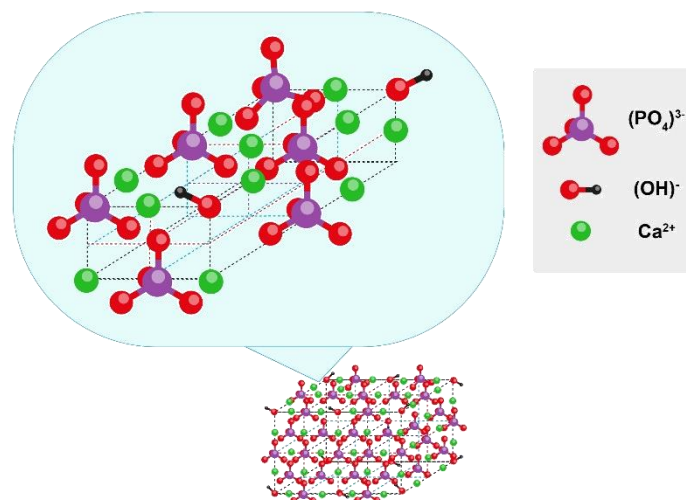


Figure 1.1: Crystal structure of hydroxyapatite. For better visualisation, some atoms have been removed from the diagram. The diagram has been constructed from the literature [20], [21].

Crystalline HA can exist as a bulky dense material but *in vivo* as a porous scaffold which has a calcium to phosphate ratio of 1.5-1.75 depending on the exact location of the mineral in the body. [22], [23] Stoichiometrically accurate HA can

be synthetically manufactured, and the density (via porosity) replicated through various processes, thus it is commonly used as a bioengineered ceramic to fix bone or teeth deformities.[24] Both natural and synthetic porous HA encourage bone in-growth within the pores by the differentiation of stem cells and HA donation of the specific ions required for bone bonding.[25], [26]

1.3 Hydroxyapatite Coating

Given that HA can entice bone growth *in vivo* and that HA deposition can be achieved on a wide range of materials, HA as a coating for orthopaedic implants is widely considered to be the industrial gold standard for promoting orthopaedic implant fixation. However, HA coatings need to be carefully prepared and controlled if they are to be effective. Fibrous build up occurs in the body as a natural (immune) response to any foreign object, causing infection and inhibiting the body's healing or bone repair around the foreign material. Some fibrous build-up is inevitable but is manageable when it does not exceed the bone's growth. [27], [28]. HA layers on implants mitigate fibrous build-up and promote fixation, Trindade et al describe this as managing the 'implant-host interaction'.[29]

Many industrial techniques such as plasma spraying, chemical vapour deposition, sol-gel deposition or ion assisted deposition can be used to form HA coatings on a surface. Plasma spraying is the most common procedure as it produces sub-micron needles and plates within micron sized lamellae which allows for the formation of a porous structure. [30], [31] Sol-gel processes can be used and can include elastic, part-polymer and ceramic composite materials. These processes are useful to study the repair of bone cartilage and are predominantly used for research purposes since control of sol-gel chemistry can be challenging in industrial environments. [32]–[35] One benefit of sol-gel processes is that they can be carried out at low temperatures. [36], [37] Biomimetic processes using simulated bodily fluids have also been studied as a means to grow HA on a surface but are difficult to scale to industrial levels. [38]–[43]

Poor porosity and thickness control, along with poor substrate adhesion are some of the unfavourable attributes of existing HA coating methods. [44] Often, intermediate thermal oxide layers are deposited to improve these properties. [45],

[46] HA deposited via the existing plasma-based method, however, does display good mechanical properties such as hardness and tensile strength. It has been shown that the hardness of these coatings, although lowered by porosity, remains above 175HV for a range of applied loads.[47], [48] The tensile strength of plasma-sprayed HA has been measured at 28-30 MPa – a satisfactory level for high load bearing implants. [49], [50] Another advantage of plasma-HA is its strong affinity for titanium implants. [51] The focus of research is mainly upon characterisation of a coating rather than characterisation of the route by which the coating has formed, although Mokabber et al [52] have used SEM and HRTEM to show that for an electrochemical process the nucleation of Ca-P species happens within the first minute of the process with pores emerging, **Figure 1.2.**

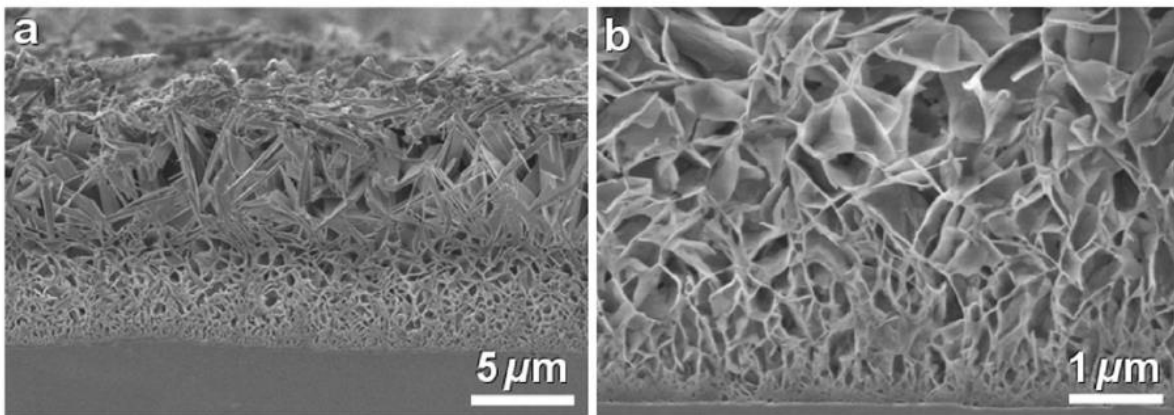


Figure 1.2: SEM images of Ca-P coating in early stages of HA deposition reproduced from experiments by Mokabber et al[52].

1.4 Bone Growth Process *in vivo*

Physiologically there are distinct stages of biological bone mineralisation: [53]–[56]

1. At the site of any bone-related trauma, mesenchymal stem cells (MSCs) arrive and differentiate into a variety of cells, including bone cells called osteoblasts. Osteoblasts are involved in bone growth while osteoclasts (derived from monocytes) reabsorb bone. [57]–[60]
2. Osteoblasts secrete and fix protein to the surface and form a matrix, leading to incorporation of collagen receptors, calcium-binding proteins, proteins that regulate osteoclasts and proteins that have a high affinity for HA.

3. Nucleation and crystallisation of calcium and phosphate ions form the beginning of an apatite matrix. Up to five different substances may form such as: amorphous calcium phosphate (ACP), tricalcium phosphate (TCP), octacalcium phosphate (OCP) or pure HA. Crystallisation *in vivo* and *in vitro* follows and starts with 10-25 nm sized amorphous apatite particles. [40] Some studies name and define these initial particles as Posner clusters of $\text{Ca}_9(\text{PO}_4)_6$, which are formed from the nucleation of phosphate-based fluid in contact with calcium semi-solid interfaces.[61], [62] These particles accumulate into clusters and act as a precursor to ACP with their shape allowing for pores and interstices in the HA as it forms. [63]

1.5 Solution-Based Hydroxyapatite Formation and Phases

Despite the anatomical knowledge about the growth of HA *in vivo*, there is no known replication of this process at engineered HA surfaces. Although chemically precipitated HA methods have been established as a means to form HA nanoparticles and nano-powders, [64], [65] thanks to their ability to control TCP and ACP phases of HA, these methods have not yet been explored as an industrial coating technique because of reproducibility and reliability issues. Previous research has demonstrated hydrothermal hydroxyapatite coating techniques but this necessitates electrochemical functionalisation prior to HA deposition on a surface. [66]–[69]

Precipitation of Ca^{2+} and phosphate ions out of solution onto a surface to form a HA layer has been achieved with relevant precursors and under specific conditions of pH and temperature. [70] Research has shown that ACP forms initially before undergoing full HA crystallisation, which is verified by studies relating to the PO_4^{3-} compound.[71] It has been established that chemically precipitated HA could allow for more precise HA phase control while mimicking the body's natural bone mineralisation process in a self-assembly manner. [72]–[74] These studies however are conducted at extreme temperatures, pressures or pH and the resulting material can be unstable; the work presented herein will replicate body conditions at a neutral pH and lower processing temperatures.

Regarding the potential of a new HA growth process with a more advanced compositional control, any process would still have to align with existing scientific data. HA consistently contains other phases of a calcium phosphate ceramic, be they amorphous or crystalline and during *in vitro* or *in vivo* formation. [75]–[78] To help with HA identification in this project, **Table 1.1** lists the specific HA phases and their Ca/P ratios along with their oxygen content as calculated from their stoichiometry.

Table 1.1: Details of HA phases reproduced from Carayon and Lacout[79] with additional column of Atomic % Oxygen.

Acronym	Mineral	Formula	Ca/P	Atomic % Oxygen
HA	Hydroxyapatite	$\text{Ca}_{10}(\text{PO}_4)_6(\text{OH})_2$	1.67	34.9
ACP	Amorphous calcium phosphate	$\text{Ca}_x(\text{H}_y(\text{PO}_4)_z \cdot n\text{H}_2\text{O})$	1.2-2.2	flexible
α -TCP	α - Tricalcium phosphate	$\alpha\text{-Ca}_3(\text{PO}_4)_2$	1.5	41
β -TCP	β - Tricalcium phosphate	$\beta\text{-Ca}_3(\text{PO}_4)_2$	1.5	41
OCP	Octacalcium phosphate	$\text{Ca}_2(\text{H}_2(\text{PO}_4)_6 \cdot 5\text{H}_2\text{O})$	1.33	39.7
CDHA	Calcium Deficient Hydroxyapatite	$\text{Ca}_9(\text{HPO}_4)(\text{PO}_4)_5\text{OH}$	1.5	43.13

All methods of HA coating deposition include ACP and other Ca-P phases amongst the crystalline HA matrix – ACP has a reabsorption and dissolution rate that differs from HA, therefore coating performance is affected.[80]–[83] **Figure 1.3** shows that ACP is the main phase adjoining titanium in an HA coating. HA coated on titanium has some parts ACP and TCP which can be differentiated by EDX due to their respective Ca/P ratios, with ACP having the lowest possible phosphate content of 20 %.[84]

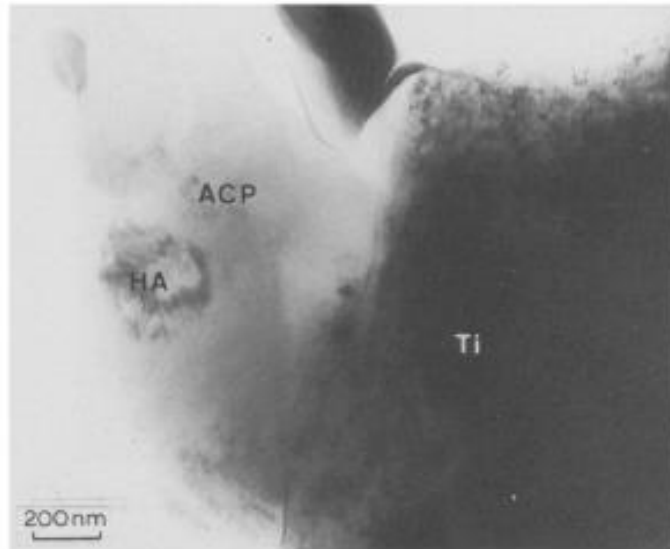


Figure 1.3: TEM images of Ti and HA interfacial layer depicting the amorphous ACP with crystalline HA phase by Ji et al. [84]

1.6 Porous Nature of Hydroxyapatite Coating

During bone mineralisation, surface adhesion of Ca-P ions to an implant is the initial step happening *in vivo* and so the rate of this process will improve the growth rate and adhesive strength of the resultant new bone. [85] Dos Santos et al [86] showed that altering the TCP content of the coating and strategically roughening the titanium prior to deposition correlates to protein adhesion at the site. It is difficult to directly measure surface roughness values for HA coatings since they are deposited to encapsulate pores at the scale of nanometres to microns. [87] However, it is known that osteoblasts preferably grow on hydrophilic surfaces, which can be verified by means of water contact angle (WCA) analysis. [88], [89] It has also been established that the porosity of a coating is affected by the deposition rates or the heat treatment during the HA deposition. [35], [83], [90]–[92] Protein adhesion to the HA pores occurs at the nanometre scale. For instance, Nagasaki et al [93] studied bovine serum albumin (BSA) and lysozyme (LSZ) proteins and their adsorption to HA. They found that the protein adsorption was debilitated if the pore was smaller than the diameter of the protein in question. At the same time the large surface areas of porous material allows for larger interfaces between the HA and the *in vivo* fluids with some of those being inter-soluble with HA. [94] This implies good phase and porosity control which are key to building a successful HA coating system.

1.7 Bulk Titanium orthopaedic joint and alternative materials

The most common bulk material for knee or hip replacement joint is titanium (specific alloys such as Ti-318 and Ti-6AL-4V) and chromium-cobalt largely due to their mechanical strength and bio-inertness. [95]–[98] Chromium-cobalt implants have declined in popularity due to the potential for heavy metal bloodstream poisoning. [96] Therefore, while titanium is the most common metal for orthopaedic implants, there are some concerns surrounding its use.

Disadvantages of titanium implants include:

1. Titanium parts can undergo surface propagated cracks in heavier subjects. [99]
2. Titanium particles (as a result of implant wear) can cause severe allergies if they enter a patient's bloodstream. [100]
3. Blood titanium levels are representative of titanium implant failure.[101]
4. The Young's modulus of titanium implants and their titanate phase is mismatched to that of bone resulting in stresses that lead to implant wear and degradation. [102]
5. Titanium implants require alloys including other elements to adjust the Young's modulus and some of these can be harmful to humans. [103]–[105]

Research in the last decade has therefore focussed on alternatives to titanium alloys. Investigations by Abitha et al[106] revealed that polytetrafluoroethylene, ultra-high molecular weight polyethylene and polyetheretherketone polymers have huge potential in orthopaedic implants due to their mechanical properties and biocompatibility. However, these materials are hindered by the poor adhesion of HA to polymers. Ismail et al [107] performed experiments on epoxy coated bamboo fibres ("*gigantochloa scortechinii*") and found that it had potential as an implant material which would incur lower aseptic loosening post joint replacement due to the fact that its stiffness was a closer correlation to that of natural bone. As recently as 2020, a publication by Andrusova et al [108] called for the need for solution based HA deposition which contains polymeric particles to be a gateway to implementing polymeric based implants. While polymers or other materials are emerging as possible replacements for large permanent metal

alloy implant parts, the greatest application of these is thought to be in developing bioabsorbable products for smaller implant devices such as screws. [109], [110] Both graphene and various 3D printed compounds and components are promising materials for implants owing to the fact that they are highly adaptable to functionalisation. [111], [112]

In conclusion, while HA coatings on titanium implants are well understood there are some drawbacks to existing fabrication approaches. A method of solution deposition, whereby phase and porosity can be controlled, could potentially outperform existing evaporation-based methods of HA deposition. Additionally, the ability to deposit HA on alternative substrates would enable an innovative approach to produce orthopaedic implants from other materials.

1.8 Doping of Hydroxyapatite Coating

Arthroplasty failures mainly arise from two core factors: 1. Aseptic loosening of the joint and 2. post-operative infection at the site of the surgery. Aseptic loosening occurs when there is an increased osteoclast presence at the implant site inhibiting new bone growth. [113] This occurs in about 10-30 % of patients depending on genetic or health factors. [114], [115] A study by Pietrzak et al [116] predicts a six-fold increase in aseptic loosening in the same hospital from the 1990s to the 2050s. Post-operative infection affecting total hip and knee replacements affects approximately 1% of patients. While this figure seems low, the impact to patients is significant, with amputation a frequent result, and recently increasing numbers are seen. [117], [118]

Much of the perspectives on the future of HA coatings are theoretical, and while bactericidal activity would be welcome in a coating, it has only been researched not implemented. [119] Attention is being given to researching inorganic doping of HA with elements that induce a more preferential differentiation of osteoblasts over osteoclasts and drug incorporated coating for antibacterial activity. Strontium intercalation to HA from a mass of 1 atomic % inhibited osteoclast production during *in vitro* studies. [120] However, Terra et al [121] hypothesise that while Sr^{2+} can substitute Ca^{2+} in the HA lattice, with increasing strontium content hydroxyl groups are diminished, and these are necessary for protein adhesion at the bone site. Studies have proven that from an atomic mass of 0.7

% Ag⁺ doped HA can suppress *staphylococcus aureus*, *escherichia coli* and *candida albicans* growth when compared to undoped HA, however the bone growth efficacy of silver -doped HA was not tested. [122], [123] Yang et al [124] have developed a method of fabricating mesoporous HA doped with europium which acts as a drug carrier for ibuprofen. While there was no biological testing carried out, they demonstrated the release of ibuprofen which would be beneficial to target post-operative inflammation *in vivo*.

Zinc metal exists in the human body in immune-essential proteins, DNA ligands and enzymes and thus aids and promotes healing.[125] Zinc incorporated in HA is studied on account of this, being both osteoclast inhibiting and antimicrobial. The role of zinc in MSC differentiation is not fully understood but the hypothesis is that zinc encourages osteoblast differentiation through certain protein signalling processes. [126] Flame sprayed[127] and pulsed laser deposited[128] zinc doped HA materials have shown potency against bacteria and biofilm formation and up to 1 atomic % Zn-doped HA does not have significant cytotoxicity to osteoblasts. Animal studies have been undertaken whereby Zn-doped HA has been implanted into rabbits and the Zn-doped parts confirmed “superior bone-implant” attachment and in a shorter time frame.[129]

1.9 Gallium

Gallium compounds have many therapeutic uses such as fighting metabolic bone disease, cancer detection or cancer treatment while also having material properties which are autoimmune suppressant and antimicrobial.[130] Gallium nitrate (Ga(NO₃)₃) is an FDA approved drug which is used to treat hypercalcemia of malignancy and other osteo-degeneration diseases such as Paget’s disease or osteoporosis in humans. Once administered, gallium nitrate transforms to Ga(OH)₃ and is stable at varying pH ranges whereby it gives rise to Ga³⁺ ions in blood plasma. [131] Osteoclast cells have an unusual, ruffled cell membrane which lends themselves to transferrin protein delivery to the cell. In turn the transferrin protein is required to convey Fe³⁺ ions where they can be reduced and metabolised. [132] Ga³⁺ and Fe³⁺ are analogous in terms of ionic radius, electronegativity and chelation action that the body cannot differentiate between them. However, when Ga³⁺ substitutes for Fe³⁺ functions such as in osteoclastic

transferrin requirements, the cell cannot reduce Ga^{3+} physiologically like it can Fe^{3+} , and thus cell proliferation is ceased. [133]

While gallium inhibits osteoclastic activity it has no effect on osteoblast growth and thus allows for bone regrowth to occur. This was shown by Gómez-Cerezo et al [134] when bringing osteo-seeding MSC in contact with gallium containing bioactive glass and Verron et al [135] when they dosed rabbit, murine and human bone cells with gallium. This is dose dependant below 100 μM concentration. Kurtjak et al [136] undertook a large study of the incorporation of Ga(III) compounds with HA and their findings demonstrated the formation of increased amounts of ACP and amorphous gallium compounds, and confirmed that Ga-HA possesses antibacterial properties against *pseudomonas aeruginosa*. Rat studies have shown that rodent bones in contact with Ga-doped HA have increased calcium content by more than pure HA implying that while ACP phase is formed with gallium, bone crystallisation is improved nonetheless. [137] Melnikov et al [138] states that gallium ions, up to 10 mass% can substitute into a synthetic HA matrix without changing any lattice parameters or grain boundary frameworks. The intercalation of gallium ions from solutions of gallium nitrate or sodium gallate are stable and do not replace calcium ions which is also supported by Cacciotti et al. [139] Further studies by Melnikov et al [140] tested Ga-doped levels of 50, 500 and 5000 $\mu\text{g}\cdot\text{ml}^{-1}$ in HA particles incubated with the kidney cells of monkeys. ANOVA analysis of the results showed no statistical difference from control implying low toxicity at these levels.

Gallium has conceivable osteogenic properties that it seems like an obvious choice of component to add to HA as both an osteoclast inhibitor and to reduce the amount of postoperative infection control procedures/requirements. The potential for gallium to enhance biological processes lies in its existing therapeutic uses, but for would only require gallium amounts on the nanoscale with the exact amount currently unknown. It is clear that gallium and to a lesser extent zinc would be good additions to HA coatings to improve osteointegration. However, the exact release mechanism and dosage of gallium from a hydroxyapatite doped coating is not superbly detailed in literature. It is for this reason that a detailed study on gallium action needs to be completed prior to the combination with HA.

1.10 Model Surfaces for Dopant Studies

As described above, dopant ions in blood would assist in bone growth and affect bacterial growth at the site of an implant regardless of HA. The controlled ionic release of ions from a surface is required for *in vitro* HA dopant testing, therefore, creating model surfaces of dopant material is required to study dopant efficacy. It may be preferable to create dopants in nano-dimensioned form. This allows rapid ionic dissolution allowing localised ion production. One convenient method to create nanosized features at a surface is by polymer self-assembly. The uptick of ions can be controlled by the size and shape of the nanofeatures. [141], [142] Our research group has pioneered these approaches using the self-assembly of block copolymer systems. [143]– [145]

Block copolymer (BCP) patterns are established in science as a means by which to create nanoscopic arrays of polymer or inorganic features. A BCP is a polymeric molecule whereby two homopolymer chains are covalently bonded to each other. BCPs can be used in bulk, in solution or as thin films cast on a substrate.[146] Infiltration of an inorganic precursor selectively into one domain of a BCP gives rise to highly ordered nanostructures that can be dimensionally accurate down to the scale of a few nanometres as demonstrated step-by step by Lopes and Jaeger. [146], [147]

Facile synthesis of inorganic arrays such as gyroid-shaped Ti nanohybrids, SiO₂, ZnO, and W nanoscopic materials using BCPs have been shown in various studies. [148], [149] BCPs are showing promise in biomedical science as a means of drug delivery.[150] Furthermore, drug quantity can be accurately estimated per mg of BCP.[151]

BCPs can be engaged to build ordered arrays of inorganic compounds and can allow controlled release of these compounds as required, therefore their use as model dopant surfaces is optimal.

1.11 Objective and Aims

Experimental work in this thesis centres around a new and novel method of depositing hydroxyapatite (HA) on orthopaedic implants using saturated solutions of calcium and phosphorous. Since this process is new, there is a wealth of knowledge still unknown on the molecular level as pertains to coating growth and

the process intricacies. One benefit of this new coating process is that it grows in a self-assembly manner mimicking the body's endogenous bone growth therefore allowing for more osteo-inductive surfaces. Another advantage of this process would be the ability to deposit HA on surfaces other than titanium metal which would allow for a new generation of implants while retaining the known attributes of HA. Understanding this new HA coating process sufficiently would also garner insight into when, where and to what amount a dopant can be added to a HA coating.

From reviewing existing literature, gallium and zinc have stood out as promising HA dopants. The mechanism of biological activity for zinc and gallium are different, gallium has both bone regenerative and antimicrobial activity due to its similarity to metabolic iron. Zinc has these tendencies due to its immunostimulant nature.

On account of gallium having osteo-inductive properties, antimicrobial activity and that it is already administered as a drug for osteo-degenerative disease it has become the primary dopant candidate for this project. On the other hand, gallium does exhibit renal toxicity and cytotoxicity in a dose dependant manner. Research and studies support its use on the nanoscale; therefore, attention needs to be given to quantification and characterisation of nano-gallium coatings prior to HA combination.

The possibility of using a block copolymer pattern as a dopant seed is explored. The polymeric material can be removed leaving dopant *in situ* and thus would allow for application of dopant to an area without complex HA crystal structure changes. BCP's are applicable to inert planar surfaces and consequently any nano-features formed are ideal test subjects of the material in the nano-features alone. Future work in this project would be to investigate if BCPs could be applied to HA coatings.

If the mechanism of hydroxyapatite growth on surfaces can be understood this not only enables process optimisation but also the ability to design the HA for function and to extend the methodology to non-conventional substrates. It would also facilitate the use of, and the action of, certain dopants to increase osteointegration and reduce damaging biofilm formation.

The specific aims of this research project were to:

1. Build a laboratory-based system for solution deposition of hydroxyapatite (HA) that allows growth for 'engineered' and more effective porous coating.
2. Perfect the deposition of HA so it is reliable in terms of composition, morphology and crystal phase.
3. Grow HA on test substrates and confirm the formation of HA coating that aligns with current literature and industrial standards.
4. Identify process and reaction parameters that impact the nature of the HA formed, which are unknown in literature.
5. Understand the role of the substrate surface chemistry that controls HA crystal structure development.
6. Investigate if the attachment of HA to titanium thin films or non-titanium substrates is possible.
7. From literature, identify inorganic compounds that would have beneficial biological responses.
8. Design a model surface to support inorganic compounds for testing against biological agents.
9. Measure the ionic release of these inorganic compounds and ratify whether this amount is antimicrobial and osteogenic.
10. Devise a means by which to dope HA coating such that there is surface elution of requisite calcium, phosphate and dopant ions.

1.12 References

- [1] D. A. Etzioni, J. H. Liu, M. A. Maggard, and C. Y. Ko, "The Aging Population and Its Impact on the Surgery Workforce," *Ann Surg*, vol. 238, no. 2, pp. 170–177, Aug. 2003, doi: 10.1097/01.SLA.0000081085.98792.3d.
- [2] G. Szczęsny, M. Kopec, D. J. Politis, Z. L. Kowalewski, A. Łazarski, and T. Szolc, "A Review on Biomaterials for Orthopaedic Surgery and Traumatology: From Past to Present," *Materials*, vol. 15, no. 10, Art. no. 10, Jan. 2022, doi: 10.3390/ma15103622.
- [3] M. Navarro, A. Michiardi, O. Castaño, and J. A. Planell, "Biomaterials in orthopaedics," *J R Soc Interface*, vol. 5, no. 27, pp. 1137–1158, Oct. 2008, doi: 10.1098/rsif.2008.0151.
- [4] H. Maradit Kremers *et al.*, "Prevalence of Total Hip and Knee Replacement in the United States," *J Bone Joint Surg Am*, vol. 97, no. 17, pp. 1386–1397, Sep. 2015, doi: 10.2106/JBJS.N.01141.
- [5] I. Shichman *et al.*, "Projections and Epidemiology of Primary Hip and Knee Arthroplasty in Medicare Patients to 2040-2060," *JB JS Open Access*, vol. 8, no. 1, p. e22.00112, Feb. 2023, doi: 10.2106/JBJS.OA.22.00112.

- [6] N. Yohe, M. D. Weisberg, M. Ciminero, A. Mannino, O. Erez, and A. Saleh, "Complications and Readmissions After Total Hip Replacement in Octogenarians and Nonagenarians," *Geriatr Orthop Surg Rehabil*, vol. 11, p. 2151459320940959, Jan. 2020, doi: 10.1177/2151459320940959.
- [7] S. K. Kunutsor *et al.*, "Risk factors for dislocation after primary total hip replacement: a systematic review and meta-analysis of 125 studies involving approximately five million hip replacements," *The Lancet Rheumatology*, vol. 1, no. 2, pp. e111–e121, Oct. 2019, doi: 10.1016/S2665-9913(19)30045-1.
- [8] T. Albrektsson and C. Johansson, "Osteoinduction, osteoconduction and osseointegration".
- [9] A. L. Overmann *et al.*, "Orthopaedic osseointegration: Implantology and future directions," *Journal of Orthopaedic Research*, vol. 38, no. 7, pp. 1445–1454, 2020, doi: 10.1002/jor.24576.
- [10] T. L. Mueller, S. E. Basler, R. Müller, and G. H. van Lenthe, "Time-lapsed imaging of implant fixation failure in human femoral heads," *Medical Engineering & Physics*, vol. 35, no. 5, pp. 636–643, May 2013, doi: 10.1016/j.medengphy.2012.07.009.
- [11] T. K. Fehring, S. Odum, W. L. Griffin, J. B. Mason, and M. Nadaud, "Early Failures in Total Knee Arthroplasty," *Clinical Orthopaedics and Related Research®*, vol. 392, p. 315, Nov. 2001.
- [12] D. R. Sumner, "Long-term implant fixation and stress-shielding in total hip replacement," *Journal of Biomechanics*, vol. 48, no. 5, pp. 797–800, Mar. 2015, doi: 10.1016/j.jbiomech.2014.12.021.
- [13] C. M. Mallon, R. Gooberman-Hill, and A. J. Moore, "Infection after knee replacement: a qualitative study of impact of periprosthetic knee infection," *BMC Musculoskelet Disord*, vol. 19, p. 352, Oct. 2018, doi: 10.1186/s12891-018-2264-7.
- [14] S. M. Kurtz, E. Lau, H. Watson, J. K. Schmier, and J. Parvizi, "Economic Burden of Periprosthetic Joint Infection in the United States," *The Journal of Arthroplasty*, vol. 27, no. 8, Supplement, pp. 61-65.e1, Sep. 2012, doi: 10.1016/j.arth.2012.02.022.
- [15] B. H. Kapadia, R. A. Berg, J. A. Daley, J. Fritz, A. Bhave, and M. A. Mont, "Periprosthetic joint infection," *The Lancet*, vol. 387, no. 10016, pp. 386–394, Jan. 2016, doi: 10.1016/S0140-6736(14)61798-0.
- [16] K. L. Ong, S. M. Kurtz, E. Lau, K. J. Bozic, D. J. Berry, and J. Parvizi, "Prosthetic Joint Infection Risk After Total Hip Arthroplasty in the Medicare Population," *The Journal of Arthroplasty*, vol. 24, no. 6, Supplement, pp. 105–109, Sep. 2009, doi: 10.1016/j.arth.2009.04.027.
- [17] S. Bose, S. Tarafder, and A. Bandyopadhyay, "7 - Hydroxyapatite coatings for metallic implants," in *Hydroxyapatite (Hap) for Biomedical Applications*, M. Mucalo, Ed., in Woodhead Publishing Series in Biomaterials. , Woodhead Publishing, 2015, pp. 143–157. doi: 10.1016/B978-1-78242-033-0.00007-9.
- [18] C. B. Carter and M. G. Norton, *Ceramic Materials: Science and Engineering*, 2nd ed. New York: Springer-Verlag, 2013. doi: 10.1007/978-1-4614-3523-5.
- [19] M. Mucalo, *Hydroxyapatite (HAp) for Biomedical Applications*. Elsevier, 2015.
- [20] L. Pramatarova and E. Pecheva, *Modified Inorganic Surfaces as a Model for Hydroxyapatite Growth*. Trans Tech Publications Limited, 2006.
- [21] S. Rujitanapanich, P. Kumpapan, and P. Wanjanoi, "Synthesis of Hydroxyapatite from Oyster Shell via Precipitation," *Energy Procedia*, vol. 56, pp. 112–117, 2014, doi: 10.1016/j.egypro.2014.07.138.
- [22] A. Kohutová, P. Honcová, L. Svoboda, P. Bezdička, and M. Maříková, "Structural characterization and thermal behaviour of biological hydroxyapatite," *Journal of Thermal Analysis and Calorimetry*, vol. 108, no. 1, pp. 163–170, Oct. 2011, doi: 10.1007/s10973-011-1942-6.

- [23] A. M. Janus, M. Faryna, K. Haberko, A. Rakowska, and T. Panz, "Chemical and microstructural characterization of natural hydroxyapatite derived from pig bones," *Microchim Acta*, vol. 161, no. 3–4, pp. 349–353, Jun. 2008, doi: 10.1007/s00604-007-0864-2.
- [24] S. T. Kao and D. D. Scott, "A Review of Bone Substitutes," *Oral and Maxillofacial Surgery Clinics of North America*, vol. 19, no. 4, pp. 513–521, Nov. 2007, doi: 10.1016/j.coms.2007.06.002.
- [25] J. E. Davies, "Bone bonding at natural and biomaterial surfaces," *Biomaterials*, vol. 28, no. 34, pp. 5058–5067, Dec. 2007, doi: 10.1016/j.biomaterials.2007.07.049.
- [26] F. Shi, D. Xiao, C. Zhang, W. Zhi, Y. Liu, and J. Weng, "The effect of macropore size of hydroxyapatite scaffold on the osteogenic differentiation of bone mesenchymal stem cells under perfusion culture," *Regen Biomater*, vol. 8, no. 6, p. rbab050, Sep. 2021, doi: 10.1093/rb/rbab050.
- [27] S. A. Wasilewski and U. Frankl, "Arthroscopy of the painful dysfunctional total knee replacement," *Arthroscopy: The Journal of Arthroscopic & Related Surgery*, vol. 5, no. 4, pp. 294–297, Dec. 1989, doi: 10.1016/0749-8063(89)90144-8.
- [28] M. D. Ries and M. Badalamente, "Arthrofibrosis After Total Knee Arthroplasty," *Clinical Orthopaedics and Related Research*, vol. 380, pp. 177–183, Nov. 2000.
- [29] R. Trindade, T. Albrektsson, P. Tengvall, and A. Wennerberg, "Foreign Body Reaction to Biomaterials: On Mechanisms for Buildup and Breakdown of Osseointegration: Foreign Body Reaction to Biomaterials," *Clinical Implant Dentistry and Related Research*, vol. 18, no. 1, pp. 192–203, Feb. 2016, doi: 10.1111/cid.12274.
- [30] Z. Zyman, J. Weng, X. Liu, X. Zhang, and Z. Ma, "Amorphous phase and morphological structure of hydroxyapatite plasma coatings," *Biomaterials*, vol. 14, no. 3, pp. 225–228, Jan. 1993, doi: 10.1016/0142-9612(93)90027-Y.
- [31] A. McCabe, M. Pickford, and J. Shawcross, "The History, Technical Specifications and Efficacy of Plasma Spray Coatings Applied to Joint Replacement Prostheses," *Reconstructive Review*, vol. 6, no. 4, Art. no. 4, Dec. 2016, doi: 10.15438/rr.6.4.136.
- [32] T. Kokubo, H.-M. Kim, and M. Kawashita, "Novel bioactive materials with different mechanical properties," *Biomaterials*, vol. 24, no. 13, pp. 2161–2175, Jun. 2003, doi: 10.1016/S0142-9612(03)00044-9.
- [33] S. Waheed, M. Sultan, T. Jamil, and T. Hussain, "Comparative Analysis of Hydroxyapatite Synthesized by Sol-gel, Ultrasonication and Microwave Assisted Technique," *Materials Today: Proceedings*, vol. 2, no. 10, Part B, pp. 5477–5484, Jan. 2015, doi: 10.1016/j.matpr.2015.11.073.
- [34] A. Jaafar, C. Hecker, P. Árki, and Y. Joseph, "Sol-Gel Derived Hydroxyapatite Coatings for Titanium Implants: A Review," *Bioengineering*, vol. 7, no. 4, Art. no. 4, Dec. 2020, doi: 10.3390/bioengineering7040127.
- [35] C. Domínguez-Trujillo *et al.*, "Sol-gel deposition of hydroxyapatite coatings on porous titanium for biomedical applications," *Surface and Coatings Technology*, vol. 333, pp. 158–162, Jan. 2018, doi: 10.1016/j.surfcoat.2017.10.079.
- [36] D.-M. Liu, Q. Yang, T. Troczynski, and W. J. Tseng, "Structural evolution of sol-gel-derived hydroxyapatite," *Biomaterials*, vol. 23, no. 7, pp. 1679–1687, Apr. 2002, doi: 10.1016/S0142-9612(01)00295-2.
- [37] G. Bezzi, G. Celotti, E. Landi, T. M. G. La Torretta, I. Sopyan, and A. Tampieri, "A novel sol-gel technique for hydroxyapatite preparation," *Materials Chemistry and Physics*, vol. 78, no. 3, pp. 816–824, Feb. 2003, doi: 10.1016/S0254-0584(02)00392-9.
- [38] Y. Abe, T. Kokubo, and T. Yamamuro, "Apatite coating on ceramics, metals and polymers utilizing a biological process," *J Mater Sci: Mater Med*, vol. 1, no. 4, pp. 233–238, Nov. 1990, doi: 10.1007/BF00701082.
- [39] L. Jonášová, F. A. Müller, A. Helebrant, J. Strnad, and P. Greil, "Biomimetic apatite formation on chemically treated titanium," *Biomaterials*, vol. 25, no. 7, pp. 1187–1194, Mar. 2004, doi: 10.1016/j.biomaterials.2003.08.009.

- [40] M. H. Uddin, T. Matsumoto, M. Okazaki, A. Nakahira, and T. Sohmura, "Biomimetic Fabrication of Apatite Related Biomaterials," *Biomimetics Learning from Nature*, Mar. 2010, doi: 10.5772/8777.
- [41] F. Baino and S. Yamaguchi, "The Use of Simulated Body Fluid (SBF) for Assessing Materials Bioactivity in the Context of Tissue Engineering: Review and Challenges," *Biomimetics (Basel)*, vol. 5, no. 4, p. 57, Oct. 2020, doi: 10.3390/biomimetics5040057.
- [42] S. Akkineni, "Biological and biomimetic mineralization via protein nanoribbon scaffolds," Thesis, 2022. Accessed: Aug. 05, 2022. [Online]. Available: <https://digital.lib.washington.edu/443/researchworks/handle/1773/49068>
- [43] N. Koju, P. Sikder, Y. Ren, H. Zhou, and S. B. Bhaduri, "Biomimetic coating technology for orthopedic implants," *Current Opinion in Chemical Engineering*, vol. 15, pp. 49–55, Feb. 2017, doi: 10.1016/j.coche.2016.11.005.
- [44] B. Beig, U. Liaqat, M. F. K. Niazi, I. Douna, M. Zahoor, and M. B. K. Niazi, "Current Challenges and Innovative Developments in Hydroxyapatite-Based Coatings on Metallic Materials for Bone Implantation: A Review," *Coatings*, vol. 10, no. 12, p. 1249, Dec. 2020, doi: 10.3390/coatings10121249.
- [45] S. Bose, D. Ke, A. A. Vu, A. Bandyopadhyay, and S. B. Goodman, "Thermal Oxide Layer Enhances Crystallinity and Mechanical Properties for Plasma-Sprayed Hydroxyapatite Biomedical Coatings," *ACS Appl. Mater. Interfaces*, vol. 12, no. 30, pp. 33465–33472, Jul. 2020, doi: 10.1021/acsami.0c05035.
- [46] M. Mittal, S. K. Nath, and S. Prakash, "Improvement in mechanical properties of plasma sprayed hydroxyapatite coatings by Al₂O₃ reinforcement," *Materials Science and Engineering: C*, vol. 33, no. 5, pp. 2838–2845, Jul. 2013, doi: 10.1016/j.msec.2013.03.005.
- [47] M. F. Hasan, J. Wang, and C. Berndt, "Evaluation of the mechanical properties of plasma sprayed hydroxyapatite coatings," *Applied Surface Science*, vol. 303, pp. 155–162, Jun. 2014, doi: 10.1016/j.apsusc.2014.02.125.
- [48] A. Ganvir, S. Nagar, N. Markocsan, and K. Balani, "Deposition of hydroxyapatite coatings by axial plasma spraying: Influence of feedstock characteristics on coating microstructure, phase content and mechanical properties," *Journal of the European Ceramic Society*, vol. 41, no. 8, pp. 4637–4649, Jul. 2021, doi: 10.1016/j.jeurceramsoc.2021.02.050.
- [49] P. L. Silva, J. D. Santos, F. J. Monteiro, and J. C. Knowles, "Adhesion and microstructural characterization of plasma-sprayed hydroxyapatite/glass ceramic coatings onto Ti-6Al-4V substrates," *Surface and Coatings Technology*, vol. 102, no. 3, pp. 191–196, Apr. 1998, doi: 10.1016/S0257-8972(97)00576-8.
- [50] G. Singh, S. Singh, and S. Prakash, "Surface characterization of plasma sprayed pure and reinforced hydroxyapatite coating on Ti6Al4V alloy," *Surface and Coatings Technology*, vol. 205, no. 20, pp. 4814–4820, Jul. 2011, doi: 10.1016/j.surfcoat.2011.04.064.
- [51] E. Mohseni, E. Zalnezhad, and A. R. Bushroa, "Comparative investigation on the adhesion of hydroxyapatite coating on Ti-6Al-4V implant: A review paper," *International Journal of Adhesion and Adhesives*, vol. 48, pp. 238–257, Jan. 2014, doi: 10.1016/j.ijadhadh.2013.09.030.
- [52] T. Mokabber, L. Q. Lu, P. van Rijn, A. I. Vakis, and Y. T. Pei, "Crystal growth mechanism of calcium phosphate coatings on titanium by electrochemical deposition," *Surface and Coatings Technology*, vol. 334, pp. 526–535, Jan. 2018, doi: 10.1016/j.surfcoat.2017.12.011.
- [53] M. Valenti, L. Dalle Carbonare, and M. Mottes, "Osteogenic Differentiation in Healthy and Pathological Conditions," *IJMS*, vol. 18, no. 1, p. 41, Dec. 2016, doi: 10.3390/ijms18010041.
- [54] P. Katsimbri, "The biology of normal bone remodelling," *European Journal of Cancer Care*, vol. 26, no. 6, p. e12740, 2017, doi: 10.1111/ecc.12740.
- [55] E. Jones and D. McGonagle, "Human bone marrow mesenchymal stem cells *in vivo*," *Rheumatology*, vol. 47, no. 2, pp. 126–131, Feb. 2008, doi: 10.1093/rheumatology/kem206.

- [56] S. P. Bruder, D. J. Fink, and A. I. Caplan, "Mesenchymal stem cells in bone development, bone repair, and skeletal regeneration therapy," *Journal of Cellular Biochemistry*, vol. 56, no. 3, pp. 283–294, 1994, doi: 10.1002/jcb.240560303.
- [57] H. K. Vaananen, H. Zhao, M. Mulari, and J. M. Halleen, "The cell biology of osteoclast function," *Journal of Cell Science*, vol. 113, no. 3, pp. 377–381, Feb. 2000, doi: 10.1242/jcs.113.3.377.
- [58] W. J. Boyle, W. S. Simonet, and D. L. Lacey, "Osteoclast differentiation and activation," *Nature*, vol. 423, no. 6937, Art. no. 6937, May 2003, doi: 10.1038/nature01658.
- [59] E. J. Mackie, "Osteoblasts: novel roles in orchestration of skeletal architecture," *The International Journal of Biochemistry & Cell Biology*, vol. 35, no. 9, pp. 1301–1305, Sep. 2003, doi: 10.1016/S1357-2725(03)00107-9.
- [60] J. Caetano-Lopes, H. Canhao, and J. E. Fonseca, "Osteoblasts and bone formation," *Acta Reumatológica Portuguesa*, vol. 32, no. 2, pp. 103–110, 2007.
- [61] M. W. Swift, C. G. V. de Walle, and M. P. A. Fisher, "Posner molecules: from atomic structure to nuclear spins," *Phys. Chem. Chem. Phys.*, vol. 20, no. 18, pp. 12373–12380, May 2018, doi: 10.1039/C7CP07720C.
- [62] J. J. Bergeron, R. Sikstrom, A. R. Hand, and B. I. Posner, "Binding and uptake of 125I-insulin into rat liver hepatocytes and endothelium. An *in vivo* radioautographic study.," *Journal of Cell Biology*, vol. 80, no. 2, pp. 427–443, Feb. 1979, doi: 10.1083/jcb.80.2.427.
- [63] L. Wang, S. Li, E. Ruiz-Agudo, C. V. Putnis, and A. Putnis, "Posner's cluster revisited: direct imaging of nucleation and growth of nanoscale calcium phosphate clusters at the calcite-water interface," *CrystEngComm*, vol. 14, no. 19, pp. 6252–6256, Aug. 2012, doi: 10.1039/C2CE25669J.
- [64] Y.-M. Sung, J.-C. Lee, and J.-W. Yang, "Crystallization and sintering characteristics of chemically precipitated hydroxyapatite nanopowder," *Journal of Crystal Growth*, vol. 262, no. 1, pp. 467–472, Feb. 2004, doi: 10.1016/j.jcrysgro.2003.10.001.
- [65] R. Kumar, K. H. Prakash, P. Cheang, and K. A. Khor, "Temperature Driven Morphological Changes of Chemically Precipitated Hydroxyapatite Nanoparticles," *Langmuir*, vol. 20, no. 13, pp. 5196–5200, Jun. 2004, doi: 10.1021/la049304f.
- [66] L.-Y. Huang, K.-W. Xu, and J. Lu, "A study of the process and kinetics of electrochemical deposition and the hydrothermal synthesis of hydroxyapatite coatings," *Journal of Materials Science: Materials in Medicine*, vol. 11, no. 11, pp. 667–673, Nov. 2000, doi: 10.1023/A:1008934522363.
- [67] D. Liu, K. Savino, and M. Z. Yates, "Coating of hydroxyapatite films on metal substrates by seeded hydrothermal deposition," *Surface and Coatings Technology*, vol. 205, no. 16, pp. 3975–3986, May 2011, doi: 10.1016/j.surfcoat.2011.02.008.
- [68] K. Suchanek *et al.*, "Crystalline hydroxyapatite coatings synthesized under hydrothermal conditions on modified titanium substrates," *Materials Science and Engineering: C*, vol. 51, pp. 57–63, Jun. 2015, doi: 10.1016/j.msec.2015.02.029.
- [69] D. He *et al.*, "Effect of hydrothermal treatment temperature on the hydroxyapatite coatings deposited by electrochemical method," *Surface and Coatings Technology*, vol. 406, p. 126656, Jan. 2021, doi: 10.1016/j.surfcoat.2020.126656.
- [70] M. J. J. M. van Kemenade and P. L. de Bruyn, "A kinetic study of precipitation from supersaturated calcium phosphate solutions," *Journal of Colloid and Interface Science*, vol. 118, no. 2, pp. 564–585, Aug. 1987, doi: 10.1016/0021-9797(87)90490-5.
- [71] A. Dey *et al.*, "The role of prenucleation clusters in surface-induced calcium phosphate crystallization," *Nature Mater*, vol. 9, no. 12, Art. no. 12, Dec. 2010, doi: 10.1038/nmat2900.
- [72] J. A. Stammeier, B. Purgstaller, D. Hippler, V. Mavromatis, and M. Dietzel, "In-situ Raman spectroscopy of amorphous calcium phosphate to crystalline hydroxyapatite transformation," *MethodsX*, vol. 5, pp. 1241–1250, 2018, doi: 10.1016/j.mex.2018.09.015.

- [73] B. Zhao, H. Hu, S. K. Mandal, and R. C. Haddon, "A Bone Mimic Based on the Self-Assembly of Hydroxyapatite on Chemically Functionalized Single-Walled Carbon Nanotubes," *Chem. Mater.*, vol. 17, no. 12, pp. 3235–3241, Jun. 2005, doi: 10.1021/cm0500399.
- [74] A. Lak *et al.*, "Self-Assembly of Dandelion-Like Hydroxyapatite Nanostructures Via Hydrothermal Method," *Journal of the American Ceramic Society*, vol. 91, no. 10, pp. 3292–3297, 2008, doi: 10.1111/j.1551-2916.2008.02600.x.
- [75] R. A. Harper and A. S. Posner, "Measurement of Non-Crystalline Calcium Phosphate in Bone Mineral.," *Proceedings of the Society for Experimental Biology and Medicine*, vol. 122, no. 1, pp. 137–142, May 1966, doi: 10.3181/00379727-122-31073.
- [76] I. Kovrlija *et al.*, "Exploring the Formation Kinetics of Octacalcium Phosphate from Alpha-Tricalcium Phosphate: Synthesis Scale-Up, Determination of Transient Phases, Their Morphology and Biocompatibility," *Biomolecules*, vol. 13, no. 3, p. 462, Mar. 2023, doi: 10.3390/biom13030462.
- [77] E. Fiume, G. Magnaterra, A. Rahdar, E. Verné, and F. Baino, "Hydroxyapatite for Biomedical Applications: A Short Overview," *Ceramics*, vol. 4, no. 4, Art. no. 4, Dec. 2021, doi: 10.3390/ceramics4040039.
- [78] C. C. Berndt, F. Hasan, U. Tietz, and K.-P. Schmitz, "A Review of Hydroxyapatite Coatings Manufactured by Thermal Spray," in *Advances in Calcium Phosphate Biomaterials*, B. Ben-Nissan, Ed., in Springer Series in Biomaterials Science and Engineering., Berlin, Heidelberg: Springer, 2014, pp. 267–329. doi: 10.1007/978-3-642-53980-0_9.
- [79] M. T. Carayon and J. L. Lacout, "Study of the Ca/P atomic ratio of the amorphous phase in plasma-sprayed hydroxyapatite coatings," *Journal of Solid State Chemistry*, vol. 172, no. 2, pp. 339–350, May 2003, doi: 10.1016/S0022-4596(02)00085-3.
- [80] L. Keller and W. A. Dollase, "X-ray determination of crystalline hydroxyapatite to amorphous calcium-phosphate ratio in plasma sprayed coatings," *J. Biomed. Mater. Res.*, vol. 49, no. 2, pp. 244–249, Feb. 2000, doi: 10.1002/(sici)1097-4636(200002)49:2<244::aid-jbm13>3.0.co;2-h.
- [81] K. Fox, P. A. Tran, and N. Tran, "Recent Advances in Research Applications of Nanophase Hydroxyapatite," *ChemPhysChem*, vol. 13, no. 10, pp. 2495–2506, 2012, doi: 10.1002/cphc.201200080.
- [82] M. Vallet-Regí and J. M. González-Calbet, "Calcium phosphates as substitution of bone tissues," *Progress in Solid State Chemistry*, vol. 32, no. 1, pp. 1–31, Jan. 2004, doi: 10.1016/j.progsolidstchem.2004.07.001.
- [83] L. Sun, C. C. Berndt, K. A. Gross, and A. Kucuk, "Material fundamentals and clinical performance of plasma-sprayed hydroxyapatite coatings: A review," *Journal of Biomedical Materials Research*, vol. 58, no. 5, pp. 570–592, 2001, doi: 10.1002/jbm.1056.
- [84] H. Ji, C. B. Ponton, and P. M. Marquis, "Microstructural characterization of hydroxyapatite coating on titanium," *J Mater Sci: Mater Med*, vol. 3, no. 4, pp. 283–287, Jul. 1992, doi: 10.1007/BF00705294.
- [85] A. Wennerberg and T. Albrektsson, "Effects of titanium surface topography on bone integration: a systematic review," *Clinical Oral Implants Research*, vol. 20, pp. 172–184, Sep. 2009, doi: 10.1111/j.1600-0501.2009.01775.x.
- [86] E. A. dos Santos, M. Farina, G. A. Soares, and K. Anselme, "Surface energy of hydroxyapatite and β -tricalcium phosphate ceramics driving serum protein adsorption and osteoblast adhesion," *J Mater Sci: Mater Med*, vol. 19, no. 6, pp. 2307–2316, Jun. 2008, doi: 10.1007/s10856-007-3347-4.
- [87] G. Mendonça, D. B. S. Mendonça, F. J. L. Aragão, and L. F. Cooper, "Advancing dental implant surface technology – From micron- to nanotopography," *Biomaterials*, vol. 29, no. 28, pp. 3822–3835, Oct. 2008, doi: 10.1016/j.biomaterials.2008.05.012.
- [88] N. Eliaz, S. Shmueli, I. Shur, D. Benayahu, D. Aronov, and G. Rosenman, "The effect of surface treatment on the surface texture and contact angle of electrochemically deposited

hydroxyapatite coating and on its interaction with bone-forming cells," *Acta Biomaterialia*, vol. 5, no. 8, pp. 3178–3191, Oct. 2009, doi: 10.1016/j.actbio.2009.04.005.

[89] M. Nakamura *et al.*, "Surface free energy predominates in cell adhesion to hydroxyapatite through wettability," *Materials Science and Engineering: C*, vol. 62, pp. 283–292, May 2016, doi: 10.1016/j.msec.2016.01.037.

[90] I. H. Arita, V. M. Castano, and D. S. Wilkinson, "Synthesis and processing of hydroxyapatite ceramic tapes with controlled porosity," *J Mater Sci: Mater Med*, vol. 6, no. 1, pp. 19–23, May 1995, doi: 10.1007/BF00121241.

[91] D.-M. Liu, "Influence of porosity and pore size on the compressive strength of porous hydroxyapatite ceramic," *Ceramics International*, vol. 23, no. 2, pp. 135–139, Jan. 1997, doi: 10.1016/S0272-8842(96)00009-0.

[92] Y.-T. Sul, C. Johansson, A. Wennerberg, L.-R. Cho, B.-S. Chang, and T. Albrektsson, "Optimum Surface Properties of Oxidized Implants for Reinforcement of Osseointegration: Surface Chemistry, Oxide Thickness, Porosity, Roughness, and Crystal Structure," vol. 20, no. 3, p. 12, 2005.

[93] T. Nagasaki, F. Nagata, M. Sakurai, and K. Kato, "Effects of pore distribution of hydroxyapatite particles on their protein adsorption behavior," *Journal of Asian Ceramic Societies*, vol. 5, no. 2, pp. 88–93, Jun. 2017, doi: 10.1016/j.jascer.2017.01.005.

[94] I. Sopyan, M. Mel, S. Ramesh, and K. A. Khalid, "Porous hydroxyapatite for artificial bone applications," *Science and Technology of Advanced Materials*, vol. 8, no. 1–2, pp. 116–123, Jan. 2007, doi: 10.1016/j.stam.2006.11.017.

[95] H. S. Dobbs and J. T. Scales, "Behavior of Commercially Pure Titanium and Ti-318 (Ti-6Al-4V) in Orthopedic Implants," *Titanium Alloys in Surgical Implants*, Jan. 1983, doi: 10.1520/STP28942S.

[96] G. M. Keegan, I. D. Learmonth, and C. Case, "A Systematic Comparison of the Actual, Potential, and Theoretical Health Effects of Cobalt and Chromium Exposures from Industry and Surgical Implants," *Critical Reviews in Toxicology*, vol. 38, no. 8, pp. 645–674, Jan. 2008, doi: 10.1080/10408440701845534.

[97] F. Guillemot, "Recent advances in the design of titanium alloys for orthopedic applications," *Expert Review of Medical Devices*, vol. 2, no. 6, pp. 741–748, Nov. 2005, doi: 10.1586/17434440.2.6.741.

[98] M. İzmir and B. Ercan, "Anodization of titanium alloys for orthopedic applications," *Front. Chem. Sci. Eng.*, vol. 13, no. 1, pp. 28–45, Mar. 2019, doi: 10.1007/s11705-018-1759-y.

[99] T. M. Grupp, T. Weik, W. Bloemer, and H.-P. Knaebel, "Modular titanium alloy neck adapter failures in hip replacement - failure mode analysis and influence of implant material," *BMC Musculoskeletal Disorders*, vol. 11, no. 1, p. 3, Jan. 2010, doi: 10.1186/1471-2474-11-3.

[100] A. Siddiqi, A. G. T. Payne, R. K. D. Silva, and W. J. Duncan, "Titanium allergy: could it affect dental implant integration?," *Clinical Oral Implants Research*, vol. 22, no. 7, pp. 673–680, 2011, doi: 10.1111/j.1600-0501.2010.02081.x.

[101] I. Swiatkowska, N. Martin, and A. J. Hart, "Blood titanium level as a biomarker of orthopaedic implant wear," *Journal of Trace Elements in Medicine and Biology*, vol. 53, pp. 120–128, May 2019, doi: 10.1016/j.jtemb.2019.02.013.

[102] M. Niinomi and M. Nakai, "Titanium-Based Biomaterials for Preventing Stress Shielding between Implant Devices and Bone," *Int J Biomater*, vol. 2011, p. 836587, 2011, doi: 10.1155/2011/836587.

[103] Y. D. Shi, L. N. Wang, S. X. Liang, Q. Zhou, and B. Zheng, "A high Zr-containing Ti-based alloy with ultralow Young's modulus and ultrahigh strength and elastic admissible strain," *Materials Science and Engineering: A*, vol. 674, pp. 696–700, Sep. 2016, doi: 10.1016/j.msea.2016.08.038.

[104] M. H. C. Tan, A. D. Baghi, R. Ghomashchi, W. Xiao, and R. H. Oskouei, "Effect of niobium content on the microstructure and Young's modulus of Ti-xNb-7Zr alloys for medical implants,"

Journal of the Mechanical Behavior of Biomedical Materials, vol. 99, pp. 78–85, Nov. 2019, doi: 10.1016/j.jmbbm.2019.07.014.

[105] M. Nakai, M. Niinomi, X. Zhao, and X. Zhao, “Self-adjustment of Young’s modulus in biomedical titanium alloys during orthopaedic operation,” *Materials Letters*, vol. 65, no. 4, pp. 688–690, Feb. 2011, doi: 10.1016/j.matlet.2010.11.006.

[106] H. Abitha, V. Kavitha, B. Gomathi, and B. Ramachandran, “A recent investigation on shape memory alloys and polymers based materials on bio artificial implants-hip and knee joint,” *Materials Today: Proceedings*, vol. 33, pp. 4458–4466, Jan. 2020, doi: 10.1016/j.matpr.2020.07.711.

[107] N. F. Ismail, S. Shuib, A. Z. Romli, and N. H. Saeid, “Epoxy-Coated of Bamboo Fibre Reinforced Polymer Composite for Uncemented Total Hip Replacement (THR) Application,” p. 11.

[108] N. N. Andrusova, E. S. Zhavoronok, O. A. Legon’kova, A. S. Goncharova, and S. A. Kedik, “Polymer–Mineral Compounds for Cementless Hip Replacement,” *Polym. Sci. Ser. D*, vol. 13, no. 1, pp. 68–72, Jan. 2020, doi: 10.1134/S1995421220010037.

[109] Y. H. An, S. K. Woolf, and R. J. Friedman, “Pre-clinical *in vivo* evaluation of orthopaedic bioabsorbable devices,” *Biomaterials*, vol. 21, no. 24, pp. 2635–2652, Dec. 2000, doi: 10.1016/S0142-9612(00)00132-0.

[110] F. Xing *et al.*, “Recent progress in Mg-based alloys as a novel bioabsorbable biomaterials for orthopedic applications,” *Journal of Magnesium and Alloys*, vol. 10, no. 6, pp. 1428–1456, Jun. 2022, doi: 10.1016/j.jma.2022.02.013.

[111] S. V. Agarwalla, A. P. Solomon, P. Neelakantan, and V. Rosa, “Novel materials and therapeutic strategies against the infection of implants,” *emergent mater.*, vol. 3, no. 4, pp. 545–557, Aug. 2020, doi: 10.1007/s42247-020-00117-x.

[112] J.-Y. Lee, J. An, and C. K. Chua, “Fundamentals and applications of 3D printing for novel materials,” *Applied Materials Today*, vol. 7, pp. 120–133, Jun. 2017, doi: 10.1016/j.apmt.2017.02.004.

[113] Y. Abu-Amer, I. Darwech, and J. C. Clohisy, “Aseptic loosening of total joint replacements: mechanisms underlying osteolysis and potential therapies,” *Arthritis Res Ther*, vol. 9, no. Suppl 1, p. S6, 2007, doi: 10.1186/ar2170.

[114] A. L. Godoy-Santos, C. O. D’Elia, W. J. Teixeira, H. B. Cabrita, and G. L. Camanho, “Aseptic Loosening of Total Hip Arthroplasty: Preliminary Genetic Investigation,” *The Journal of Arthroplasty*, vol. 24, no. 2, pp. 297–302, Feb. 2009, doi: 10.1016/j.arth.2008.08.006.

[115] R. Marks, “Body mass characteristics of hip osteoarthritis patients experiencing aseptic loosening, periprosthetic fractures, dislocation, and infections after total hip replacement,” *Clinicoecon Outcomes Res*, vol. 1, pp. 7–16, May 2009.

[116] J. Pietrzak, H. Common, H. Migaud, G. Pasquier, J. Girard, and S. Putman, “Have the frequency of and reasons for revision total knee arthroplasty changed since 2000? Comparison of two cohorts from the same hospital: 255 cases (2013–2016) and 68 cases (1991–1998),” *Orthopaedics & Traumatology: Surgery & Research*, vol. 105, no. 4, pp. 639–645, Jun. 2019, doi: 10.1016/j.otsr.2019.01.025.

[117] A. W. Blom, J. Brown, A. H. Taylor, G. Pattison, S. Whitehouse, and G. C. Bannister, “Infection after total knee arthroplasty,” *The Journal of Bone and Joint Surgery. British volume*, vol. 86-B, no. 5, pp. 688–691, Jul. 2004, doi: 10.1302/0301-620X.86B5.14887.

[118] S. M. Kurtz, E. Lau, J. Schmier, K. L. Ong, K. Zhao, and J. Parvizi, “Infection Burden for Hip and Knee Arthroplasty in the United States,” *The Journal of Arthroplasty*, vol. 23, no. 7, pp. 984–991, Oct. 2008, doi: 10.1016/j.arth.2007.10.017.

[119] S. Awasthi, S. K. Pandey, E. Arunan, and C. Srivastava, “A review on hydroxyapatite coatings for the biomedical applications: experimental and theoretical perspectives,” *J. Mater. Chem. B*, vol. 9, no. 2, pp. 228–249, Jan. 2021, doi: 10.1039/D0TB02407D.

[120] C. Capuccini, P. Torricelli, E. Boanini, M. Gazzano, R. Giardino, and A. Bigi, “Interaction of Sr-doped hydroxyapatite nanocrystals with osteoclast and osteoblast-like cells,” *Journal of*

Biomedical Materials Research Part A, vol. 89A, no. 3, pp. 594–600, 2009, doi: 10.1002/jbm.a.31975.

[121] J. Terra, E. Rodrigues Dourado, J.-G. Eon, D. E. Ellis, G. Gonzalez, and A. Malta Rossi, "The structure of strontium-doped hydroxyapatite: an experimental and theoretical study," *Physical Chemistry Chemical Physics*, vol. 11, no. 3, pp. 568–577, 2009, doi: 10.1039/B802841A.

[122] M. Riaz, R. Zia, A. Ijaz, T. Hussain, M. Mohsin, and A. Malik, "Synthesis of monophasic Ag doped hydroxyapatite and evaluation of antibacterial activity," *Materials Science and Engineering: C*, vol. 90, pp. 308–313, Sep. 2018, doi: 10.1016/j.msec.2018.04.076.

[123] V. Stanić *et al.*, "Synthesis of antimicrobial monophasic silver-doped hydroxyapatite nanopowders for bone tissue engineering," *Applied Surface Science*, vol. 257, no. 9, pp. 4510–4518, Feb. 2011, doi: 10.1016/j.apsusc.2010.12.113.

[124] P. Yang, Z. Quan, C. Li, X. Kang, H. Lian, and J. Lin, "Bioactive, luminescent and mesoporous europium-doped hydroxyapatite as a drug carrier," *Biomaterials*, vol. 29, no. 32, pp. 4341–4347, Nov. 2008, doi: 10.1016/j.biomaterials.2008.07.042.

[125] H. Tapiero and K. D. Tew, "Trace elements in human physiology and pathology: zinc and metallothioneins," *Biomed Pharmacother*, vol. 57, no. 9, pp. 399–411, Nov. 2003, doi: 10.1016/s0753-3322(03)00081-7.

[126] K. H. Park, Y. Choi, D. S. Yoon, K.-M. Lee, D. Kim, and J. W. Lee, "Zinc Promotes Osteoblast Differentiation in Human Mesenchymal Stem Cells Via Activation of the cAMP-PKA-CREB Signaling Pathway," *Stem Cells and Development*, vol. 27, no. 16, pp. 1125–1135, Aug. 2018, doi: 10.1089/scd.2018.0023.

[127] Y.-C. Yang, C.-C. Chen, J.-B. Wang, Y.-C. Wang, and F.-H. Lin, "Flame sprayed zinc doped hydroxyapatite coating with antibacterial and biocompatible properties," *Ceramics International*, vol. 43, pp. S829–S835, Aug. 2017, doi: 10.1016/j.ceramint.2017.05.318.

[128] B. M. Hidalgo-Robatto *et al.*, "Pulsed laser deposition of copper and zinc doped hydroxyapatite coatings for biomedical applications," *Surface and Coatings Technology*, vol. 333, pp. 168–177, Jan. 2018, doi: 10.1016/j.surfcoat.2017.11.006.

[129] P. Bhattacharjee, H. Begam, A. Chanda, and S. K. Nandi, "Animal trial on zinc doped hydroxyapatite: A case study," *Journal of Asian Ceramic Societies*, vol. 2, no. 1, pp. 44–51, Mar. 2014, doi: 10.1016/j.jascer.2014.01.005.

[130] C. R. Chitambar, "Medical Applications and Toxicities of Gallium Compounds," *IJERPH*, vol. 7, no. 5, pp. 2337–2361, May 2010, doi: 10.3390/ijerph7052337.

[131] A. Sigel, H. Sigel, E. Freisinger, and R. K. O. Sigel, *Metallo-Drugs: Development and Action of Anticancer Agents*. Walter de Gruyter GmbH & Co KG, 2018.

[132] H. Palokangas, M. Mulari, and H. K. Vaananen, "Endocytic pathway from the basal plasma membrane to the ruffled border membrane in bone-resorbing osteoclasts," *Journal of Cell Science*, vol. 110, no. 15, pp. 1767–1780, Aug. 1997.

[133] L. R. Bernstein, "Mechanisms of Therapeutic Activity for Gallium," *Pharmacol Rev*, vol. 50, no. 4, pp. 665–682, Dec. 1998.

[134] N. Gómez-Cerezo *et al.*, "The response of pre-osteoblasts and osteoclasts to gallium containing mesoporous bioactive glasses," *Acta Biomaterialia*, vol. 76, pp. 333–343, Aug. 2018, doi: 10.1016/j.actbio.2018.06.036.

[135] E. Verron *et al.*, "Gallium modulates osteoclastic bone resorption *in vitro* without affecting osteoblasts," *British Journal of Pharmacology*, vol. 159, no. 8, pp. 1681–1692, 2010, doi: 10.1111/j.1476-5381.2010.00665.x.

[136] M. Kurtjak, M. Vukomanović, A. Krajnc, L. Kramer, B. Turk, and D. Suvorov, "Designing Ga(III)-containing hydroxyapatite with antibacterial activity," *RSC Adv.*, vol. 6, no. 114, pp. 112839–112852, 2016, doi: 10.1039/C6RA23424K.

[137] R. S. Bockman, A. L. Boskey, N. C. Blumenthal, N. W. Alcock, and R. P. Warrell, "Gallium increases bone calcium and crystallite perfection of hydroxyapatite," *Calcif Tissue Int*, vol. 39, no. 6, pp. 376–381, Nov. 1986, doi: 10.1007/BF02555174.

- [138] P. Melnikov, A. R. Teixeira, A. Malzac, and M. de B. Coelho, "Gallium-containing hydroxyapatite for potential use in orthopedics," *Materials Chemistry and Physics*, vol. 117, no. 1, pp. 86–90, Sep. 2009, doi: 10.1016/j.matchemphys.2009.05.046.
- [139] I. Cacciotti, "Cationic and Anionic Substitutions in Hydroxyapatite," in *Handbook of Bioceramics and Biocomposites*, I. V. Antoniac, Ed., Cham: Springer International Publishing, 2015, pp. 1–68. doi: 10.1007/978-3-319-09230-0_7-1.
- [140] P. Melnikov, M. de Fatima Cepa Matos, A. Malzac, A. Rainho Teixeira, and D. M. de Albuquerque, "Evaluation of *in vitro* toxicity of hydroxyapatite doped with gallium," *Materials Letters*, vol. 253, pp. 343–345, Oct. 2019, doi: 10.1016/j.matlet.2019.06.095.
- [141] A. Selkirk *et al.*, "Optimization and Control of Large Block Copolymer Self-Assembly via Precision Solvent Vapor Annealing," *Macromolecules*, vol. 54, no. 3, pp. 1203–1215, Feb. 2021, doi: 10.1021/acs.macromol.0c02543.
- [142] R. Lundy *et al.*, "Controlled solvent vapor annealing of a high χ block copolymer thin film," *Physical Chemistry Chemical Physics*, vol. 19, no. 4, pp. 2805–2815, 2017, doi: 10.1039/C6CP07633E.
- [143] C. Cummins, T. Ghoshal, J. D. Holmes, and M. A. Morris, "Strategies for Inorganic Incorporation using Neat Block Copolymer Thin Films for Etch Mask Function and Nanotechnological Application," *Advanced Materials*, vol. 28, no. 27, pp. 5586–5618, 2016, doi: 10.1002/adma.201503432.
- [144] C. Cummins, R. Lundy, J. J. Walsh, V. Ponsinet, G. Fleury, and M. A. Morris, "Enabling future nanomanufacturing through block copolymer self-assembly: A review," *Nano Today*, vol. 35, p. 100936, Dec. 2020, doi: 10.1016/j.nantod.2020.100936.
- [145] M. A. Morris, "Directed self-assembly of block copolymers for nanocircuitry fabrication," *Microelectronic Engineering*, vol. 132, pp. 207–217, Jan. 2015, doi: 10.1016/j.mee.2014.08.009.
- [146] F. S. Bates and G. H. Fredrickson, "Block Copolymer Thermodynamics: Theory and Experiment," p. 33.
- [147] W. A. Lopes and H. M. Jaeger, "Hierarchical self-assembly of metal nanostructures on diblock copolymer scaffolds," *Nature*, vol. 414, no. 6865, pp. 735–738, Dec. 2001, doi: 10.1038/414735a.
- [148] H.-Y. Hsueh and R.-M. Ho, "Bicontinuous Ceramics with High Surface Area from Block Copolymer Templates," *Langmuir*, vol. 28, no. 22, pp. 8518–8529, Jun. 2012, doi: 10.1021/la3009706.
- [149] Q. Peng, Y.-C. Tseng, S. B. Darling, and J. W. Elam, "A Route to Nanoscopic Materials via Sequential Infiltration Synthesis on Block Copolymer Templates," *ACS Nano*, vol. 5, no. 6, pp. 4600–4606, Jun. 2011, doi: 10.1021/nn2003234.
- [150] A. B. Kutikov and J. Song, "Biodegradable PEG-Based Amphiphilic Block Copolymers for Tissue Engineering Applications," *ACS Biomater Sci Eng*, vol. 1, no. 7, pp. 463–480, Jul. 2015, doi: 10.1021/acsbiomaterials.5b00122.
- [151] W. Li, S.-S. Feng, and Y. Guo, "Block copolymer micelles for nanomedicine," *Nanomedicine*, vol. 7, no. 2, pp. 169–172, Feb. 2012, doi: 10.2217/nnm.11.182.

Chapter 2: Development of hydroxyapatite coatings for orthopaedic implants from colloidal solutions, Part 1: effect of solution concentration and deposition kinetics.

Abstract

This chapter introduces and explores the use of supersaturated solutions of calcium and phosphate ions to generate well-defined hydroxyapatite coatings for orthopaedic implants. The deposition of hydroxyapatite is conducted via solutions of metastable precursors that precipitate insoluble hydroxyapatite minerals at a substrate–solution interface. Solutions of this nature are intrinsically unstable, but this chapter outlines process windows in terms of time, temperature, concentration and pH in which coating deposition is controlled via the stop/go reaction. To understand the kinetics of the deposition process, comparisons based on ionic strength, particle size, electron imaging, elemental analyses and mass of the formed coating for various deposition solutions are conducted. This comprehensive dataset enables the measurement of deposition kinetics and identification of an optimum solution and its reaction mechanism. This study has established stable and reproducible process windows, which are precisely controlled, leading to the successful formation of desired hydroxyapatite films. The data demonstrates that this process is a promising and highly repeatable method for forming hydroxyapatites with desirable thickness, morphology and chemical composition at low temperatures and low capital cost compared to the existing techniques.

2.1 Introduction

Orthopaedic implant fixation is hindered by fibrosis encapsulation, which is the body's natural response to a foreign object [1–4]. Coating metallic implants with a bio-compatible layer can mitigate fibrous build-up and promote implant fixation [5,6].

As the main ceramic component of bones and teeth in the human body, with properties of rigidity and compressive strength and a brittle nature,

hydroxyapatite (HA) coatings are used to improve the osteointegration of orthopaedic implants. The use of synthetic HA coating aids orthopaedic recovery since it mimics natural bone, and when deposited in a porous structure, it encourages new bone-ingrowth directly onto an implant [7]. HA coating is particularly important for total hip and total knee replacements as it accelerates implant fixation at these load-bearing joints [8].

HA is a crystalline phase of calcium, phosphate and hydroxyl groups of chemical formula $\text{Ca}_{10}(\text{PO}_4)_6(\text{OH})_2$ and hexagonal crystal structure of space group $\text{P6}_3/\text{m}$. Biological HA is a product of the nucleation and crystallisation of calcium and phosphate ions *in vivo*, but these ions in solution can also synthetically initiate HA formation. Synthetic HA can enhance bone growth *in vivo*, and its deposition can be achieved on a wide range of materials [9–13]. Certain types of synthetic HA as doped HA or HA nanoparticles are being explored for their antimicrobial performance to aid in post-orthopaedic operative infections [14,15]. However, synthetic methods of coating metallic parts with HA are far from facile.

Solution-based HA processes highlight a requirement to regulate the ionic strength of solutions [16–19]. Chemical precipitation is advantageous in forming HA nanoparticles and nano-powders because the phases of HA can be controlled during this process, but it has not yet been extensively explored as a coating technique [20–25]. Similarly, precipitation of Ca^{2+} and PO_4^{3-} ions out of a solution onto a surface to form a HA layer has been achieved with relevant precursors under specific conditions of pH and temperature on collagen or bone interfaces [26,27]. In general, formation of a complex crystalline structure with the desired morphology, adhesion properties and mechanical strength remains a significant challenge. Despite a plethora of methods that lead to HA formation, few replicate the body's natural process of HA growth, and those that do are limited by poor porosity, phase and thickness control, along with limited substrate adhesion to a relevant orthopaedic implant [28,29].

HA crystallisation *in vivo* is thought to start with 10–25 nm sized amorphous apatite particles [30]. Studies suggest these initial particles are Posner clusters of $\text{Ca}_9(\text{PO}_4)_6$, which are formed from the nucleation of phosphate-based fluid in contact with calcium semi-solid interfaces [31–33]. These particles agglomerate into clusters and function as a precursor to amorphous calcium phosphate (ACP),

with their shape allowing for pores and interstices in the HA as it forms [34–36]. Formation of synthetic HA under aqueous conditions might allow for ACP nucleation followed by HA crystal growth which replicates the body's endogenous bone growth process [37]. However, the formation of HA at surfaces is not well understood; the focus of research has mainly been on characterisation rather than the mechanism of film formation. This study builds upon the findings of the scientific community regarding other HA deposition methods, both biologically and synthetically. With a focus on the required outcomes of porosity, herein, chemical structure analysis is undertaken at various stages to tie the characterisation outcomes back to the process itself.

This method of depositing hydroxyapatite (HA) on orthopaedic implant-type substrates mimics biological-like self-assembly growth processes. One novelty of this process lies in the use of chemical precipitation directly onto a substrate to be coated without intermediate steps. Using these saturated solutions of calcium and phosphorous gives rise to coatings with adequate coverage, thickness and morphology control that are relevant to manufacturing requirements. This method also allows for a non-line of sight HA deposition, which is also another of its advantages over the existing material evaporation techniques [38–40]. It is possible to build on the existing literature and studies to hypothesise how a colloidal method might work. At a near biological pH of 7 in aqueous supersaturated conditions, studies show that HA will form via apatitic precursors [41,42]. The precursors formed should follow Ostwald's rule of 4, whereby the most thermodynamically unstable phase forms first [43].

Our results detail a proposed nucleation and growth pathway for HA within this deposition system. With the aim of identifying the ideal process solutions, analysis is conducted on pH, ionic strength, and dynamic light scattering (DLS) properties. Subsequently, HA films are formed with different solutions and are analysed. Weight analysis, scanning electron microscopy (SEM) and energy dispersive X-ray spectroscopy (EDX) of the deposited films reveals the solutions which generated HA films with coverage, morphology and chemical structure best aligned to osetoinduction HA coatings.

2.2 Materials and Methods

All materials and reagents were used as received. Monobasic potassium phosphate (KH_2PO_4) United States Pharmacopeia (USP) reference standard, Honeywell Fluka hydrochloric (HCl) acid solution 6M, tris(hydroxymethyl)-aminomethane (TRIS) ACS reagent, 99.8% sodium chloride (NaCl) BioXtra, 99.5% calcium nitrate tetrahydrate ($\text{Ca}(\text{NO}_3)_2 \cdot 4\text{H}_2\text{O}$) ACS reagent all from Sigma Aldrich. A calibrated benchtop pH meter with a temperature enabled probe (Orion Star A111, Thermo Scientific™, U.K) was used for pH measurements with an accuracy of 0.001 pH. Titanium coupons of Ti-6Al-4V alloy were used as substrates. These coupons were received from the industry co-funding partner, DePuy Synthes. All substrates were submerged in hot basic solutions to increase roughness and yield a negatively charged surface for calcium ion attachment. [44–47]

KH_2PO_4 , TRIS and NaCl were mixed in deionised water (DIW) to yield a supersaturated phosphate concentrate. HCl was added to increase stability of the concentrate to prevent precipitation. $\text{Ca}(\text{NO}_3)_2 \cdot 4\text{H}_2\text{O}$ was mixed with DIW to yield a supersaturated calcium concentrate. The ratio of calcium to phosphate in the syrups remained 09:1 Ca to P with $\text{Ca}(\text{NO}_3)_2 \cdot 4\text{H}_2\text{O}$ having a molarity of $36\mu\text{M}$ and KH_2PO_4 having a molarity of $40\mu\text{M}$. For deposition, the supersaturated concentrates were combined and diluted to various concentrations for deposition process runs. See **Appendix 2.5.1** for all molarities, CAS numbers and water solubility of reagents.

Solutions of varying dilution were identified by %v/v which is percentage concentrate volume to process solution volume. Solutions were warmed to 40-50 °C for deposition of hydroxyapatite. To design a process around body temperature a range of temperature around 30-35°C would have been optimum. However, due to the solubility of NaCl, a slightly higher range of 40-50°C was chosen, this is still lower than other chemically prepared methods.

Ionic strength is a well-established modifier in hydroxyapatite formation since it increases or decreases the ions present in a solution. [48,49] Ionic strength was calculated as follows.

Equation 2.1: Ionic Strength (I) formula

$$I = \frac{1}{2} \sum \left((C_{KH_2PO_4} \cdot (z_{KH_2PO_4})^2) + (C_{TRIS} \cdot (z_{TRIS})^2) + (C_{NaCl} \cdot (z_{NaCl})^2) + (C_{Ca(NO_3)_2} \cdot (z_{Ca(NO_3)_2})^2) \right)$$

Where $C = \text{mol} \cdot \text{L}^{-1}$ and $z = \text{electric charge}$

Despite the ratio of components remaining fixed, ionic strength of the supersaturated solutions was increased via sodium chloride addition (increasing the ratio of concentrate in solution), see **Table 2.1** for a list of the solution data.

Table 2.1: Table containing list of process solutions used (1-7) in this work, with their corresponding percent solution to syrup (%v/v) and ionic strength values ($\text{mmol} \cdot \text{L}^{-1}$).

ID	Syrup to Solution Dilution [%v/v]	Ionic Strength [$\text{mmol} \cdot \text{L}^{-1}$]
Solution 1	3.1	163.08
Solution 2	4.6	244.71
Solution 3	6.2	326.81
Solution 4	7.7	407.71
Solution 5	9.2	489.74
Solution 6	10.8	570.76
Solution 7	12.3	652.36

A custom-designed experimental apparatus was used for deposition, See **Figure 2.1**. A sample holder, thermometer, and pH probe for in situ temperature and acidity measurements, and overhead stirrer to agitate the solution were inserted into the vessel. High agitation rates of 1000 RPM prevented gross precipitation of mineral from the solution.

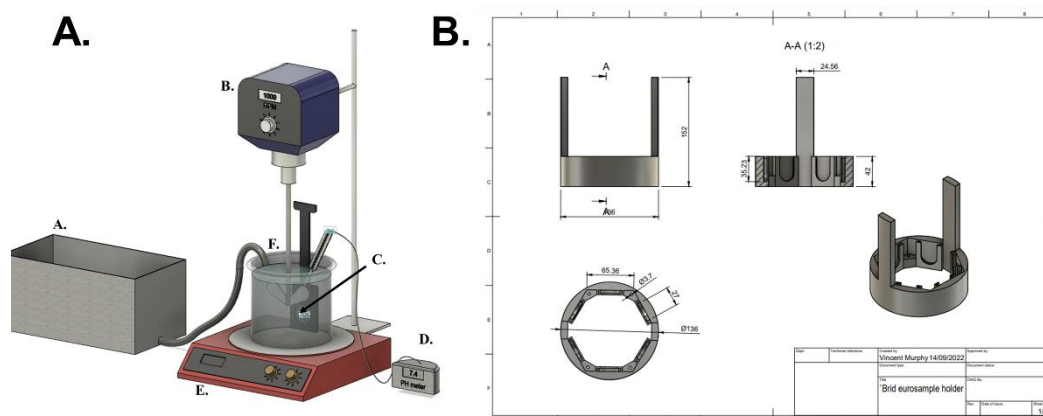


Figure 2.1: **A.** Schematic of deposition rig with the following labels: (A): Solution bath, B: Overhead Stirrer, C: customised 3D printer sample holders, D: pH meter attached to probe, E: Large hot plate and F: stainless steel reaction vessel. And (B). CAD rendering of sample holder used in this studies containing 6 identical Ti coupons for deposition.

Substrates were placed in the reaction vessel for deposition then removed and rinsed with DIW, this process was repeated several times with fresh solutions to grow a coherent layer of HA at the solution-substrate interface of desired thickness. Between deposition steps substrates were removed from solution and allowed to dry for a minimum of 15 min in ambient conditions (to ensure active sites are available for subsequent process runs). More data behind the drying rationale is provided in **Appendix 2.5.2**. To assess the effect of different solutions on eventual film growth, identical substrates were subjected to several deposition process runs of each solution and analysed intermittently, i.e., 6 substrates underwent 7 deposition runs using solution 1, 6 substrates underwent 7 deposition runs using solution 2 etc. This was repeated for 3 sets and data is the average of all the results except where some SEM images are selected.

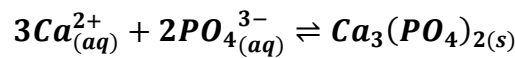
Dynamic Light Scattering (DLS) was performed using Malvern Zetasizer Nano ZS, with 633 nm HeNe laser. Samples were added to glass cuvette which had a 10 mm pathlength and allowed to equilibrate for 120 s at 47 °C prior to sampling. The machine was operated in backscatter mode at an angle of 173 °. Scanning Electron Microscopy (SEM) images were recorded on a Zeiss Ultra Plus system with the accelerating voltages in the range of 5-10 kV, at a working distance between 3 to 10 mm and an in-lens detector. Energy-dispersive X-ray spectroscopy (EDX) spectra were acquired at 15 kV on an Oxford Inca EDX detector.

2.3 Results

2.3.1 Kinetics of Process Solutions

The solution reactions are complex but may be thought of using the following reaction schemes which detail the formation of hydroxyapatite (HA). At equilibrium, calcium and phosphate ions in solution form a tricalcium phosphate (TCP) mineral product as shown by **Equation 2.2**.

Equation 2.2: Equilibrium chemical reaction for the formation of tricalcium phosphate (TCP) from calcium and phosphate ions.



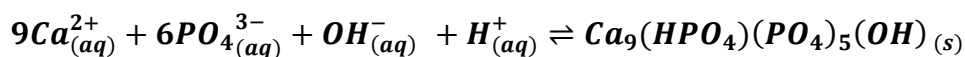
At stoichiometric proportions and in the presence of hydroxyl ions, the formation of TCP is thermodynamically favoured. To form pure hydroxyapatite (HA) under solution excess calcium ions as Ca^{2+} or $Ca(OH)_2$ are required, **Equation 2.3**.

Equation 2.3: Example of one reaction where additional calcium ions with tricalcium phosphate and hydroxyl ions can form hydroxyapatite (HA).

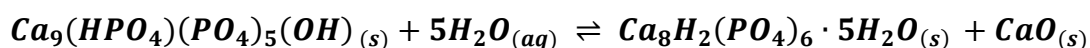


In this work, as the concentration of solutions are equally supersaturated with respect to calcium and phosphate ions, they drive the precipitation of thermodynamically unstable phases of octacalcium phosphate (OCP), as shown in **Equation 2.4 and 2.5**. [50–52]

Equation 2.4: Formation of calcium deficient (CDHA) precursor to octacalcium phosphate (OCP) particles in aqueous solution.



Equation 2.5: Nucleation of octacalcium phosphate (OCP) particle in aqueous solution



Whilst the experimental solutions at room temperature contain metastable intermediaries (which form and then re-dissolve continually), their nucleation into stable precipitates only occurred above a critical temperature and deposition only

occurred between 44 and 50 °C. There is an upper temperature limit because of redissolution. Data temperature from more than 100 process runs (including process runs from various solutions) shows a mean of 46.9 °C.

Precipitation of Ca-P phases from solution should be associated with a pH drop as a result of decreased calcium ion concentration. [53] As **Equations 1,2,3** show, the formation of HA species initiates a drop in calcium ion concentration and OH⁻ concentration. Within this study pH dropped by 0.12 ± 0.02 from 0 to 30 min with almost no change after that, therefore, process runs were ceased at 30 min for all solutions, **Figure 2.2(a)**. The pH reduction confirmed ions are removed from solution, their concentration decreases with the solution becoming more thermodynamically stable until the rate of deposition becomes kinetically too slow.

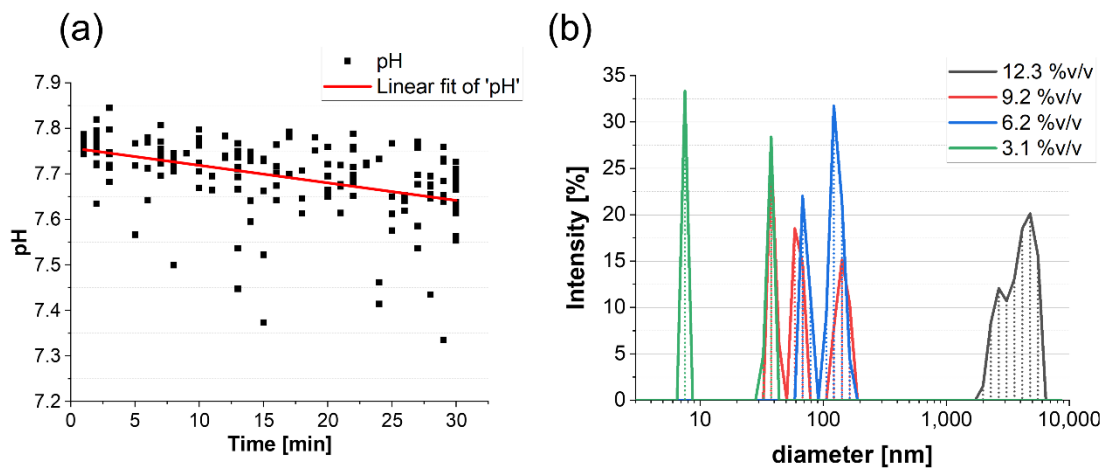


Figure 2.2:(a) pH data from all runs graphed against process time fitted with linear line of best fit and (c) Dynamic light scattering (DLS) data of different solutions, intensity versus particle size.

While all constituent parts were accounted for in the ionic strength calculations, 95% of the ionic strength value for each solution was due to the NaCl component, see **Table 2.1** for values.

DLS data from various process solutions shows that the particle size in solution varies significantly with dilution becoming smaller with increased dilution, **Figure 2.2(b)**. Solution of 12 %v/v has particle size with a mean of 5.2 μm whereas concentrations between 6 and 9 %v/v have a particle size around 100 nm, with the concentration of 3 %v/v having 35 % of particles < 8 nm. The hypothesis

herein is that particles above 100nm aggregate too readily in solution and hinder self-assembly growth on the sub-micron scale at the surface of the substrates during deposition.

2.3.2 Analysis of HA films formed from various process solutions.

When a substrate is added to the solutions at the correct temperature, heterogeneous nucleation at the substrate occurs forming a deposit. A photograph of samples, side-by-side post 7 deposition runs reveals a colour gradient of the HA film across solutions, **Figure 2.3**. This number of deposition runs was chosen to grow a layer of HA up to 6/7 μ m thick, due to the porosity of the layer each deposition run did not provide significant amounts of material. It is clear from this photograph that solutions 5,6 &7 have more white material and we postulate that some of this is just apatite mineral deposited on the surface as it is easily removed. The darker colour gradient seen in solutions 3 and 4 is more well adhered crystal growth bonded onto the substrates as it cannot be removed without significant effort.



Figure 2.3: Photograph of HA samples on Ti coupons as deposited by Solutions 1-7.

The porosity of a HA film is fundamental to the success of the coating *in vivo* and should be on the few hundred nm to micron scale. [54,55] SEM imaging was performed on samples of the HA film deposited by solutions 1-7 after 2,4 and 7 process runs (**Appendix 2.5.3**). A subset of these SEM images is included in **Figure 2.4** to assess their mineral coverage and porosity. From **Figure 2.4(a-b)** it can be concluded that solution 1 generated little or no coverage of mineral with

the topography unchanged compared to the blank substrate after 7 process runs, see **Figure 2.4 (g)**.

Solution 4 showed the beginning of a porous network after 2 process runs, with mineral clusters forming a porous layer amidst needle like interconnectivity, **Figure 2.4(c)**. After 7 process runs, solution 4 shows thorough coverage and porosity on the sub-micron scale. Solution 7 shows large build-up of mineral after 2 process runs, without any needle-like interconnectivity apparent, **Figure 2.4(e)**. After 7 process runs solution 7 has good film coverage, and, although pores can be seen, morphological features are larger, flatter and show evidence of cracking typical of poor adhesion. When compared with lower concentration solutions, inference can be suggested that this solution results in a coating of high coverage but low porosity/high density. We postulate that this is related to the larger particle size of this solution 7, particles should be on the nanometres scale to nucleate and formed a film with features sub-micron.

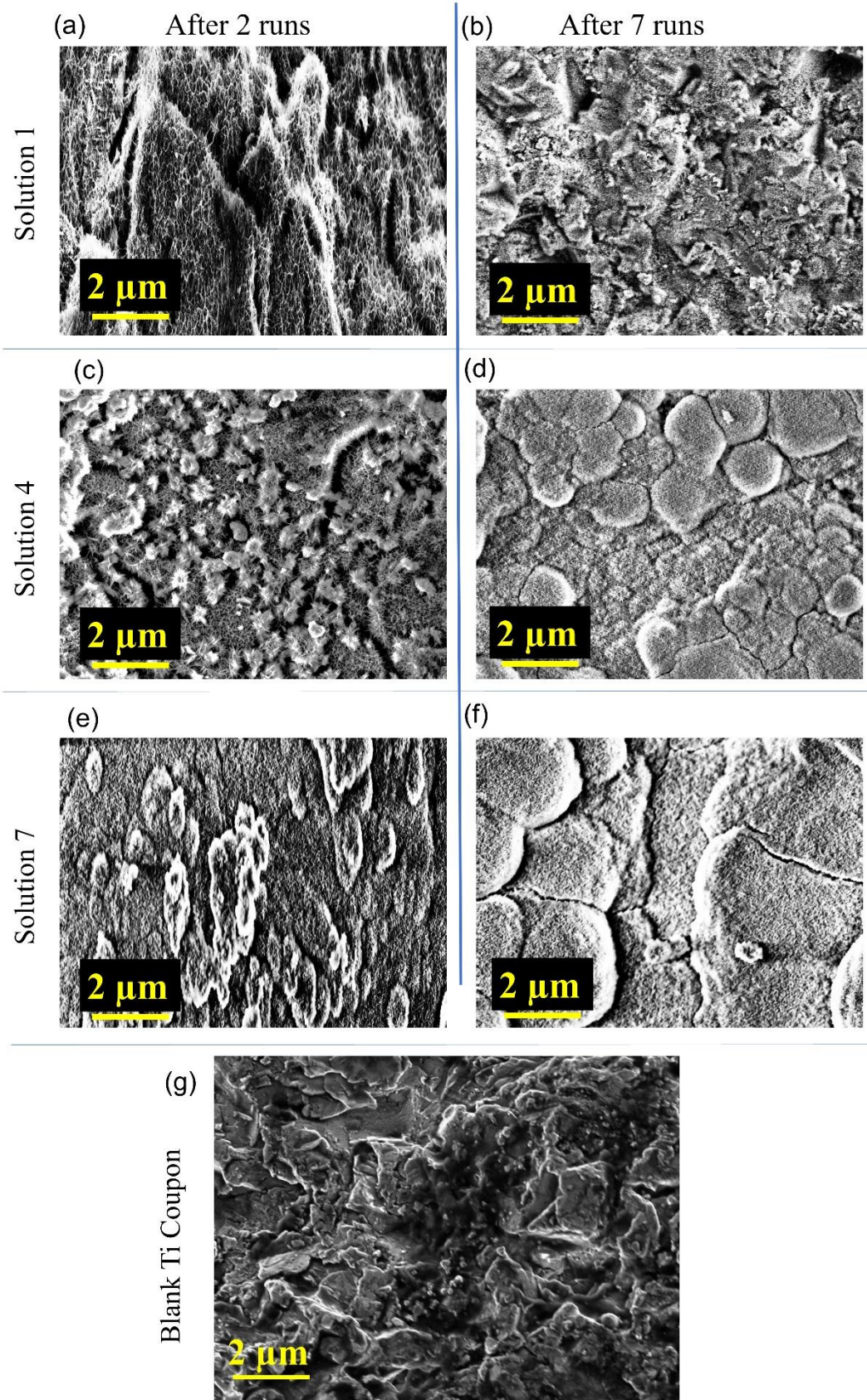


Figure 2.4: Scanning electron micrograph images of hydroxyapatite mineral formed on Ti-6AL-4V alloy. (a) image of the mineral deposited using solution 1 after 2 process runs, (b) image of the mineral deposited using solution 1 after 7

process runs, (c) image of the mineral deposited using solution 4 after 2 process runs, (d) image of the mineral deposited using solution 4 after 7 process runs, (e) image of the mineral deposited using solution 7 after 2 process runs, (f) image of the mineral deposited using solution 7 after 7 process runs and (g) Scanning Electron Microscope (SEM) images of titanium alloy coupons after basic activation. Image recorded using a Zeiss Ultra Plus system with the accelerating voltage of 5 kV, at a working distance of 7.8mm and an in-lens detector.

EDX analysis enhanced SEM observations. Lower titanium signals indicated higher HA coverage, and it can be seen in **Figure 2.5(a)** that the more concentrated solutions 5-7 show < 5 at.% titanium after just 2 process runs but at lower concentration the HA layers are thinner. Solution 7 had no titanium detection at all post-7 process runs. Calcium and phosphorus signals are minimal for solutions 1 and 2, solutions 3 and 4 show clear increases in these elements with process runs, while solutions 5-7 show greater than 12 at.% Ca and 10 at.% P following two process runs, **Figure 2.5(b-c)**. Oxygen is 50-60 at.% for all samples consistent with the presence of oxide containing phases, **Figure 2.5(d)**. Surface-bound carbon is universally observed across all samples, a typical occurrence with hydroxyapatite (HA) due to its well-known adsorption properties. [56] Notably, the carbon content exhibits an upward trend with increasing solution concentration, attributed to the greater availability of apatitic minerals for adsorption, as illustrated in **Figure 2.5(e)**. **Figure 2.5(f)** shows the NaCl content of the films. The NaCl concentration is small for all samples regardless of the ionic strength (Na at.% < 2.5 % and Cl at.% < 2 %) consistent with expectations because of its high solubility. It is clear from these data that the NaCl only acts to increase the ionic concentration and improve the availability of other ions for the precipitation process.

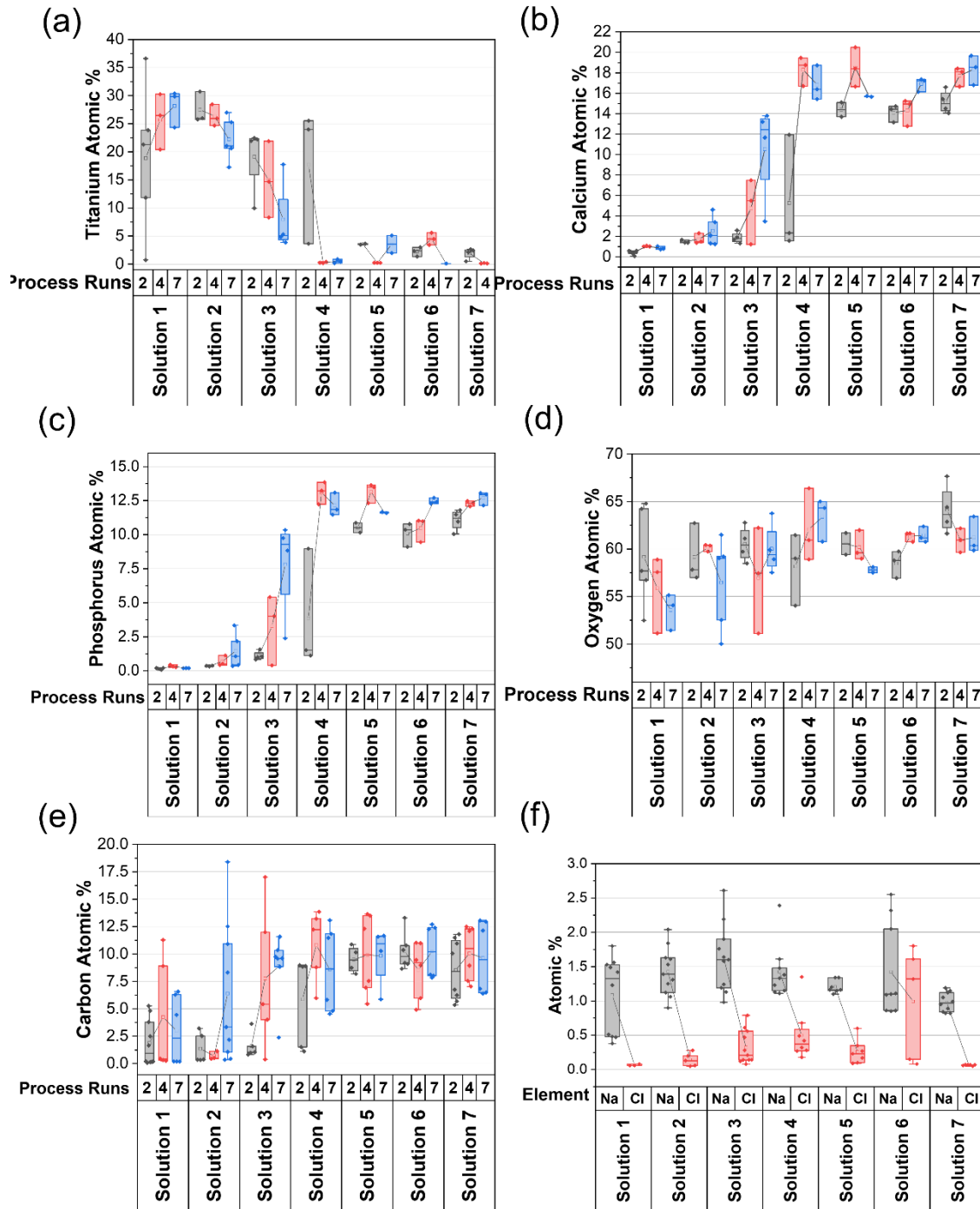


Figure 2.5: Energy-dispersive X-ray spectroscopy (EDX) spectra of deposited films recording various elements pertinent to hydroxyapatite deposition. All data points are the mean of 3 areas within a sample, grouped on the x-axis by solution ID: 1-7 and number of processes runs complete for each film (2,4 or7). (a: titanium atomic %, b: calcium atomic %, c: phosphorus atomic %, d: oxygen atomic %, e: carbon atomic %, f: sodium and chlorine atomic %).

It was possible to quantify the amount of film deposited from the weight of samples after each process run, **Figure 2.6(a)**. This data is the mean of the mass

added after every run per solution. Mass uptake for solutions 1 and 2 is minimal. There is a linear trend of mass uptake per run with increasing concentration. Solutions 4-7 have upwards of 1 mg per run with solution 7 having 4 mg of film attachment per run.

The calcium to phosphate at.% ratio (Ca/P), along with the oxygen at.% are widely used to identify hydroxyapatite phases, see **Table 2.2** with data for the relevant phases listed. [57,58] From **Figure 2.6(b)** it is seen there is generally a decrease of the Ca/P ratio as the number of process runs increases (where deposition is significant: solutions 3-7). Solutions 1 or 2 show the highest Ca/P ratios, and the data suggest that calcium attachment is preferential in the preliminary stages of film development (nucleation), and this is consistent with the substrate having negatively charged hydroxyl groups that attract Ca^{2+} from solution. For solution 1 and 2 there are not enough available ions to form TCP or OCP mineral as per **equations 1** and **2**. After 2 process runs both solutions 3 and 4 show a higher Ca/P aligning with **equation 2** since a TCP content would increase the Ca/P. As deposition progresses (4,7 runs) the OCP phase dominates, **Figure 2.6(b)**. **Figure 2.6(b)** shows that solutions 3-7 are very closely aligned near the level of OCP in terms of Ca/P after 7 runs. Solutions 3-7 however, have an Oxygen at.% > 40% implying that there is ACP present also since ACP can have a flexible oxygen at.%.

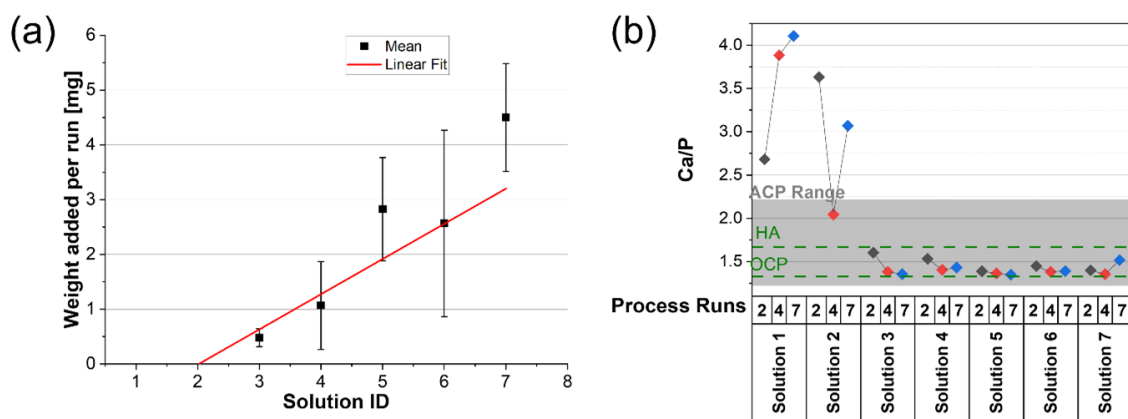


Figure 2.6: (a) graph of weight added per run in mg versus solution ID and (b) the calcium to phosphate ratio (Ca/P) of films calculated for each solution after 2,4, and 7 process runs.

Table 2.2: Tabular data of hydroxyapatite phases; their acronym, mineral name, stoichiometric formula, calcium to phosphate ratio (Ca/P) and stoichiometric atomic percentage of oxygen[59].

Acronym	Mineral	Formula	Ca/P	Atomic % Oxygen
HA	Hydroxyapatite	$\text{Ca}_{10}(\text{PO}_4)_6(\text{OH})_2$	1.67	34.9
ACP	Amorphous calcium phosphate	$\text{Ca}_x\text{H}_y(\text{PO}_4)_z \cdot n\text{H}_2\text{O}$	1.2–2.2	flexible
OCP	Octacalcium phosphate	$\text{Ca}_8\text{H}_2(\text{PO}_4)_6 \cdot 5\text{H}_2\text{O}$	1.33	39.7
TCP	Tricalcium phosphate	$\text{Ca}_3(\text{PO}_4)_2$	1.5	41.3
CDHA	Calcium deficient hydroxyapatite	$\text{Ca}_9(\text{HPO}_4)(\text{PO}_4)_5\text{OH}$	1.5	43.13

When considered together these data sets reveal that solutions 1 and 2 had minimal apatite film attachment across all process runs, implying that their concentration and ionic strength are too low. Solutions 3 and 4 showed slower apatite film growth kinetics but the most adhered layer with a measurable mg of material added per run. Solutions 3 and 4 also showed the best morphological development after 7 process runs, mirrored through EDX data of the relevant elements at 2, 4 and 7 process runs. Compared to other studies this morphology and phase composition are advantageous since the presence of TCP can accelerate coating degradation whereas the mix of ACP and OCP allows for ease of integration and the structure encourages bone growth. [60,61] Solutions 5, 6 and 7 had large-scale apatite film attachment after only 2 process runs but morphologically showed some cracks emerging after 7 process runs with material having fewer interconnecting needles and pores. Solutions 6 and 7 also exhibit high carbonate content coincident to HA-based material. The chemical composition of HA film from solutions 3-7 was matched at 7 process runs indicating an OCP crystalline phase with ACP material also. It is clear from this data that by altering the concentration and ionic strength of solutions, it is possible

to expediate or remediate HA growth. However, growth follows the same nucleation and growth mechanism. Further detailed investigation of the crystallinity of HA phases is conducted in the next chapter including XRD analysis after various process runs to identify the growth mechanism of OCP, HA and ACP as they emerge from this solution process.

2.4. Conclusion

This study has shown HA film can be deposited and controlled using a colloidal solution process. The repeatability of the process at 47 °C is confirmed through consistent dropping of pH in 30min runs. Calcium ions bonding to the substrate lead to pH drop, as explained in the proposed chemical pathway. DLS data shows various particle sizes in solutions, with ~100 nm particles preferred for porous and coherent films (because of the denser packing). SEM topography showed that the various solutions used gave rise to a morphologically porous and chemically consistent HA coating. Solution concentration influences film thickness, coverage, and coating rate, with NaCl having no role in HA bonding. Lower concentration solutions formed very thin films, with calcium and phosphate content being <5 at.% after 7 deposition runs. While some films contained carbonates at higher concentrations, all films had similar oxygen content. Where HA film was formed at >1 mg per run, there is a strong indication that the phase of HA formed is consistent to all solutions. Ca/P ratio data strongly indicated the OCP phase, and an oxygen atomic percentage additionally indicated the presence of water and ACP. This HA phase lines up with the proposed nucleation and growth pathway from **Equations 2,3,4 and 5**.

The optimal process solution is between solution 3 and 4 based off the data shown. Solutions 3 and 4 very clearly followed the proposed chemical nucleation and growth. The advantage of this slower crystal growth allows for excellent porosity and morphology to be seen at SEM, and through photography the adhesion of the layer can be conveniently ratified.

Overall, this body of work had outlined that colloidal solutions can be used as a novel HA coating process whereby crystallisation happens in a timely manner at low temperatures.

2.5 Appendix Chapter 2

Appendix 2.5.1. Molarity and Solubility of Chemicals Used.

Table A2.1: List of Reagents used and their exact CAS number, the molarity (and molarity tolerance) to which they were included in the concentrates, and their water solubility at 20°C.

Reagent	Molarity (mM)	Molarity tolerance	Water Solubility at 20°C
KH_2PO_4 CAS# 7778-77-0	40	0.015	222 g/L
TRIS = $(\text{HOCH}_2)_3\text{CNH}_2$ CAS# 77-86-1	157.16	2	678 g/L
NaCl CAS# 7647-14-5	4683	0.02	317 g/L
$\text{Ca}(\text{NO}_3)_2 \cdot 4\text{H}_2\text{O}$ CAS# 13477-34-4	36.364	0.015	1,293 g/L

Appendix 2.5.2 Brief explanation behind allowing HA samples to Dry in ambient conditions.

Studies were run whereby HA films were deposited onto a functionalised Quartz Crystal microbalance, the change in dissipation of this crystal represents a phase change. Dissipation data was collected through the deposition runs (30 min/1800 s) and up to 35 minutes afterwards (4000 s) and it became clear that the HA film dehydrated 15mins post process run (2700s on the below graph). On this graph there is a sharp peak after 15 min which represents dehydration of the layer.

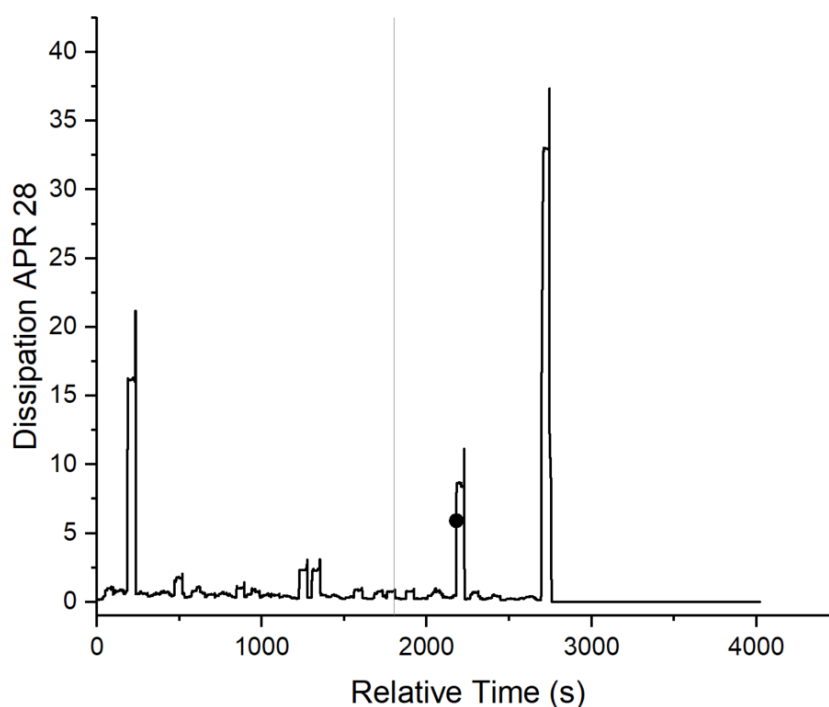


Figure A2.1: Dissipation versus relative time of a quartz crystal microbalance which has undergone HA deposition, the data shows the sample gathering HA film growth through this colloidal solution process (up to 1800s) and afterwards during drying.

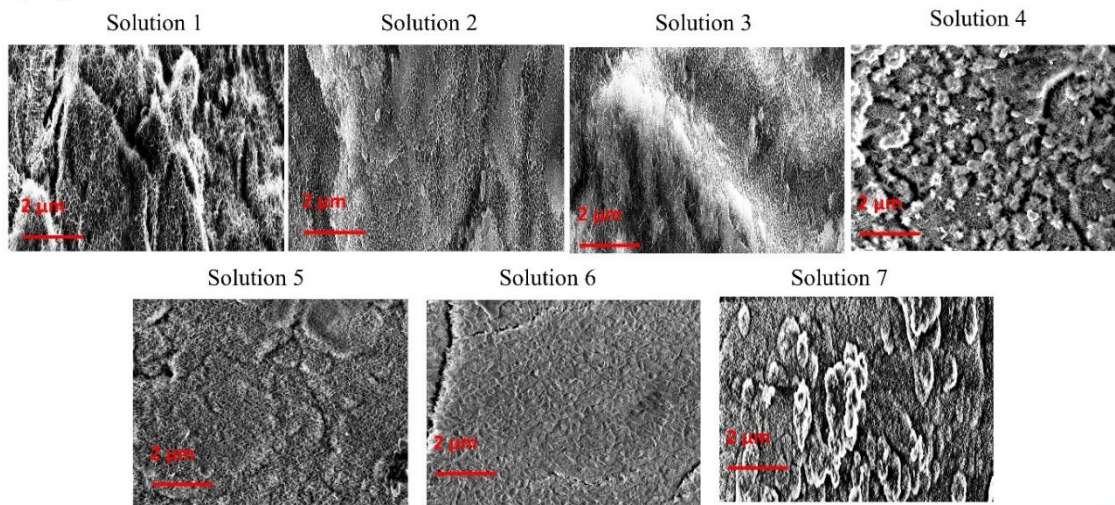
Further to this, studies were conducted whereby Ha was deposited onto substrates without letting them dry at all, only rinsing and refilling in between 30 min process runs. Using solution 3 gave the following weights for 6 samples. When analysed this data reflects a 40% decrease in film growth versus what it could be if parts were allowed to dry in ambient conditions for 15 min. There is no error included in this data since just 7 individual coupons were ran.

Table A2.2: Weight recorded for titanium coupons that were subject to HA deposition without allowing them to dry in between process runs.

Coupon	Before (g)	After 7 Runs (g)	Weight Added (g)
1	7.17	7.1239	-0.0461
2	7.0901	7.0976	0.0075
3	6.9931	6.9999	0.0068
4	6.9649	6.9715	0.0066
5	7.0269	7.0329	0.006
6	6.971	6.9766	0.0056

Appendix 2.5.3 Supplemental SEM Images

(2a)



(2b)

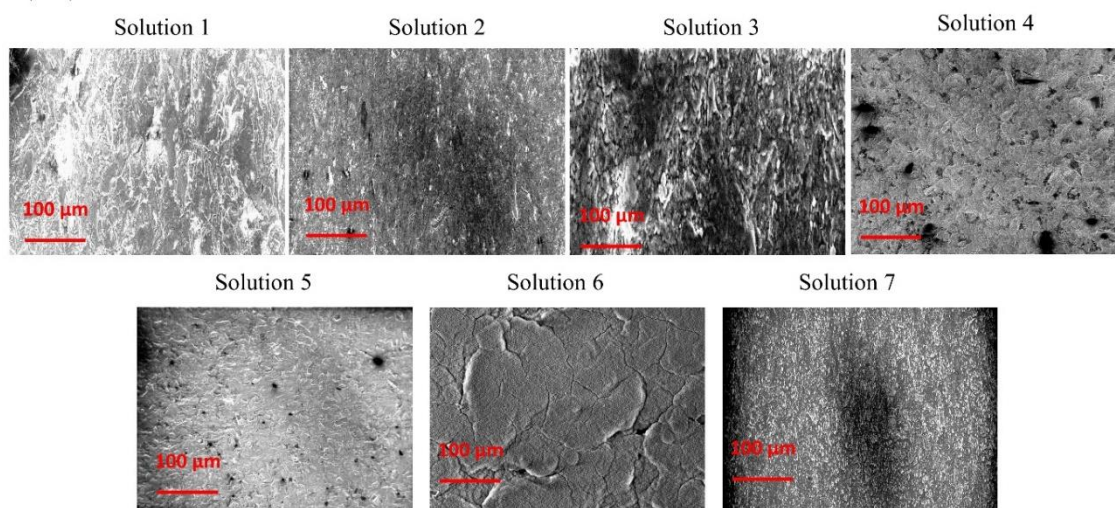


Figure A2.2: Scanning Electron Microscope (SEM) images of hydroxyapatite film on titanium alloy coupons after 2 hydroxyapatite solution deposition runs using Solutions 1-7. Images are recorded using a Zeiss Ultra Plus system with the accelerating voltage of 5 kV, at a working distance between 3 to 10 mm and an in-lens detector or secondary electron detector. 1a: SEM images with a scale bar of 2 μm to show nature of the porous film. 1b: SEM images with a scale bar of 100 μm to show overall sample coverage.

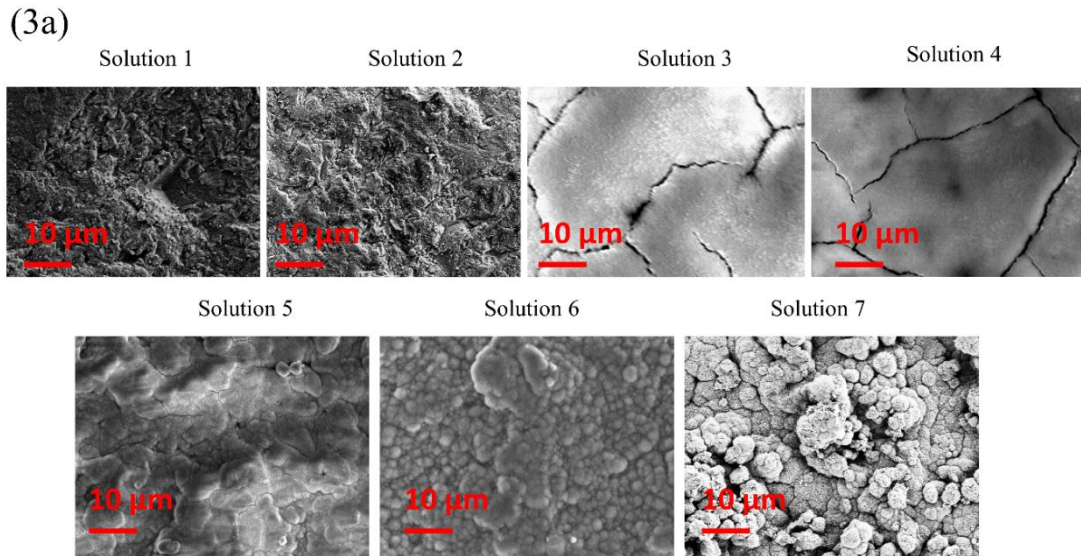


Figure A2.3: Scanning Electron Microscope (SEM) images of hydroxyapatite film on titanium alloy coupons after 4 hydroxyapatite solution deposition runs using Solutions 1-7. Images are recorded using a Zeiss Ultra Plus system with the accelerating voltage of 5 kV, at a working distance between 3 to 10 mm and an in-lens detector or secondary electron detector, all images have a 10 μ m scale bar.

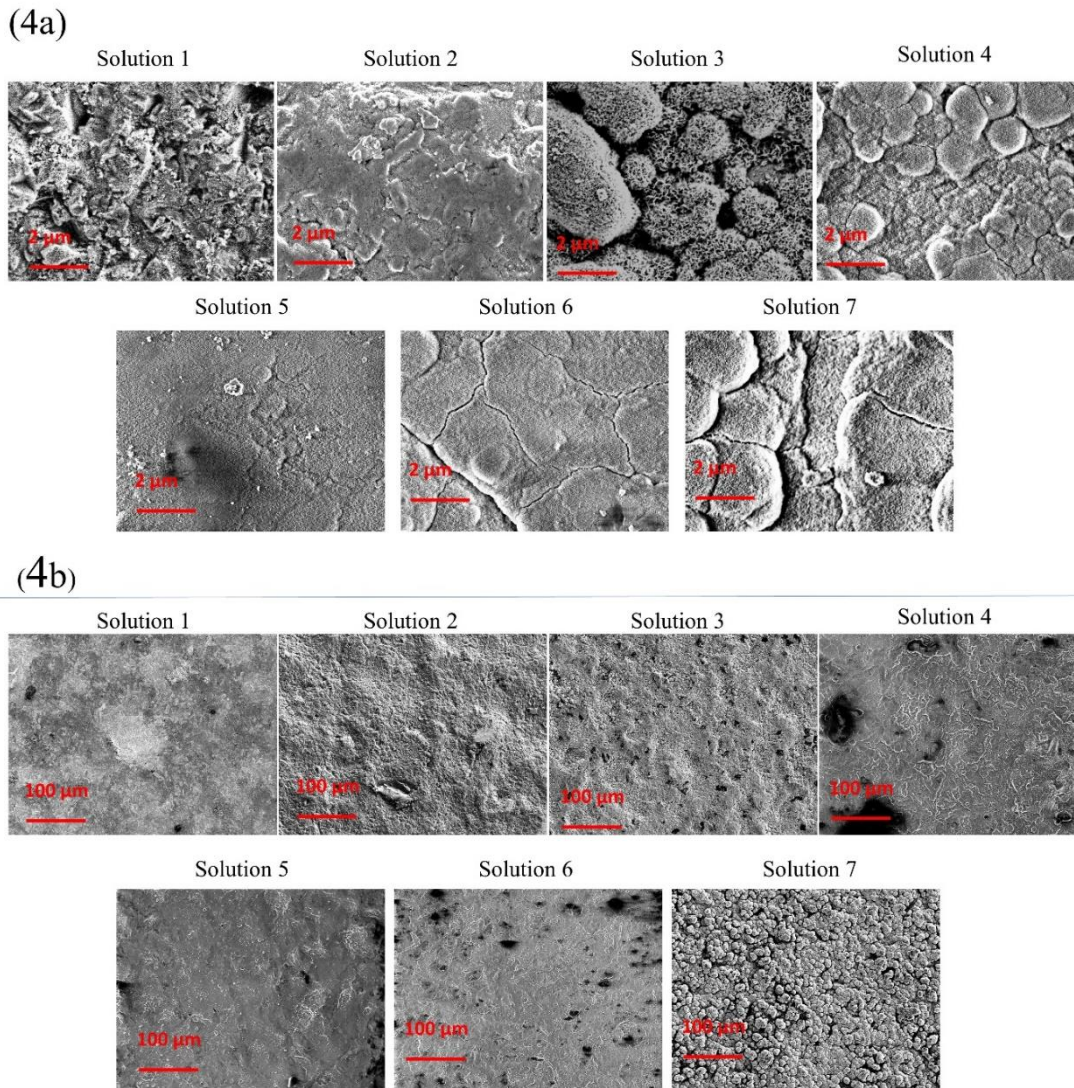


Figure A2.4: Scanning Electron Microscope (SEM) images of hydroxyapatite film on titanium alloy coupons after 7 hydroxyapatite solution deposition runs using Solutions 1-7. Images are recorded using a Zeiss Ultra Plus system with the accelerating voltage of 5 kV, at a working distance between 3 to 10 mm and an in-lens detector or secondary electron detector. 1a: SEM images with a scale bar of 2 μ m to show nature of the porous film. 1b: SEM images with a scale bar of 100 μ m to show overall sample coverage.

2.6 References

- [1] N. Noskovicova, B. Hinz, and P. Pakshir, "Implant Fibrosis and the Underappreciated Role of Myofibroblasts in the Foreign Body Reaction," *Cells*, vol. 10, no. 7, p. 1794, Jul. 2021, doi: 10.3390/cells10071794.
- [2] G. Szczęśny, M. Kopec, D. J. Politis, Z. L. Kowalewski, A. Łazarski, and T. Szolc, "A Review on Biomaterials for Orthopaedic Surgery and Traumatology: From Past to Present," *Materials*, vol. 15, no. 10, Art. no. 10, Jan. 2022, doi: 10.3390/ma15103622.

- [3] M. Kaur and K. Singh, "Review on titanium and titanium based alloys as biomaterials for orthopaedic applications," *Materials Science and Engineering: C*, vol. 102, pp. 844–862, Sep. 2019, doi: 10.1016/j.msec.2019.04.064.
- [4] U. Filipović, R. G. Dahmane, S. Ghannouchi, A. Zore, and K. Bohinc, "Bacterial adhesion on orthopedic implants," *Advances in Colloid and Interface Science*, vol. 283, p. 102228, Sep. 2020, doi: 10.1016/j.cis.2020.102228.
- [5] N. Walter, T. Stich, D. Docheva, V. Alt, and M. Rupp, "Evolution of implants and advancements for osseointegration: A narrative review," *Injury*, vol. 53, pp. S69–S73, Nov. 2022, doi: 10.1016/j.injury.2022.05.057.
- [6] A. Bandyopadhyay, I. Mitra, S. B. Goodman, M. Kumar, and S. Bose, "Improving biocompatibility for next generation of metallic implants," *Progress in Materials Science*, vol. 133, p. 101053, Mar. 2023, doi: 10.1016/j.pmatsci.2022.101053.
- [7] A. Kothari, R. A. Razdan, R. Jain, V. Patel, N. Parihar, and D. Pandey, "Role of Hydroxyapatite (HA) Coatings in Implants: A Review," *UNIVERSITY JOURNAL OF DENTAL SCIENCES*, vol. 8, no. 4, Jul. 2022, doi: 10.21276/ujds.2022.8.4.21.
- [8] T. Horváth *et al.*, "Hydroxyapatite-coated implants provide better fixation in total knee arthroplasty. A meta-analysis of randomized controlled trials," *PLOS ONE*, vol. 15, no. 5, p. e0232378, May 2020, doi: 10.1371/journal.pone.0232378.
- [9] J. Jiang, G. Han, X. Zheng, G. Chen, and P. Zhu, "Characterization and biocompatibility study of hydroxyapatite coating on the surface of titanium alloy," *Surface and Coatings Technology*, vol. 375, pp. 645–651, Oct. 2019, doi: 10.1016/j.surfcoat.2019.07.067.
- [10] S. U. Zaman, M. Irfan, M. Irfan, M. K. U. Zaman, and N. Muhammad, "Overview of hydroxyapatite; composition, structure, synthesis methods and its biomedical uses," vol. 6, pp. 84–99, Jun. 2020.
- [11] J. Litak *et al.*, "Hydroxyapatite Use in Spine Surgery—Molecular and Clinical Aspect," *Materials*, vol. 15, no. 8, Art. no. 8, Jan. 2022, doi: 10.3390/ma15082906.
- [12] M. U. Munir, S. Salman, A. Ihsan, and T. Elsaman, "Synthesis, Characterization, Functionalization and Bio-Applications of Hydroxyapatite Nanomaterials: An Overview," *International Journal of Nanomedicine*, vol. 17, pp. 1903–1925, Dec. 2022, doi: 10.2147/IJN.S360670.
- [13] V. G. DileepKumar *et al.*, "A review on the synthesis and properties of hydroxyapatite for biomedical applications," *Journal of Biomaterials Science, Polymer Edition*, vol. 33, no. 2, pp. 229–261, Jan. 2022, doi: 10.1080/09205063.2021.1980985.
- [14] X. Ge *et al.*, "Cicada-inspired fluoridated hydroxyapatite nanostructured surfaces synthesized by electrochemical additive manufacturing," *Materials & Design*, vol. 193, p. 108790, Aug. 2020, doi: 10.1016/j.matdes.2020.108790.
- [15] S. Lamkhao *et al.*, "Synthesis of Hydroxyapatite with Antibacterial Properties Using a Microwave-Assisted Combustion Method," *Sci Rep*, vol. 9, no. 1, Art. no. 1, Mar. 2019, doi: 10.1038/s41598-019-40488-8.
- [16] J. Gil *et al.*, "Mineralization of Titanium Surfaces: Biomimetic Implants," *Materials*, vol. 14, no. 11, Art. no. 11, Jan. 2021, doi: 10.3390/ma14112879.
- [17] A. K. Riau, S. S. Venkatraman, and J. S. Mehta, "Biomimetic vs. Direct Approach to Deposit Hydroxyapatite on the Surface of Low Melting Point Polymers for Tissue Engineering," *Nanomaterials*, vol. 10, no. 11, Art. no. 11, Nov. 2020, doi: 10.3390/nano10112162.
- [18] C. Huang *et al.*, "Biomimetic composite scaffold from an in situ hydroxyapatite coating on cellulose nanocrystals," *RSC Advances*, vol. 9, no. 10, pp. 5786–5793, 2019, doi: 10.1039/C8RA09523J.
- [19] J. Jiang, W. Liu, Z. Xiong, Y. Hu, and J. Xiao, "Effects of biomimetic hydroxyapatite coatings on osteoimmunomodulation," *Biomaterials Advances*, vol. 134, p. 112640, Mar. 2022, doi: 10.1016/j.msec.2021.112640.

- [20] B. Murphy, J. Baez, and M. A. Morris, "Characterising Hydroxyapatite Deposited from Solution onto Novel Substrates: Growth Mechanism and Physical Properties," *Nanomaterials*, vol. 13, no. 17, Art. no. 17, Jan. 2023, doi: 10.3390/nano13172483.
- [21] S. György *et al.*, "Effect of the reaction temperature on the morphology of nanosized HAp," *J Therm Anal Calorim*, vol. 138, no. 1, pp. 145–151, Oct. 2019, doi: 10.1007/s10973-019-08255-z.
- [22] B. A. Correa-Piña, O. M. Gomez-Vazquez, S. M. Londoño-Restrepo, L. F. Zubieta-Otero, B. M. Millan-Malo, and M. E. Rodriguez-García, "Synthesis and characterization of nano-hydroxyapatite added with magnesium obtained by wet chemical precipitation," *Progress in Natural Science: Materials International*, vol. 31, no. 4, pp. 575–582, Aug. 2021, doi: 10.1016/j.pnsc.2021.06.006.
- [23] M. Bin Mobarak *et al.*, "Probing the photocatalytic competency of hydroxyapatite synthesized by solid state and wet chemical precipitation method," *Journal of Molecular Structure*, vol. 1252, p. 132142, Mar. 2022, doi: 10.1016/j.molstruc.2021.132142.
- [24] N. A. S. Mohd Pu'ad, J. Alipal, H. Z. Abdullah, M. I. Idris, and T. C. Lee, "Synthesis of eggshell derived hydroxyapatite via chemical precipitation and calcination method," *Materials Today: Proceedings*, vol. 42, pp. 172–177, Jan. 2021, doi: 10.1016/j.matpr.2020.11.276.
- [25] O. M. Gomez-Vazquez, B. A. Correa-Piña, L. F. Zubieta-Otero, A. M. Castillo-Paz, S. M. Londoño-Restrepo, and M. E. Rodriguez-García, "Synthesis and characterization of bioinspired nano-hydroxyapatite by wet chemical precipitation," *Ceramics International*, vol. 47, no. 23, pp. 32775–32785, Dec. 2021, doi: 10.1016/j.ceramint.2021.08.174.
- [26] J. A. Stammeier, B. Purgstaller, D. Hippler, V. Mavromatis, and M. Dietzel, "In-situ Raman spectroscopy of amorphous calcium phosphate to crystalline hydroxyapatite transformation," *MethodsX*, vol. 5, pp. 1241–1250, 2018, doi: 10.1016/j.mex.2018.09.015.
- [27] D. J. Patty, A. D. Nugraheni, I. Dewi Ana, and Y. Yusuf, "Mechanical Characteristics and Bioactivity of Nanocomposite Hydroxyapatite/Collagen Coated Titanium for Bone Tissue Engineering," *Bioengineering*, vol. 9, no. 12, Art. no. 12, Dec. 2022, doi: 10.3390/bioengineering9120784.
- [28] B. Beig, U. Liaqat, M. F. K. Niazi, I. Douna, M. Zahoor, and M. B. K. Niazi, "Current Challenges and Innovative Developments in Hydroxyapatite-Based Coatings on Metallic Materials for Bone Implantation: A Review," *Coatings*, vol. 10, no. 12, p. 1249, Dec. 2020, doi: 10.3390/coatings10121249.
- [29] S. Awasthi, S. K. Pandey, E. Arunan, and C. Srivastava, "A review on hydroxyapatite coatings for the biomedical applications: experimental and theoretical perspectives," *J. Mater. Chem. B*, vol. 9, no. 2, pp. 228–249, Jan. 2021, doi: 10.1039/D0TB02407D.
- [30] S. Jiang, Y. Cao, S. Li, Y. Pang, and Z. Sun, "Dual function of poly(acrylic acid) on controlling amorphous mediated hydroxyapatite crystallization," *Journal of Crystal Growth*, vol. 557, p. 125991, Mar. 2021, doi: 10.1016/j.jcrysgro.2020.125991.
- [31] A. S. Posner, "Crystal chemistry of bone mineral," *Physiological Reviews*, vol. 49, no. 4, pp. 760–792, Oct. 1969, doi: 10.1152/physrev.1969.49.4.760.
- [32] A. S. Posner, A. Perloff, and A. F. Diorio, "Refinement of the hydroxyapatite structure," *Acta Cryst*, vol. 11, no. 4, Art. no. 4, Apr. 1958, doi: 10.1107/S0365110X58000815.
- [33] R. A. Harper and A. S. Posner, "Measurement of Non-Crystalline Calcium Phosphate in Bone Mineral.," *Proceedings of the Society for Experimental Biology and Medicine*, vol. 122, no. 1, pp. 137–142, May 1966, doi: 10.3181/00379727-122-31073.
- [34] B. Jin, C. Shao, Y. Wang, Z. Mu, Z. Liu, and R. Tang, "Anisotropic Epitaxial Behavior in the Amorphous Phase-Mediated Hydroxyapatite Crystallization Process: A New Understanding of Orientation Control," *J. Phys. Chem. Lett.*, vol. 10, no. 24, pp. 7611–7616, Dec. 2019, doi: 10.1021/acs.jpcclett.9b03109.
- [35] K. He *et al.*, "Revealing nanoscale mineralization pathways of hydroxyapatite using in situ liquid cell transmission electron microscopy," *Science Advances*, vol. 6, no. 47, p. eaaz7524, Nov. 2020, doi: 10.1126/sciadv.aaz7524.

- [36] L. Degli Esposti and M. Iafisco, "Amorphous calcium phosphate, the lack of order is an abundance of possibilities," *Biomaterials and Biosystems*, vol. 5, p. 100037, Mar. 2022, doi: 10.1016/j.bbiosy.2021.100037.
- [37] G. R. Sauer, W. B. Zunic, J. R. Durig, and R. E. Wuthier, "Fourier transform raman spectroscopy of synthetic and biological calcium phosphates," *Calcif Tissue Int*, vol. 54, no. 5, pp. 414–420, May 1994, doi: 10.1007/BF00305529.
- [38] A. Evcin and B. Buyukleblebici, "Ti6Al4V coating with B₂O₃ and Al₂O₃ containing hydroxyapatite by HVOF technique," *Scientia Iranica*, vol. 26, no. 3, pp. 1980–1989, Jun. 2019, doi: 10.24200/sci.2019.50994.1958.
- [39] S. F. Robertson, A. Bandyopadhyay, and S. Bose, "Titania nanotube interface to increase adhesion strength of hydroxyapatite sol-gel coatings on Ti-6Al-4V for orthopedic applications," *Surface and Coatings Technology*, vol. 372, pp. 140–147, Aug. 2019, doi: 10.1016/j.surfcoat.2019.04.071.
- [40] M. Lu *et al.*, "Electrochemical Deposition of Nanostructured Hydroxyapatite Coating on Titanium with Enhanced Early Stage Osteogenic Activity and Osseointegration," *International Journal of Nanomedicine*, vol. 15, pp. 6605–6618, Dec. 2020, doi: 10.2147/IJN.S268372.
- [41] M. Sawada, K. Sridhar, Y. Kanda, and S. Yamanaka, "Pure hydroxyapatite synthesis originating from amorphous calcium carbonate," *Sci Rep*, vol. 11, no. 1, Art. no. 1, Jun. 2021, doi: 10.1038/s41598-021-91064-y.
- [42] I. Roohani, S. Cheong, and A. Wang, "How to build a bone? - Hydroxyapatite or Posner's clusters as bone minerals," *Open Ceramics*, vol. 6, p. 100092, Jun. 2021, doi: 10.1016/j.oceram.2021.100092.
- [43] J. J. De Yoreo, "Casting a bright light on Ostwald's rule of stages," *Proc Natl Acad Sci U S A*, vol. 119, no. 7, p. e2121661119, Feb. 2022, doi: 10.1073/pnas.2121661119.
- [44] N. N. Andrusova, E. S. Zhavoronok, O. A. Legon'kova, A. S. Goncharova, and S. A. Kedik, "Polymer–Mineral Compounds for Cementless Hip Replacement," *Polym. Sci. Ser. D*, vol. 13, no. 1, pp. 68–72, Jan. 2020, doi: 10.1134/S1995421220010037.
- [45] T. Moskalewicz, M. Warcaba, Ł. Cieniek, M. Sitarz, M. Gajewska, and A. R. Boccaccini, "Hydroxyapatite/sodium alginate coatings electrophoretically deposited on titanium substrates: microstructure and properties," *Applied Surface Science*, vol. 540, p. 148353, Feb. 2021, doi: 10.1016/j.apsusc.2020.148353.
- [46] O. Janson *et al.*, "Titanium surface modification to enhance antibacterial and bioactive properties while retaining biocompatibility," *Materials Science and Engineering: C*, vol. 96, pp. 272–279, Mar. 2019, doi: 10.1016/j.msec.2018.11.021.
- [47] J. Zheng, L. Chen, D. Chen, C. Shao, M. Yi, and B. Zhang, "Effects of pore size and porosity of surface-modified porous titanium implants on bone tissue ingrowth," *Transactions of Nonferrous Metals Society of China*, vol. 29, no. 12, pp. 2534–2545, Dec. 2019, doi: 10.1016/S1003-6326(19)65161-7.
- [48] K.-W. Jung, S. Y. Lee, J.-W. Choi, and Y. J. Lee, "A facile one-pot hydrothermal synthesis of hydroxyapatite/biochar nanocomposites: Adsorption behavior and mechanisms for the removal of copper(II) from aqueous media," *Chemical Engineering Journal*, vol. 369, pp. 529–541, Aug. 2019, doi: 10.1016/j.cej.2019.03.102.
- [49] A. Ribeiro, Y. A. Manrique, M. F. Barreiro, J. C. B. Lopes, and M. M. Dias, "Effect of temperature, pH and ionic strength on hydroxyapatite stabilised Pickering emulsions produced in batch and continuous mode," *Food Biophysics*, vol. 17, no. 3, pp. 422–436, Sep. 2022, doi: 10.1007/s11483-022-09732-z.
- [50] O. V. Frank-Kamenetskaya, D. Y. Vlasov, E. G. Panova, and S. N. Lessovaia, *Processes and Phenomena on the Boundary Between Biogenic and Abiogenic Nature*. Springer Nature, 2019.
- [51] A. Prihanto, S. Muryanto, R. Ismail, J. Jamari, and A. P. Bayuseno, "Hydrothermal Production of Nanoparticles, Thermostable Hydroxyapatite with Varying Ph and Temperatures." Rochester, NY, Mar. 23, 2022. doi: 10.2139/ssrn.4050023.

- [52] J. Kim, S. kim, and I. song, "Octacalcium phosphate, a promising bone substitute material: a narrative review," *JYMS*, May 2023, doi: 10.12701/jyms.2023.00010.
- [53] F. Bakan, "A Systematic Study of the Effect of pH on the Initialization of Ca-deficient Hydroxyapatite to β -TCP Nanoparticles," *Materials (Basel)*, vol. 12, no. 3, Jan. 2019, doi: 10.3390/ma12030354.
- [54] M. Nakhaei, N. Jirofti, M. H. Ebrahimzadeh, and A. Moradi, "Different methods of hydroxyapatite-based coatings on external fixator pin with high adhesion approach," *Plasma Processes and Polymers*, vol. 20, no. 6, p. e2200219, 2023, doi: 10.1002/ppap.202200219.
- [55] J. Botterill and H. Khatkar, "The role of hydroxyapatite coating in joint replacement surgery – Key considerations," *Journal of Clinical Orthopaedics and Trauma*, vol. 29, p. 101874, Jun. 2022, doi: 10.1016/j.jcot.2022.101874.
- [56] M. Ibrahim, M. Labaki, J.-M. Giraudon, and J.-F. Lamonier, "Hydroxyapatite, a multifunctional material for air, water and soil pollution control: A review," *Journal of Hazardous Materials*, vol. 383, p. 121139, Feb. 2020, doi: 10.1016/j.jhazmat.2019.121139.
- [57] Z. Yuan *et al.*, "A novel synthesis method and properties of calcium-deficient hydroxyapatite/ α -TCP biphasic calcium phosphate," *J Biomater Appl*, vol. 36, no. 9, pp. 1712–1719, Apr. 2022, doi: 10.1177/08853282211068597.
- [58] V. Bystrov, E. Paramonova, L. Avakyan, J. Coutinho, and N. Bulina, "Simulation and Computer Study of Structures and Physical Properties of Hydroxyapatite with Various Defects," *Nanomaterials*, vol. 11, no. 10, Art. no. 10, Oct. 2021, doi: 10.3390/nano11102752.
- [59] L. Deng and B. R. Dhar, "Phosphorus recovery from wastewater via calcium phosphate precipitation: A critical review of methods, progress, and insights," *Chemosphere*, vol. 330, p. 138685, Jul. 2023, doi: 10.1016/j.chemosphere.2023.138685.
- [60] A. M. Vilardell *et al.*, "In-vitro comparison of hydroxyapatite coatings obtained by cold spray and conventional thermal spray technologies," *Materials Science and Engineering: C*, vol. 107, p. 110306, Feb. 2020, doi: 10.1016/j.msec.2019.110306.
- [61] Y. Su, K. Li, F. Tielens, and J. Wang, "Effect of sprayed techniques on the surface microstructure and in vitro behavior of nano-HAp coatings," *Materials Science and Engineering: C*, vol. 117, p. 111318, Dec. 2020, doi: 10.1016/j.msec.2020.111318.

Chapter 3: Development of hydroxyapatite coatings for orthopaedic implants from colloidal solutions, Part 2: detailed characterisation of the coatings and their growth mechanism

Abstract

This chapter is the second part of a two-part study whereby supersaturated solutions of calcium and phosphate ions generate well-defined hydroxyapatite coatings for orthopaedic implants. An 'ideal' process solution is selected from Chapter 2 and detailed characterisation of films produced from this solution is undertaken here in Chapter 3.

Analysis is presented on the hydroxyapatite produced, in both powder form and as a film upon titanium substrates representative of orthopaedic implants. From thermal analysis data it is shown that there is chemically bound, and interstitial water present in the hydroxyapatite. Nuclear magnetic resonance data allows for the distinction between an amorphous and a crystalline component of the material. As hydroxyapatite coatings are generated, their growth mechanism is tracked across repeated process runs. Clear understanding of the growth mechanism is achieved through crystallinity and electron imaging data. Transmission electron imaging data supports the proposed crystal growth and deposition mechanism. The data concludes that this process has a clear propensity to grow the hydroxyapatite phase of octacalcium phosphate.

The investigation of the hydroxyapatite coating and its growth mechanism establishes that a stable and reproducible process window has been identified. Precise control is achieved, leading to successful formation of desired hydroxyapatite films.

3.1 Introduction

The coating of metal titanium alloy implants (or other metals such as chromium cobalt) is key to improving the bodily response to a metal. As mentioned in Chapter 2 [1] of this thesis, hydroxyapatite (HA) coatings on orthopaedic implants mitigate fibrous build-up and promote implant fixation [2,3]. In Chapter 3, the

evolution of HA as it grows on a substrate and the resulting film is extensively characterised. How HA film emerges with different mechanical properties from any coating process depends on various parameters, such as temperature, pressure and process time [4–6]. Similarly, HA will grow differently based on its precursors, be they synthetic or biologically derived; for example, mammalian or shell-derived HA can have variations in particle size or phase composition [7,8]. HA film will have different crystallinity based on its substrate chemistry [9–11]. Some methods of HA coating also incur water content which requires dehydration [12,13]. The interaction between all these process parameters on the eventual film formed vary greatly by coating process.

There are many industrial techniques for HA coating, such as plasma spraying, chemical vapour deposition, electrochemical deposition, sol-gel deposition or ion assisted deposition, which can be used to form HA coatings on a surface. Within any synthetic process different calcium phosphate (Ca-P) phases can be created: amorphous calcium phosphate (ACP), α/β -tricalcium phosphate (α/β -TCP), octacalcium phosphate (OCP) or pure HA [14]. These other Ca-P phases have reabsorption and dissolution rates *in vivo* that differ from HA, thus affecting coating performance [15–19]. HA coatings must be sufficiently porous to encourage protein and mineral deposition in order to form new bone at the site [20–24].

The most common industrial HA coating techniques, plasma spraying and electrochemical deposition, have poor porosity control, poor crystalline phase control, require expensive tools (elevated temperatures or currents) and have poor coating adhesion [25]. Plasma spraying produces sub-micron needles and plates within micron-sized lamellae which allows for a porous structure [26,27]. Plasma spraying induces the less desirable α/β -TCP and relies upon post-deposition heating to crystallise the HA, which can result in low porosity [28,29]. Electrochemical HA coating deposits may sometimes suffer from defects in the coatings taking the form of certain Ca-P phases or hydrogen bubbles [30,31]. Sol-gel and biomimetic methods are commonly used in hydroxyapatite coating research [32]. Sol-gel processes can include elastic, part-polymer and ceramic composite materials which are useful to study the repair of bone cartilage [33–35]. Biomimetic processes using simulated bodily fluids have been studied as a

means to grow HA on a surface [36,37]. Sol-gel deposited HA coatings have the highest coating adhesion of all methods, whereas biomimetic HA coating is the closest in nature to the body's endogenous bone growth pathway [32,38]. Sol-gel and biomimetic processes are hindered by time-consuming steps and, in the case of biomimetic processes, rely heavily on the use of simulated body fluid [39–42]. Although as stated, poor porosity and thickness control, along with poor substrate adhesion, are some of the unfavourable attributes of existing HA coating methods [43]. The advantages of existing methods lie within their mechanical properties and their easy affinity for titanium surfaces [44].

As outlined in Chapter 2, this method of depositing hydroxyapatite (HA) on orthopaedic implant-type substrates, using saturated solutions of calcium and phosphorous, has the benefits of sol-gel techniques and biomimetic techniques. Coating crystallisation occurs at low temperatures, unlike in other methods. This process entices HA to grow in a self-assembly manner, encouraging high porosity and strict phase control. Chapter 2 provides us with an ideal process solution, process time and process temperature at which to grow hydroxyapatite coatings from solution. The formation of HA at surfaces is not well understood; the focus of research has mainly been on characterisation rather than the mechanism of film formation.

Further work is conducted herein on the mechanism of film formation upon a titanium alloy surface. Through thermal analysis, nuclear magnetic resonance (NMR), X-ray diffraction (XRD) and transmission electron microscopy (TEM), we identify the initial nucleation of Ca-P through to the final film characteristics. Once surface coating has commenced, XRD is performed at distinct stages of the process to identify each phase's composition and how they emerge during the process. By proving the repeatable and reliable physiochemical outcomes of this process, a new generation of HA coatings can be engineered, ultimately improving patient prognoses post-implantation.

3.2. Materials and Methods

All materials and reagents were used as received. Monobasic potassium phosphate (KH_2PO_4) United States Pharmacopeia (USP) reference standard, Honeywell Fluka hydrochloric (HCl) acid solution 6 M, tris(hydroxymethyl)-

aminomethane (TRIS) ACS reagent, 99.8% sodium chloride (NaCl) BioXtra and 99.5% calcium nitrate tetrahydrate ($\text{Ca}(\text{NO}_3)_2 \cdot 4\text{H}_2\text{O}$) ACS reagent were all from Sigma Aldrich. A calibrated benchtop pH meter with a temperature enabled probe (Orion Star A111, [Thermo Scientific™, UK]) was used for pH measurements with an accuracy of 0.001 pH. Titanium coupons of Ti-6Al-4V alloy were used as substrates. These coupons were received from the industry co-funding partner, DePuy Synthes. All substrates were submerged in hot basic solutions to increase roughness and yield a negatively charged surface for the calcium ion attachment [45, 46].

KH_2PO_4 , TRIS and NaCl were mixed in deionised water (DIW) to yield a supersaturated phosphate concentrate. HCl was added to increase the stability of the concentrate to prevent precipitation. $\text{Ca}(\text{NO}_3)_2 \cdot 4\text{H}_2\text{O}$ was mixed with DIW to yield a supersaturated calcium concentrate. Solutions 3-4 from **Chapter 2** were used in this work, meaning, for deposition, the supersaturated concentrates were combined before a dilution factor of between 15 and 17 was applied. The process solution was heated to 46 °C. A custom-designed experimental apparatus was used for deposition. A sample holder, thermometer and pH probe for in situ temperature and acidity measurements, and an overhead stirrer to agitate the solution, were inserted into the vessel. High agitation rates of 1000 RPM prevented gross precipitation of the minerals from the solution. Substrates were placed in the reaction vessel for deposition then removed and rinsed with DIW; this process was repeated several times with fresh solutions to grow a coherent layer of HA at the solution–substrate interface. In between process runs, samples were left to dry for a minimum of 15 min in ambient conditions. To facilitate some powder analyses two powders were collected; (i) HA powder was collected by scraping it from surfaces post-solution deposition (for thermal analysis and nuclear magnetic resonance) and (ii) the process solutions underwent filtration and evaporation to remove the solvent and the dried solute was collected (for crystallinity analysis).

Solid-state nuclear magnetic resonance spectroscopy (NMR) was performed using a 9.4T Bruker Avance III HD NMR spectrometer equipped with a 3.2 mm H-F/X CP-MAS probe with TopSpin software version 3.6.5. The spectra were recorded at a Larmor frequency of 400.13 and 161.97 MHz for ^1H and ^{31}P ,

respectively. Chemical shifts were externally referenced to $\text{NH}_4(\text{H}_2\text{PO}_4)$ and Tetramethyl silane for ^{31}P and ^1H , respectively. A powder HA sample was added to a zirconia rotor, which was then spun at a magic angle spinning of 20 kHz. All spectra were run at room temperature. The ^{31}P MAS spectra were measured at a spin rate of 20 kHz and with 50 kHz proton decoupling. An exponential window function of 20 Hz line broadening was applied to each free induction decay before the Fourier transformation. The 2D $^{31}\text{P}\{^1\text{H}\}$ heteronuclear correlation (HETCOR) experiments were run with a contact time (τ_{CP}) of 0.5 ms and a recycling delay of 8 s at 20 °C. Thermogravimetric analysis (TGA) was carried out using Perkin Elmer Pyris 1 TGA under nitrogen; samples were held at 30 °C for 15 min and then heated from 30 °C to 900 °C at 10.00 °C min^{-1} . DSC was carried out using the Perkin Elmer Diamond DSC 800 under nitrogen; the sample was heated from 20°C to 500 °C at 10.00 °C min^{-1} , held for 1.0 min at 500 °C before cooling to 20 °C at 100 °C min^{-1} , held for 5.0 min at 20 °C and reheated to 500 °C at 10.00 °C min^{-1} . However, it is the first heating which is reported on. X-ray Diffraction (XRD) patterns were acquired using a Bruker Advance Powder Diffractometer (Cu-K α radiation with $\lambda = 1.5406 \text{ \AA}$, an operating voltage of 40 kV and a current of 40 mA). Measurements were performed in the 2θ range from 10° to 60° with steps of 0.004°. XRD diffractograms of HA powder from the dried process solution and HA films (after two, four and seven deposition runs) were collected. XRD was also performed on the blank titanium substrate. Scanning Electron Microscope (SEM) images were recorded using a Zeiss Ultra Plus system with the accelerating voltage of 5 kV, at a working distance between 3 and 10 mm and using an in-lens detector or secondary electron detector.

Lamellae for TEM cross-section images were prepared on a Zeiss AURIGA Focused Ion Beam (FIB), with accelerating voltages of 5–30 kV and ion beam currents of 50 pA–2 nA. Transmission Electron Microscopy (TEM) coupled with EDX analyses were performed on a FEI Titan 80–300 microscope with a Schottky-type field emission electron gun operated at 300 kV and a Bruker XFlash 6T-30 detector (resolution 129 eV).

3.3 Results

3.3.1 Analysis of HA generated from within this process in powder form.

Powder analysis was performed on apatite mineral to understand how phases emerge within solution and upon solution–surface interaction. TGA analysis of this HA powder revealed the presence of adsorbed water and interstitial water, similar to other HA studies [47–49]. In the TGA data, **Figure 3.1a** showed a 4% weight loss by 600 °C at a steady rate. From 0 °C to 200 °C the weakly adsorbed water loss was ~2%. This was accompanied by a large heat flow in the DSC data (**Figure 3.1b**). **Figure 3.1b** showed a large peak at 113 °C which corresponded to a change in enthalpy of 101.2 Jg⁻¹. The TGA data showed a decrease in mass from 200 °C to 400 °C likely due to chemically bound water loss of ~2%. Again, this was accompanied by a significant heat flow, shown in the DSC data by a smaller peak at 368 °C, which corresponded to a change in enthalpy of 29.7 Jg⁻¹. There was no sign of phosphate decomposition, which only occurs significantly at temperatures >600 °C. The TGA analysis of HA compounds commonly show a weight gain at 700 °C upwards; this is a bounce back in weight due to the recrystallisation of the mineral and it is seen in **Figure 3.1a** [50, 51].

Solid state NMR of HA powder was performed and the 1D spectra of ¹H and ³¹P were collected, **Appendix 3.5.1**. The 1D spectra gave little information because of low resolution about the hydration state of the phosphorous species. However, 2D heteronuclear correlation (2D HETCOR) experiments which correlated ¹H chemical shifts with ³¹P (or other X-nuclei) chemical shifts provided excellent ¹H resolution in the indirect dimension, **Figure 3.1(c)**. Cross-polarisation dynamics are different for ACP versus crystalline HA due to different proton pair correlations. [52–54] ACP is correlated by the proton in water with the P proton of a phosphate: ¹H₂O ↔ ³¹P O₄³⁻. Crystalline HA material is correlated by the proton of the hydroxyl functional group with the P proton of a phosphate O¹H ↔ ³¹P O₄³⁻. Two distinct areas could be seen on the HETCOR spectrum (τ_{cp} = 0.5 ms) through contour vectors at the location of the cross peaks, **Figure 3.1(c)**. The cross correlated peak at ¹H 0 ppm was due to apatitic OH⁻ and can be assigned to a more well-formed crystalline HA. The broader cross peak between ¹H 5 and 10 ppm was due to correlations between hydrogen phosphates, ACP, free and bound water, i.e., less well-formed HA. The NMR data indicated the existence of

two distinct types of HA within the powder, one crystalline and one amorphous. The ACP peak also manifested the presence of water nuclei in and around all HA phases.

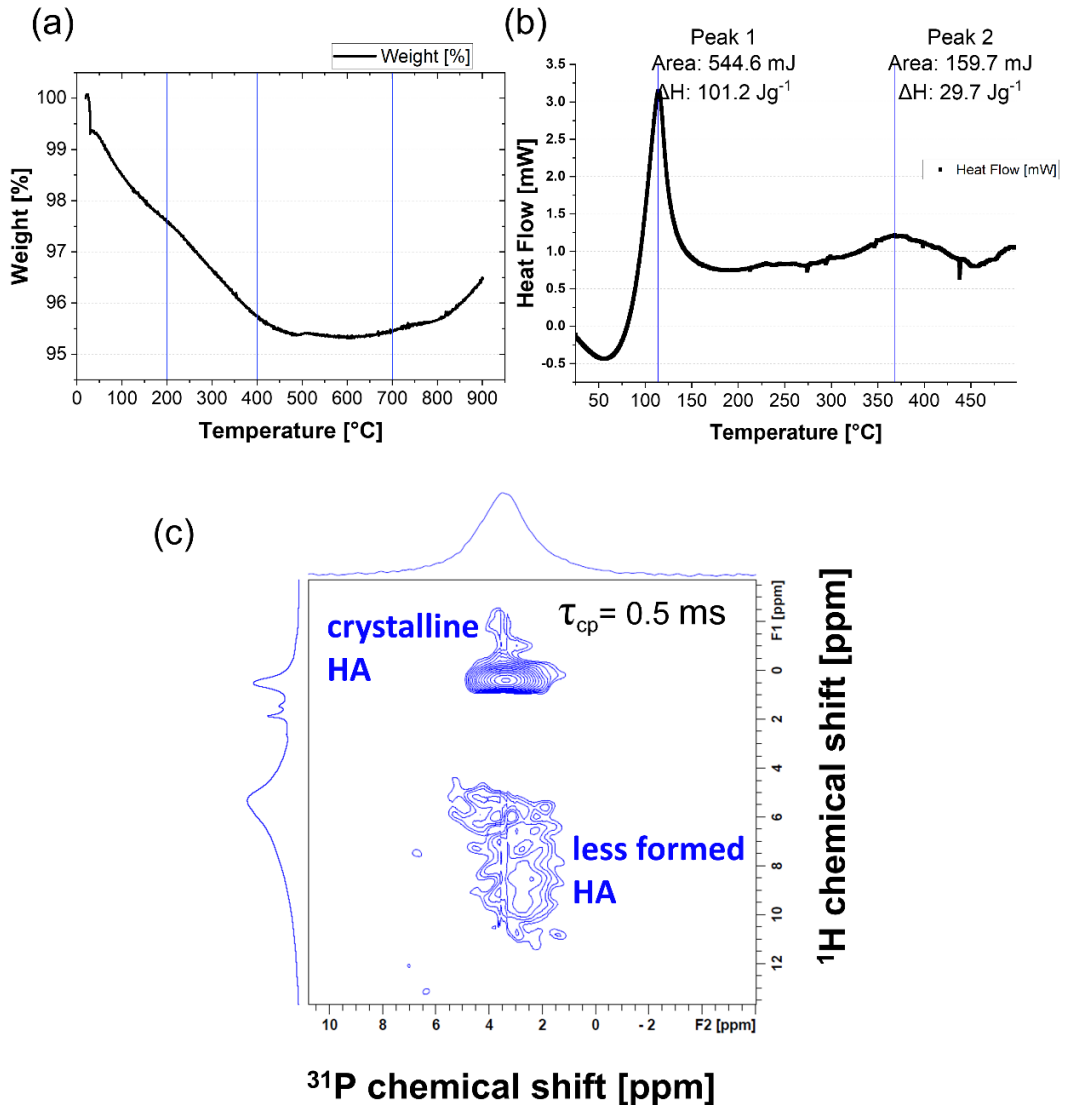


Figure 3.1:(a) Thermogravimetric data (TGA) showing weight loss as percentage loss from the samples versus temperature, (b) Differential scanning calorimetry (DSC) data for the first heating of a sample, graph of heat flow [mW] versus temperature, (c) Solid state Nuclear Magnetic Resonance 2D Heteronuclear correlation sequence (NMR 2D HETCOR) measuring cross-polarisation of ^1H and ^{31}P proton spectra at a relaxation time (τ) of 0.5ms, showing two distinct peak regions as blue contours

3.3.2 Growth Mechanism of HA film on a titanium substrate

Films were also analysed *in situ* to identify relationships between the properties of the solution and the films formed plus characterisation of the film itself.

To identify the specific crystalline phases of HA present, extensive XRD analysis was performed, **Figure 3.2(a)** and tabulated in **Table 3.1**

Table 3.1. Peak assignment of peaks seen in X-ray Diffraction (XRD) diffractograms in **Figure 3.2**.

Peak Assignment				
Sample	OCP [002] (26.2°)	HA [210] (28.5°)	HA Triple Peak (32°-33°)	Titanium (35.8°)
Dried Process Solute	Medium	Weak	Strong	Absent
7 × Runs HA film on Ti	Strong	Weak	Medium	Weak
4 × Runs HA film on Ti	Strong	Weak	Medium	Medium
2 × Runs HA film on Ti	Weak	Absent	Strong	Strong
Blank Ti substrate	Absent	Absent	Absent	Strong

The titanium alloy has a strong reflection at a 2θ angle of 35.8° , denoted in **Figure 3.2(a)** as 'Ti'. [55,56] This titanium peak can be seen on HA coated substrates and the peak decreases in intensity as the number of HA deposition cycles increase. There are three peaks of interest in this study with respect to HA: [57–62]

1. OCP [002] is indicative of a calcium deficient plane [002] (26.2°)
2. HA [210] (28.5°)
3. HA Triple Peak containing the planes [211], [112] and [310] in varying degrees and could be masking the presence of TCP which would be observed at a similar position.

Powder solute obtained directly from process solution rather than substrate gave an XRD pattern which shows amorphous build up around the peaks with a strong indication of HA triple peak, **Figure 3.2(a)**. After two process runs, HA film on the substrate shows a weak OCP [002] peak and a strong characteristic HA triple peak. This may suggest that the initial attachment could be TCP. After four

process runs, the HA layer on the Ti substrate shows a strong OCP [210] peak, emergence of a HA [210] peak and a broadening of the triplet peak with shoulders implying a mixture of planes. Clearly while HA is forming, the unstable phase of OCP begins to dominate within this solution process. Pure HA can have a peak around 26° but the intensity of it is lower than the HA Triple Peak, unlike in this study where the OCP peak at 26° surpasses the HA triple peak intensity. By the 7th run of HA on the Ti substrate, the OCP [002] peak remains narrow and sharp and rises in intensity relative to pure HA phases in the diffractogram. This implies that the coating grows preferentially along the [002] calcium deficient plane within this process. [63] The comparison of diffractograms between HA film on the surfaces to dried HA solute shows that the substrate encourages much sharper peaks shapes. This confirms that the presence of a substrate in solution causes heterogenous nucleation and orientation of the crystallites, with OCP more prevalent than pure HA. This process could be driven by surface alignment or epitaxy between the substrate and the HA type coating.

The SEM images in **Figure 3.2(b,c)** represent the HA film at 7 and 2 process runs, respectively. The film develops cobweb-like interconnectivity with pores which develop to a full coverage of a porous film after 7 process runs. This morphological structure has been shown in various *in vitro* studies to be the most advantageous HA structure by which to proliferate bone-growth cells. [64-66] As the coverage grows from **Figure 3.2(c)** to **Figure 3.2(b)** it rationalises the diminishing Ti substrate peak.

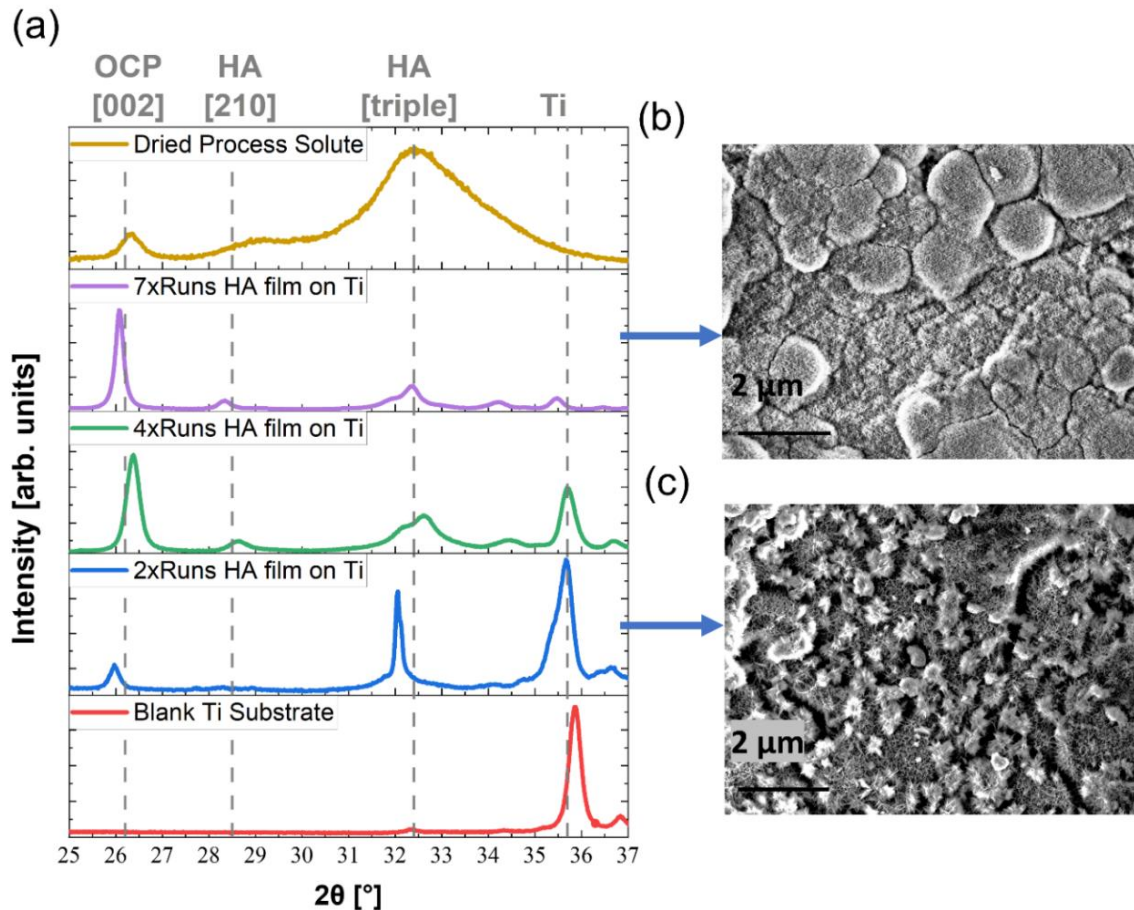


Figure 3.2: (a) X-ray diffraction (XRD) diffractograms in the region of 2θ angle 25° to 37° , separate trends shown for a blank titanium substrate, films of hydroxyapatite on a titanium substrate after 2,4 and 7 process runs and a trend from the dried process solute. (b) Scanning Electron Microscope (SEM) image of hydroxyapatite film on titanium alloy coupon after 7 hydroxyapatite solution deposition runs and (c) SEM image of hydroxyapatite film on titanium alloy coupon after 2 hydroxyapatite solution deposition runs.

It should be noted that OCP, $\text{Ca}_8(\text{HPO}_4)_2(\text{PO}_4)_4 \cdot 5\text{H}_2\text{O}$, has an apatitic structure with a ‘hydrated’ water layer along the c axis. [67,68] These repeating OCP crystallites can be confirmed by the sharp [002] peak at XRD for our HA films. Correspondingly our HA films also show the water content in TGA, DSA and NMR data.

To further analyse the specific planes within the HA film on the titanium substrate, FIB lamellae were cut from the deposited films for cross-sectional TEM analysis. TEM indicates a coating thickness of $6\mu\text{m}$, see **Figure 3.3(a)**. **Figures 3.3(b-d)** show $<20\text{nm}$ segments of dark and light features which are thought to be layers of pores developed through the coating process. Dark areas are small

nanoparticles, possibly gallium implanted during FIB sectioning. **Figures 3.3(e-f)** show crystalline areas circled, suggesting that the coating consists of polycrystalline domains within an amorphous matrix. The HRTEM images, **Figures 3.3(g-h)** depict areas of high crystallinity with lattice fringes that are highly uniform and perfectly orientated with respect to each other. FFT analysis was performed on crystalline areas, **Figure 3.3(i)**. From the FFT diffractogram, we found the d-spacings of $d=0.344\text{nm}$ and $d=0.284\text{nm}$, corresponding to XRD peaks at 26° and 32° and correlating with the XRD data shown in **Figure 3.2(a)**. [69,70] In **Figure 3.3(i)** strong $[002]$ and $[00\bar{2}]$ reflections are consistent with the XRD data. The absence of the $[001]$ reflection suggests that here is still some pure HA phase present since this phase has a symmetry assignment of $P6_3/m$ where this reflection is phase forbidden. [71] FFT diffractograms were fitted with crystallographic information file (cif) 1534327 which is a mixture of OCP and HA using CrystalMaker and CrystalDiffract software and showed excellent alignment.

Appendix 3.5.2.

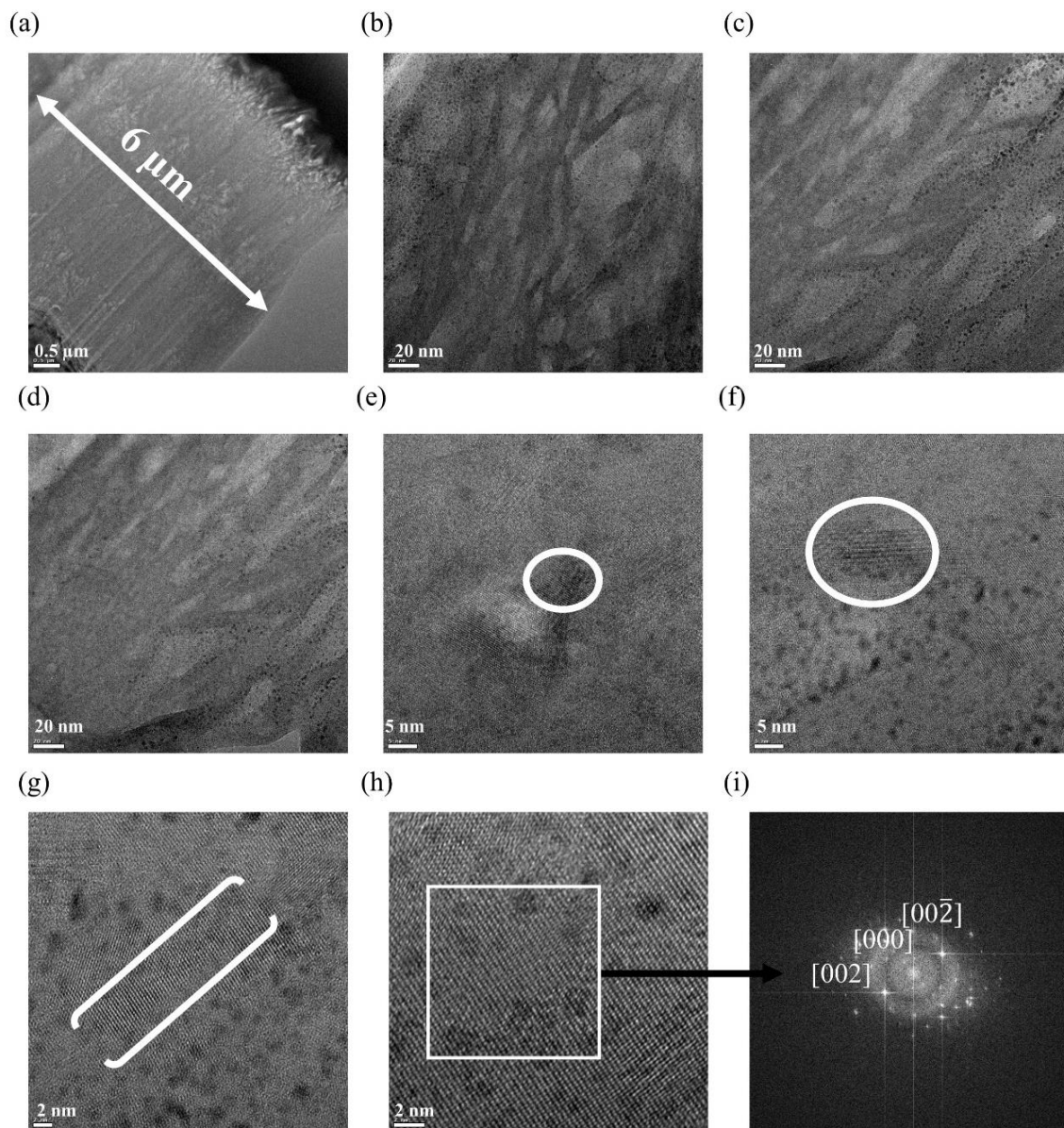


Figure 3.3: (a-h) Transmission electron microscope (TEM) images of lamellae cut into the HA film over titanium substrate, (e-g) have areas of high crystallinity outlined by white circles or brackets (i) fast Fourier transform (FFT) performed on crystalline areas present in white square in (h) to identify lattice parameters.

The crystallinity analysis presented here shows a coating comprising of amorphous and distinct crystalline zones. The combination of these phases of ACP, OCP and some pure HA are desired for HA bone cement since these phases stimulate bone reformation *in vitro*. [72,73] New studies relating to the coating of Mg alloys for orthopaedic implants are also highlighting these ACP,

OCP and HA phases as being beneficial for controlled resorption. [74,75] The phases, combined with the morphological structure of our HA coating confirm that we have designed a process of making highly osteoinductive coatings.

3.4 Conclusion

This work has proved the efficacy of a coating process whereby an orthopaedic quality film of hydroxyapatite can be generated at a surface from supersaturated solutions of calcium and phosphate ions. Based off findings in Part 1 of this study, films were generated herein using process solutions of specific concentrations. The subsequent growth of HA was investigated through various characterisation methods. Thermal analysis highlighted a hydrated nature within the HA film grown which is to be expected from an aqueous process. However, some of the water content can be assigned to hydrated interstitial water content from the OCP phase. NMR data proved that there are two distinct types of material being formed within this process: amorphous and crystalline.

Crystallinity analysis reveals the specific planes of HA that are present post deposition. XRD data shows that the presence of a substrate alters the formation mechanism and HA on a surface favours growth along the calcium deficient plane of [002] after 7 process runs. SEM data shows the comprehensive HA coverage achieved without compromising on the porosity of the film. TEM data shows that after 7 process runs the thickness of the coating is 6 μm . TEM data supports that the film is an amorphous layer with crystalline pockets. FFT analysis of these crystalline pockets show again that both OCP and HA is present through reflection and d-spacing data.

From these results, solution deposition of HA is shown to produce excellent HA coatings on titanium parts. The deposition can be tracked as the coating grows and the phase composition and morphology of the HA generated is advantageous for a low temperature and cost process. This body of work highlights that there is a large opportunity here in industrialising methods which have thus far only been used in research. Since the results are consistent across the full surface of the coupon which is 2.5cm, and we have shown that we can achieved these results on 1 up to 6 parts per run, we deem this process is readily scalable.

3.5 Appendix Chapter 3

Appendix 3.5.1 1D NMR Spectra

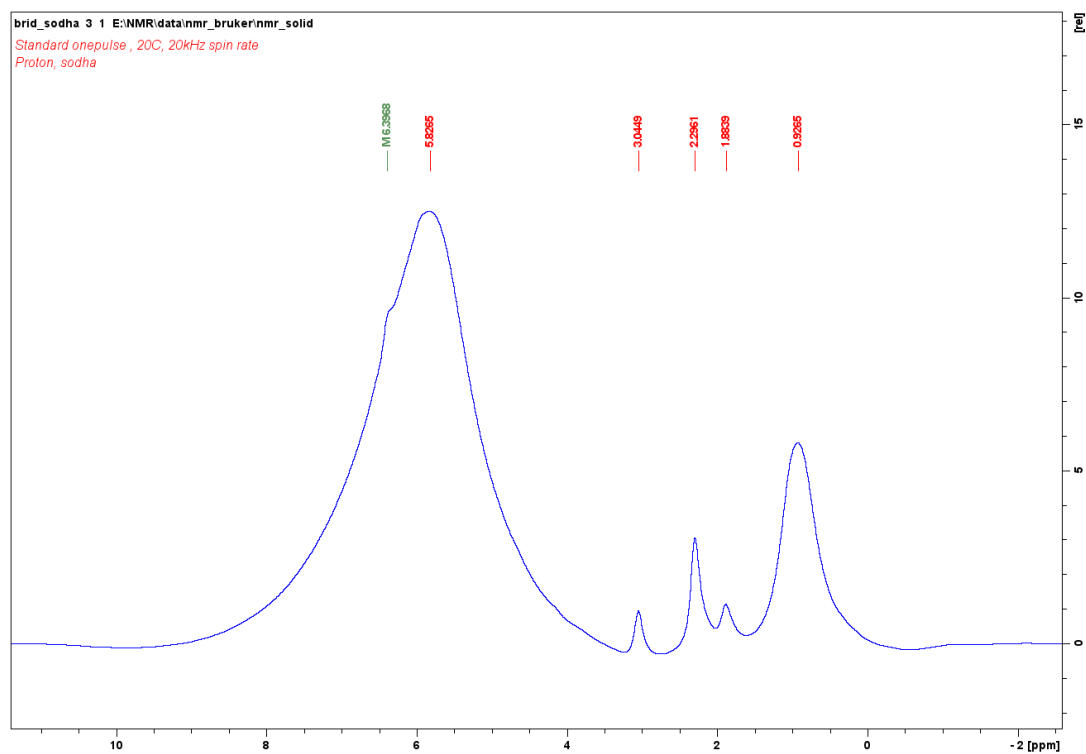


Figure A3.1: Solid state Nuclear Magnetic Resonance 1D ^1H proton spectrum from a standard one pulse sequence at 20kHz spin rate.

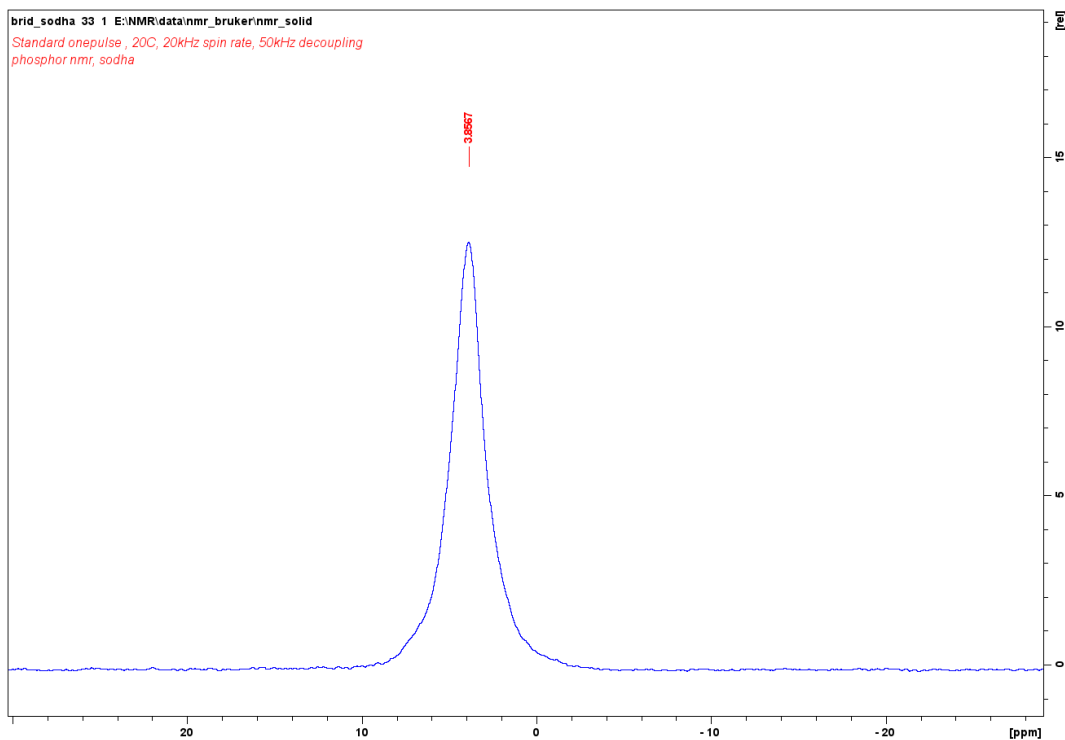


Figure A3.2: Solid state Nuclear Magnetic Resonance 1D ^{31}P (phosphorus) spectrum from a standard one pulse sequence at 20kHz spin rate with 50kHz decoupling.

Appendix 3.5.2 TEM FFT fitting on Single Crystal

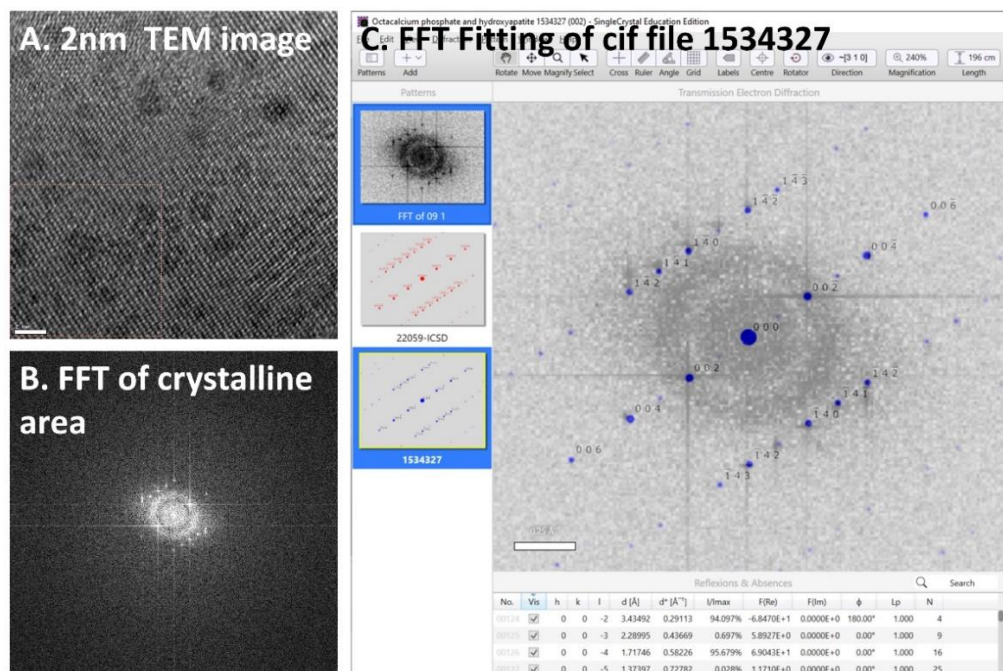


Figure A3.3: (A) high magnitude Transmission electron microscope (TEM) image of crystalline area within the deposited HA (B) Fast Fourier Transform measurement as applied to the highlighted square in A. and (C) Software

interface from Single Crystal software (education edition) fitting the crystallographic information file (cif) number 1534327 to the FFT image in C.

3.6 References

- [1] B. Murphy, M. A. Morris, and J. Baez, "Development of Hydroxyapatite Coatings for Orthopaedic Implants from Colloidal Solutions: Part 1—Effect of Solution Concentration and Deposition Kinetics," *Nanomaterials*, vol. 13, no. 18, Art. no. 18, Jan. 2023, doi: 10.3390/nano13182577.
- [2] S. Keyhani *et al.*, "Is posterior knee arthroscopy using posterior portals necessary for orthopedic surgeons? The latest evidence on applications and techniques," *EFORT Open Reviews*, vol. 8, no. 4, pp. 189–198, Apr. 2023, doi: 10.1530/EOR-22-0133.
- [3] A. Josyula, K. S. Parikh, I. Pitha, and L. M. Ensign, "Engineering biomaterials to prevent post-operative infection and fibrosis," *Drug Deliv. and Transl. Res.*, vol. 11, no. 4, pp. 1675–1688, Aug. 2021, doi: 10.1007/s13346-021-00955-0.
- [4] J. Guillem-Marti *et al.*, "Porous titanium-hydroxyapatite composite coating obtained on titanium by cold gas spray with high bond strength for biomedical applications," *Colloids and Surfaces B: Biointerfaces*, vol. 180, pp. 245–253, Aug. 2019, doi: 10.1016/j.colsurfb.2019.04.048.
- [5] A.-R. Ibrahim *et al.*, "Ultra-fast route to synthesizing biogenic carbonate hydroxyapatite: Consequence of a high-pressure solid-solid preparation technique," *Chemical Engineering and Processing - Process Intensification*, vol. 142, p. 107549, Aug. 2019, doi: 10.1016/j.cep.2019.107549.
- [6] M. A. Hussain *et al.*, "Influence of spark plasma sintering temperature and hydroxyapatite nanoparticles on properties of HA based functionally graded materials for bone prosthesis," *Ceramics International*, vol. 48, no. 10, pp. 14481–14490, May 2022, doi: 10.1016/j.ceramint.2022.01.341.
- [7] T. Varadavenkatesan, R. Vinayagam, S. Pai, B. Kathirvel, A. Pugazhendhi, and R. Selvaraj, "Synthesis, biological and environmental applications of hydroxyapatite and its composites with organic and inorganic coatings," *Progress in Organic Coatings*, vol. 151, p. 106056, Feb. 2021, doi: 10.1016/j.porgcoat.2020.106056.
- [8] R. Kumar and S. Mohanty, "Hydroxyapatite: A Versatile Bioceramic for Tissue Engineering Application," *J Inorg Organomet Polym*, vol. 32, no. 12, pp. 4461–4477, Dec. 2022, doi: 10.1007/s10904-022-02454-2.
- [9] B. Murphy, J. Baez, and M. A. Morris, "Characterising Hydroxyapatite Deposited from Solution onto Novel Substrates: Growth Mechanism and Physical Properties," *Nanomaterials*, vol. 13, no. 17, Art. no. 17, Jan. 2023, doi: 10.3390/nano13172483.
- [10] B. Murphy, J. Baez, and M. A. Morris, "Characterizing Hydroxyapatite Deposited from Solution onto Novel Substrates in Terms of Growth Mechanism and Physical Chemical Properties," *Materials Proceedings*, vol. 14, no. 1, Art. no. 1, 2023, doi: 10.3390/IOC2023-14491.
- [11] P. Rajkumar and B. K. Sarma, "Substrate dependent structural variations of biomimetic carbonated hydroxyapatite deposited on glass, Ti and sputtered ZnO thin films," *Materials Characterization*, vol. 191, p. 112120, Sep. 2022, doi: 10.1016/j.matchar.2022.112120.
- [12] L. C. Hua *et al.*, "The dehydration effect on mechanical properties of tooth enamel," *Journal of the Mechanical Behavior of Biomedical Materials*, vol. 95, pp. 210–214, Jul. 2019, doi: 10.1016/j.jmbbm.2019.04.013.
- [13] R. B. Heimann, "Structural Changes of Hydroxylapatite during Plasma Spraying: Raman and NMR Spectroscopy Results," *Coatings*, vol. 11, no. 8, Art. no. 8, Aug. 2021, doi: 10.3390/coatings11080987.
- [14] M. Prakasam, J. Locs, K. Salma-Ancane, D. Loca, A. Largeteau, and L. Berzina-Cimdina, "Fabrication, Properties and Applications of Dense Hydroxyapatite: A Review," *Journal of Functional Biomaterials*, vol. 6, no. 4, Art. no. 4, Dec. 2015, doi: 10.3390/jfb6041099.

- [15] L. Schröter, F. Kaiser, S. Stein, U. Gbureck, and A. Ignatius, "Biological and mechanical performance and degradation characteristics of calcium phosphate cements in large animals and humans," *Acta Biomaterialia*, vol. 117, pp. 1–20, Nov. 2020, doi: 10.1016/j.actbio.2020.09.031.
- [16] H. Zhou, L. Yang, U. Gbureck, S. B. Bhaduri, and P. Sikder, "Monetite, an important calcium phosphate compound—Its synthesis, properties and applications in orthopedics," *Acta Biomaterialia*, vol. 127, pp. 41–55, Jun. 2021, doi: 10.1016/j.actbio.2021.03.050.
- [17] M. Bohner, B. L. G. Santoni, and N. Döbelin, "β-tricalcium phosphate for bone substitution: Synthesis and properties," *Acta Biomaterialia*, vol. 113, pp. 23–41, Sep. 2020, doi: 10.1016/j.actbio.2020.06.022.
- [18] D. Liu, C. Cui, W. Chen, J. Shi, B. Li, and S. Chen, "Biodegradable Cements for Bone Regeneration," *Journal of Functional Biomaterials*, vol. 14, no. 3, Art. no. 3, Mar. 2023, doi: 10.3390/jfb14030134.
- [19] O. Suzuki, R. Hamai, and S. Sakai, "The material design of octacalcium phosphate bone substitute: increased dissolution and osteogenicity," *Acta Biomaterialia*, vol. 158, pp. 1–11, Mar. 2023, doi: 10.1016/j.actbio.2022.12.046.
- [20] S. Bhat, U. T. Uthappa, T. Altalhi, H.-Y. Jung, and M. D. Kurkuri, "Functionalized Porous Hydroxyapatite Scaffolds for Tissue Engineering Applications: A Focused Review," *ACS Biomater. Sci. Eng.*, vol. 8, no. 10, pp. 4039–4076, Oct. 2022, doi: 10.1021/acsbmaterials.1c00438.
- [21] S. Awasthi, S. K. Pandey, E. Arunan, and C. Srivastava, "A review on hydroxyapatite coatings for the biomedical applications: experimental and theoretical perspectives," *J. Mater. Chem. B*, vol. 9, no. 2, pp. 228–249, Jan. 2021, doi: 10.1039/D0TB02407D.
- [22] D. Xiao *et al.*, "The role of calcium phosphate surface structure in osteogenesis and the mechanisms involved," *Acta Biomaterialia*, vol. 106, pp. 22–33, Apr. 2020, doi: 10.1016/j.actbio.2019.12.034.
- [23] M. Du, J. Chen, K. Liu, H. Xing, and C. Song, "Recent advances in biomedical engineering of nano-hydroxyapatite including dentistry, cancer treatment and bone repair," *Composites Part B: Engineering*, vol. 215, p. 108790, Jun. 2021, doi: 10.1016/j.compositesb.2021.108790.
- [24] S. Kang, A. Haider, K. C. Gupta, H. Kim, and I. Kang, "Chemical Bonding of Biomolecules to the Surface of Nano-Hydroxyapatite to Enhance Its Bioactivity," *Coatings*, vol. 12, no. 7, Art. no. 7, Jul. 2022, doi: 10.3390/coatings12070999.
- [25] M. S. Safavi, F. C. Walsh, M. A. Surmeneva, R. A. Surmenev, and J. Khalil-Allafi, "Electrodeposited Hydroxyapatite-Based Biocoatings: Recent Progress and Future Challenges," *Coatings*, vol. 11, no. 1, Art. no. 1, Jan. 2021, doi: 10.3390/coatings11010110.
- [26] A. McCabe, M. Pickford, and J. Shawcross, "The History, Technical Specifications and Efficacy of Plasma Spray Coatings Applied to Joint Replacement Prostheses," *Reconstructive Review*, vol. 6, no. 4, Art. no. 4, Dec. 2016, doi: 10.15438/rr.6.4.136.
- [27] M. S. Safavi and M. Etminanfar, "A review on the prevalent fabrication methods, microstructural, mechanical properties, and corrosion resistance of nanostructured hydroxyapatite containing bilayer and multilayer coatings used in biomedical applications," *Journal of Ultrafine Grained and Nanostructured Materials*, vol. 52, no. 1, pp. 1–17, Jun. 2019, doi: 10.22059/JUFGNSM.2019.01.01.
- [28] A. T. Guner and C. Meran, "A review on plasma sprayed titanium and hydroxyapatite coatings on polyetheretherketone implants," *International Journal of Surface Science and Engineering*, vol. 13, no. 4, pp. 237–262, Jan. 2019, doi: 10.1504/IJSURFSE.2019.103923.
- [29] H. Singh, R. Kumar, C. Prakash, and S. Singh, "HA-based coating by plasma spray techniques on titanium alloy for orthopedic applications," *Materials Today: Proceedings*, vol. 50, pp. 612–628, Jan. 2022, doi: 10.1016/j.matpr.2021.03.165.
- [30] P. Ranjan Dev, C. Parambil Anand, D. Samuvel Michael, and P. Wilson, "Hydroxyapatite coatings: a critical review on electrodeposition parametric variations influencing crystal facet

orientation towards enhanced electrochemical sensing,” *Materials Advances*, vol. 3, no. 21, pp. 7773–7809, 2022, doi: 10.1039/D2MA00620K.

[31] F. Lissandrello and L. Magagnin, “Pulsed electrochemical deposition of calcium phosphate coatings for biomedical applications,” *Transactions of the IMF*, vol. 101, no. 4, pp. 173–178, Jul. 2023, doi: 10.1080/00202967.2023.2207334.

[32] A. Jaafar, C. Hecker, P. Árki, and Y. Joseph, “Sol-Gel Derived Hydroxyapatite Coatings for Titanium Implants: A Review,” *Bioengineering*, vol. 7, no. 4, Art. no. 4, Dec. 2020, doi: 10.3390/bioengineering7040127.

[33] Z. Ansari, M. Kalantar, M. Kharaziha, L. Ambrosio, and M. G. Raucci, “Polycaprolactone/fluoride substituted-hydroxyapatite (PCL/FHA) nanocomposite coatings prepared by in-situ sol-gel process for dental implant applications,” *Progress in Organic Coatings*, vol. 147, p. 105873, Oct. 2020, doi: 10.1016/j.porgcoat.2020.105873.

[34] H. Chen, R. Wang, L. Qian, H. Liu, J. Wang, and M. Zhu, “Surface modification of urchin-like serried hydroxyapatite with sol-gel method and its application in dental composites,” *Composites Part B: Engineering*, vol. 182, p. 107621, Feb. 2020, doi: 10.1016/j.compositesb.2019.107621.

[35] A. X. S. Sebastin and V. Uthirapathy, “In Vitro Electrochemical Behavior of Sol-Gel Derived Hydroxyapatite/Graphene Oxide Composite Coatings on 316L SS for Biomedical Applications,” *ChemistrySelect*, vol. 5, no. 39, pp. 12140–12147, 2020, doi: 10.1002/slct.202003368.

[36] B. Tan *et al.*, “Biomimetic hydroxyapatite coating on the 3D-printed bioactive porous composite ceramic scaffolds promoted osteogenic differentiation via PI3K/AKT/mTOR signaling pathways and facilitated bone regeneration in vivo,” *Journal of Materials Science & Technology*, vol. 136, pp. 54–64, Feb. 2023, doi: 10.1016/j.jmst.2022.07.016.

[37] J. Jiang, W. Liu, Z. Xiong, Y. Hu, and J. Xiao, “Effects of biomimetic hydroxyapatite coatings on osteoimmunomodulation,” *Biomaterials Advances*, vol. 134, p. 112640, Mar. 2022, doi: 10.1016/j.msec.2021.112640.

[38] N. Koju, P. Sikder, Y. Ren, H. Zhou, and S. B. Bhaduri, “Biomimetic coating technology for orthopedic implants,” *Current Opinion in Chemical Engineering*, vol. 15, pp. 49–55, Feb. 2017, doi: 10.1016/j.coche.2016.11.005.

[39] F. Baino and S. Yamaguchi, “The Use of Simulated Body Fluid (SBF) for Assessing Materials Bioactivity in the Context of Tissue Engineering: Review and Challenges,” *Biomimetics (Basel)*, vol. 5, no. 4, p. 57, Oct. 2020, doi: 10.3390/biomimetics5040057.

[40] T. Suchý *et al.*, “Various Simulated Body Fluids Lead to Significant Differences in Collagen Tissue Engineering Scaffolds,” *Materials (Basel)*, vol. 14, no. 16, p. 4388, Aug. 2021, doi: 10.3390/ma14164388.

[41] F. Ghorbani, A. Zamanian, A. Behnamghader, and M. Daliri-Joupari, “Bone-like hydroxyapatite mineralization on the bio-inspired PDA nanoparticles using microwave irradiation,” *Surfaces and Interfaces*, vol. 15, pp. 38–42, Jun. 2019, doi: 10.1016/j.surfin.2019.01.007.

[42] G. Wei, C. Gong, K. Hu, Y. Wang, and Y. Zhang, “Biomimetic Hydroxyapatite on Graphene Supports for Biomedical Applications: A Review,” *Nanomaterials*, vol. 9, no. 10, Art. no. 10, Oct. 2019, doi: 10.3390/nano9101435.

[43] B. Beig, U. Liaqat, M. F. K. Niazi, I. Douna, M. Zahoor, and M. B. K. Niazi, “Current Challenges and Innovative Developments in Hydroxyapatite-Based Coatings on Metallic Materials for Bone Implantation: A Review,” *Coatings*, vol. 10, no. 12, p. 1249, Dec. 2020, doi: 10.3390/coatings10121249.

[44] C. Domínguez-Trujillo *et al.*, “Sol-gel deposition of hydroxyapatite coatings on porous titanium for biomedical applications,” *Surface and Coatings Technology*, vol. 333, pp. 158–162, Jan. 2018, doi: 10.1016/j.surfcoat.2017.10.079.

[45] N. N. Andrusova, E. S. Zhavoronok, O. A. Legon'kova, A. S. Goncharova, and S. A. Kedik, “Polymer–Mineral Compounds for Cementless Hip Replacement,” *Polym. Sci. Ser. D*, vol. 13, no. 1, pp. 68–72, Jan. 2020, doi: 10.1134/S1995421220010037.

- [46] J. Sánchez-Bodón, J. Andrade del Olmo, J. M. Alonso, I. Moreno-Benítez, J. L. Vilas-Vilela, and L. Pérez-Álvarez, "Bioactive Coatings on Titanium: A Review on Hydroxylation, Self-Assembled Monolayers (SAMs) and Surface Modification Strategies," *Polymers*, vol. 14, no. 1, Art. no. 1, Jan. 2022, doi: 10.3390/polym14010165.
- [47] R. Durga, N. Jimenez, S. Ramanathan, P. Suraneni, and W. J. Pestle, "Use of thermogravimetric analysis to estimate collagen and hydroxyapatite contents in archaeological bone," *Journal of Archaeological Science*, vol. 145, p. 105644, Sep. 2022, doi: 10.1016/j.jas.2022.105644.
- [48] N. Ebadipour, S. Paul, B. Katryniok, and F. Dumeignil, "Calcium Hydroxyapatite: A Highly Stable and Selective Solid Catalyst for Glycerol Polymerization," *Catalysts*, vol. 11, no. 10, Art. no. 10, Oct. 2021, doi: 10.3390/catal11101247.
- [49] J. H. Roque-Ruiz, J. A. Garibay-Alvarado, N. A. Medellín-Castillo, and S. Y. Reyes-López, "Preparation of Electrospun Hydroxyapatite-Glass Fibers for Removal of Cadmium (Cd²⁺) and Lead (Pb²⁺) from Aqueous Media," *Water Air Soil Pollut*, vol. 231, no. 10, p. 497, Sep. 2020, doi: 10.1007/s11270-020-04856-9.
- [50] M. Greiner *et al.*, "The bone mineral is carbonato-hydro-apatite and it transforms into hydroxyapatite by heating (cremation) beyond 700°C," *Acta Crystallographica Section A: Foundations and Advances*, vol. 75, pp. e199–e199, Aug. 2019, doi: 10.1107/S2053273319093574.
- [51] K. P. Malla *et al.*, "Extraction and Characterization of Novel Natural Hydroxyapatite Bioceramic by Thermal Decomposition of Waste Ostrich Bone," *International Journal of Biomaterials*, vol. 2020, p. e1690178, Aug. 2020, doi: 10.1155/2020/1690178.
- [52] Y. Jiang, C. Ren, H. Guo, M. Guo, and W. Li, "Speciation Transformation of Phosphorus in Poultry Litter during Pyrolysis: Insights from X-ray Diffraction, Fourier Transform Infrared, and Solid-State NMR Spectroscopy," *Environ. Sci. Technol.*, vol. 53, no. 23, pp. 13841–13849, Dec. 2019, doi: 10.1021/acs.est.9b03261.
- [53] J. Wang, C. Ren, Z. Li, and W. Li, "Two-dimensional solid-state NMR spectroscopy investigations of surface precipitation of phosphate onto calcite," *Science of The Total Environment*, vol. 890, p. 164444, Sep. 2023, doi: 10.1016/j.scitotenv.2023.164444.
- [54] V. Klimavicius *et al.*, "Step-by-step from amorphous phosphate to nano-structured calcium hydroxyapatite: monitoring by solid-state ¹H and ³¹P NMR and spin dynamics," *Physical Chemistry Chemical Physics*, vol. 24, no. 31, pp. 18952–18965, 2022, doi: 10.1039/D2CP02108K.
- [55] H. M. Hamza, K. M. Deen, and W. Haider, "Microstructural examination and corrosion behavior of selective laser melted and conventionally manufactured Ti6Al4V for dental applications," *Materials Science and Engineering: C*, vol. 113, p. 110980, Aug. 2020, doi: 10.1016/j.msec.2020.110980.
- [56] F. R. Kaschel *et al.*, "Mechanism of stress relaxation and phase transformation in additively manufactured Ti-6Al-4V via in situ high temperature XRD and TEM analyses," *Acta Materialia*, vol. 188, pp. 720–732, Apr. 2020, doi: 10.1016/j.actamat.2020.02.056.
- [57] K. A. Gross, C. Petzold, L. Pluduma-LaFarge, M. Kumermanis, and H. J. Haugen, "Structural and Chemical Hierarchy in Hydroxyapatite Coatings," *Materials*, vol. 13, no. 19, Art. no. 19, Jan. 2020, doi: 10.3390/ma13194447.
- [58] T.-T. Li *et al.*, "Properties and Mechanism of Hydroxyapatite Coating Prepared by Electrodeposition on a Braid for Biodegradable Bone Scaffolds," *Nanomaterials*, vol. 9, no. 5, Art. no. 5, May 2019, doi: 10.3390/nano9050679.
- [59] S. M. Londoño-Restrepo, B. M. Millán-Malo, A. del Real-López, and M. E. Rodríguez-García, "In situ study of hydroxyapatite from cattle during a controlled calcination process using HT-XRD," *Materials Science and Engineering: C*, vol. 105, p. 110020, Dec. 2019, doi: 10.1016/j.msec.2019.110020.
- [60] D. Q. Pham *et al.*, "Antibacterial Longevity of a Novel Gallium Liquid Metal/Hydroxyapatite Composite Coating Fabricated by Plasma Spray," *ACS Appl. Mater. Interfaces*, vol. 14, no. 16, pp. 18974–18988, Apr. 2022, doi: 10.1021/acsami.2c03695.

- [61] S. M. Londoño-Restrepo, M. Herrera-Lara, L. R. Bernal-Alvarez, E. M. Rivera-Muñoz, and M. E. Rodríguez-García, "In-situ XRD study of the crystal size transition of hydroxyapatite from swine bone," *Ceramics International*, vol. 46, no. 15, pp. 24454–24461, Oct. 2020, doi: 10.1016/j.ceramint.2020.06.230.
- [62] A. S. Khan and M. Awais, "Low-Cost Deposition of Antibacterial Ion-Substituted Hydroxyapatite Coatings onto 316L Stainless Steel for Biomedical and Dental Applications," *Coatings*, vol. 10, no. 9, Art. no. 9, Sep. 2020, doi: 10.3390/coatings10090880.
- [63] I. Grigoraviciute-Puroniene, Y. Tanaka, V. Vegelyte, Y. Nishimoto, K. Ishikawa, and A. Kareiva, "A novel synthetic approach to low-crystallinity calcium deficient hydroxyapatite," *Ceramics International*, vol. 45, no. 12, pp. 15620–15623, Aug. 2019, doi: 10.1016/j.ceramint.2019.05.072.
- [64] A. M. Vilardell *et al.*, "In-vitro comparison of hydroxyapatite coatings obtained by cold spray and conventional thermal spray technologies," *Materials Science and Engineering: C*, vol. 107, p. 110306, Feb. 2020, doi: 10.1016/j.msec.2019.110306.
- [65] M. Lu *et al.*, "The morphological effect of nanostructured hydroxyapatite coatings on the osteoinduction and osteogenic capacity of porous titanium," *Nanoscale*, vol. 12, no. 47, pp. 24085–24099, 2020, doi: 10.1039/D0NR06306A.
- [66] Y. Sun *et al.*, "Plasma Spray vs. Electrochemical Deposition: Toward a Better Osteogenic Effect of Hydroxyapatite Coatings on 3D-Printed Titanium Scaffolds," *Frontiers in Bioengineering and Biotechnology*, vol. 9, 2021, Accessed: Sep. 05, 2023. [Online]. Available: <https://www.frontiersin.org/articles/10.3389/fbioe.2021.705774>
- [67] T. Yokoi, M. Shimabukuro, and M. Kawashita, "Octacalcium phosphate with incorporated carboxylate ions: a review," *Science and Technology of Advanced Materials*, vol. 23, no. 1, pp. 434–445, Dec. 2022, doi: 10.1080/14686996.2022.2094728.
- [68] R. Hamai *et al.*, "Octacalcium phosphate crystals including a higher density dislocation improve its materials osteogenicity," *Applied Materials Today*, vol. 26, p. 101279, Mar. 2022, doi: 10.1016/j.apmt.2021.101279.
- [69] H. Nosrati, R. Sarraf-Mamoory, A. H. Ahmadi, and M. Canillas, "Synthesis of Graphene Nanoribbons-Hydroxyapatite Nanocomposite Applicable in Biomedicine and Theranostics," vol. 1, p. 2, Apr. 2020, doi: 10.3390/jnt1010002.
- [70] Y. In, U. Amornkitbamrung, M.-H. Hong, and H. Shin, "On the Crystallization of Hydroxyapatite under Hydrothermal Conditions: Role of Sebacic Acid as an Additive," *ACS Omega*, vol. 5, no. 42, pp. 27204–27210, Oct. 2020, doi: 10.1021/acsomega.0c03297.
- [71] J. Reyes-Gasga, E. I. Martínez-Piñeiro, and É. f. Brès, "Crystallographic structure of human tooth enamel by electron microscopy and x-ray diffraction: hexagonal or monoclinic?," *Journal of Microscopy*, vol. 248, no. 1, pp. 102–109, 2012, doi: 10.1111/j.1365-2818.2012.03653.x.
- [72] J. L. Bystrom and M. Pujari-Palmer, "Phosphoserine Functionalized Cements Preserve Metastable Phases, and Reprecipitate Octacalcium Phosphate, Hydroxyapatite, Dicalcium Phosphate, and Amorphous Calcium Phosphate, during Degradation, In Vitro," *Journal of Functional Biomaterials*, vol. 10, no. 4, Art. no. 4, Dec. 2019, doi: 10.3390/jfb10040054.
- [73] Y. Lukina, L. Bionyshev-Abramov, S. Kotov, N. Serejnikova, D. Smolentsev, and S. Sivkov, "Carbonate-Hydroxyapatite Cement: The Effect of Composition on Solubility In Vitro and Resorption In Vivo," *Ceramics*, vol. 6, no. 3, Art. no. 3, Sep. 2023, doi: 10.3390/ceramics6030086.
- [74] S. Mahmud, M. Rahman, M. Kamruzzaman, H. Khatun, M. O. Ali, and M. M. Haque, "Recent developments in hydroxyapatite coating on magnesium alloys for clinical applications," *Results in Engineering*, vol. 17, p. 101002, Mar. 2023, doi: 10.1016/j.rineng.2023.101002.
- [75] A.-M. Zhang, P. Lenin, R.-C. Zeng, and M. B. Kannan, "Advances in hydroxyapatite coatings on biodegradable magnesium and its alloys," *Journal of Magnesium and Alloys*, vol. 10, no. 5, pp. 1154–1170, May 2022, doi: 10.1016/j.jma.2022.01.001.

Chapter 4: Characterising Hydroxyapatite Deposited from Solution onto Novel Substrates: Growth Mechanism and Physical Properties

Abstract: Whilst titanium, stainless steel and cobalt-chrome alloys are the most common materials for use in orthopaedic implant devices, there are significant advantages in moving to alternative non-metallic substrates. Substrates such as polymers may have advantageous mechanical biological properties whilst other substrates may bring unique capabilities. A key challenge in the use of non-metal products is producing substrates which can be modified to allow the formation of well-adhered hydroxyapatite films which promote osteointegration and have other beneficial properties. In this work we aim to develop a methodology for the growth of hydroxyapatite films on surfaces other than bulk metallic parts using a wet chemical coating process and we provide detailed characterisation of the coatings. In this study, hydroxyapatite is grown from saturated solutions onto thin titanium films and silicon substrates and compared to results from titanium alloy substrates. The coating process efficacy is shown to be dependent on substrate roughness, hydrophilicity and activation. The mechanism of the hydroxyapatite growth is investigated in terms of initial attachment and morphological development using SEM and XPS analysis. XPS analysis reveals the exact chemical state of the hydroxyapatite compositional elements of Ca, P and O. Characterisation of grown hydroxyapatite layers by XRD reveal that the hydroxyapatite forms from amorphous phases, displaying preferential crystal growth along the [002] direction, with TEM imagery confirming polycrystalline pockets amid an amorphous matrix. SEM-EDX and FTIR confirmed the presence of hydroxyapatite phases through elemental atomic weight percentages and bond assignment. All data are collated and reviewed for the different substrates. The results demonstrate that once hydroxyapatite seeds, it crystallises in the same manner as bulk titanium whether that be on a titanium or silicon substrate. These data suggest that a range of substrates may be coated using this facile hydroxyapatite deposition technique allowing for the broadening of substrate choice for a particular function.

4.1. Introduction

The most commonly used materials for knee or hip replacements are stainless steel, cobalt-chromium, or titanium alloys due to their mechanical strength and bio-inertness [1–4]. Although it is a common metal for use in orthopaedic implants, there are concerns surrounding titanium's (and the other metals') use. Specifically, the disadvantages of titanium parts include surface propagated cracks, titanium leeching, patient allergies, and mechanical requirements that require the addition of other metals [5–7]. There is also a problematic difference in the Young's Modulus of the implant alloy and natural bone (somewhat worse for Co-Cr) because of a higher density of the metals [8–12].

Research over the last decade has focused on alternatives to titanium alloys. Dental applications often use zirconia-based implants and researchers are showing data whereby these could replace titanium for bulk orthopaedic implants since they have the same mechanical properties but improved antimicrobial and osteointegrative properties [13,14]. Polymers have considerable potential for use in orthopaedic implants due to their mechanical properties, density similarity to bone, and biocompatibility [15,16]. Experiments on epoxy-coated bamboo fibres found that it had potential as an implant material that would incur lower aseptic loosening post-joint replacement because its stiffness is close to that of natural bone [17]. Biodegradable magnesium-based alloys have considerable potential for orthopaedic implants but on the lower size scale, such as screws or clips, not large joints [18,19]. The advent of 3D printing has opened huge opportunities to produce patient-specific orthopaedic implants from metals or composite-type materials [20–23]. Despite numerous investigations of alternative, promising materials, many of these require very different processing methods and modification, including, most importantly, surface modification [24]. This is because a key barrier to the use of new substrate materials such as plastics for implant devices is surface functionality, which enables covalent bonding to bone. Specifically, the development of materials for orthopaedic parts is hindered by the challenges of developing osteoinductive hydroxyapatite (HA) layers at the substrate surface which is well-developed for metal parts, particularly titanium [25–27].

There are various long-standing methods of depositing HA onto metallic orthopaedic parts such as chemical vapour deposition, electro spraying, and plasma spraying [28–31]. These are often inconsistent with the use of alternative materials. The plasma spraying of HA, the established industry method, has been evaluated to coat novel materials such as polyetheretherketone (PEEK), bioresorbable Mg alloys, or zirconia implants [32–34]. A key parameter outlined for successful coating of Mg-based and composite materials with HA by plasma or cold-spraying is the surface hydrophilicity of the substrate [35–37]. In general for most polymer type parts, the plasma spraying of hydroxyapatite is impeded by this disparity in hydrophilicity, while the temperatures required for plasma spraying are also incompatible with polymers [38,39]. There are studies published whereby the plasma spraying of HA onto polymers with a varying degree of success is assisted by other materials such as nanoparticles or carbon-based materials [40–43]. Electrochemical methods of depositing HA exist but are an obvious challenge for non-conductors [44,45]. Laser deposition methods of depositing HA have shown potential for titanium alloys but are challenged by scale, the formation of intermediary layers between the part, and also substrate temperature issues for coating for non-metallic parts [46–48].

As outlined, there is a clear need to develop appropriate HA coating methods for non-metallic surfaces that result in coatings with equivalent properties to metallic coatings and which can be readily scaled. Solution-based methods have been explored for HA powder formation but have no widespread application as a coating technique [49,50]. However, hydrothermal synthesis of the HA coating has shown promise on novel materials, such as magnesium, but requires high temperature and pressure [51–53]. Correspondingly, solution-based HA deposition, which uses a material containing polymeric particles, could be deployed as a gateway to implementing polymeric-based implants [54]. Other solution-based techniques rely on the use of simulated body fluids [55,56]. However, the composition and bioactivity of these simulated body fluids often vary across studies [57,58]. Under solution, the formation of HA occurs at active sites, whereby mineral precipitation begins [59]. To this end, we postulate that if we can generate active sites on novel substrates, using a colloidal-solution-based coating process, we can grow a coherent HA layer on these substrates. This new

and exciting solution-based coating technique has never been studied as a direct solution for substrate technique. The main objective of this work is to apply this novel coating technique to different substrates and to rationalise the HA film in terms of growth mechanisms and chemical composition. The aim is to show the efficacy of this HA coating system for non-bulk Ti. We highlight this system as having immense potential for change in the material used in orthopaedic implants.

The research presented in this paper demonstrates a facile and scalable solution for the deposition of HA onto non-metallic substrates that would enable the effective coating of non-traditional orthopaedic substrates. Unlike other studies, this work probes the adhesion of HA films as they evolve on novel substrates without any significant pre-preparation or the use of additional materials. The crystal phase, porosity, and integrity of the coating are compared to existing HA thin films (on titanium). Titanium coupons (Ti coupons) are used to model standard orthopaedic parts. Novel substrates (planar silicon and titanium thin films) were used as indicators that the methodology could form HA films formed on non-metals. All substrates that undergo basic activation are studied afterwards physically to assess their roughness and water contact angles, but also chemically to determine if the pre-activation has caused any intermediate layers. We present the results of an extensive XPS study that shows how varying the surface activation of Ti thin-film substrates gives rise to HA elements such as Ca, P, and O attaching to the surface in difference chemical bond states. Electron microscopy data compare the films of HA which are formed on the three different substrates from this solution process. The crystallinity of the HA formed is assessed at distinct stages in film growth, and from it a clear picture emerges of the phase evolution of the HA from this process. HA grows in the same manner for titanium bulk parts and Ti thin-film parts, which have characteristic HA lattice peaks and a dominant calcium-deficient peak. However, the silicon part's growth is less characteristic than HA mineral growth. Further transmission electron data show that the thickness of the Ti-formed HA films are comparable and that all substrates have HA mineral material with polycrystalline areas within an amorphous matrix.

The results suggest that these methods should be further explored as a way to develop functional alternative implant devices. The data prove that a <100 nm

titanium layer, which could be applied to any material, will allow for HA film growth. The HA film will be fully aligned with the HA growth on a bulk titanium part when it is deposited using this colloidal solution system. Separately, while the silicon parts do not give rise to HA films as heterogeneously as the Ti parts, we have shown that once the HA seeds, it evolves in a comparable manner to HA on Ti. This finding indicates that this coating method is easily applied to other materials once an activation is applied.

4.2. Materials and Methods

All materials and reagents were used as received. Monobasic potassium phosphate (KH_2PO_4) United States pharmacopeia (USP) reference standard, Honeywell Fluka hydrochloric (HCl) acid solution 6 M, tris(hydroxymethyl)-aminomethane (TRIS) ACS reagent, 99.8% sodium chloride (NaCl) BioXtra, and 99.5% calcium nitrate tetrahydrate ($\text{Ca}(\text{NO}_3)_2 \cdot 4\text{H}_2\text{O}$) ACS reagent were all obtained from Sigma Aldrich. KH_2PO_4 , TRIS, and NaCl were mixed in deionised water (DIW) to yield a supersaturated phosphate solution. HCl was added to increase solubility, stability, and prevent precipitation. $\text{Ca}(\text{NO}_3)_2 \cdot 4\text{H}_2\text{O}$ was mixed with DIW to yield a supersaturated calcium solution. For deposition, the supersaturated solutions were combined before dilution by a factor of 10–20 and with warming to 40–50 °C. The mixture was then agitated in a reaction vessel. Four-inch silicon wafers were used as received and a subset of these underwent e-beam evaporation–deposition (Temescal FC-2000) to generate 100 nm titanium thin films. Titanium coupons of a Ti-6Al-4V alloy were also used. All substrates were submerged in hot basic solutions to increase their roughness and foster a more negatively charged surface to which calcium ions could attach [60,61]. Substrates were placed in the reaction vessel for deposition and then removed and rinsed with DIW. This process was repeated several times with fresh solutions to grow a coherent layer of HA at the solution–substrate interface. For characterisation, some samples are analysed after one solution deposition run and some are analysed after up to six solution deposition runs.

Scanning electron microscopy (SEM) data were collected using a Carl Zeiss Ultra Microscope equipped with an in-lens detector. An accelerating voltage of 5 to 10 kV was used. Energy-dispersive X-ray spectroscopy (EDX) spectra were

acquired at 15 kV on an Oxford Inca EDX detector. Water contact angles (WCAs) of the samples were measured on a custom-built device using a fast shutter camera and a 60 Hz sampling rate. Ten microlitre drops of pure water were placed on the sample. Image J software (version 1.4.3) with 'DropSnake' plug-in was used to measure the water contact angle. Atomic force microscopy (AFM) was performed using an aXE-7, Park Systems AFM with non-contact cantilevers. AFM images were imported to Parks Systems' XEI imaging software (version 4.3.0 Build 5) which allows for quantitative and statistical analyses of images. Using the 'Region' tab, average roughness values as average roughness (Ra) and peak-to-valley roughness (Rpv) were calculated for each substrate from their corresponding AFM images. X-ray Photoelectron Spectroscopy (XPS) data were gathered using an Al K α X-ray source, 1486.6 eV, CTX400 (PSP Vacuum Technology) with ultra-high vacuum conditions ($<5 \times 10^{-10}$ mbar). Each spectrum was calibrated using a C 1s binding energy of 284.8 eV. Analysis was conducted using CasaXPS software (version 2.3.23.PR1.0). X-ray diffraction (XRD) patterns were acquired using a Bruker Advance Powder Diffractometer (Cu-K α radiation with $\lambda = 1.5406$ Å, operating voltage of 40 kV, and current of 40 mA). Measurements were performed in the 2θ range from 10° to 60° at steps of 0.004° . Transmission electron microscopy (TEM) was performed on an FEI Titan 80–300 microscope. Lamellae for TEM cross-section images were prepared using a Zeiss AURIGA Focused Ion Beam (FIB), obtaining accelerating voltages of 5–30 kV and ion beam currents of 50 pA–2 nA. Fourier-transform infrared spectroscopy (FTIR) spectra were obtained using a Perkin Elmer's Spotlight 200i benchtop device with attenuated total reflectance (ATR, 4000–500 cm^{-1} , 8 scans, and 4 cm^{-1} resolution diamond crystal).

4.3. Results

After the activation of the substrates, analysis was performed using SEM-EDX, WCA measurements, and AFM with XEI software. The available literature suggests that when titanium alloy parts are treated with NaOH, it forms a sodium titanate layer, which promotes the formation of apatite [60–63]. In this work, the SEM-EDX of substrates post NaOH did not show evidence of a sodium titanate layer, likely because the treatment time was less than an hour, i.e., much lower than in other studies. The aim of the activation herein is to generate active sites

such as OH⁻ groups on the surface, and so the minimalistic Na amounts are not imperative. Secondly, the presence of a sodium-titanate layer is only possible for bulk titanium parts, and the purpose of our work is to show how NaOH activation can be used for non-bulk titanium. SEM images and EDX mapping showed that there was no concentrated layer of sodium but low-level sodium detection, <1 at.% across the whole sampling area for all substrates, see **Figure 4.1A**. **Figure 4.1A (i,ii,v)**, shows cross-section SEM images of each substrate post activation; samples were cut to perform this, and the pink boxes highlight the EDX area which includes the edge of the substrate. Each pink box has an EDX spectrum **Figure 4.1A (ii,iv,vi)** and the insert is a map of the Na content within it. It is shown by the EDX that substrates have a small amount of Na detected, but the mapping shows that Na is in no specific pattern; there is no Na layer along the edge. This probably results from Na contamination post NaOH activation. **Figure 4.1A (ii,iv,vi)** sub-images show the elemental mapping, where Na was green for silicon (ii), red on Ti thin film (iv), and white on Ti coupon (vi).

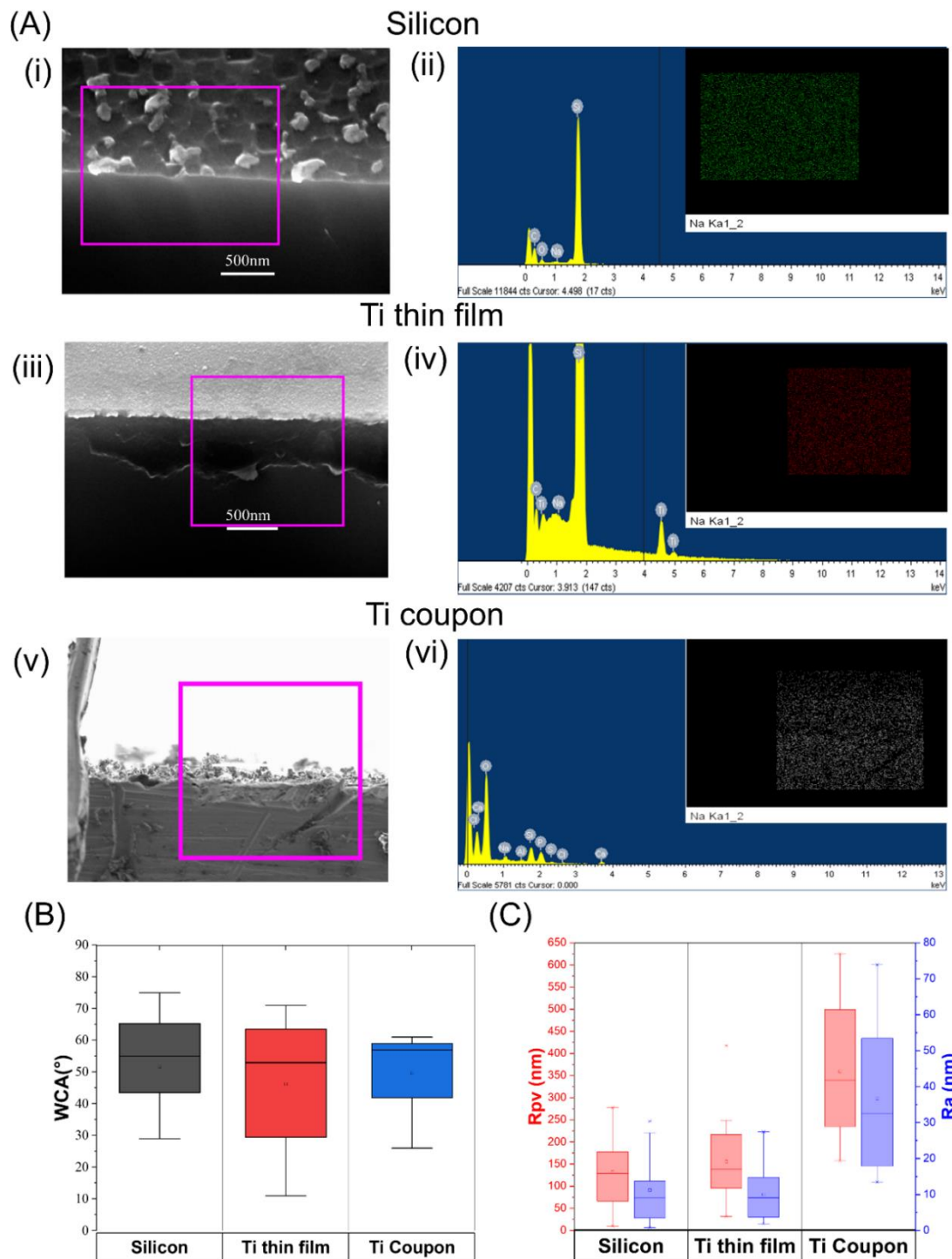


Figure 4.1: (A) Scanning electron microscope (SEM) energy dispersive X-ray (EDX) data of substrates post activation: (i) Cross-sectional SEM image of a silicon substrate with area of EDX mapping highlighted in pink, (ii) corresponding EDX spectrum and insert of elemental map of sodium, (iii) cross-sectional SEM image of a Ti thin-film substrate with area of EDX mapping highlighted in pink, (iv) corresponding EDX spectrum and insert of elemental map of sodium, (v) cross-sectional SEM image of a Ti coupon substrate with area of EDX mapping highlighted in pink, (vi) corresponding EDX spectrum and insert of elemental map of sodium. (B) Water contact angle (WCA) in $^{\circ}$

measured for each substrate post activation; (C) the average roughness (Ra) and peak-to-valley (Rpv) roughness of the three substrates post-activation as measured by atomic force microscopy

Roughness and WCA were also used to investigate the effect of NaOH treatment, with pre-activation data shown in **Appendix 4.5.1**. We postulate that the NaOH treatment used rendered the substrates hydrophilic, with all three substrates having WCA $< 90^\circ$, as seen in **Figure 4.1B**. As well as being hydrophilic, all three substrates have similar average WCAs, all measuring between 45 and 55° . Ti Coupons had a WCA distribution of 40 – 60° , while both novel substrates had a wider distribution. AFM was used to calculate the roughness of each substrate. The Ra of the novel substrates was < 30 nm, with the mean Rpv being 125 – 150 nm. Although this was lower than that of the titanium coupons, the roughness was in the same order of magnitude, as shown in **Figure 4.1C**. Thus, these data showed that the sodium content and WCA are similar for all substrates and despite somewhat of a difference in roughness, the wettability and chemical functionality of the novel substrates were comparable to the typical titanium part. This is incredibly important since the deposition process used herein depends on a colloidal solution wetting and bonding with the surface of the substrate, triggering attachment.

For further clarity, comparative tests were conducted on the Ti thin-film substrate (see **Table 4.1** for the result summary). Samples were activated for different time durations: 5 min (sample 1), 10 min (sample 2), and 15 min (sample 3) before their roughness and WCA was measured. Samples 1, 2, and 3 showed increasing roughness with an Rpv of 32.9, 93.2, and 208.9 nm, respectively. The WCA for the samples ranged from 46° to 63° . Samples 1, 2, and 3 were placed in the reaction vessel and underwent HA solution deposition together, thus experiencing matching deposition.

Table 4.1: Tabulated data of the water contact angle and roughness of Ti thin-film samples post-activation, and their resulting chemical composition as measured by XPS post HA deposition.

Ti thin film Sample	WCA [°]	Rpv [nm]	Ra [nm]	Ca at.%	P at.%	O at.%	Ti at %
1 (A,D,G)	46	32.9	2.4	1.5	0	47.9	14.6
2 (B, E, H)	63	93.2	10.8	21.9	17.8	45.9	0
3 (C, F, I)	58	205.9	33.7	20.8	16.7	42.7	0

X-ray Photon Spectroscopy (XPS) was performed on three HA-coated Ti substrates to detect slight changes in chemical composition at the surface. The samples were activated in NaOH for 5, 10 and 15mins each as a proof of concept study. The resulting chemical compositions calculated from the XPS survey scans (**Appendix 4.5.2**) included in **Table 4.1**. Sample 1 which had the lowest roughness had the least mineral attachment, demonstrated by a Ti at.% of 14.6. Samples 2 and 3 had no titanium detected; therefore, both had a coherent layer of HA mineral on the surface that was sufficient to prevent emission from the sub-layer titanium. Presented in **Table 4.1** are also the results for Ca, P, and O at.% from XPS survey scans. Sample 1 has 1.5 at.% Ca and no P. Samples 2 and 3 have similar values of 20–22 at.% Ca and 16–18 at.% P.

A further understanding of the nature of the HA formed on these surfaces was provided through the XPS core scans of O1s, Ca 2p, and P 2p (**Figure 4.2**). The core scan of Ca, O, and P reveals the local bond nature of each element and thus provides more information than the XPS Survey scans alone.

Calcium: The Ca 2p core scan, **Figure 4.2A**, showed that Sample 1 had a low calcium concentration as seen from the CPS and the line shape being noisy. The location of the Ca 2p 3/2 peak at 347.8 eV implies that the low level of Ca is due to contamination or minimal uptake from the colloidal solution. Samples 2 and 3 had significantly higher Ca signals, higher CPS, and smooth lines, **Figure 4.2B,C**.

The Ca 2p 3/2 peak at the lower binding energies of 347.1 and 346.9 eV, respectively, indicated the deposition of calcium phosphate [64,65].

Oxygen: The O 1s core scan, **Figure 4.2D**, revealed that Sample 1 had different oxygen bonding compared to Samples 2 and 3, **Figure 4.2E,F**, since Sample 1 had a double peak and Samples 2 and 3 had just one peak. All three samples showed a broad O 1s feature at around 532 eV, representative of absorbed hydroxyl species and large oxide features (due to oxides and phosphates) around 530 eV [66]. The double-peak line shape of O 1s for sample 1 indicated that it also had a metal carbonate peak at 533 eV, **Figure 4.2D** [67]; this O1s scan for Sample 1 aligns with the XPS survey scan detecting titanium.

Phosphorus: **Figure 4.2G** is the P 2p core scan of Sample 1, showing no P detection at all through both low CPS and the lack of a peak. **Figure 4.2H** is the P 2p core scan of Sample 2 and it shows P detection at a low level. By comparing Sample 2 (**Figure 4.2H**) and Sample 3 (**Figure 4.2I**), Sample 3 had a higher CPS and smoother line shape, implying more P detection. Since **Figure 4.2I** showed Sample 3 having the greatest P signal, it was indicative of mineral growth. The binding energies showed that both Sample 2 and 3 had a 2p 3/2 peak at 133 eV, indicative of HA phosphates [64].

We suggest that these three samples are representative of distinct stages of attachment. Sample 1 was hydrophilic, had the lowest roughness, had minimal calcium, no phosphates, and evidence of metal carbonate deposition. We can conclude that the sample is *activated but limited in sorptive capacity*. Sample 2 was hydrophilic, had greater roughness, and obvious calcium attachment. However, in the O1s scan line shape, there was no evidence of metal carbonates present but only oxide and hydroxide-bonded oxygens, i.e., *calcium started to bond to the active sites of the substrate*. Sample 3 was hydrophilic and had the highest roughness and had the same calcium and oxygen species and amounts as Sample 2. However, Sample 3 had a much higher P 2p signal, indicating increased phosphate build-up around the previously bonded calcium, i.e., *phosphate groups started to bond to the calcium and HA mineral formation was underway*.

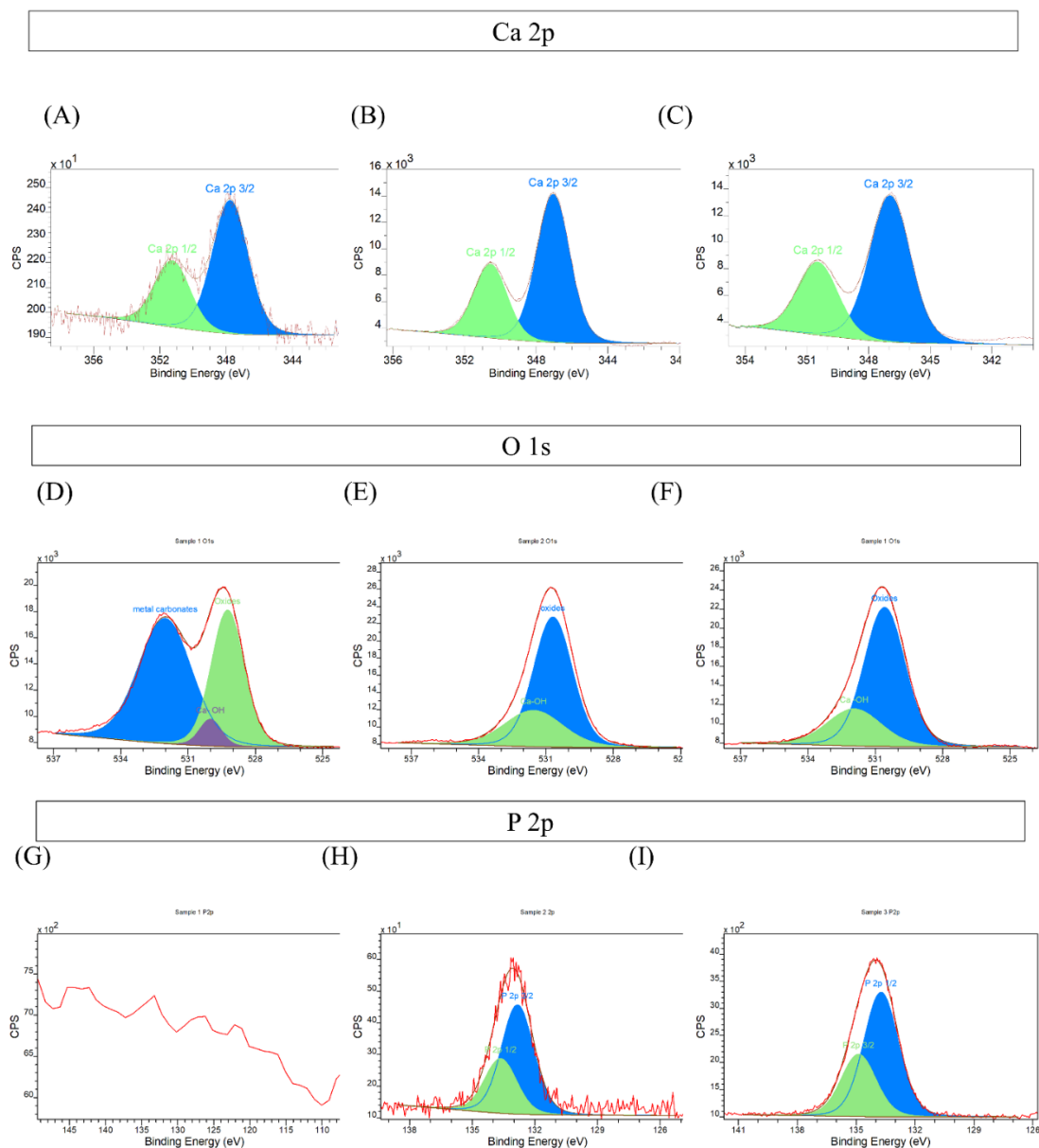


Figure 4.2: X-ray Photoelectron spectroscopy (XPS) core scans. (A) Calcium 2p orbital of Sample 1, (B) calcium 2p orbital of Sample 2, and (C) calcium 2p orbital of Sample 3. (D) Oxygen 1s orbital of Sample 1, (E) oxygen 1s orbital of Sample 2, and (F) oxygen 1s orbital of Sample 3. (G) Phosphorous 2p orbital of Sample 1, (H) phosphorous 2p orbital of Sample 2, and (I) phosphorous 2p orbital of Sample 3.

This XPS study was proof that under the correct conditions of activation, hydrophilicity, and roughness, novel substrates will lend themselves to HA mineral growth under these solution conditions. This mineral growth was further studied for all substrates via SEM imaging after they had undergone one HA deposition run. SEM images showed lighter areas of mineral deposits for all three

substrates, as depicted in **Figure 4.3A–C**. All three substrates generated this initial calcium attachment in discrete areas where there were surface groups for bonding. From this initial nucleation, the heterogeneous growth of a needle-like cobweb structure emerged as phosphate groups bonded to the calcium. This structure is what aids porosity as the coverage grows since air is still present in between the needles/cobwebs. Additionally, wider surface coverage was achieved identically for all three substrates after more HA deposition runs, as shown in **Figure 4.3D–F**. All samples had good coating integrity and similar morphologies for both Ti samples, but the silicon samples had less repeatable porosity and interconnectivity, as shown in **Figure 4.3D–F**. This morphological difference between silicon (**Figure 4.3D**) and the titanium substrates (**Figure 4.3E,F**) implied a slightly slower and less homogenous growth pattern for silicon. Overall, SEM data further confirm that once a substrate has active sites for bonding, regardless of the substrate, HA mineral growth will progress within this process akin to a bulk titanium part.

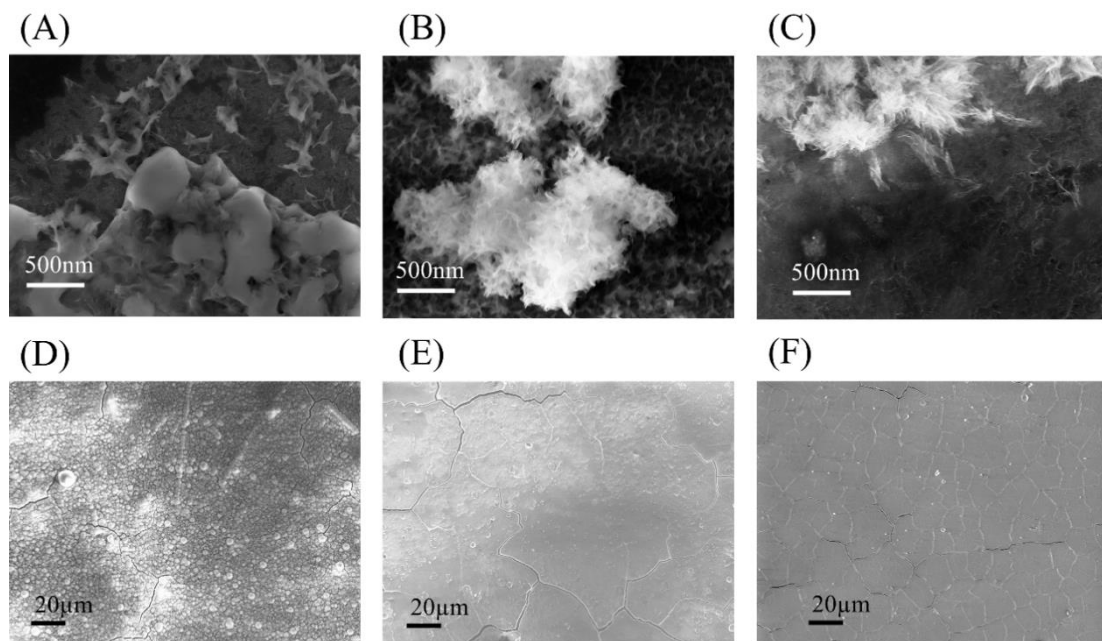


Figure 4.3: Scanning Electron Microscopy (SEM) images taken at 5 kv using inLens detector of samples after the first hydroxyapatite deposition run (a): silicon substrate, (b): titanium thin film substrate and (c): titanium coupon part. SEM images taken at 5 kv using inLens detector of samples after 6 HA deposition runs; (d): silicon substrate; (e): Ti thin film substrate; and (f): titanium coupon part.

To further probe the growth mechanism through multiple HA deposition runs, XRD patterns were recorded after two, four, and six process runs, as shown in **Figure 4.4B–D**. This XRD study compared the evolution of different HA phases as they formed on the different substrates. Both Ti thin films and silicon had substrate peaks around 33° , see **Figure 4.4A**. These diminished as the HA layer grew on the surface, **Figure 4.4B**. After two process runs, the XRD diffractogram showed that the first detection of mineral growth was characteristic of HA planes (HA), i.e., [211], [112], and [310] around 32° , **Figure 4.4B**. However, as the process continued, the mineral formed was calcium-deficient HA (CDHA), as indicated by the [002] plane emerging at 26° [68–70], **Figure 4.4C,D**. After two process runs, the Ti thin-film parts showed dominant and sharp peaks of HA, but the silicon substrate did not show these until after four process runs, implying slower and less mineral growth for silicon, as shown in **Figure 4.4B,C**. The Ti thin-film samples followed the growth pattern of a typical titanium part through the emergence of CDHA and HA characteristic peaks at given stages in the deposition. The XRD study implied that (i) silicon had some CDHA phase, but that it also had the least counts and therefore the least material, and (ii) that the Ti thin film had a lower quantity of the same phases as the Ti coupon.

FIB lamellae of HA films deposited onto all three substrate types were taken, and subsequent TEM cross-sectional analysis allowed for film thickness to be measured. Silicon's HA coating measured roughly $1.5\ \mu\text{m}$, Ti thin films' HA coating roughly $5\ \mu\text{m}$, and Ti coupon parts' HA coating roughly $6\text{--}7\ \mu\text{m}$ in thickness, as shown in **Figure 4.4E(i–iii)**. TEM imagery showed HA with clear layers from the deposition cycles and pockets of differing crystal orientation within an amorphous matrix, as shown in **Figure 4.4E(iv–vi)**. High resolution TEM images showed ordered lattice fringes for all three substrates, and, under analysis, these d-spacings were comparable to the XRD data peaks (CDHA of $0.34\ \text{nm}$ and Pure HA $0.274\text{--}0.28\ \text{nm}$) in **Figure 4.4D** [71]. These data again suggest that once HA seeds, it grows similarly for all.

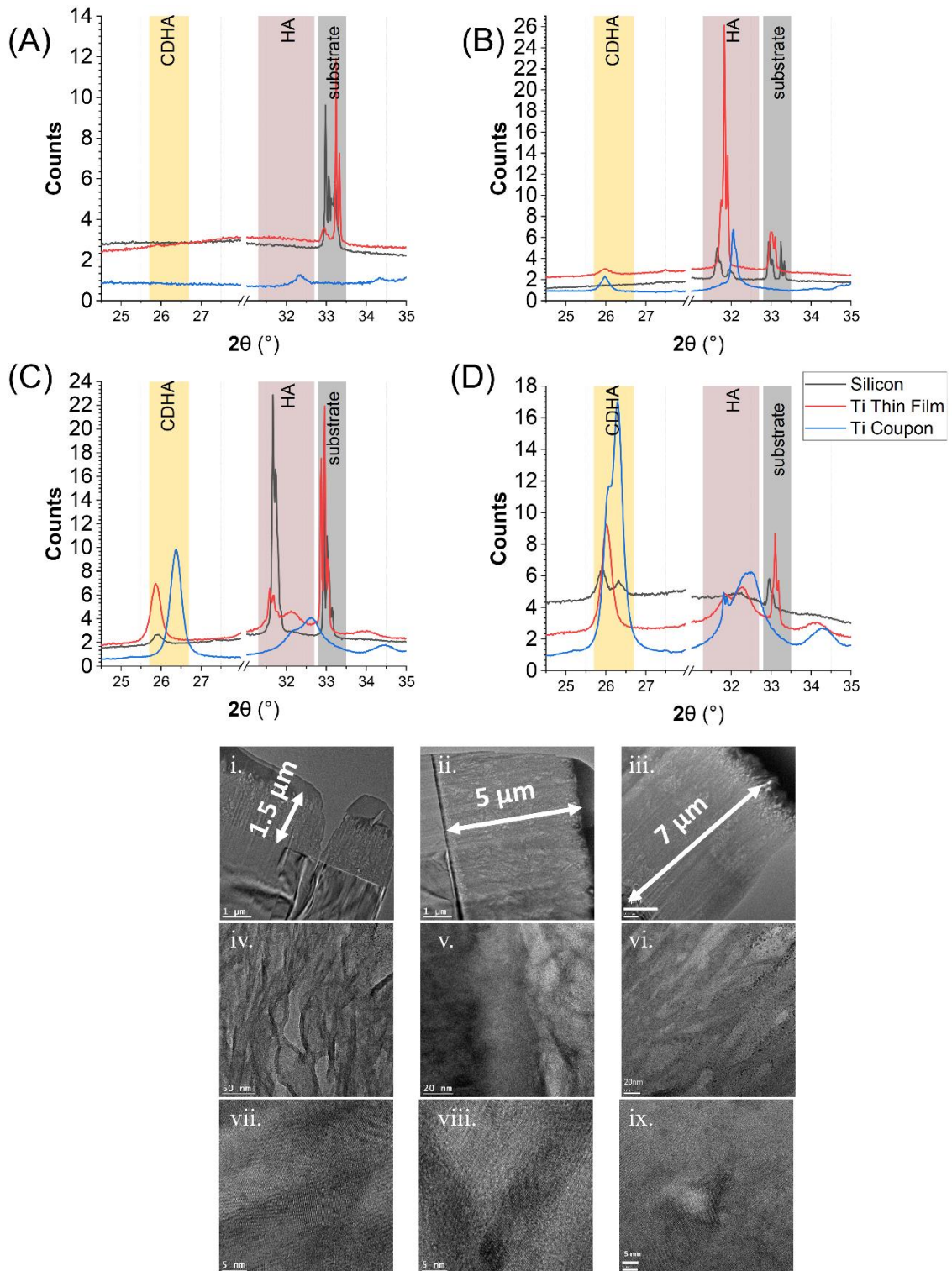


Figure 4.4: (A–D): X-ray diffraction (XRD) patterns in terms of counts per second versus diffraction angle of 2θ collected for all three substrates: silicon (grey line), Ti thin film (red line), and Ti coupon (blue line). (A) Post-activation prior to any HA deposition; (B) post 2 HA deposition runs; (C) post 4 HA deposition runs; and (D) post 6 HA deposition runs. (E) Transmission electron microscopy (TEM) cross-sectional images of lamellae cut through HA layers, 1 μm scale, 50 nm scale bar, and higher magnification nanometre scale; (i,iv,vi) cross-section of the HA layer over silicon substrate; (ii,v,vii) cross-section of the

HA layer over Ti thin-film substrate; (iii,vi,ix) cross-section of the HA layer over Ti coupon part.

An elemental and chemical analysis of the HA layers was conducted on samples post full deposition using FTIR and SEM-EDX characterisation. From FTIR, the silicon substrate had the strongest indication of absorbed water in the HA layer, as shown in **Figure 4.5A**. All substrates had strong vibrational peaks within the known phosphate region of 700 to 1300 cm^{-1} , as shown in **Figure 4.5B** [72,73]. All substrates demonstrated a matching ratio between the largest peak for $\nu^3 \text{PO}_4^{3-}$ and shoulder peak of $\nu^1 \text{PO}_4^{3-}$. Compared to the titanium samples, the silicon samples showed a greater absorbance of HPO_4^{2-} in agreement with the XRD data having less fully formed HA peaks. Only Ti coupon samples had a shoulder peak for pure HA.

The EDX analysis of the HA on each substrate supported the calculation of the calcium-to-phosphate ratio (Ca/P) and oxygen atomic percentage (O at.%) of the films, as shown in **Figure 4.5C,D**. Samples in this study had O at.% of $52 \pm 6\%$ for silicon, $60 \pm 3.5\%$ for Ti thin film, and $62 \pm 2\%$ for Ti coupon, **Figure 4.5C**. Separately, silicon had the lowest Ca/P at 1.25 ± 0.12 , but the Ti thin film was 1.36 ± 0.14 , very close to Ti coupon at 1.38 ± 0.07 , **Figure 4.5D**. Both the relatively low O at.% and Ca/P of silicon HA layer illustrate that it is in keeping with the Ti thin-film sample that had early-stage HA growth, i.e., Sample 1 in **Table 4.1**.

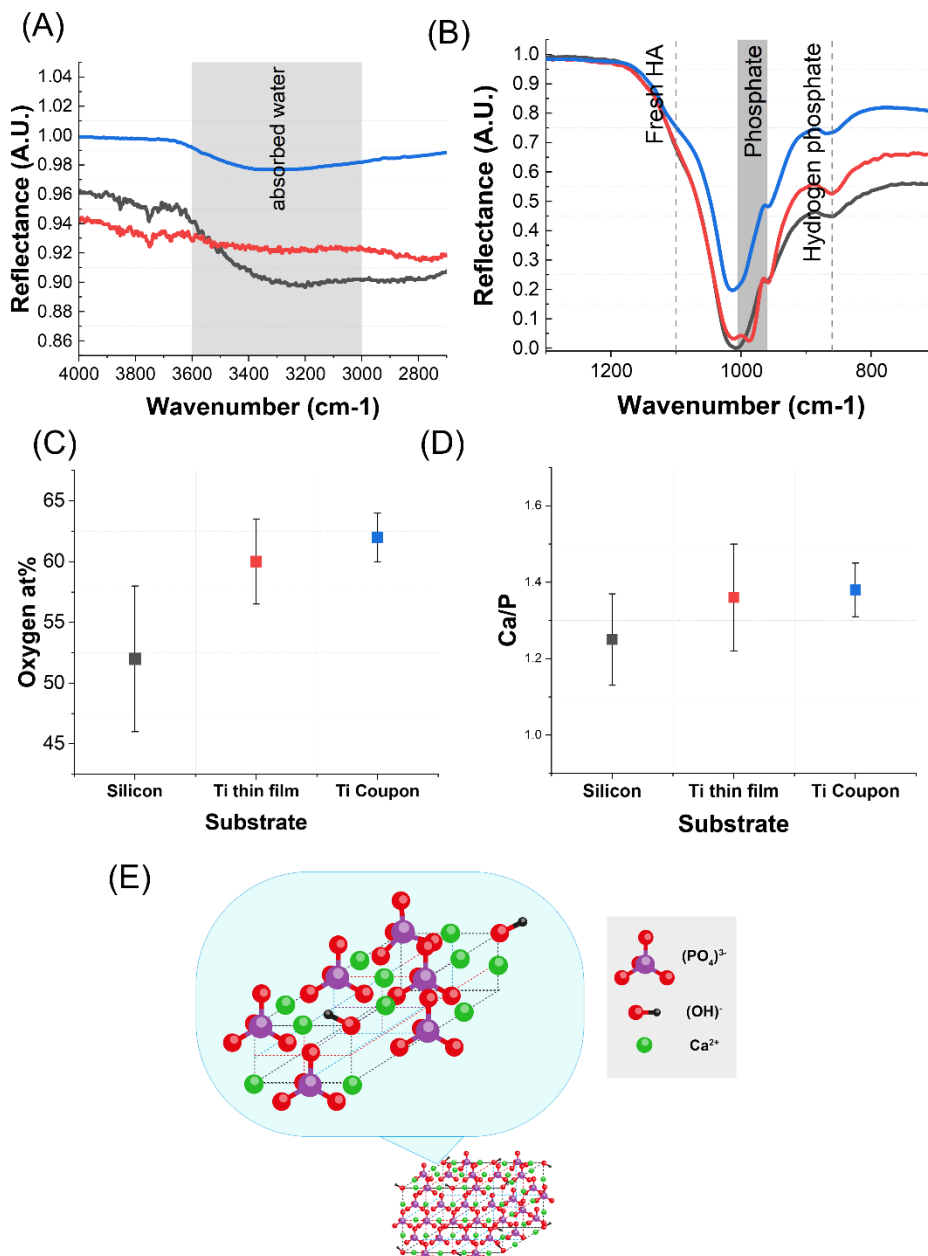


Figure 4.5:(A,B) Fourier-transform infrared spectra (FTIR) (A) in the absorbed water region of 4000–2000 cm^{-1} and (B) in the phosphate region of 1300–700 cm^{-1} of the full deposited HA layer over all three substrates: silicon (grey line), Ti thin film (red line), and Ti coupon (blue line). (C,D) . (E) Crystal structure of hydroxyapatite. For better visualisation, some atoms have been removed from the diagram. The diagram has been constructed from the literature [74,75].

The unit cell of pure HA, formula $\text{Ca}_{10}(\text{PO}_4)_6(\text{OH})$, has hydroxyl ions at the corners of the planes; additionally, phosphate anions and Ca^{2+} cations formed a hexagonal $\text{P6}_3/\text{m}$ space group, as seen in **Figure 4.5E**. Other phases of HA exist, and from the data herein it became clear that HA films formed from this solution deposition process were a combination of phases. From the literature, pure HA

has a Ca/P of 1.67 and O at.% of 34.9% and amorphous calcium phosphate (ACP) $\text{Ca}_x\text{H}_y(\text{PO}_4)_z \cdot n\text{H}_2\text{O}$ has a varying Ca/P and O at.%. Most pertinent to this work was octacalcium phosphate (OCP) $\text{Ca}_8\text{H}_2(\text{PO}_4)_6 \cdot 5\text{H}_2\text{O}$, a phase which has a Ca/P of 1.33 with an O at.% of 39.7% [76]. The Ca/P of all three samples heavily indicated the dominant formation of OCP, which supported the XRD observations since the intensity of the OCP peak is greater than the intensity of the HA triple peak. OCP is similar to pure HA but has hydrated layers along the *c* axis of the lattice which would contribute to increased oxygen aided by this aqueous colloidal-solution-based deposition. It is interesting to recall the Ti thin-film samples that underwent XPS analysis, **Table 4.1**. These initial stages of deposition gave rise to Ca/P in the region of 1.23–1.24 with lower O at.% than fully formed samples at EDX. This would demonstrate that the initial phases are calcium phosphate compounds such as $\text{Ca}_3(\text{PO}_4)_2$, and we can see from XRD that it is only after two or more deposition runs that HA phases start to form, **Figure 4.4B–D**. The rate at which HA phases form is slower for silicon and less-rough Ti thin films than Ti coupons, but they are similar compositionally. Samples in this study all possessed a higher oxygen content than the known phases. This implied the presence of ACP and hydrogen phosphates, but also the presence of adsorbed water and oxides around the lattice. Silicon samples showed the highest % of O, again implying the lowest pure HA content.

4.4. Conclusion

A successful method of deposition of hydroxyapatite films using a novel colloidal solution deposition process was developed and its efficacy in coating non-bulk titanium parts was confirmed in this work. SEM-EDX data of all substrates post NaOH activation show that there is equivalent low-level sodium present across the surface of all three. However, the importance of the formation of a sodium titanate film in an activation process is very much less than previously thought. AFM and WCA analysis showed that although the two novel-type substrates were less rough than a typical titanium part, they had similar hydrophilicity. XPS data gathered from HA on Ti thin-film samples proved that the roughness of a novel substrate will alter the propensity of the substrate for HA deposition showing that, once suitable activation is reached, HA will grow. SEM data suggested that HA mineral deposits were generated after the first process run in discrete regions of

the surface. SEM also showed that after six process runs, all three substrates had widespread HA film coverage. XRD revealed the pathway by which HA grows within this process for a typical titanium part and that Ti thin-film parts follow this mechanism closely, but also that silicon has a slower growth mechanism. Through TEM analysis, the thickness and crystallinity of layers were compared. While silicon was found to have less material, all three substrates had crystalline regions within an amorphous matrix. The chemical composition of the film, determined from FTIR and SEM-EDX data, showed that all three had ACP and OCP present with a limited proportion of pure HA, but that the silicon had higher impurities.

Overall, we confirmed that a Ti thin film can support the growth of an HA layer in an equivalent manner as a Ti coupon part. This opens the possibility of coating non-bulk metallic orthopaedic implants, such as plastic, via simple titanium deposition. Ongoing work suggests these methods can be applied for many different substrates.

4.5 Appendix Chapter 4

Appendix 4.5.1 Water contact angle and Roughness data

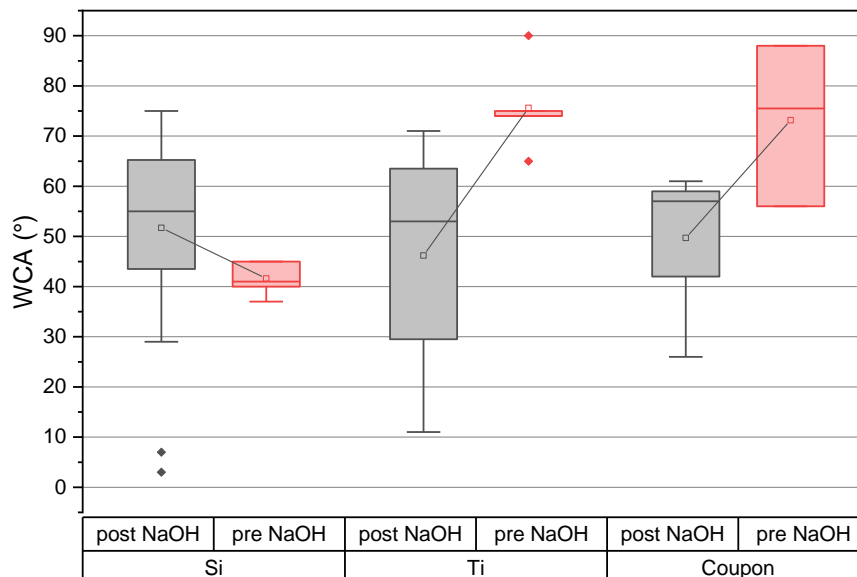


Figure A4.1: WCA in ° measured for each substrate pre and post activation.

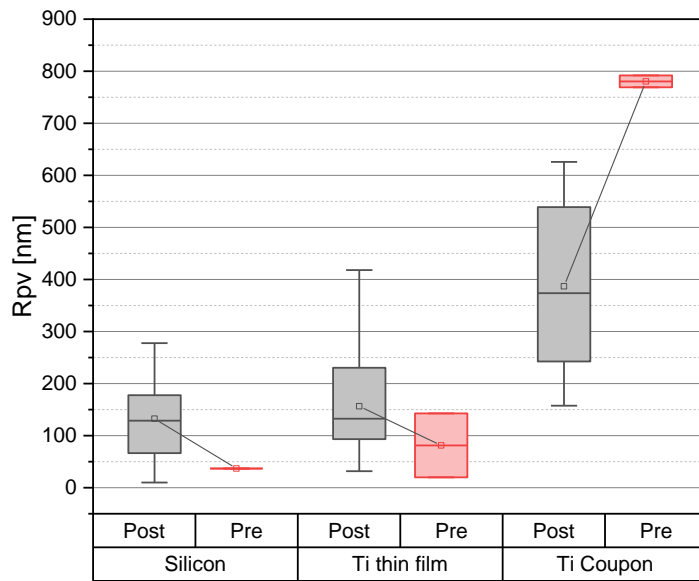


Figure A4.2: The peak-to-valley (Rpv) roughness of the three substrates pre- and post-activation as measured by atomic force microscopy.

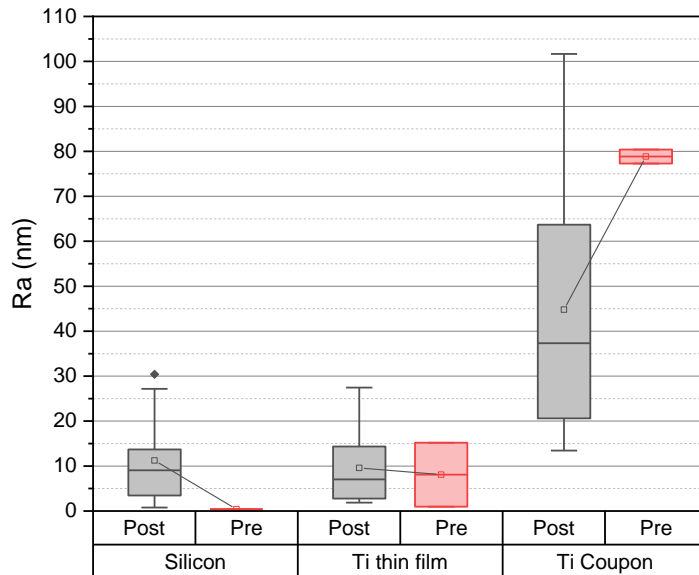


Figure A4.3: The average roughness (Ra) of the three substrates pre- and post-activation as measured by atomic force microscopy.

In **Figure A4.2** and **A4.3** it is clear that the roughness of the coupons decreases post NaOH activation, this is likely due to the cleaning effect that the NaOH has on the coupons. Since the coupons have been sourced from the industry partner

and unlike the wafer have not been used 'fresh' a certain amount of inorganic matter and oxidation would have occurred prior NaOH and thus this is removed by the treatment.

Appendix 4.5.2 XPS Survey scans of Ti thin film samples

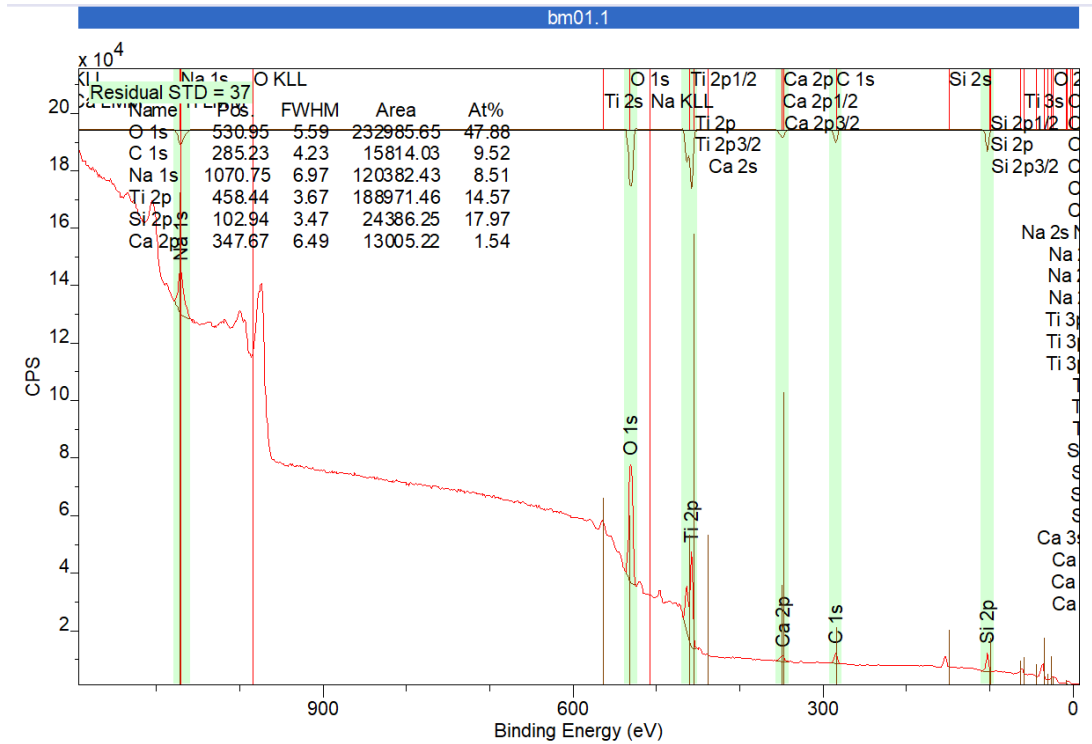


Figure A4.4: X-ray Photoelectron spectroscopy analysis, showing the Survey Scan of HA coated titanium thin film (Sample 1), Y-axis: counts per second [CPS] versus X-axis: binding energy [eV]

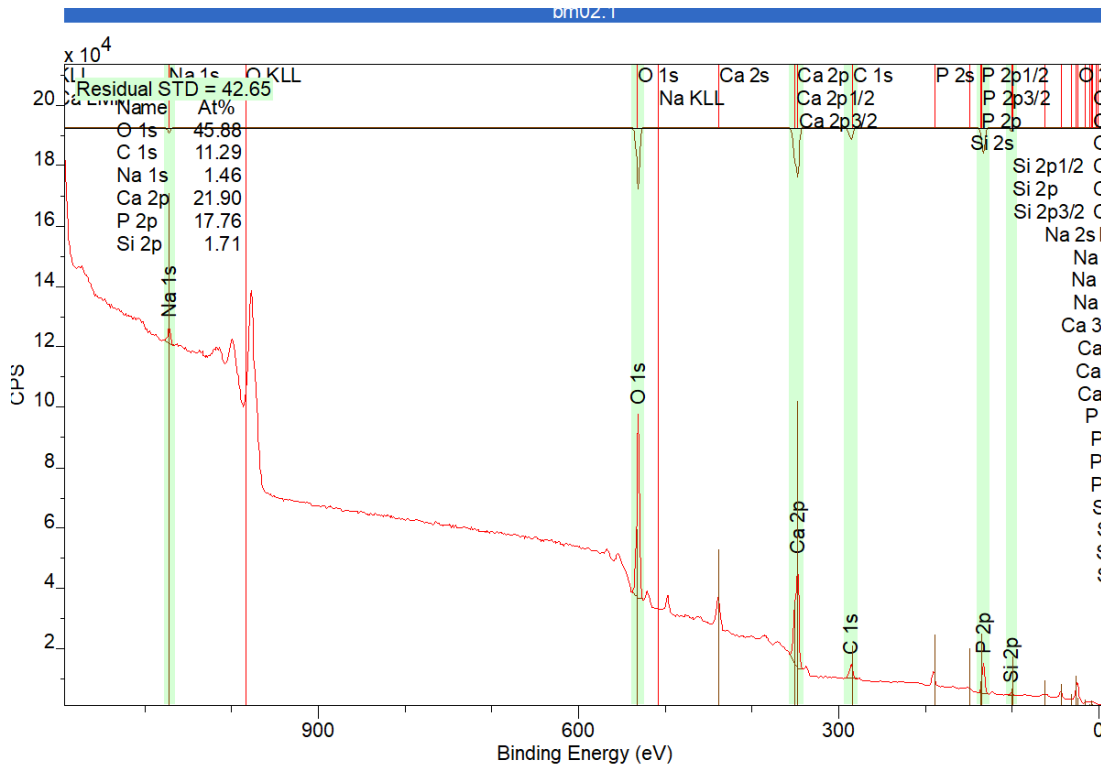


Figure A4.5: X-ray Photoelectron spectroscopy analysis, showing the Survey Scan of HA coated titanium thin film (Sample 2), Y-axis: counts per second [CPS] versus X-axis: binding energy [eV]

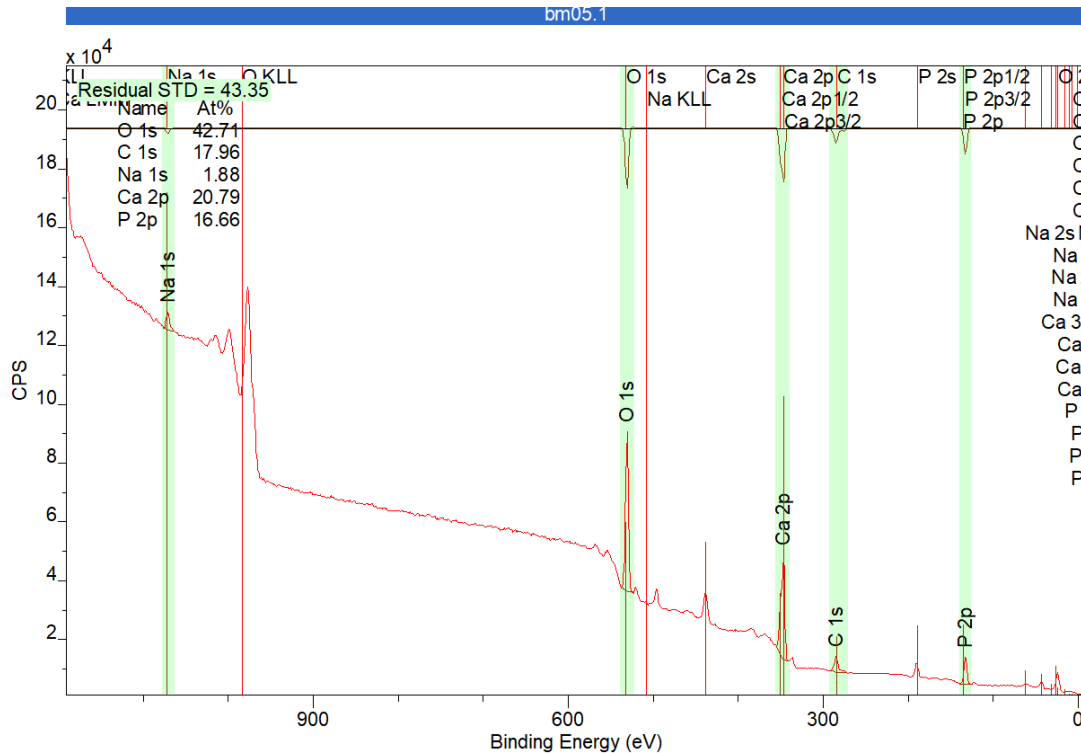


Figure A4.6: X-ray Photoelectron spectroscopy analysis, showing the Survey Scan of HA coated titanium thin film (Sample 3), Y-axis: counts per second [CPS] versus X-axis: binding energy [eV]

4.6 References

- [1] H. S. Dobbs and J. T. Scales, "Behavior of Commercially Pure Titanium and Ti-318 (Ti-6Al-4V) in Orthopedic Implants," *Titanium Alloys in Surgical Implants*, Jan. 1983, doi: 10.1520/STP28942S.
- [2] G. M. Keegan, I. D. Learmonth, and C. Case, "A Systematic Comparison of the Actual, Potential, and Theoretical Health Effects of Cobalt and Chromium Exposures from Industry and Surgical Implants," *Critical Reviews in Toxicology*, vol. 38, no. 8, pp. 645–674, Jan. 2008, doi: 10.1080/10408440701845534.
- [3] C. Skjöldebrand, J. L. Tipper, P. Hatto, M. Bryant, R. M. Hall, and C. Persson, "Current status and future potential of wear-resistant coatings and articulating surfaces for hip and knee implants," *Materials Today Bio*, vol. 15, p. 100270, Jun. 2022, doi: 10.1016/j.mtbio.2022.100270.
- [4] E. Chua and D. Shah, "Hip and Knee Arthroplasty: A Review of Complications and Advances in Imaging," *Journal of Arthroscopy and Joint Surgery*, vol. 10, no. 2, p. 44, Jun. 2023, doi: 10.4103/jajs.jajs_142_22.
- [5] T. M. Grupp, T. Weik, W. Bloemer, and H.-P. Knaebel, "Modular titanium alloy neck adapter failures in hip replacement - failure mode analysis and influence of implant material," *BMC Musculoskeletal Disorders*, vol. 11, no. 1, p. 3, Jan. 2010, doi: 10.1186/1471-2474-11-3.
- [6] A. Siddiqi, A. G. T. Payne, R. K. D. Silva, and W. J. Duncan, "Titanium allergy: could it affect dental implant integration?," *Clinical Oral Implants Research*, vol. 22, no. 7, pp. 673–680, 2011, doi: 10.1111/j.1600-0501.2010.02081.x.
- [7] I. Swiatkowska, N. Martin, and A. J. Hart, "Blood titanium level as a biomarker of orthopaedic implant wear," *Journal of Trace Elements in Medicine and Biology*, vol. 53, pp. 120–128, May 2019, doi: 10.1016/j.jtemb.2019.02.013.
- [8] M. Niinomi and M. Nakai, "Titanium-Based Biomaterials for Preventing Stress Shielding between Implant Devices and Bone," *Int J Biomater*, vol. 2011, p. 836587, 2011, doi: 10.1155/2011/836587.
- [9] Y. D. Shi, L. N. Wang, S. X. Liang, Q. Zhou, and B. Zheng, "A high Zr-containing Ti-based alloy with ultralow Young's modulus and ultrahigh strength and elastic admissible strain," *Materials Science and Engineering: A*, vol. 674, pp. 696–700, Sep. 2016, doi: 10.1016/j.msea.2016.08.038.
- [10] M. H. C. Tan, A. D. Baghi, R. Ghomashchi, W. Xiao, and R. H. Oskouei, "Effect of niobium content on the microstructure and Young's modulus of Ti-xNb-7Zr alloys for medical implants," *Journal of the Mechanical Behavior of Biomedical Materials*, vol. 99, pp. 78–85, Nov. 2019, doi: 10.1016/j.jmbbm.2019.07.014.
- [11] M. Nakai, M. Niinomi, X. Zhao, and X. Zhao, "Self-adjustment of Young's modulus in biomedical titanium alloys during orthopaedic operation," *Materials Letters*, vol. 65, no. 4, pp. 688–690, Feb. 2011, doi: 10.1016/j.matlet.2010.11.006.
- [12] C. M. Arnholt *et al.*, "Corrosion Damage and Wear Mechanisms in Long-Term Retrieved CoCr Femoral Components for Total Knee Arthroplasty," *The Journal of Arthroplasty*, vol. 31, no. 12, pp. 2900–2906, Dec. 2016, doi: 10.1016/j.arth.2016.05.006.
- [13] L. P. Webber, H.-L. Chan, and H.-L. Wang, "Will Zirconia Implants Replace Titanium Implants?," *Applied Sciences*, vol. 11, no. 15, Art. no. 15, Jan. 2021, doi: 10.3390/app11156776.
- [14] M. F. Kunrath, S. Gupta, F. Lorusso, A. Scarano, and S. Noubissi, "Oral Tissue Interactions and Cellular Response to Zirconia Implant-Prosthetic Components: A Critical Review," *Materials*, vol. 14, no. 11, Art. no. 11, Jan. 2021, doi: 10.3390/ma14112825.
- [15] H. Abitha, V. Kavitha, B. Gomathi, and B. Ramachandran, "A recent investigation on shape memory alloys and polymers based materials on bio artificial implants-hip and knee joint," *Materials Today: Proceedings*, vol. 33, pp. 4458–4466, Jan. 2020, doi: 10.1016/j.matpr.2020.07.711.

- [16] M. Saad, S. Akhtar, and S. Srivastava, "Composite Polymer in Orthopedic Implants: A Review," *Materials Today: Proceedings*, vol. 5, no. 9, Part 3, pp. 20224–20231, Jan. 2018, doi: 10.1016/j.matpr.2018.06.393.
- [17] N. F. Ismail, S. Shuib, A. Z. Romli, and N. H. Saeid, "Epoxy-Coated of Bamboo Fibre Reinforced Polymer Composite for Uncemented Total Hip Replacement (THR) Application," p. 11.
- [18] D. Bairagi and S. Mandal, "A comprehensive review on biocompatible Mg-based alloys as temporary orthopaedic implants: Current status, challenges, and future prospects," *Journal of Magnesium and Alloys*, vol. 10, no. 3, pp. 627–669, Mar. 2022, doi: 10.1016/j.jma.2021.09.005.
- [19] V. Tsakiris, C. Tardei, and F. M. Clicinschi, "Biodegradable Mg alloys for orthopedic implants – A review," *Journal of Magnesium and Alloys*, vol. 9, no. 6, pp. 1884–1905, Nov. 2021, doi: 10.1016/j.jma.2021.06.024.
- [20] M. J. Zafar, D. Zhu, and Z. Zhang, "3D Printing of Bioceramics for Bone Tissue Engineering," *Materials*, vol. 12, no. 20, Art. no. 20, Jan. 2019, doi: 10.3390/ma12203361.
- [21] R. Rodriguez Colon *et al.*, "The presence of 3D printing in orthopedics: A clinical and material review," *Journal of Orthopaedic Research*, vol. 41, no. 3, pp. 601–613, 2023, doi: 10.1002/jor.25388.
- [22] Y. Wu *et al.*, "An overview of 3D printed metal implants in orthopedic applications: Present and future perspectives," *Heliyon*, vol. 9, no. 7, Jul. 2023, doi: 10.1016/j.heliyon.2023.e17718.
- [23] Z. Jing *et al.*, "Functionalization of 3D-printed titanium alloy orthopedic implants: a literature review," *Biomed. Mater.*, vol. 15, no. 5, p. 052003, Aug. 2020, doi: 10.1088/1748-605X/ab9078.
- [24] G. Szczęsny, M. Kopec, D. J. Politis, Z. L. Kowalewski, A. Łazarski, and T. Szolc, "A Review on Biomaterials for Orthopaedic Surgery and Traumatology: From Past to Present," *Materials*, vol. 15, no. 10, Art. no. 10, Jan. 2022, doi: 10.3390/ma15103622.
- [25] C. Auclair-Daigle, M. N. Bureau, J.-G. Legoux, and L. Yahia, "Bioactive hydroxyapatite coatings on polymer composites for orthopedic implants," *Journal of Biomedical Materials Research Part A*, vol. 73A, no. 4, pp. 398–408, 2005, doi: 10.1002/jbm.a.30284.
- [26] G. Balasundaram and T. J. Webster, "An Overview of Nano-Polymers for Orthopedic Applications," *Macromolecular Bioscience*, vol. 7, no. 5, pp. 635–642, 2007, doi: 10.1002/mabi.200600270.
- [27] J. Qi *et al.*, "Influence of a hard transition layer on the microstructure and properties of diamond-like carbon/hydroxyapatite composite coating prepared by magnetron sputtering," *Journal of the European Ceramic Society*, vol. 41, no. 6, pp. 3731–3742, Jun. 2021, doi: 10.1016/j.jeurceramsoc.2021.01.006.
- [28] S. Awasthi, S. K. Pandey, E. Arunan, and C. Srivastava, "A review on hydroxyapatite coatings for the biomedical applications: experimental and theoretical perspectives," *J. Mater. Chem. B*, vol. 9, no. 2, pp. 228–249, Jan. 2021, doi: 10.1039/D0TB02407D.
- [29] V. G. DileepKumar *et al.*, "A review on the synthesis and properties of hydroxyapatite for biomedical applications," *Journal of Biomaterials Science, Polymer Edition*, vol. 33, no. 2, pp. 229–261, Jan. 2022, doi: 10.1080/09205063.2021.1980985.
- [30] C.-H. Huang and M. Yoshimura, "Biocompatible hydroxyapatite ceramic coating on titanium alloys by electrochemical methods via Growing Integration Layers [GIL] strategy: A review," *Ceramics International*, vol. 49, no. 14, Part B, pp. 24532–24540, Jul. 2023, doi: 10.1016/j.ceramint.2022.12.248.
- [31] J. Singh, J. P. Singh, S. Kumar, and H. S. Gill, "Short review on hydroxyapatite powder coating for SS 316L," *Journal of Electrochemical Science and Engineering*, vol. 13, no. 1, pp. 25–39, Feb. 2023, doi: 10.5599/jese.1611.
- [32] A. T. Guner and C. Meran, "A review on plasma sprayed titanium and hydroxyapatite coatings on polyetheretherketone implants," *International Journal of Surface Science and Engineering*, vol. 13, no. 4, pp. 237–262, Jan. 2019, doi: 10.1504/IJSURFSE.2019.103923.

- [33] B. Singh, G. Singh, B. S. Sidhu, and N. Bhatia, "In-vitro assessment of HA-Nb coating on Mg alloy ZK60 for biomedical applications," *Materials Chemistry and Physics*, vol. 231, pp. 138–149, Jun. 2019, doi: 10.1016/j.matchemphys.2019.04.037.
- [34] F. Sharifianjazi *et al.*, "Hydroxyapatite consolidated by zirconia: applications for dental implant," *Journal of Composites and Compounds*, vol. 2, no. 2, Art. no. 2, Mar. 2020, doi: 10.29252/jcc.2.1.4.
- [35] P. Bansal, G. Singh, and H. S. Sidhu, "Investigation of surface properties and corrosion behavior of plasma sprayed HA/ZnO coatings prepared on AZ31 Mg alloy," *Surface and Coatings Technology*, vol. 401, p. 126241, Nov. 2020, doi: 10.1016/j.surfcoat.2020.126241.
- [36] H.-L. Yao *et al.*, "Improved corrosion resistance of AZ91D magnesium alloy coated by novel cold-sprayed Zn-HA/Zn double-layer coatings," *Ceramics International*, vol. 46, no. 6, pp. 7687–7693, Apr. 2020, doi: 10.1016/j.ceramint.2019.11.271.
- [37] W. Yu *et al.*, "Novel fluoridated hydroxyapatite/MAO composite coating on AZ31B magnesium alloy for biomedical application," *Applied Surface Science*, vol. 464, pp. 708–715, Jan. 2019, doi: 10.1016/j.apsusc.2018.09.148.
- [38] A. M. Fathi, M. K. Ahmed, M. Afifi, A. A. Menazea, and V. Uskoković, "Taking Hydroxyapatite-Coated Titanium Implants Two Steps Forward: Surface Modification Using Graphene Mesolayers and a Hydroxyapatite-Reinforced Polymeric Scaffold," *ACS Biomater. Sci. Eng.*, vol. 7, no. 1, pp. 360–372, Jan. 2021, doi: 10.1021/acsbiomaterials.0c01105.
- [39] G. Prashar and H. Vasudev, "Understanding cold spray technology for hydroxyapatite deposition," *Journal of Electrochemical Science and Engineering*, vol. 13, no. 1, pp. 41–62, Feb. 2023, doi: 10.5599/jese.1424.
- [40] S. M. Baligheid, A. C. Maharudresh, T. Arunkumar, K. N. Bharath, and S. Abdullah, "Investigation on performance of hybrid coating of hydroxyapatite and reduced graphene oxide on polyether ether ketone for orthopaedic application," *Prog Addit Manuf*, Jun. 2023, doi: 10.1007/s40964-023-00464-1.
- [41] T. G. P. Galindo, Y. Chai, and M. Tagaya, "Hydroxyapatite Nanoparticle Coating on Polymer for Constructing Effective Biointeractive Interfaces," *Journal of Nanomaterials*, vol. 2019, p. e6495239, Jan. 2019, doi: 10.1155/2019/6495239.
- [42] J. Li *et al.*, "A two-step strategy to deposit a hydroxyapatite coating on polydopamine-coated polymer fibers," *Biomed. Mater.*, vol. 18, no. 1, p. 015025, Dec. 2022, doi: 10.1088/1748-605X/aca85a.
- [43] N. Kaushik, L. Nhat Nguyen, J. H. Kim, E. H. Choi, and N. Kumar Kaushik, "Strategies for Using Polydopamine to Induce Biomineralization of Hydroxyapatite on Implant Materials for Bone Tissue Engineering," *International Journal of Molecular Sciences*, vol. 21, no. 18, Art. no. 18, Jan. 2020, doi: 10.3390/ijms21186544.
- [44] M. Li *et al.*, "Electrophoretic deposition and electrochemical behavior of novel graphene oxide-hyaluronic acid-hydroxyapatite nanocomposite coatings," *Applied Surface Science*, vol. 284, pp. 804–810, Nov. 2013, doi: 10.1016/j.apsusc.2013.08.012.
- [45] P. Strąkowska, R. Beutner, M. Gnyba, A. Zielinski, and D. Scharnweber, "Electrochemically assisted deposition of hydroxyapatite on Ti6Al4V substrates covered by CVD diamond films — Coating characterization and first cell biological results," *Materials Science and Engineering: C*, vol. 59, pp. 624–635, Feb. 2016, doi: 10.1016/j.msec.2015.10.063.
- [46] S.-H. Um *et al.*, "Robust Hydroxyapatite Coating by Laser-Induced Hydrothermal Synthesis," *Advanced Functional Materials*, vol. 30, no. 48, p. 2005233, 2020, doi: 10.1002/adfm.202005233.
- [47] M. Badiceanu, S. Anghel, N. Mihailescu, A. I. Visan, C. N. Mihailescu, and I. N. Mihailescu, "Coatings Functionalization via Laser versus Other Deposition Techniques for Medical Applications: A Comparative Review," *Coatings*, vol. 12, no. 1, Art. no. 1, Jan. 2022, doi: 10.3390/coatings12010071.
- [48] A. J. Haider, T. Alawsi, M. J. Haider, B. A. Taha, and H. A. Marhoon, "A comprehensive review on pulsed laser deposition technique to effective nanostructure production: trends and

challenges," *Opt Quant Electron*, vol. 54, no. 8, p. 488, Jun. 2022, doi: 10.1007/s11082-022-03786-6.

[49] S. S. A. Abidi and Q. Murtaza, "Synthesis and Characterization of Nano-hydroxyapatite Powder Using Wet Chemical Precipitation Reaction," *Journal of Materials Science & Technology*, vol. 30, no. 4, pp. 307–310, Apr. 2014, doi: 10.1016/j.jmst.2013.10.011.

[50] S. György *et al.*, "Effect of the reaction temperature on the morphology of nanosized HAp," *J Therm Anal Calorim*, vol. 138, no. 1, pp. 145–151, Oct. 2019, doi: 10.1007/s10973-019-08255-z.

[51] S. Wen *et al.*, "Hydrothermal synthesis of hydroxyapatite coating on the surface of medical magnesium alloy and its corrosion resistance," *Progress in Natural Science: Materials International*, vol. 31, no. 2, pp. 324–333, Apr. 2021, doi: 10.1016/j.pnsc.2020.12.013.

[52] Zhang Chunyan, M. Yanlong, and L. Chenglong, "Hydroxyapatite Coating on Fluorine-treated Magnesium Alloy by Hydrothermal Method and Its Electrochemical Corrosion Behaviour in Hank's Solution," *Prot Met Phys Chem Surf*, vol. 55, no. 1, pp. 127–135, Jan. 2019, doi: 10.1134/S207020511901009X.

[53] D. He *et al.*, "Effect of hydrothermal treatment temperature on the hydroxyapatite coatings deposited by electrochemical method," *Surface and Coatings Technology*, vol. 406, p. 126656, Jan. 2021, doi: 10.1016/j.surfcoat.2020.126656.

[54] N. N. Andrusova, E. S. Zhavoronok, O. A. Legon'kova, A. S. Goncharova, and S. A. Kedik, "Polymer–Mineral Compounds for Cementless Hip Replacement," *Polym. Sci. Ser. D*, vol. 13, no. 1, pp. 68–72, Jan. 2020, doi: 10.1134/S1995421220010037.

[55] H. Zamin, T. Yabutsuka, S. Takai, and H. Sakaguchi, "Role of Magnesium and the Effect of Surface Roughness on the Hydroxyapatite-Forming Ability of Zirconia Induced by Biomimetic Aqueous Solution Treatment," *Materials*, vol. 13, no. 14, Art. no. 14, Jan. 2020, doi: 10.3390/ma13143045.

[56] J. Sun, S. Cai, J. Sun, K. Shen, J. Liu, and G. Xu, "Ultrasonic aqueous synthesis of corrosion resistant hydroxyapatite coating on magnesium alloys for the application of long-term implant," *Ultrasonics Sonochemistry*, vol. 58, p. 104677, Nov. 2019, doi: 10.1016/j.ultsonch.2019.104677.

[57] B. Yilmaz, A. E. Pazarceveren, A. Tezcaner, and Z. Evis, "Historical development of simulated body fluids used in biomedical applications: A review," *Microchemical Journal*, vol. 155, p. 104713, Jun. 2020, doi: 10.1016/j.microc.2020.104713.

[58] T. Kokubo and S. Yamaguchi, "Simulated body fluid and the novel bioactive materials derived from it," *Journal of Biomedical Materials Research Part A*, vol. 107, no. 5, pp. 968–977, 2019, doi: 10.1002/jbm.a.36620.

[59] S. Ferraris *et al.*, "Bioactive materials: In vitro investigation of different mechanisms of hydroxyapatite precipitation," *Acta Biomaterialia*, vol. 102, pp. 468–480, Jan. 2020, doi: 10.1016/j.actbio.2019.11.024.

[60] M. C. de Andrade, M. R. Figueiras, and T. Ogasawara, "Nucleation and growth of hydroxyapatite on titanium pretreated in NaOH solution: experiments and thermodynamic explanation," *J Biomed Mater Res*, vol. 46, no. 4, pp. 441–446, Sep. 1999, doi: 10.1002/(sici)1097-4636(19990915)46:4<441::aid-jbm1>3.0.co;2-9.

[61] C. Kim *et al.*, "Comparison of titanium soaked in 5 M NaOH or 5 M KOH solutions," *Mater Sci Eng C Mater Biol Appl*, vol. 33, no. 1, pp. 327–339, Jan. 2013, doi: 10.1016/j.msec.2012.08.047.

[62] D. K. Pattanayak, S. Yamaguchi, T. Matsushita, and T. Kokubo, "Nanostructured positively charged bioactive TiO₂ layer formed on Ti metal by NaOH, acid and heat treatments," *J Mater Sci: Mater Med*, vol. 22, no. 8, pp. 1803–1812, Aug. 2011, doi: 10.1007/s10856-011-4372-x.

[63] Y. Luo, Y. Jiang, J. Zhu, J. Tu, and S. Jiao, "Surface treatment functionalization of sodium hydroxide onto 3D printed porous Ti6Al4V for improved biological activities and osteogenic

potencies," *Journal of Materials Research and Technology*, vol. 9, no. 6, pp. 13661–13670, Nov. 2020, doi: 10.1016/j.jmrt.2020.09.076.

[64] C. C. Chusuei, D. W. Goodman, M. J. Van Stipdonk, D. R. Justes, and E. A. Schweikert, "Calcium Phosphate Phase Identification Using XPS and Time-of-Flight Cluster SIMS," *Anal. Chem.*, vol. 71, no. 1, pp. 149–153, Jan. 1999, doi: 10.1021/ac9806963.

[65] B. Demri and D. Muster, "XPS study of some calcium compounds," *Journal of Materials Processing Technology*, vol. 55, no. 3, pp. 311–314, Dec. 1995, doi: 10.1016/0924-0136(95)02023-3.

[66] M. P. Casaletto, S. Kaciulis, G. Mattocono, A. Mezzi, L. Ambrosio, and F. Branda, "XPS characterization of biocompatible hydroxyapatite–polymer coatings," *Surface and Interface Analysis*, vol. 34, no. 1, pp. 45–49, 2002, doi: 10.1002/sia.1249.

[67] J. Stoch and J. Gablankowska-Kukucz, "The effect of carbonate contaminations on the XPS O 1s band structure in metal oxides," *Surf. Interface Anal.*, vol. 17, no. 3, pp. 165–167, Mar. 1991, doi: 10.1002/sia.740170308.

[68] L. Keller and P. Rey-Fessler, "Nondestructive Characterization of Hydroxylapatite Coated Dental Implants by XRD Method," in *Characterization and Performance of Calcium Phosphate Coatings for Implants - Emanuel Horowitz, Jack E. Parr, E. Horowitz and J. E. Parr, Eds.*, Miami, Floride, USA: ASTM International, Nov. 1992. Accessed: Aug. 17, 2022. [Online]. Available: [https://books.google.ie/books?id=BLWyUIAj9JgC&pg=PR3&lpg=PR3&dq=Characterization+and+Performance+of+Calcium+Phosphate+Coatings+for+Implants+Editor\(s\):+Emanuel+Horowitz,+Jack+E.+Parr&source=bl&ots=LWoK99oz1v&sig=ACfU3U2WnTxiblb52Tv03kAJCGT19hqS5g&hl=en&sa=X&ved=2ahUKEwi-qluz9c35AhXqSEEAHQJcAFcQ6AF6BAgCEAM#v=onepage&q=Characterization%20and%20Performance%20of%20Calcium%20Phosphate%20Coatings%20for%20Implants%20Editor\(s\)%3A%20Emanuel%20Horowitz%2C%20Jack%20E.%20Parr&f=false](https://books.google.ie/books?id=BLWyUIAj9JgC&pg=PR3&lpg=PR3&dq=Characterization+and+Performance+of+Calcium+Phosphate+Coatings+for+Implants+Editor(s):+Emanuel+Horowitz,+Jack+E.+Parr&source=bl&ots=LWoK99oz1v&sig=ACfU3U2WnTxiblb52Tv03kAJCGT19hqS5g&hl=en&sa=X&ved=2ahUKEwi-qluz9c35AhXqSEEAHQJcAFcQ6AF6BAgCEAM#v=onepage&q=Characterization%20and%20Performance%20of%20Calcium%20Phosphate%20Coatings%20for%20Implants%20Editor(s)%3A%20Emanuel%20Horowitz%2C%20Jack%20E.%20Parr&f=false)

[69] A. Ślósarczyk, Z. Paszkiewicz, and C. Paluszkiwicz, "FTIR and XRD evaluation of carbonated hydroxyapatite powders synthesized by wet methods," *Journal of Molecular Structure*, vol. 744–747, pp. 657–661, Jun. 2005, doi: 10.1016/j.molstruc.2004.11.078.

[70] C. Chappard, G. André, M. Daudon, and D. Bazin, "Analysis of hydroxyapatite crystallites in subchondral bone by Fourier transform infrared spectroscopy and powder neutron diffraction methods," *Comptes Rendus Chimie*, vol. 19, no. 11–12, pp. 1625–1630, Nov. 2016, doi: 10.1016/j.crci.2015.03.015.

[71] W. E. Brown, J. P. Smith, J. R. Lehr, and A. W. Frazier, "Octacalcium Phosphate and Hydroxyapatite: Crystallographic and Chemical Relations between Octacalcium Phosphate and Hydroxyapatite," *Nature*, vol. 196, no. 4859, pp. 1050–1055, Dec. 1962, doi: 10.1038/1961050a0.

[72] I. Rehman and W. Bonfield, "Characterization of hydroxyapatite and carbonated apatite by photo acoustic FTIR spectroscopy," *Journal of Materials Science: Materials in Medicine*, vol. 8, no. 1, pp. 1–4, 1997, doi: 10.1023/A:1018570213546.

[73] A. Ślósarczyk, C. Paluszkiwicz, M. Gawlicki, and Z. Paszkiewicz, "The FTIR spectroscopy and QXRD studies of calcium phosphate based materials produced from the powder precursors with different ratios," *Ceramics International*, vol. 23, no. 4, pp. 297–304, Jan. 1997, doi: 10.1016/S0272-8842(96)00016-8.

[74] S. Rujitanapanich, P. Kumpapan, and P. Wanjanoi, "Synthesis of Hydroxyapatite from Oyster Shell via Precipitation," *Energy Procedia*, vol. 56, pp. 112–117, 2014, doi: 10.1016/j.egypro.2014.07.138.

[75] L. Pramatarova and E. Pecheva, *Modified Inorganic Surfaces as a Model for Hydroxyapatite Growth*. Trans Tech Publications Limited, 2006.

[76] M. T. Carayon and J. L. Lacout, "Study of the Ca/P atomic ratio of the amorphous phase in plasma-sprayed hydroxyapatite coatings," *Journal of Solid State Chemistry*, vol. 172, no. 2, pp. 339–350, May 2003, doi: 10.1016/S0022-4596(02)00085-3.

Chapter 5: Nano Sized Gallium Oxide Surface Features for Enhanced Antimicrobial and Osteo-Integrative Responses

Abstract

Gallium oxide has known beneficial osteo-integrative properties. This may have importance for improving the osteointegration of orthopaedic implants. At high concentrations gallium is cytotoxic. Therefore, integration of gallium into implant devices must be carefully controlled to limit its concentration and release. A strategy based on surface doping of gallium, although challenging, seems an appropriate approach to limit dose amounts to minimise cytotoxicity and maximise osteointegration benefits. In this work we develop a novel form of patterned surface doping via a block copolymer-based surface chemistry that enables extremely low gallium content but enhanced osteogenesis as proven by comprehensive bioassays. Polystyrene-b-poly 4vinyl pyridine (PS-b-P4VP) BCP (block copolymer) films were produced on surfaces. Selective infiltration of the BCP pattern with a gallium salt precursor solution and subsequent UV-ozone treatment produced a surface pattern of gallium oxide nanodots as evidenced by atomic force and scanning electron microscopy. A comprehensive study of the bioactivity was conducted, including antimicrobial and sterility testing, gallium ion release kinetics and the interaction with human marrow mesenchymal stromal cells and mononuclear cells. Comparing the data from osteogenesis media assay tests with osteoclastogenesis tests demonstrated the potential for the gallium oxide nanodot doping to improve osteointegration properties of a surface.

5.1. Introduction

Orthopaedic implants are profoundly important to human health in maintaining patient mobility and well-being. Improving osteointegration of the implants is a key target since surgery is not always as beneficial or as long lasting as hoped, often due to underlying patient conditions but also due to problems derived from poor initial, or degradation of, fixation. Pooled registry data suggests that the survivorship after 25 years for total knee replacement is 82% but much lower for total hip replacement at 58%. [1,2] Arthroplasty failures mainly arise from a number of factors including three core factors.[3,4] These are: 1. aseptic

loosening of the joint, 2. post-operative infection at the site of the surgery and 3. particle-induced osteolysis around the implant. Aseptic loosening can be the result of inadequate initial fixation, mechanical loss of fixation over time, or biologic loss of fixation, and is associated with elevated osteoclast activity inhibiting bone growth.[5–7] Overall failure occurs in about 10-30% of patients and depends on genetic or health factors and is predicted to increase into the future as life expectancy improves.[8–10]

Surface engineering of the implant is a key strategy in overcoming aseptic loosening and research is being directed towards novel materials or enhancement of existing materials by doping with active materials that control osteoclasts and enhance osteoblast formation.[11–13] Current non-cemented knee or hip implants are generally cobalt-chromium or titanium alloys, often with a pre-deposited hydroxyapatite (HA) coating for improved osteointegration.[14,15] Inorganic doping of HA with elements such as strontium, silver, europium and zinc can induce a preferential biological response.[16–22] However, the drawback to some of these emerging methods is reduction in the necessary hydroxyl groups for bone growth[23] and strong antimicrobial activity resulting in reduced bone growth.[24] There are also issues regarding the intercalation of ions into HA[25–27] and, despite both laboratory and animal studies, there remains a need for more detailed understanding or optimisation of bone regeneration from these compounds.[28,29] There is a significant need to study the effects of dopant ions on bone stem cells prior to incorporating them into existing orthopaedic systems and this necessitates a suitable compound and delivery surface to be created.

Gallium nitrate ($\text{Ga}(\text{NO}_3)_3$) is an FDA approved drug which is used to treat hypercalcemia of malignancy and other osteo-degeneration diseases such as Paget's disease or osteoporosis in humans.[30–32] Once administered gallium nitrate forms to the aqueous ion $\text{Ga}(\text{OH})_4^-$ which is stable across a range of pH and is active as Ga^{3+} ions in blood plasma. [33] According to the FDA approval package (19-961/S-009) for the gallium nitrate drug 'Ganite' the dosage applied leads to 1134 – 2300 ng. mL⁻¹ of gallium present in blood plasma, which converted to ppm is 1.13ppm-2.3ppm. [34] Osteoclast cells have a ruffled cell membrane which promotes transferrin protein delivery and the transport of Fe^{3+}

ions which can be reduced and metabolised.[35–37] Ga^{3+} and Fe^{3+} are similar in terms of ionic radius, electronegativity and chelation action such that the body cannot differentiate between them. [38,39] Ga^{3+} substitution for Fe^{3+} prevents cell proliferation because of the highly stable redox state of the Ga^{3+} ion.[40] While gallium inhibits osteoclastic activity it has no effect on osteoblast growth and thus allows for bone regrowth to occur.[41–43] Gallium ionic levels measuring < 3 ppm in simulated bodily fluid has been shown to encourage bone growth. [44–47] Separate tests have shown that gallium ions at a concentration of 2.5mol% Ga[48] can enhance osteogenic response when incorporated into Ca-P ceramics, or, when applied directly to monocyte cells at a rate of 10^{-7} to 10^{-2} M for 7 days osteoclast proliferation was inhibited.[49]

As gallium has such strong osteogenic properties, it is an obvious choice to promote aseptic fixation and furthermore, it has beneficial antimicrobial properties.[50,51] However, the gallium concentration must be minimised as it exhibits renal toxicity. [52,53] The exact release mechanism and dosage of gallium as an orthopaedic coating is not well detailed in literature and requires model surfaces of characterised material to study biological efficacy.[54]

This work is based on the postulation that an engineered gallium doped surface is needed to control the properties for maximum effect – high concentration bulk doping may affect the bulk HA properties; partial coverage of the surface would enable both gallium release and maintain the surface HA properties and nano dimensioned features would enable rapid gallium release that could be tuned with size. We propose a unique solution for controlled osteointegration by adapting an established method of surface engineering on planar substrate surfaces. BCP self-assembly is now established technology for the development of nanoscopic arrays of polymer or inorganic features.[55,56] BCPs can be used as thin films cast on a substrate. [57–59] Infiltration of an inorganic precursor selectively into one domain of a BCP gives rise to highly ordered inorganic nanostructures that can be dimensionally accurate down to the scale of a few nanometres[60–62] but there are no studies available to show how BCP based coatings can support subsequent ionic release.[63–65] BCPs are showing promise in drug delivery via the infiltration of the BCP with conjugated drugs. [66–68] Changing the molecular weight or block ratio in a BCP allows for tuneable feature size which could be

used to control ion release for an optimum/tuneable activity[69–71] i.e. maximising osteointegration and minimising cytotoxicity. Block copolymer PS (polystyrene)-b-P4VP (poly(4-vinylpyridine)) is used in this work since the pyridine groups present in P4VP have affinity to bind metallic ions.[72,73] The use of BCP methods to nanopattern a titanium surface through oxidation has been shown to improve osteointegration but the methods used do not allow active doping or engineering of HA surfaces as described here.[74]

In congruence with the wave of emerging BCP science this work aims to harness nanoscale BCP patterns to measure the osteoinduction of gallium oxide leading to use as novel coatings or dopants for existing orthopaedic implants. In the following data, sections 5.2.4, 5.3.4 and 5.3.5 were undertaken by collaborative researchers: Mimma Maggio and Carolina Martens with the supervision of David Hoey.

5.2. Experimental Methods

5.2.1 Block Copolymer Materials

PS-b-P4VP BCP of molecular weight 32-b-4, 50-b-6 and 100-b-15.5 kg mol⁻¹ were purchased from Polymer Source Inc and used as received. A selection of molecular weights was chosen to show how nanodot size can vary by molecular weight while the geometry of the nanodots remains bcc spherical once the ratio of PS to P4VP remains between 6:1 and 8:1. All other chemicals/solvents were ex-Sigma Aldrich or Fisher Scientific. BCPs were dissolved in a solvent mixture comprising 4:1 toluene (99%): tetrahydrofuran (99%). BCP solutions were made to 0.5 wt.% concentration and stirred for 24 h. Gallium precursor solution was made up in the range of 0.1 wt.% to 2 wt.% using gallium (III)nitrate hydrate 99.9% in anhydrous ethanol (99.8%). Solutions were stirred for 1 h to ensure full dissolution of the salt.

As substrates, Ted Pella, Inc Ultra-Flat 4-inch silicon wafers were used. These ultra-flat surfaces allowed effects of surface roughness to be ignored. Some of these wafers were used as received and a subset of these underwent e-beam evaporation-deposition (Temescal FC-2000) to generate 50 nm titanium layers. All wafers were then cut to 13 mm x 13 mm coupons. To clean the coupons, they were each submerged in deionised water, acetone (>99%) and isopropyl alcohol

(>99%) for 20 min and placed into an ultra-sonic bath. Substrates were then dried using nitrogen.

5.2.2 Block Copolymer and Metal Infiltration Method

Polymer solutions were deposited onto cleaned substrates using an SCS G3 Spin Coater for 30 s. As spun samples were then solvent annealed towards an ordered BCP arrangement by placement at the bottom of a glass solvent vapor annealing jar. A 7 ml vial of chloroform was also placed into this jar and the jar was sealed in a fridge at 4 °C for 2 h. To fully enhance the micro-phase separation of the BCP film, samples are next immersed in 100% ethanol for 15 min.

Infiltration was performed by spin-on of the gallium-ethanol solutions. Samples were then placed in a Novascan PSD Pro UV Lamp for 3 h at a distance of 2 cm; this removed the organic polymeric layer and resulted in gallium oxide nanodots.

5.2.3 Characterisation of Gallium Nanodot Samples

Atomic Force Microscopy (AFM) was performed using an aXE-7, Park Systems AFM with non-contact cantilevers. Scanning Electron Microscopy (SEM) data were collected using a Carl Zeiss Ultra Microscope equipped with an in-Lens detector. An accelerating voltage of 5 to 10 kV was used. X-ray Photoelectron Spectroscopy (XPS) data were gathered using VG Scientific ESCA lab Mk II performed under ultrahigh vacuum conditions ($<5 \times 10^{-10}$ mbar). Analysis was conducted using CasaXPS software. Sterility Testing was conducted by submergence in nutrient broth and incubated at 30 °C for 20 days. Nutrient broth was made up of 2 parts tryptone, 1-part meat extract and 1-part NaCl.

5.3. Results and Discussion

5.3.1. Gallium Included into a Nanodot Array on a Surface

Post solvent annealing, polymer patterns were infiltrated with gallium salt solutions and oxidised to give rise to metallic nanodots. Atomic Force Microscopy (AFM) data revealed well-ordered patterns for silicon and titanium substrates, see **Figure 5.1(A-F)** which shows results obtained using PS-*b*-P4VP Block Copolymer (BCP) of molecular weight 32-*b*-4, 50-*b*-6 and 100-*b*-15.5 kg mol⁻¹ formed from 0.5 wt% gallium precursor. The block composition ensures the BCP self-assembly yields a body centre cubic spherical array.[55,78] The dot size as measured by AFM was tightly aligned within its BCP grouping, with the polymer 100-*b*-15.5 kg mol⁻¹ having the largest diameter (59±3 nm for Si and 55±3 nm for

Ti) and height (5 ± 1 nm for Si and 6 ± 2 nm for Ti). The overall dot coverage as a percentage of total area was between 70% and 83% for all samples, **Figure 5.1 (G-I)**. Scanning electron microscopy reveals good sample coverage with silicon samples having clearer dot definition, **Figure 5.1 (J and K)**. This data proves that the ratio between the PS and P4VP components of the BCP along with the SVA settings gives rise to matching arrays of nanodots. However, by changing the magnitude of the PS and P4VP molecular weights, it was proven that the nanodot itself could be increased or decreased in size. The ability to alter geometry and size within BCP chemistry is one of the reasons they have been chosen in this work. To keep certain process variables constant, within sample sets only one polymer was used, for example all biological testing was conducted using 100-b-15.5 kg mol⁻¹ with varying gallium precursor solution concentrations.

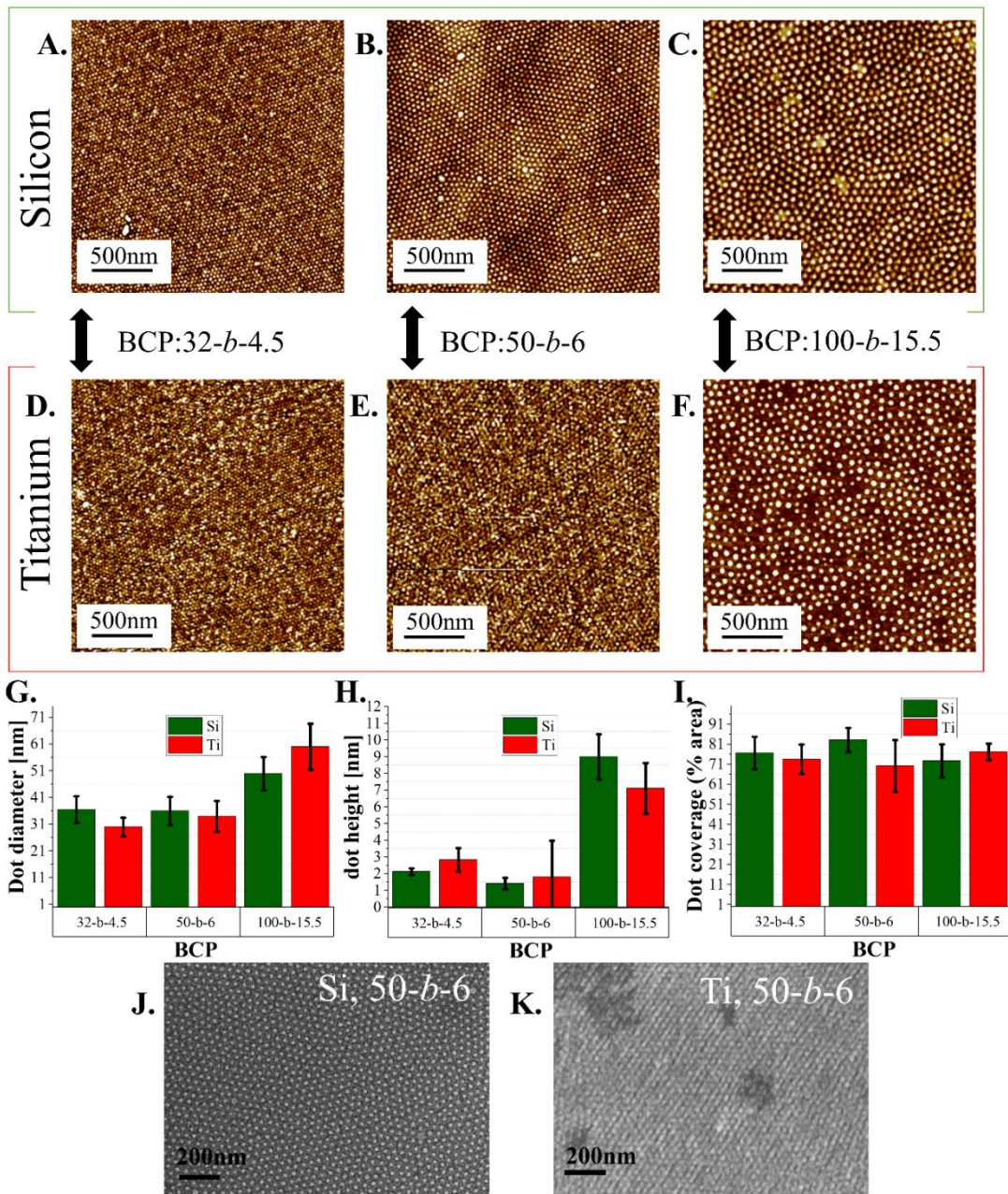


Figure 5.1: A-F: Atomic Force Microscopy (non-contact mode) images of nanodot arrays post gallium infiltration and oxidation yielding regular patterning dot array. Images are grouped by BCP used and specific substrate. G: Bar chart of mean nanodot diameter in nm grouped by BCP and coloured by substrate. H: Bar chart of mean nanodot height in nm grouped by BCP and coloured by substrate. I: Percentage area covered by the dots as measured by Image J particle analysis grouped by BCP and coloured by substrate. J: Scanning electron micrograph of gallium nanodots formed on silicon substrate using 50-b-6 BCP and K: Scanning electron micrograph of gallium nanodots formed on titanium substrate using 50-b-6 BCP

The inclusion of gallium post UV-ozone oxidation into the P4VP dot in the BCP matrix was confirmed by X-ray Photoelectron Spectroscopy (XPS), **Figure 5.2(A-C)**, Energy Dispersive X-ray Spectroscopy (**Appendix 5.4.2**) and was similar for both substrates. **Figure 5.2A** shows XPS Survey data with gallium features for Ga 2s, Ga 2p, Ga Auger (LMM) and Ga 3d transitions while also showing the presence of O1s and C1s. There was no indication of a N1s feature confirming full removal of the polymeric material. **Figure 5.2(B,C)** depict core scans of the Ga 2p doublet peaks which are narrow peaks without shoulders implying a single Ga gallium oxidation state. The binding energy of the Ga 2p 3/2 and 1/2 peaks at 1119.5 and 1146.5 eV respectively (for both substrates) and an area ratio of 1:2 suggest the compound is Ga₂O₃. [79,80]

5.3.2 Nano Surfaces Facilitate a Controlled Release of Gallium

Analysing the ionic release of gallium from the surface on these samples is important as their intended biological response would be dependent on a controlled dissolution *in vitro*. Both silicon and titanium surfaces coated with nanodots infiltrated with a precursor of 0.5 wt.% gallium concentration were immersed in PBS to replicate *in vivo* conditions for 1,2,3,5,10,15, and 20 days (**Figure 5.2D**). Inductively Coupled Plasma Optical Emission Spectroscopy (ICP-OES) was used to measure the gallium concentration in PBS. **Figure 5.2D** shows that after 1 day 0.09-0.095 ppm gallium is detected increasing to 0.11-0.12 ppm after 5 days before reaching limiting values of 0.12-0.13 ppm after 20 days. The levels detected in parts per million are at the lower end of medical gallium levels (i.e., < 4 ppm) and consistent with target values to limit cytotoxicity, demonstrating a localised release of therapeutically relevant gallium.

To allow for a comparative measure of gallium dosage, nanodot samples were made from gallium precursor of 0.125, 0.5 and 1 wt.% on silicon and immersed in PBS for 24 hours. Data shown in **Figure 5.2E** proves that higher gallium precursor concentration presents a higher ionic release. This data demonstrates the tuneability of the gallium release and is purposely targeted far below existing drugs as it represents a smaller surface area than an implant but is also creating readily active gallium oxide for media interaction unlike existing methods. Samples provided for further biological testing were 1 wt.% Ga (0.18 ppm ± 0.02)

and a much smaller ionic release 0.125 wt.% sample (0.04 ppm \pm 0.02, it is worth noting that this is near the detection limit of the ICP device.)

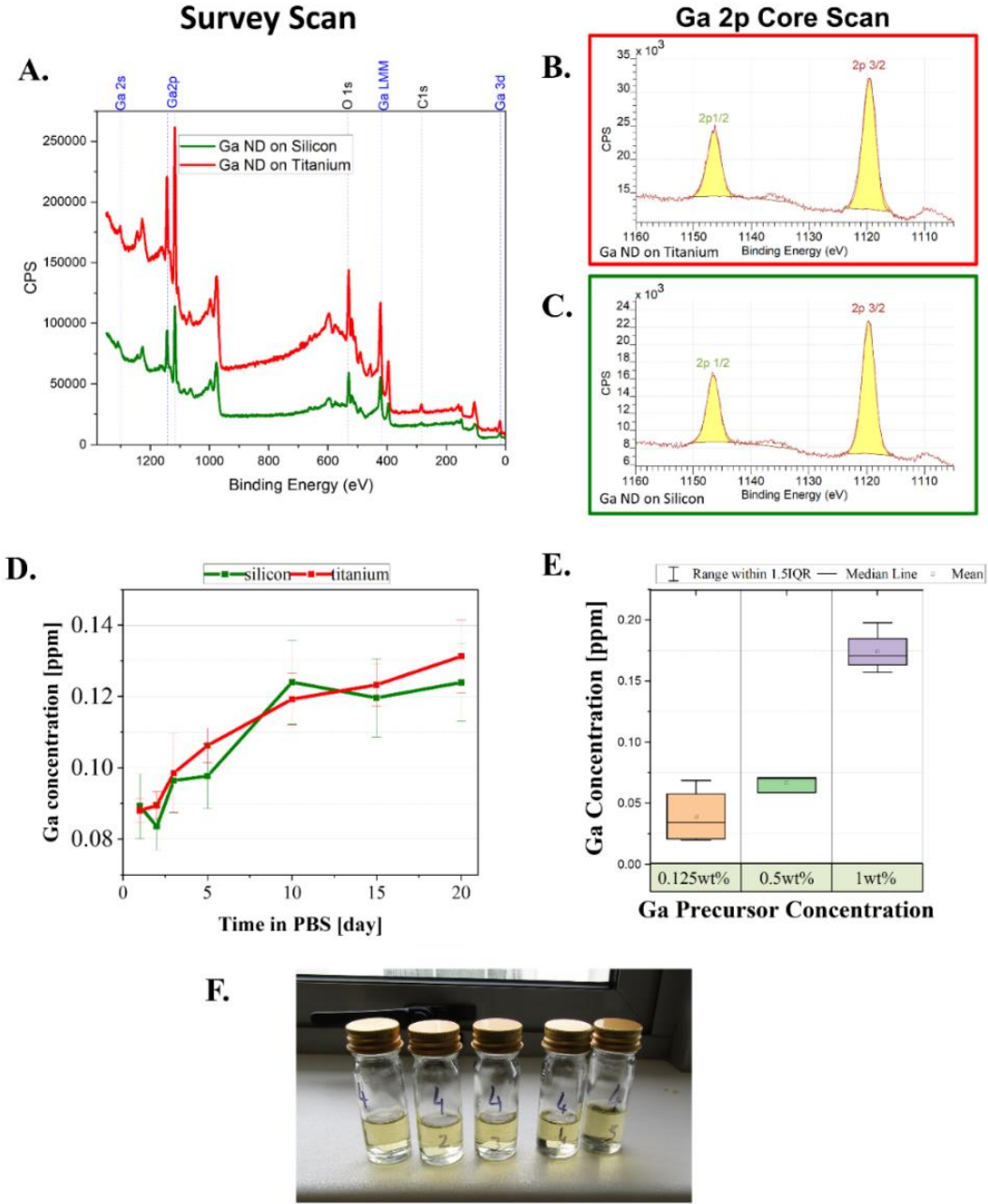


Figure 5.2: A-C: X-ray Photoelectron spectroscopy analysis of gallium nanodot samples on silicon and titanium substrates, Y-axis: counts per second [CPS] versus X-axis: binding energy [eV] (A: Survey Scan graph of gallium nanodot on both substrates, B: Ga 2p Core Scan of gallium nanodots on titanium, C: Ga 2p Core Scan of gallium nanodots on silicon), D: Gallium ionic concentration [ppm] as measured by Ionic Coupled Plasma Optical Emission Spectroscopy of PBS solution in which nanodot samples were immersed for a finite number of days, E: Gallium ionic concentration [ppm] as measured by Inductively Coupled Plasma Optical Emission Spectroscopy of PBS solution in which nanodot samples made from varying gallium precursor concentrations [wt.%] were

immersed for 24 hours and F: Photograph of a batch of gallium nanodot samples in nutrient broth after 20 days showing all vials remaining clear

5.3.3 Nano Gallium Surfaces Demonstrate Excellent Sterility and Antimicrobial Activity.

Twenty silicon nanodot samples made using 0.5 wt.% gallium concentration from four different batches were aseptically transferred into 10 ml of 20 gL⁻¹ sterile nutrient broth. The presence of any impurities would result in the opaquing of the nutrient broth. Indicative data in **Figure 5.2F** shows the clarity of samples confirming their sterility[81–83]. Nanodot samples exhibited no bacterial growth in inhibition zone tests, see **Appendix 5.4.3**

5.4. Conclusion

Block copolymer self-assembly can be used to develop gallium oxide nanostructures on silicon and titanium surfaces. This coating represents what could be a simple addendum to existing orthopaedic implant manufacturing lines. The system shows an 88% reduction in osteoclast formation within 1% Ga sample group at a ppm dosage far below current clinical standard.

The methodology is a simple, solution-based process and demonstrated in laboratory conditions but would be relatively easily scaled for use in implant devices at the manufacturing level. The methodology allows size and hence the ion release to be tuned for efficacy. The gallium oxide processing features offered some antimicrobial activity and did not compromise sterility. Using these samples to generate conditioned media for anabolic and anti-catabolic testing showed that there was no impact on stem cell viability and minimal effects on osteogenesis. The effect on osteoclastogenesis demonstrated a robust inhibition of osteoclast formation. Based on these results the 1wt.% gallium sample would be the best candidate for improved osteogenesis. When considered in tandem these results prove that BCP generated gallium surfaces were ideal model substrates for gallium testing and characterisation on the nanoscale. The subsequent concentration of gallium eluted into media inhibited osteoclast differentiation with no inhibitor effect on osteoblast formation, thus resulting in a net gain in bone formation.

5.5 Appendix Chapter 5

Appendix 5.5.1 Water Contact Angle Data

The Water Contact Angle (WCA) of samples was recorded on a custom built WCA device using fast shutter camera, 60 Hz sampling. 10microlitre drops of pure water were placed on the sample and Image J software with dropsnake plugin was used to measure the advancing water contact angle. WCAs in the region of 50°-90° are optimum for biological testing [1,2].

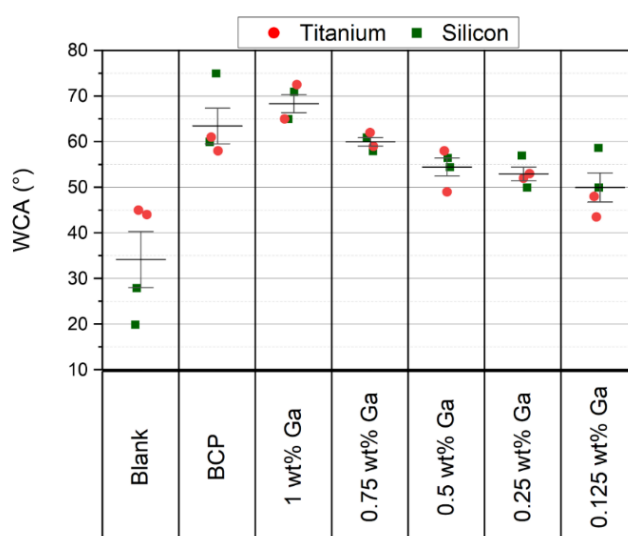


Figure A5.1: Water Contact angles of blank substrates, substrates with BCP nanodots, and substrates with gallium nanodots of decreasing gallium content.

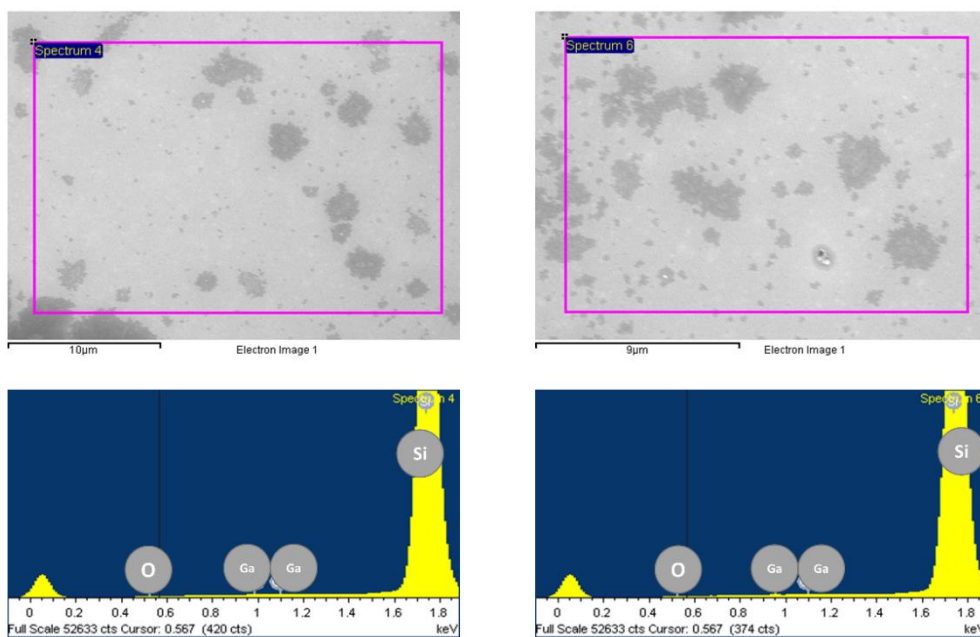
Figure A5.1 shows that the WCA of the blank substrates are in the range of 20° to 45° indicating hydrophilicity and large variation of values. The BCP dots post SVA have WCA values the range of 55° to 75° and as the gallium nanodots are infiltrated with gallium precursors of varying concentration the WCA decreases slightly with decreasing gallium content. The conversion of BCP nanodots to gallium nanodots sees a decrease in WCA due to the inherent hydrophilicity of a metal but that data suggests that it is the dot architecture that drives the WCA of the sample surfaces since lower gallium content would also mean lower gallium

nanodot volume. This hypothesis is supported by the fact that patterned surface samples groups have WCA values with a standard deviation of less than 10° meaning that the WCA of the samples is maintained by the nanodot shape as opposed to substrate nature or metallic content.

Appendix 5.5.2 Energy Dispersive X-ray Spectroscopy

Energy-dispersive X-ray spectroscopy (EDX) spectra were acquired at 15-20 kV on an Oxford Inca EDX detector at a working distance of 10mm. Gallium nanodots on silicon and gallium nanodots on titanium substrates were analysed. Both samples showed gallium present in the spectrum.

Ga nanodots on Silicon



Ga nanodots on Titanium

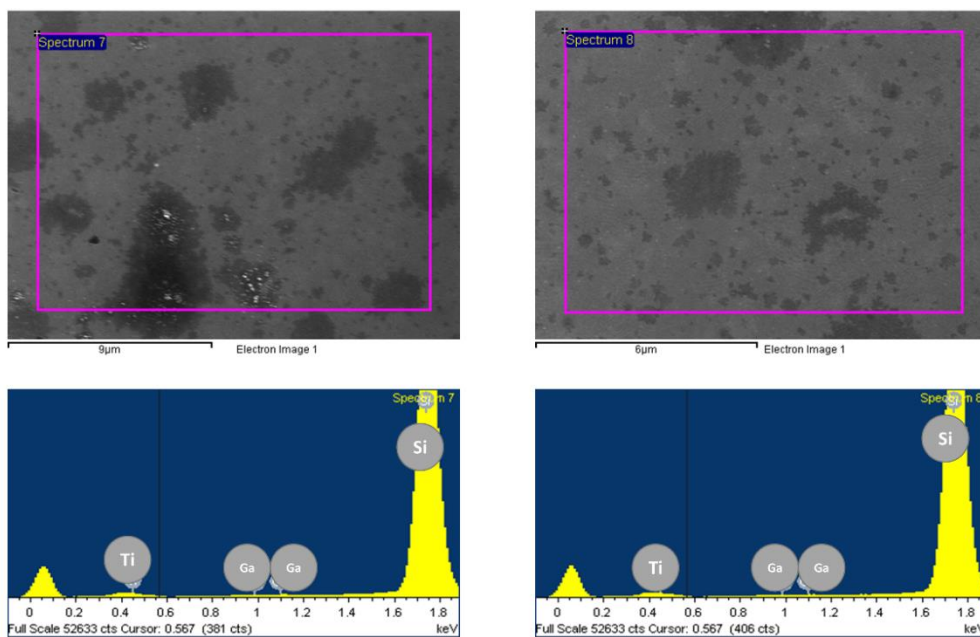


Figure A5.2: Energy-dispersive X-ray spectroscopy (EDX) spectra were acquired at 15-20 kV on an Oxford Inca EDX detector at a working distance of 10mm. Gallium nanodots on silicon and gallium nanodots on titanium substrates were analysed. Both samples showed gallium present in the spectrum.

Appendix 5.5.3 Antimicrobial Testing

Antimicrobial inhibition zones were performed as described by Azlin-Hasim et al[3]. Nanodot samples were formed on Silicon from 50-b-6 kg mol⁻¹ polymer and infiltration with 0.25 wt.% Ga, 0.5 wt.% Ga and 2 wt. % Ga. Three sets of each sample set were provided for testing along with 3 silicon blanks. Resulting images, however showed little bacterial growth at all in the vicinity implying that gallium may be completely prolific against *Escherichia coli*, **Figure A5.3** and *Staphylococcus aureus*, **Figure A5.4**. This data has some limitations since the inhibition zone in each sample is both images difficult to identify and there is no control sample included. To support these results, many tests are carried out in literature that detail gallium nitrate being highly effective against pathogens within inhibition zone tests[4–6]. Herein however, it is ionic gallium present and this, we postulate, leads to high inhibition against any bacterial growth.

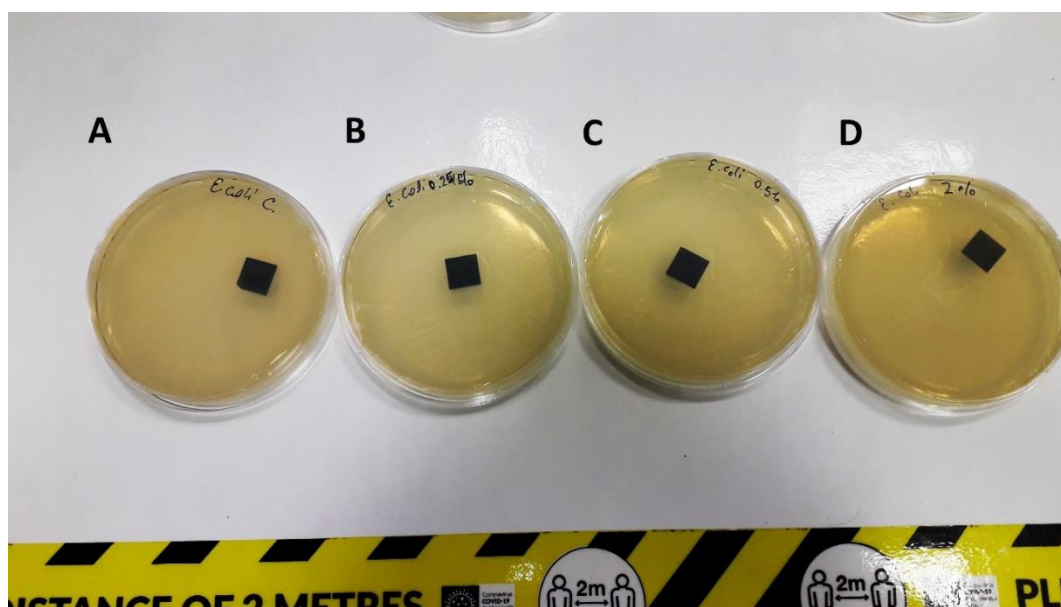


Figure A5.3: Inhibition zone photograph of A. Silicon control, B. 0.25 wt.% Ga sample, C. 0.5 wt.% Ga sample, and D. 2 wt. % Ga sample against strain of *E.coli*

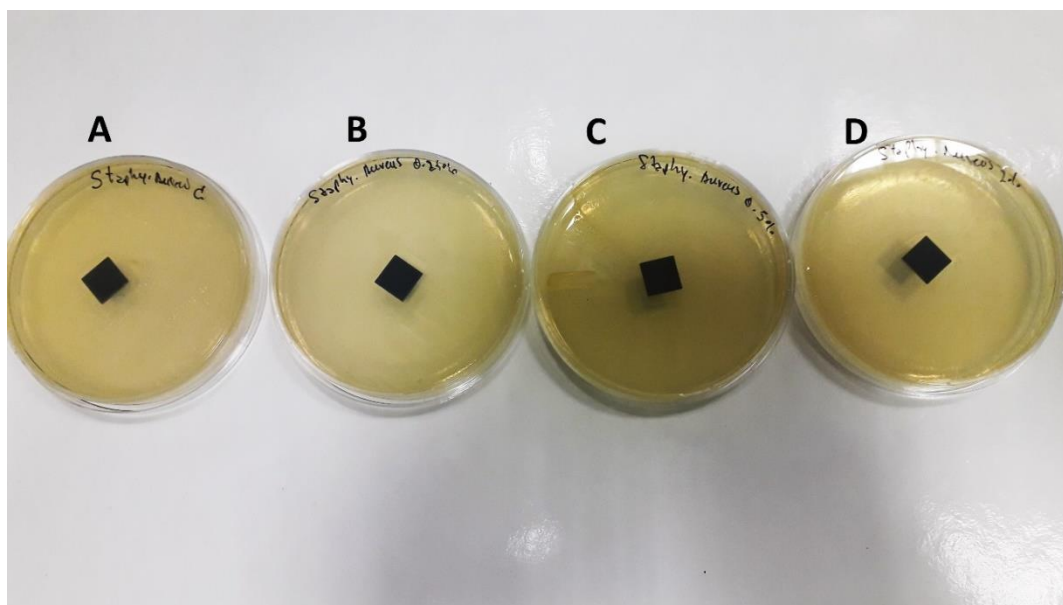


Figure A5.4: Inhibition zone photograph of A. Silicon control, B. 0.25 wt.% Ga sample, C. 0.5 wt.% Ga sample, and D. 2 wt. % Ga sample against strain of Staph. A

Appendix 5.5.3 - References

- [1] Huhtamäki, T.; Tian, X.; Korhonen, J. T.; Ras, R. H. A. Surface-Wetting Characterization Using Contact-Angle Measurements. *Nature Protocols* **2018**, *13* (7), 1521–1538. <https://doi.org/10.1038/s41596-018-0003-z>.
- [2] Oh, J. K.; Yegin, Y.; Yang, F.; Zhang, M.; Li, J.; Huang, S.; Verkhoturov, S. V.; Schweikert, E. A.; Perez-Lewis, K.; Scholar, E. A.; Taylor, T. M.; Castillo, A.; Cisneros-Zevallos, L.; Min, Y.; Akbulut, M. The Influence of Surface Chemistry on the Kinetics and Thermodynamics of Bacterial Adhesion. *Scientific Reports* **2018**, *8* (1), 17247. <https://doi.org/10.1038/s41598-018-35343-1>.
- [3] Azlin-Hasim, S.; Cruz-Romero, M. C.; Ghoshal, T.; Morris, M. A.; Cummins, E.; Kerry, J. P. Application of Silver Nanodots for Potential Use in Antimicrobial Packaging Applications. *Innovative Food Science & Emerging Technologies* **2015**, *27*, 136–143. <https://doi.org/10.1016/j.ifset.2014.10.012>.
- [4] Gugala, N.; Vu, D.; Parkins, M. D.; Turner, R. J. Specificity in the Susceptibilities of Escherichia Coli, Pseudomonas Aeruginosa and Staphylococcus Aureus Clinical Isolates to Six Metal Antimicrobials. *Antibiotics (Basel)* **2019**, *8* (2), 51. <https://doi.org/10.3390/antibiotics8020051>.
- [5] Xu, Z.; Zhao, X.; Chen, X.; Chen, Z.; Xia, Z. Antimicrobial Effect of Gallium Nitrate against Bacteria Encountered in Burn Wound Infections. *RSC Advances* **2017**, *7* (82), 52266–52273. <https://doi.org/10.1039/C7RA10265H>.
- [6] Guerrini, M.; d'Agostino, S.; Grepioni, F.; Braga, D.; Lekhan, A.; Turner, R. J. Antimicrobial Activity of Supramolecular Salts of Gallium(III) and Proflavine and the Intriguing Case of a Trioxalate Complex. *Sci Rep* **2022**, *12* (1), 3673. <https://doi.org/10.1038/s41598-022-07813-0>.

Appendix 5.5.4 Biological Testing of Gallium Nanodot surfaces

5.5.4.1 Conditioned media collection

Gallium nanodot coated silicon samples were formed using 1 wt.% Ga (1% Ga) and 0.125wt.% Ga (0.125% Ga) precursor. These samples and silicon control

(0 % Ga) samples were immersed in α -minimum essential medium (α -MEM) containing 10% foetal bovine serum (FBS), 1% penicillin/streptomycin (P/S) and 1% L-glutamine (L-G) (Growth media), for 24h at 37 °C to simulate physiological conditions of an implant and generate condition media (CM).

5.5.4.2 Cell Isolation

Human bone marrow stromal/stem cells (hMSCs) were isolated from bone marrow (Lonza), characterised by tri-lineage differentiation (data not shown), and maintained in Dulbecco's modified eagle medium (DMEM) with 10% foetal bovine serum (FBS, Gibco, 10270106) and 1% penicillin/streptomycin (P/S, Sigma) unless otherwise stated (Growth media). All cells were cultured at 37°C and 5% CO₂.

Peripheral blood mononuclear cells (PBMCs) were isolated from leukocyte-enriched human buffy coats using density gradient centrifugation with LymphoPrep™ solution (Progen). CD14⁺ monocytes were isolated from PBMCs by magnetic sorting using MagniSort Human CD14 Positive Selection Kit (Invitrogen) according to the manufacturer's instructions.

Leukocyte-enriched buffy coats from anonymous healthy donors were obtained with permission from the Irish Blood Transfusion Service (IBTS), St. James's Hospital, Dublin and approved by the research ethics committee of Trinity College Dublin (Inst code 004/group no. 039) and in accordance with the Helsinki Declaration. Donors provided informed written consent to the IBTS for their blood to be used for research purposes.

5.5.4.3 Conditioned Media effect on hMSC Viability and Osteogenic Differentiation

To assess the effect of the Conditioned Media (CM) on hMSC viability, hMSCs were seeded at 6500 cells cm⁻² in 12-well plates and allowed to settle for 24 h in normal growth media. hMSCs were then treated with each CM for an additional 24 h followed by LIVE/DEAD™ (Invitrogen, L3224) staining. Quantification of cell viability was performed using ImageJ.

To evaluate the effect of the CM on the osteogenic differentiation of hMSCs, cells were seeded and treated with the conditioned media as described above for 3 days, followed by further 14 days in DMEM GlutaMAX™ (Gibco, 10566016) supplemented with osteogenic supplements (100 nM dexamethasone, 0.05 mM

L-ascorbic acid and 10 mM β -glycerol phosphate). Following this culture period, the media was collected, and cells fixed and lysed for DNA analysis and markers of osteogenesis.

5.5.4.4 DNA Quantification

Cells were fixed and lysed for DNA quantification which was performed using the Quant-iT™ PicoGreen™ dsDNA Assay (Invitrogen, P7589) with excitation at 480 nm and read at 520 nm.

2.4.5 Alkaline Phosphatase Quantification

To determine alkaline phosphate (ALP) expression, media was collected from the cells following 14 days in osteogenic media and cells were lysed using a Triton-X based lysis buffer as described above. Intracellular and extracellular ALP was quantified using a SigmaFast p-nitrophenyl phosphate (pNPP) kit (Sigma Aldrich, N1891), as previously described.[75] The test samples were diluted, 1:2 for media samples and 1:16 for cell lysates and added to wells as well as 50 μ l of a 5mM pNPP solution. ALP content was normalised to DNA content.

5.5.4.6 Alizarin red staining and quantification

Alizarin red staining (ARS) and quantification was used to assess mineral/calcium deposition. Cells were fixed in 4% paraformaldehyde (PFA) for 10 min. Following fixation, cells and 1ml of 1% alizarin red stain (ARS) was added to each well for 20 minutes. Background staining was removed with sequential washes in H₂O, and the wells were imaged using an Olympus CKX53 inverted microscope with a 10x objective. Quantification was performed as previously described [75] with standards made through serial dilutions of ARS and 100 μ l of each test sample and standard added to a 96-well plate. Absorbance was then read at 405nm.

5.5.4.7 Conditioned Media effect on Osteoclast differentiation.

To assess the effect of CM on osteoclast differentiation [76,77] CD14+monocytes (625000 cells/cm²) were seeded into 96-well plates, cultured with CM and supplemented with 25 ng/mL M-CSF (Miltenyi Biotec) and 50 ng/mL Recombinant Human sRANK Ligand (sRANKL) (PeproTech) to induce osteoclastogenesis for 7 days. An additional group (Untreated) which was not supplement with RANKL functioned as a negative control for osteoclastogenesis. CM was replenished every 3.5 days. On day 7, cells were fixed with 2% paraformaldehyde (PFA) and stained for tartrate-resistant acid phosphatase

(TRAP) activity with a leukocyte acid Phosphatase (TRAP) Kit (Sigma) and with DAPI (1:200) (Sigma) according to the manufacturer's protocols. TRAP-positive multinuclear cells containing three or more nuclei were counted as osteoclasts. These cells and the number of nuclei were imaged using an Olympus IX81 inverted microscope with 10x objective and counted using the cell counter plugin on Image-J software (NIH, USA).

Appendix 5.5.5 Effect of Silicon conditioned media on Human MSC and Monocyte viability

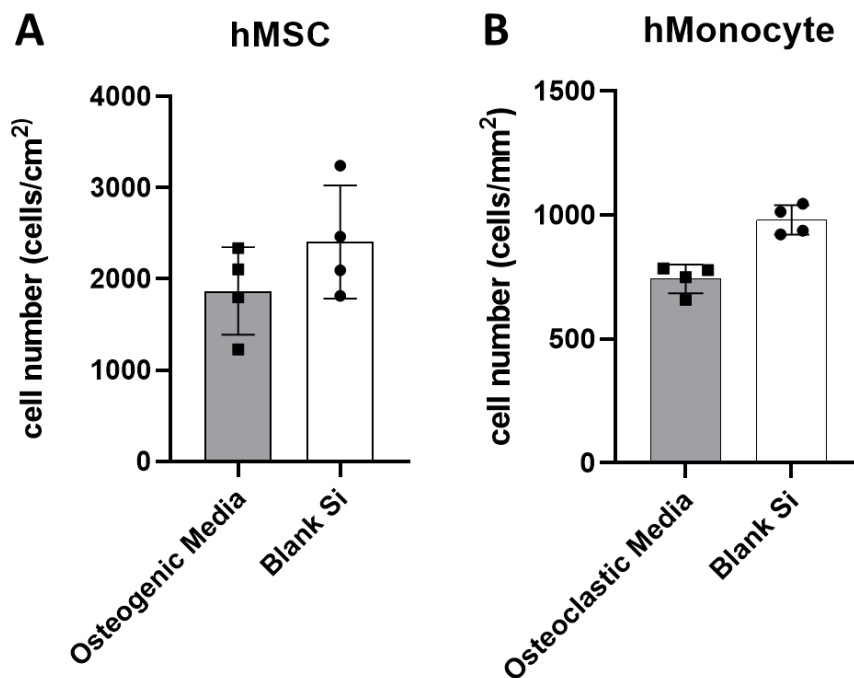


Figure A5.5: Effect of Silicon conditioned media on Human MSC and Monocyte viability. (A) hMSC cells cultured for in osteogenic media or Silicon conditioned osteogenic media (B) CD14+ cells cultured for in Osteoclast media or Silicon conditioned osteoclast media

5.4.5.1 Nano sized gallium surfaces do not influence hMSC viability.

Figure A5.6 demonstrates the effect of gallium release from the nanodot surfaces on hMSC viability. After 24 hours there is no effect seen for gallium samples versus bare silicon in terms of live/dead staining, where no dead cells could be detected in any groups (**Figure A5.6A**). Quantification of cell density indicated a slight trend of increased cell number in gallium condition media (CM) samples when compared to silicon control (**Figure A5.6B**). This is consistent with that

seen following DNA quantification (**Figure A5.6C**), where DNA content present for gallium 0.125 wt.% is 1094 ng and gallium 1 wt.% is 1079 ng, which are both higher than for silicon which is 838 ng.

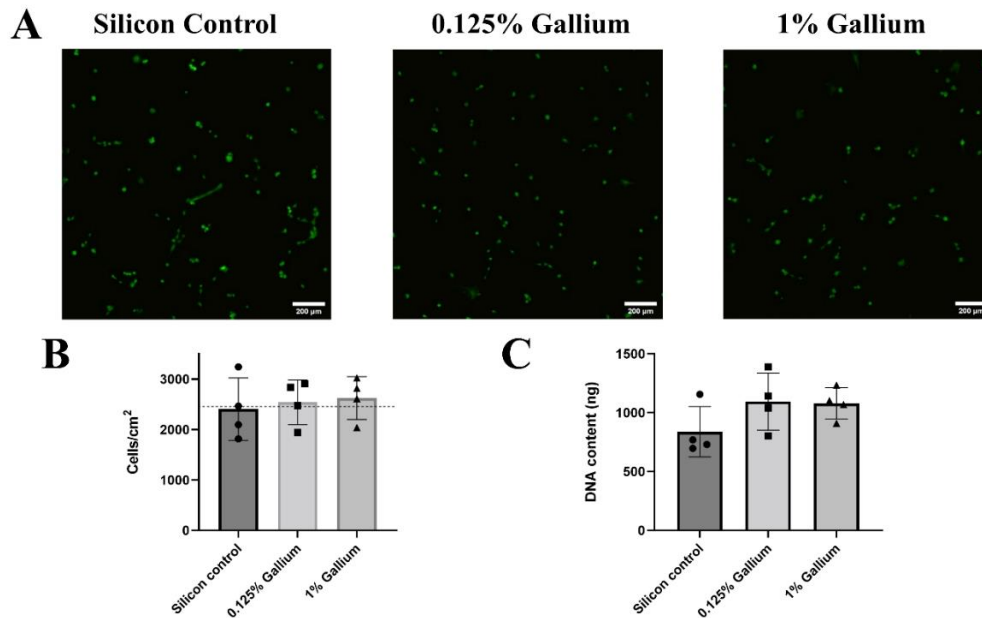


Figure A5.6: Effect of conditioned media from gallium nanodots on the viability of hMSCs. (A) live/dead staining and (B) quantification. (C) DNA content following 3 days in conditioned media and 14 days in osteogenic media. Scale bar= 200 μ m. Results shown are means \pm SD (n=4).

5.5.5.2 Nano Sized Gallium Surfaces do not Inhibit Osteoblastic Differentiation but can Adversely Affect Mineralisation at High Concentrations.

Osteogenesis assays were conducted to study the effect of gallium release on osteoblastic differentiation and late-stage mineralisation as determined by ALP expression and mineral deposition respectively as a proxy for anabolic responses upon implantation, the results of which are shown in **Figure A5.7**. Both intracellular and extracellular ALP were not affected by gallium released from the nanodot surfaces at either low or high concentration (**Figure A5.7A, B**), indicating that this novel surface coating does not adversely affect osteogenic differentiation and early osteogenesis.[84,85] With respect to later stage mineral deposition as measured by ARS staining, [86,87] calcium deposition displayed a negative trend with increasing gallium concentration. Despite a short 14-day culture period, mineral nodules are present in all groups with robust staining in the Silicon and 0.125% Gallium groups. While ARS staining is present in the 1% Gallium group, indicative of late stage hMSC differentiation, the staining is less pronounced

(**Figure A5.7C**). This trend is verified upon quantification where calcium levels normalised to DNA decrease with increasing Gallium concentration, reaching significance with 1% Gallium ($p < 0.05$; **Figure A5.7D**). This decrease in mineral production per cell could potentially be attributed to the increased proliferation rates identified in these groups (**Figure A5.6**). Interestingly, despite a 36% decrease in mineral produced per cell following treatment (**Figure A5.7D**), this only corresponds to a non-significant 15% decrease in total mineral because of increased cellular proliferation following Gallium treatment (**Figure A5.7E**). A similar analysis can be done for the 1% Gallium, where a 50% decrease in mineral deposition per cell only results in a 35% drop in total mineral deposition. While this latter example is a significant decrease ($p < 0.05$), the trade-off between proliferation and mineralisation may indicate that longer time points may result in even greater anabolic responses following gallium treatment from nanodot surfaces. Overall, this data demonstrates that nanosized gallium surfaces do not inhibit osteoblastic differentiation but can adversely affect mineralisation at high concentrations.

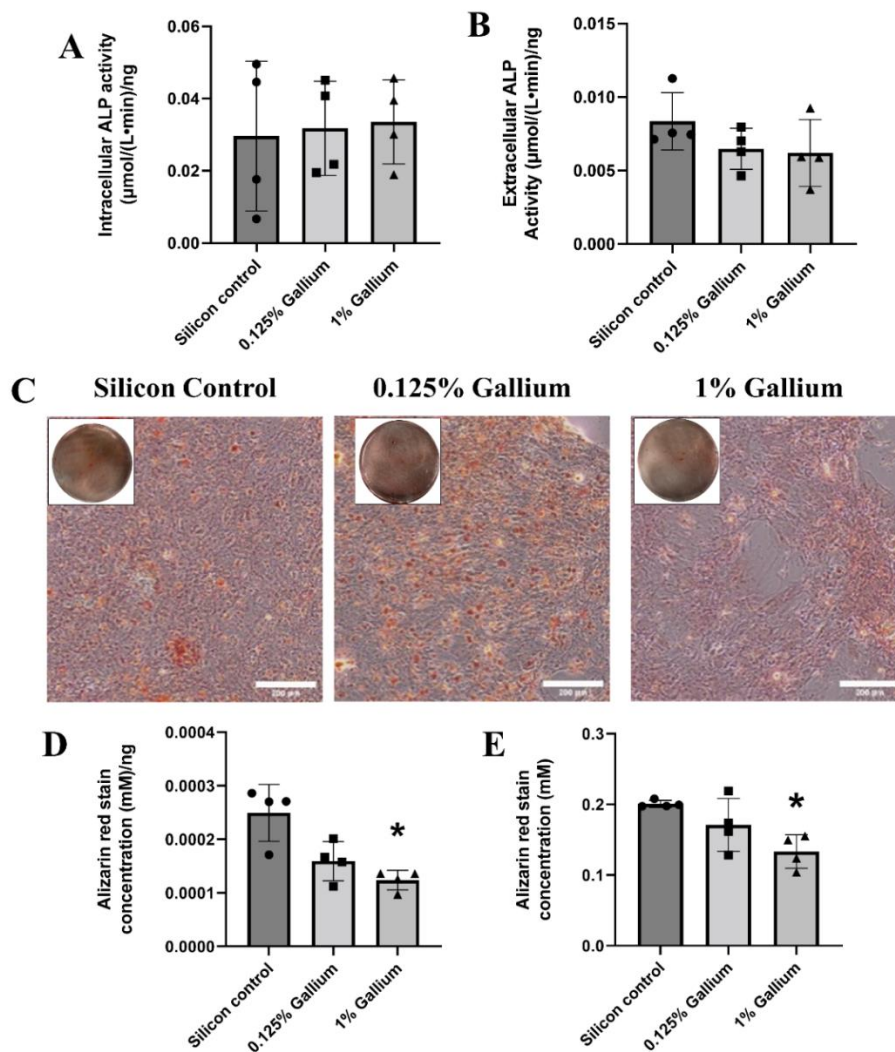


Figure A5.7: Effect of conditioned media from gallium nanodots on the osteogenic differentiation of hMSCs. (A) Intracellular and (B) extracellular ALP activity normalised to DNA content (C) Alizarin red staining and (D) quantification normalised to DNA content and (E) total staining quantification. Scale bar= 200 μm . Results shown are means \pm SD (n=4). *p<0.05 compared to silicon control.

5.5.5.3 Nano Sized Gallium Surfaces Inhibit Osteoclastogenesis at High Concentrations

Osteoclastogenesis tests were carried out to study the effect of Gallium CM on CD14+ monocyte differentiation into osteoclasts as a proxy for catabolic responses upon implantation, the results of which are shown in **Figure A5.8**. The quantification of TRAP positive cells with 3 or more nuclei post treatment with CM is used as these are biological markers for osteoclast formation and function.[88,89] Large multi-nucleated TRAP+ cells are present following

treatment with RANKL indicating successful osteoclastic differentiation when compared to untreated groups **Figure A5.8A**. While some osteoclasts are present following treatment with 0.125% Gallium, there is a clear decrease in osteoclast number following 1% Gallium treatment (**Figure A5.8A**). Following quantification there was a significant decrease in cell number found following treatment with 1% Gallium indicating that these high concentrations can adversely affect the viability of human monocytes (27% decrease when compared to Treated control, $p < 0.05$; (**Figure A5.8B**). No effect on cell viability was identified with the lower 0.125% Gallium treatment. Despite the modest decrease in cell number, 1% Gallium treatment resulted in a robust and significant 88% inhibition of osteoclastogenesis **Figure A5.8C, D**, with the number of osteoclast cells per unit area reducing from 13.2 in treated groups to 1.5 following treatment with 1% Gallium, a level that was not significantly different to untreated controls. No effect of 0.125% Gallium was seen on osteoclastogenesis suggesting that this concentration is too low to elicit a response. Taken together, this data demonstrates that gallium released from the nanodot surfaces is effectively preventing osteoclastogenesis and thus represents a robust anti-catabolic coating for orthopaedic implants.

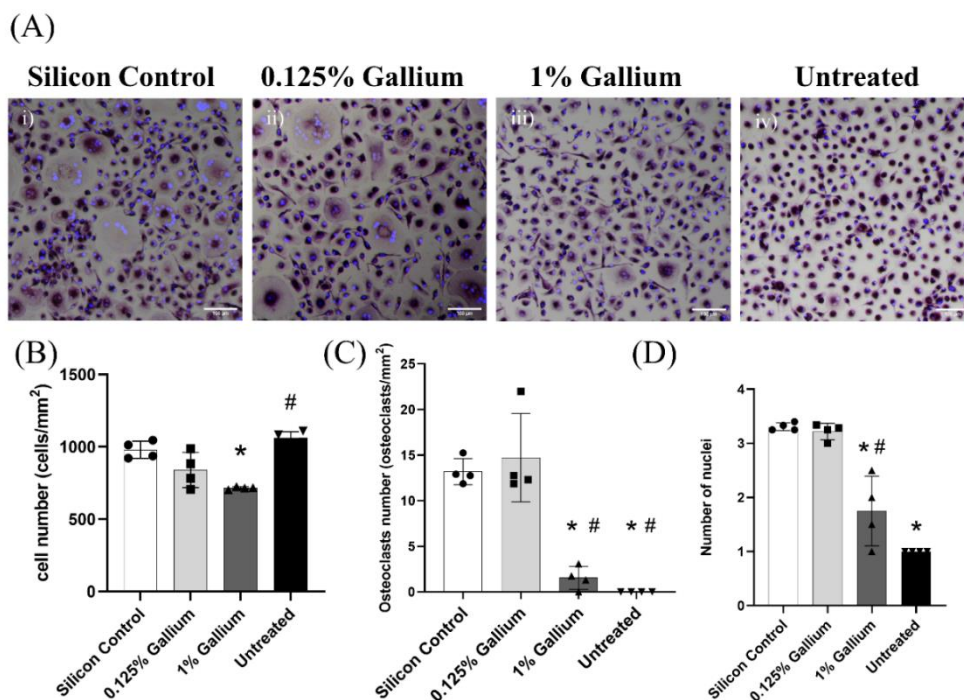


Figure A5.8: Effect of Gallium Conditioned media on osteoclast formation. (A) CD14+ cells cultured for 7 days in Silicon Control conditioned media (i) ,0.125 wt% Gallium conditioned media (ii), 1 wt% Gallium conditioned media (iii) and in

growth media supplemented with M-CSF (iv). (B) Total cell number. (C) Osteoclasts number expressed as cells/surface. (D) Number of nuclei. * $p < 0.05$ compared to the silicon control and # $p < 0.05$ compared to the 0.125 wt% Gallium.

5.6 References

- [1] J. T. Evans, R. W. Walker, J. P. Evans, A. W. Blom, A. Sayers, and M. R. Whitehouse, "How long does a knee replacement last? A systematic review and meta-analysis of case series and national registry reports with more than 15 years of follow-up," *Lancet*, vol. 393, no. 10172, pp. 655–663, Feb. 2019, doi: [https://doi.org/10.1016/S0140-6736\(18\)32531-5](https://doi.org/10.1016/S0140-6736(18)32531-5).
- [2] J. T. Evans, J. P. Evans, R. W. Walker, A. W. Blom, M. R. Whitehouse, and A. Sayers, "How long does a hip replacement last? A systematic review and meta-analysis of case series and national registry reports with more than 15 years of follow-up," *The Lancet*, vol. 393, no. 10172, pp. 647–654, Feb. 2019, doi: [10.1016/S0140-6736\(18\)31665-9](https://doi.org/10.1016/S0140-6736(18)31665-9).
- [3] K. T. Kim, S. Lee, D. O. Ko, B. S. Seo, W. S. Jung, and B. K. Chang, "Causes of Failure after Total Knee Arthroplasty in Osteoarthritis Patients 55 Years of Age or Younger," *Knee Surg Relat Res*, vol. 26, no. 1, pp. 13–19, Mar. 2014, doi: [10.5792/ksrr.2014.26.1.13](https://doi.org/10.5792/ksrr.2014.26.1.13).
- [4] R. Narkbunnam and K. Chareancholvanich, "Causes of failure in total knee arthroplasty," *J Med Assoc Thai*, vol. 95, no. 5, pp. 667–673, May 2012.
- [5] Y. Abu-Amer, I. Darwech, and J. C. Clohisy, "Aseptic loosening of total joint replacements: mechanisms underlying osteolysis and potential therapies," *Arthritis Res Ther*, vol. 9, no. Suppl 1, p. S6, 2007, doi: [10.1186/ar2170](https://doi.org/10.1186/ar2170).
- [6] L. A. Cordova *et al.*, "Orthopaedic implant failure: aseptic implant loosening—the contribution and future challenges of mouse models in translational research," *Clinical Science*, vol. 127, no. 5, pp. 277–293, Sep. 2014, doi: [10.1042/CS20130338](https://doi.org/10.1042/CS20130338).
- [7] E. M. Greenfields, Y. Bi, A. A. Ragab, V. M. Goldberg, and R. R. Van De Motter, "The role of osteoclast differentiation in aseptic loosening," *J. Orthop. Res.*, vol. 20, no. 1, pp. 1–8, Jan. 2002, doi: [10.1016/S0736-0266\(01\)00070-5](https://doi.org/10.1016/S0736-0266(01)00070-5).
- [8] A. L. Godoy-Santos, C. O. D'Elia, W. J. Teixeira, H. B. Cabrita, and G. L. Camanho, "Aseptic Loosening of Total Hip Arthroplasty: Preliminary Genetic Investigation," *The Journal of Arthroplasty*, vol. 24, no. 2, pp. 297–302, Feb. 2009, doi: [10.1016/j.arth.2008.08.006](https://doi.org/10.1016/j.arth.2008.08.006).
- [9] R. Marks, "Body mass characteristics of hip osteoarthritis patients experiencing aseptic loosening, periprosthetic fractures, dislocation, and infections after total hip replacement," *Clinicoecon Outcomes Res*, vol. 1, pp. 7–16, May 2009.
- [10] J. Pietrzak, H. Common, H. Migaud, G. Pasquier, J. Girard, and S. Putman, "Have the frequency of and reasons for revision total knee arthroplasty changed since 2000? Comparison of two cohorts from the same hospital: 255 cases (2013–2016) and 68 cases (1991–1998)," *Orthopaedics & Traumatology: Surgery & Research*, vol. 105, no. 4, pp. 639–645, Jun. 2019, doi: [10.1016/j.otsr.2019.01.025](https://doi.org/10.1016/j.otsr.2019.01.025).
- [11] J. Vishnu and G. Manivasagam, "Surface Modification and Biological Approaches for Tackling Titanium Wear-Induced Aseptic Loosening," *J Bio Tribo Corros*, vol. 7, no. 1, p. 32, Jan. 2021, doi: [10.1007/s40735-021-00474-y](https://doi.org/10.1007/s40735-021-00474-y).
- [12] P. Wang, G. Shang, S. Xiang, H. Zhang, Y. Wang, and H. Xu, "Zoledronic acid and teriparatide have a complementary therapeutic effect on aseptic loosening in a rabbit model," *BMC Musculoskeletal Disorders*, vol. 22, no. 1, p. 580, Jun. 2021, doi: [10.1186/s12891-021-04458-4](https://doi.org/10.1186/s12891-021-04458-4).
- [13] H. Prock-Gibbs, C. A. Pumilia, T. Meckmongkol, J. Lovejoy, A. Mumith, and M. Coathup, "Incidence of Osteolysis and Aseptic Loosening Following Metal-on-Highly Cross-Linked

Polyethylene Hip Arthroplasty: A Systematic Review of Studies with Up to 15-Year Follow-up," *JBJS*, vol. 103, no. 8, pp. 728–740, Apr. 2021, doi: 10.2106/JBJS.20.01086.

[14] M. Marsh and S. Newman, "Trends and developments in hip and knee arthroplasty technology," *J Rehabil Assist Technol Eng*, vol. 8, p. 2055668320952043, Feb. 2021, doi: 10.1177/2055668320952043.

[15] S. Santavirta *et al.*, "Materials in total joint replacement," *Current Orthopaedics*, vol. 12, no. 1, pp. 51–57, Jan. 1998, doi: 10.1016/S0268-0890(98)90008-1.

[16] F. He *et al.*, "Alliance of gallium and strontium potently mediates the osteoclastic and osteogenic activities of β -tricalcium phosphate bioceramic scaffolds," *Chemical Engineering Journal*, vol. 412, p. 128709, May 2021, doi: 10.1016/j.cej.2021.128709.

[17] V. Stanić *et al.*, "Synthesis of antimicrobial monophasic silver-doped hydroxyapatite nanopowders for bone tissue engineering," *Applied Surface Science*, vol. 257, no. 9, pp. 4510–4518, Feb. 2011, doi: 10.1016/j.apsusc.2010.12.113.

[18] P. Yang, Z. Quan, C. Li, X. Kang, H. Lian, and J. Lin, "Bioactive, luminescent and mesoporous europium-doped hydroxyapatite as a drug carrier," *Biomaterials*, vol. 29, no. 32, pp. 4341–4347, Nov. 2008, doi: 10.1016/j.biomaterials.2008.07.042.

[19] B. M. Hidalgo-Robatto *et al.*, "Pulsed laser deposition of copper and zinc doped hydroxyapatite coatings for biomedical applications," *Surface and Coatings Technology*, vol. 333, pp. 168–177, Jan. 2018, doi: 10.1016/j.surfcoat.2017.11.006.

[20] Y.-C. Yang, C.-C. Chen, J.-B. Wang, Y.-C. Wang, and F.-H. Lin, "Flame sprayed zinc doped hydroxyapatite coating with antibacterial and biocompatible properties," *Ceramics International*, vol. 43, pp. S829–S835, Aug. 2017, doi: 10.1016/j.ceramint.2017.05.318.

[21] K. H. Park, Y. Choi, D. S. Yoon, K.-M. Lee, D. Kim, and J. W. Lee, "Zinc Promotes Osteoblast Differentiation in Human Mesenchymal Stem Cells Via Activation of the cAMP-PKA-CREB Signaling Pathway," *Stem Cells and Development*, vol. 27, no. 16, pp. 1125–1135, Aug. 2018, doi: 10.1089/scd.2018.0023.

[22] C. Capuccini, P. Torricelli, E. Boanini, M. Gazzano, R. Giardino, and A. Bigi, "Interaction of Sr-doped hydroxyapatite nanocrystals with osteoclast and osteoblast-like cells," *Journal of Biomedical Materials Research Part A*, vol. 89A, no. 3, pp. 594–600, 2009, doi: 10.1002/jbm.a.31975.

[23] J. Terra, E. Rodrigues Dourado, J.-G. Eon, D. E. Ellis, G. Gonzalez, and A. Malta Rossi, "The structure of strontium-doped hydroxyapatite: an experimental and theoretical study," *Physical Chemistry Chemical Physics*, vol. 11, no. 3, pp. 568–577, 2009, doi: 10.1039/B802841A.

[24] S. Awasthi, S. K. Pandey, E. Arunan, and C. Srivastava, "A review on hydroxyapatite coatings for the biomedical applications: experimental and theoretical perspectives," *J. Mater. Chem. B*, vol. 9, no. 2, pp. 228–249, Jan. 2021, doi: 10.1039/D0TB02407D.

[25] E. Munting, "The contributions and limitations of hydroxyapatite coatings to implant fixation: A histomorphometric study of load bearing implants in dogs," *International Orthopaedics SICOT*, vol. 20, no. 1, pp. 1–6, Feb. 1996, doi: 10.1007/PL00006691.

[26] M. Riaz, R. Zia, A. Ijaz, T. Hussain, M. Mohsin, and A. Malik, "Synthesis of monophasic Ag doped hydroxyapatite and evaluation of antibacterial activity," *Materials Science and Engineering: C*, vol. 90, pp. 308–313, Sep. 2018, doi: 10.1016/j.msec.2018.04.076.

[27] K. F. Eichholz, S. Von Euw, R. Burdis, D. J. Kelly, and D. A. Hoey, "Development of a New Bone-Mimetic Surface Treatment Platform: Nanoneedle Hydroxyapatite (nnHA) Coating," *Adv Healthc Mater*, vol. 9, no. 24, p. e2001102, Dec. 2020, doi: 10.1002/adhm.202001102.

[28] H. Tapiero and K. D. Tew, "Trace elements in human physiology and pathology: zinc and metallothioneins," *Biomed Pharmacother*, vol. 57, no. 9, pp. 399–411, Nov. 2003, doi: 10.1016/s0753-3322(03)00081-7.

[29] P. Bhattacharjee, H. Begam, A. Chanda, and S. K. Nandi, "Animal trial on zinc doped hydroxyapatite: A case study," *Journal of Asian Ceramic Societies*, vol. 2, no. 1, pp. 44–51, Mar. 2014, doi: 10.1016/j.jascer.2014.01.005.

- [30] S. Aldridge and A. J. Downs, *The Group 13 Metals Aluminium, Gallium, Indium and Thallium: Chemical Patterns and Peculiarities*. John Wiley & Sons, 2011.
- [31] A. B. Kelson, M. Carnevali, and V. Truong-Le, "Gallium-based anti-infectives: targeting microbial iron-uptake mechanisms," *Current Opinion in Pharmacology*, vol. 13, no. 5, pp. 707–716, Oct. 2013, doi: 10.1016/j.coph.2013.07.001.
- [32] G. Apseloff, "Therapeutic uses of gallium nitrate: past, present, and future. - Abstract - Europe PMC," *American Journal of Therapeutics*, vol. 6, no. 6, pp. 327–339, Sep. 1999.
- [33] T. Katagiri and N. Takahashi, "Regulatory mechanisms of osteoblast and osteoclast differentiation," *Oral Diseases*, vol. 8, no. 3, pp. 147–159, 2002, doi: 10.1034/j.1601-0825.2002.01829.x.
- [34] <https://www.drugs.com/pro/ganite.html>, "Ganite: Package Insert / Prescribing Information," Drugs.com. Accessed: May 12, 2023. [Online]. Available: <https://www.drugs.com/pro/ganite.html>
- [35] H. Palokangas, M. Mulari, and H. K. Vaananen, "Endocytic pathway from the basal plasma membrane to the ruffled border membrane in bone-resorbing osteoclasts," *Journal of Cell Science*, vol. 110, no. 15, pp. 1767–1780, Aug. 1997.
- [36] K. Yamasaki and H. Hagihara, "Excess iron inhibits osteoblast metabolism," *Toxicology Letters*, vol. 191, no. 2, pp. 211–215, Dec. 2009, doi: 10.1016/j.toxlet.2009.08.023.
- [37] G. D. Roodman, "Osteoclasts Pump Iron," *Cell Metabolism*, vol. 9, no. 5, pp. 405–406, May 2009, doi: 10.1016/j.cmet.2009.04.005.
- [38] M. Merckx and B. A. Averill, "Ga³⁺ as a functional substitute for Fe³⁺: preparation and characterization of the Ga³⁺+Fe²⁺ and Ga³⁺+Zn²⁺ forms of bovine spleen purple acid phosphatase," *Biochemistry*, vol. 37, no. 23, pp. 8490–8497, Jun. 1998, doi: 10.1021/bi972929a.
- [39] K. D. Weaver *et al.*, "Ga³⁺ as a mechanistic probe in Fe³⁺ transport: characterization of Ga³⁺ interaction with FbpA," *J Biol Inorg Chem*, vol. 13, no. 6, pp. 887–898, Aug. 2008, doi: 10.1007/s00775-008-0376-5.
- [40] V. Nikolova, S. Angelova, N. Markova, and T. Dudev, "Gallium as a Therapeutic Agent: A Thermodynamic Evaluation of the Competition between Ga³⁺ and Fe³⁺ Ions in Metalloproteins," *J. Phys. Chem. B*, vol. 120, no. 9, pp. 2241–2248, Mar. 2016, doi: 10.1021/acs.jpcc.6b01135.
- [41] N. Gómez-Cerezo *et al.*, "The response of pre-osteoblasts and osteoclasts to gallium containing mesoporous bioactive glasses," *Acta Biomaterialia*, vol. 76, pp. 333–343, Aug. 2018, doi: 10.1016/j.actbio.2018.06.036.
- [42] M. Kurtjak, M. Vukomanović, A. Krajnc, L. Kramer, B. Turk, and D. Suvorov, "Designing Ga(iii)-containing hydroxyapatite with antibacterial activity," *RSC Adv.*, vol. 6, no. 114, pp. 112839–112852, 2016, doi: 10.1039/C6RA23424K.
- [43] R. S. Bockman, A. L. Boskey, N. C. Blumenthal, N. W. Alcock, and R. P. Warrell, "Gallium increases bone calcium and crystallite perfection of hydroxyapatite," *Calcif Tissue Int*, vol. 39, no. 6, pp. 376–381, Nov. 1986, doi: 10.1007/BF02555174.
- [44] S. Yamaguchi *et al.*, "Two-in-One Biointerfaces—Antimicrobial and Bioactive Nanoporous Gallium Titanate Layers for Titanium Implants," *Nanomaterials*, vol. 7, no. 8, Art. no. 8, Aug. 2017, doi: 10.3390/nano7080229.
- [45] C. Mellier *et al.*, "Design and properties of novel gallium-doped injectable apatitic cements," *Acta Biomaterialia*, vol. 24, pp. 322–332, Sep. 2015, doi: 10.1016/j.actbio.2015.05.027.
- [46] E. Zeimaran *et al.*, "Antibacterial properties of poly (octanediol citrate)/gallium-containing bioglass composite scaffolds," *J Mater Sci: Mater Med*, vol. 27, no. 1, p. 18, Jan. 2016, doi: 10.1007/s10856-015-5620-2.
- [47] H. Qiao *et al.*, "Gallium loading into a polydopamine-functionalised SrTiO₃ nanotube with combined osteoinductive and antimicrobial activities," *Ceramics International*, vol. 45, no. 17, Part A, pp. 22183–22195, Dec. 2019, doi: 10.1016/j.ceramint.2019.07.240.

- [48] C. Qiu *et al.*, "Influences of gallium substitution on the phase stability, mechanical strength and cellular response of β -tricalcium phosphate bioceramics," *Ceramics International*, vol. 46, no. 10, Part B, pp. 16364–16371, Jul. 2020, doi: 10.1016/j.ceramint.2020.03.195.
- [49] M. Yu, Y. Wang, Y. Zhang, D. Cui, G. Gu, and D. Zhao, "Gallium ions promote osteoinduction of human and mouse osteoblasts via the TRPM7/Akt signaling pathway," *Molecular Medicine Reports*, vol. 22, no. 4, pp. 2741–2752, Oct. 2020, doi: 10.3892/mmr.2020.11346.
- [50] S. P. Valappil *et al.*, "Controlled delivery of antimicrobial gallium ions from phosphate-based glasses," *Acta Biomaterialia*, vol. 5, no. 4, pp. 1198–1210, May 2009, doi: 10.1016/j.actbio.2008.09.019.
- [51] Y. Kaneko, M. Thoendel, O. Olakanmi, B. E. Britigan, and P. K. Singh, "The transition metal gallium disrupts *Pseudomonas aeruginosa* iron metabolism and has antimicrobial and antibiofilm activity," *J. Clin. Invest.*, vol. 117, no. 4, pp. 877–888, Apr. 2007, doi: 10.1172/JCI30783.
- [52] M. Gómez, D. J. Sánchez, J. L. Domingo, and J. Corbella, "Developmental toxicity evaluation of gallium nitrate in mice," *Arch Toxicol*, vol. 66, no. 3, pp. 188–192, 1992, doi: 10.1007/BF01974013.
- [53] M. M. Hart, C. F. Smith, S. T. Yancey, and R. H. Adamson, "Toxicity and Antitumor Activity of Gallium Nitrate and Periodically Related Metal Salts²²," *JNCI: Journal of the National Cancer Institute*, vol. 47, no. 5, pp. 1121–1128, Nov. 1971, doi: 10.1093/jnci/47.5.1121.
- [54] F. Li, F. Liu, K. Huang, and S. Yang, "Advancement of Gallium and Gallium-Based Compounds as Antimicrobial Agents," *Frontiers in Bioengineering and Biotechnology*, vol. 10, 2022, Accessed: Apr. 14, 2022. [Online]. Available: <https://www.frontiersin.org/article/10.3389/fbioe.2022.827960>
- [55] M. Aizawa and J. M. Buriak, "Block Copolymer Templated Chemistry for the Formation of Metallic Nanoparticle Arrays on Semiconductor Surfaces," *Chem. Mater.*, vol. 19, no. 21, pp. 5090–5101, Oct. 2007, doi: 10.1021/cm071382b.
- [56] L. Leibler, "Theory of Microphase Separation in Block Copolymers," *Macromolecules*, vol. 13, no. 6, pp. 1602–1617, Nov. 1980, doi: 10.1021/ma60078a047.
- [57] J. Bang *et al.*, "Facile Routes to Patterned Surface Neutralization Layers for Block Copolymer Lithography," *Adv. Mater.*, vol. 19, no. 24, pp. 4552–4557, Dec. 2007, doi: 10.1002/adma.200701866.
- [58] A. Blanz, S. P. Armes, and A. J. Ryan, "Self-Assembled Block Copolymer Aggregates: From Micelles to Vesicles and their Biological Applications," *Macromolecular Rapid Communications*, vol. 30, no. 4–5, pp. 267–277, 2009, doi: 10.1002/marc.200800713.
- [59] I. Cacciotti, "Cationic and Anionic Substitutions in Hydroxyapatite," in *Handbook of Bioceramics and Biocomposites*, I. V. Antoniac, Ed., Cham: Springer International Publishing, 2015, pp. 1–68. doi: 10.1007/978-3-319-09230-0_7-1.
- [60] W. A. Lopes and H. M. Jaeger, "Hierarchical self-assembly of metal nanostructures on diblock copolymer scaffolds," *Nature*, vol. 414, no. 6865, pp. 735–738, Dec. 2001, doi: 10.1038/414735a.
- [61] H.-Y. Hsueh and R.-M. Ho, "Bicontinuous Ceramics with High Surface Area from Block Copolymer Templates," *Langmuir*, vol. 28, no. 22, pp. 8518–8529, Jun. 2012, doi: 10.1021/la3009706.
- [62] Q. Peng, Y.-C. Tseng, S. B. Darling, and J. W. Elam, "A Route to Nanoscopic Materials via Sequential Infiltration Synthesis on Block Copolymer Templates," *ACS Nano*, vol. 5, no. 6, pp. 4600–4606, Jun. 2011, doi: 10.1021/nn2003234.
- [63] Z. Zhang, J. Krajniak, J. R. Keith, and V. Ganesan, "Mechanisms of Ion Transport in Block Copolymeric Polymerized Ionic Liquids," *ACS Macro Lett.*, vol. 8, no. 9, pp. 1096–1101, Sep. 2019, doi: 10.1021/acsmacrolett.9b00478.

- [64] Y. He, Z. Li, P. Simone, and T. P. Lodge, "Self-Assembly of Block Copolymer Micelles in an Ionic Liquid," *J. Am. Chem. Soc.*, vol. 128, no. 8, pp. 2745–2750, Mar. 2006, doi: 10.1021/ja058091t.
- [65] J. Min, H. Y. Jung, S. Jeong, B. Lee, C. Y. Son, and M. J. Park, "Enhancing ion transport in charged block copolymers by stabilizing low symmetry morphology: Electrostatic control of interfaces," *Proc Natl Acad Sci U S A*, vol. 118, no. 32, p. e2107987118, Aug. 2021, doi: 10.1073/pnas.2107987118.
- [66] A. B. Kutikov and J. Song, "Biodegradable PEG-Based Amphiphilic Block Copolymers for Tissue Engineering Applications," *ACS Biomater Sci Eng*, vol. 1, no. 7, pp. 463–480, Jul. 2015, doi: 10.1021/acsbiomaterials.5b00122.
- [67] W. Li, S.-S. Feng, and Y. Guo, "Block copolymer micelles for nanomedicine," *Nanomedicine*, vol. 7, no. 2, pp. 169–172, Feb. 2012, doi: 10.2217/nnm.11.182.
- [68] S. Mondal, S. V. Dorozhkin, and U. Pal, "Recent progress on fabrication and drug delivery applications of nanostructured hydroxyapatite," *WIREs Nanomedicine and Nanobiotechnology*, vol. 10, no. 4, p. e1504, 2018, doi: 10.1002/wnan.1504.
- [69] M. A. Morris, "Directed self-assembly of block copolymers for nanocircuitry fabrication," *Microelectronic Engineering*, vol. 132, pp. 207–217, Jan. 2015, doi: 10.1016/j.mee.2014.08.009.
- [70] A. P. Marencic and R. A. Register, "Controlling Order in Block Copolymer Thin Films for Nanopatterning Applications," *Annual Review of Chemical and Biomolecular Engineering*, vol. 1, no. 1, pp. 277–297, 2010, doi: 10.1146/annurev-chembioeng-073009-101007.
- [71] S. Schrickler, M. Palacio, B. T. S. Thirumamagal, and B. Bhushan, "Synthesis and morphological characterization of block copolymers for improved biomaterials," *Ultramicroscopy*, vol. 110, no. 6, pp. 639–649, May 2010, doi: 10.1016/j.ultramic.2010.02.025.
- [72] G. de Ruiter, M. Lahav, and M. E. van der Boom, "Pyridine Coordination Chemistry for Molecular Assemblies on Surfaces," *Acc. Chem. Res.*, vol. 47, no. 12, pp. 3407–3416, Dec. 2014, doi: 10.1021/ar500112b.
- [73] S. Pal, "Pyridine: A Useful Ligand in Transition Metal Complexes," *Pyridine*, Nov. 2018, doi: 10.5772/intechopen.76986.
- [74] T. Sjöström, L. E. McNamara, R. M. D. Meek, M. J. Dalby, and B. Su, "2D and 3D Nanopatterning of Titanium for Enhancing Osteoinduction of Stem Cells at Implant Surfaces," *Advanced Healthcare Materials*, vol. 2, no. 9, pp. 1285–1293, Sep. 2013, doi: 10.1002/adhm.201200353.
- [75] K. F. Eichholz *et al.*, "Human bone marrow stem/stromal cell osteogenesis is regulated via mechanically activated osteocyte-derived extracellular vesicles," *Stem Cells Translational Medicine*, vol. 9, no. 11, pp. 1431–1447, Nov. 2020, doi: 10.1002/sctm.19-0405.
- [76] D. Abdallah *et al.*, "An Optimized Method to Generate Human Active Osteoclasts From Peripheral Blood Monocytes," *Frontiers in Immunology*, vol. 9, 2018, Accessed: Jan. 09, 2023. [Online]. Available: <https://www.frontiersin.org/articles/10.3389/fimmu.2018.00632>
- [77] W. Liu *et al.*, "LncRNA-mRNA expression profiles and functional networks in osteoclast differentiation," *J Cell Mol Med*, vol. 24, no. 17, pp. 9786–9797, Sep. 2020, doi: 10.1111/jcmm.15560.
- [78] J. N. L. Albert and T. H. Epps, "Self-assembly of block copolymer thin films," *Materials Today*, vol. 13, no. 6, pp. 24–33, Jun. 2010, doi: 10.1016/S1369-7021(10)70106-1.
- [79] V. Thakur and S. M. Shivaprasad, "Electronic structure of GaN nanowall network analysed by XPS," *Applied Surface Science*, vol. 327, pp. 389–393, Feb. 2015, doi: 10.1016/j.apsusc.2014.11.082.
- [80] M. Senthil Kumar and J. Kumar, "XRD, XPS, SEM, PL and Raman scattering analysis of synthesised GaN powder," *Materials Chemistry and Physics*, vol. 77, no. 2, pp. 341–345, Jan. 2003, doi: 10.1016/S0254-0584(02)00012-3.

- [81] W. Brittle *et al.*, "Improvement in Mycobacterial Yield and Reduced Time to Detection in Pediatric Samples by Use of a Nutrient Broth Growth Supplement," *Journal of Clinical Microbiology*, vol. 47, no. 5, pp. 1287–1289, May 2009, doi: 10.1128/JCM.02320-08.
- [82] V. S. M. Saegeman, D. Lismont, B. Verduyckt, N. L. Ectors, and J. Verhaegen, "Comparison of microbiological culture methods in screening allograft tissue. Swab versus nutrient broth," *Journal of Microbiological Methods*, vol. 70, no. 2, pp. 374–378, Aug. 2007, doi: 10.1016/j.mimet.2007.05.014.
- [83] D. J. Stokely, J. T. C. Kwan, M. R. Bending, A. T. L. Chin, and A. J. Eisinger, "Isolation of organisms in CAPD peritonitis: use of nutrient broth cultures and Bactec blood culture media," *Journal of Hospital Infection*, vol. 11, no. 1, pp. 77–81, Jan. 1988, doi: 10.1016/0195-6701(88)90042-4.
- [84] L. Kuru, G. S. Griffiths, A. Petrie, and I. Olsen, "Alkaline phosphatase activity is upregulated in regenerating human periodontal cells," *J Periodontal Res*, vol. 34, no. 2, pp. 123–127, Feb. 1999, doi: 10.1111/j.1600-0765.1999.tb02231.x.
- [85] A. Sabokbar, P. J. Millett, B. Myer, and N. Rushton, "A rapid, quantitative assay for measuring alkaline phosphatase activity in osteoblastic cells in vitro," *Bone and Mineral*, vol. 27, no. 1, pp. 57–67, Jan. 1994, doi: 10.1016/S0169-6009(08)80187-0.
- [86] A. Serguienko, M. Y. Wang, and O. Myklebost, "Real-Time Vital Mineralization Detection and Quantification during In Vitro Osteoblast Differentiation," *Biological Procedures Online*, vol. 20, no. 1, p. 14, Aug. 2018, doi: 10.1186/s12575-018-0079-4.
- [87] K. Subramani, S. N. Pandravadra, D. A. Puleo, J. K. Hartsfield, and S. S. Huja, "In vitro evaluation of osteoblast responses to carbon nanotube-coated titanium surfaces," *Progress in Orthodontics*, vol. 17, no. 1, p. 23, Jul. 2016, doi: 10.1186/s40510-016-0136-y.
- [88] P. Ballanti *et al.*, "Tartrate-resistant acid phosphate activity as osteoclastic marker: sensitivity of cytochemical assessment and serum assay in comparison with standardized osteoclast histomorphometry," *Osteoporos Int*, vol. 7, no. 1, pp. 39–43, 1997, doi: 10.1007/BF01623458.
- [89] C. Ghayor, R. M. Correro, K. Lange, L. S. Karfeld-Sulzer, K. W. Grätz, and F. E. Weber, "Inhibition of Osteoclast Differentiation and Bone Resorption by N-Methylpyrrolidone," *J Biol Chem*, vol. 286, no. 27, pp. 24458–24466, Jul. 2011, doi: 10.1074/jbc.M111.223297.

Chapter 6: Incorporating an additive layer over hydroxyapatite coating using polymeric patterns and inorganic infiltration.

Abstract

Hydroxyapatite is used to improve surgical outcomes of orthopaedic surgeries because it promotes bone growth at the site of the implant. Despite this, there remains some issues with regards to post-operative or hospital-based infections as hydroxyapatite itself is not inherently antimicrobial. Research is ongoing around adding other elements to the hydroxyapatite to improve the antimicrobial performance of orthopaedic implants. Gallium and zinc are particularly important as they are known to promote osteointegration whilst they also have antimicrobial properties.

This chapter shows how a nano-polymer template can be used as a sacrificial layer for inorganic materials to be applied to hydroxyapatite coatings. The results demonstrate, through atomic force and electron microscopy, that the crystalline structure and morphology of the deposited HA layer is unaffected by the application of a polymer template. Data shows that this template can be infiltrated with gallium precursors and the polymer layer completely removed during processing leaving gallium oxide at the surface. Chemical analysis comparison using infra-red, and electron dispersive spectroscopy shows no difference in the hydroxyapatite post-doping. Data proves that a measurable gallium ionic release into *in vitro* fluids can be achieved from the gallium oxide nanofeatures. Furthermore, an optimum patterning and precursor concentration is selected, and this also supports the application of zinc over hydroxyapatite. X-ray fluorescence data shows that on a larger millimetre scale the doping of hydroxyapatite has been successful implying easy replication of this process for larger orthopaedic implants.

6.1 Introduction

Orthopaedic surgeons use metallic based implants for a variety of reasons, including, but not limited to the repair of bone fractures, bone graft post- tumours,

prosthetic implants, joint replacements, maxillofacial or cranial reconstruction surgery. [1] To increase the osteoinduction of metals, synthetic hydroxyapatite as a scaffold or coating is used which mimics biological hydroxyapatite (the brittle part of natural teeth and bone mineral consisting of calcium, phosphate and hydroxyl groups.) [2]–[5] Synthetic hydroxyapatite (HA) also accelerates bone fixation and encourages stronger bone bonding via tight engineering control of its physiochemical properties. Parameters such as phase composition, porosity, roughness and thickness dictate the outcome of a coating *in vivo*. [6]–[9]

HA itself does not have antimicrobial properties and infection can be a serious complication of orthopaedic implant surgery. Post operative infections lead to severe physiological damage, require follow up surgical procedures or amputations in rare cases. [10] Separately, there is a global surge in antibiotic resistant strains of bacteria, and these affect all patients who undergo surgery in general as surgeries expose internal organs to external microbes.[11]–[13] As well as this, patients who are immunocompromised, overweight or have certain conditions such as osteoporosis do not generally have good replacement outcomes when compared to the general population. [14]–[17] In light of these clinical challenges the need to engineer a more antimicrobial, osteoinductive HA has become apparent, but retaining the existing benefits must be considered paramount before any additional elements can be added to a system.

Biological HA has naturally occurring non-HA ions at very low concentrations, such as trace amounts of sodium, fluorine, zinc, carbonates or many more. [18] Within the HA lattice anions can replace PO_4^{3-} or OH^- groups whereas cations can replace Ca^{2+} ions, this happens by surface absorption or chemical incorporation. [19] Accordingly, synthetic HA can be doped with antimicrobial elements, most commonly gallium, strontium, magnesium, zinc, iron, copper, silver or fluorine. [20] Even the addition of unusual elements such as uranium, europium, carbon nanotubes or various nanoparticles to HA have been studied for their effects on the antimicrobial, physical and chemical properties. [21]–[26] Various reviews have been undertaken in the field of biomedical advances regarding the atomic doping of hydroxyapatite to improve its performance.[27], [28] A plethora of different elements or even combinations of them have all shown promise in research but an industrial realisation of this potential has not

been achieved [29], [30]. Despite all the research completed, the presence and intercalation of non-HA ions affects the crystallinity, mechanical properties, biological degradation and cellular response of HA which in turn may hinder its osteointegrative function. [22] [20], [30]. Conventional coating methods incur changes to the physical and chemical properties of HA and may create toxic intermediary compounds when additional elements are added. [27], [31] Unfortunately, while doping is a convenient way of improving the antimicrobial performance of HA its comes at the detriment of the structural and chemical integrity of the HA.[32] Therefore, a methodology where dopant features are formed at the surface of the HA films may be preferred. It may also be important to control the size and shape of any dopant material features at the surface as this allows for high surface areas and thus rapid release, and control of release rate (through size and shape control).

This research proposes a polymer coating method to deposit nano-amounts of dopant over HA without affecting the physical composition. Block Copolymer (BCP) self-assembly and polymer brush (PB) grafting methods have been used in other scientific areas for controlled formation of precise material nanopatterns which may facilitate feature formation and control. [33]–[39] Infiltration of a metallic precursor selectively into one domain of a BCP or PB gives rise to highly ordered metal or oxide nanostructures that can be dimensionally accurate down to the scale of a few nanometres. [40], [41] Polymers templates such as these have also been shown to have biomedical uses for drug delivery and diagnostics due to their tuneable uptick of bioactive compounds. [42]–[45]

This work demonstrates that the use of the polymer poly(4-vinylpyridine). Polystyrene-*b*-poly(4-vinylpyridine) (PS-*b*-P4VP) BCP, when deposited on a silicon substrate and separated into different geometries selectively uptakes metal ions such as iron or gallium into the P4VP block since it has a strong affinity to bind metallic ions unlike the PS block. [46], [47]

As well as inorganic patterns being created by BCP self-assembly, thin films of the inorganic can be formed at the HA surface. Poly(4-vinylpyridine) (P4VP) polymer brushes (short chain polymers that are end functionalised to covalently bond hydroxyl surfaces) have the same propensity for infiltration and capture of inorganic materials. [48], [49] In this work we coat HA with a P4VP-based

polymer layer which covalently bonds with excess hydroxyl groups present in the hydroxyapatite. To prove our concept, we have paired the polymer techniques with gallium infiltration and evaluated the concept with zinc infiltration. Both zinc and gallium are proven to promote bone growth stems cells; osteoclasts and inhibit bone adsorptive stem cells; osteoclasts, while being antimicrobial. [50]–[53] The dosage of the additive element is controlled by the polymer thickness and solution strength and can even allow for dosage of more than one element at a time.[54], [55]. Once the BCP or brush is infiltrated with an additive element, the coated HA part is placed under Ultraviolet Ozone, the polymer dissolves but the added element from the solution remains in place on top of the hydroxyapatite, **Figure 6.1**.

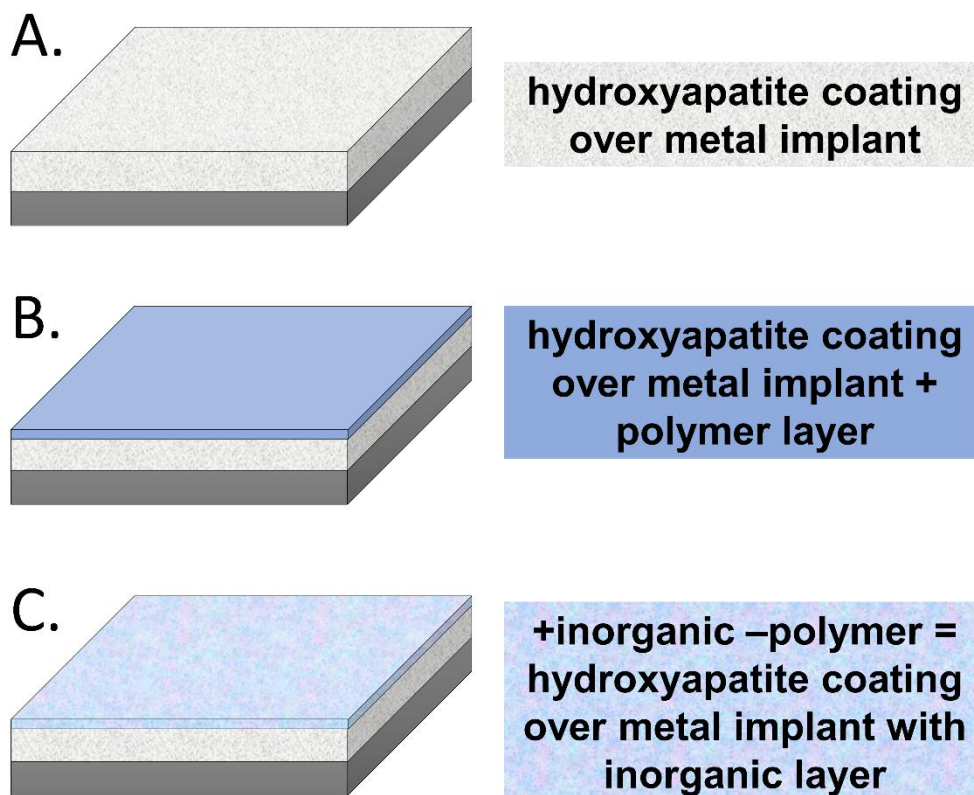


Figure 6.1: Diagram to represent three different steps in this coating process whereby A: the initial coating is just hydroxyapatite over a metallic part, B: the deposition of a polymeric layer has been added on top of the hydroxyapatite and C: the polymeric layer has been infiltrated with an inorganic element, polymer

removed and the result is a hydroxyapatite layer with a nano layer of an additive inorganic element on top of it.

In these experiments we use hydroxyapatite coatings on various substrates which have previously been extensively studied, meaning the exact composition, morphology and structure of them is known.[56]–[58] These HA coated substrates are analogues of orthopaedic implants and gallium and iron as dopants will illustrate the approach which could be used for doping real metallic-HA coated devices. Upon gallium coating we undertake atomic force microscopy on the nanostructure. X-ray diffraction data paired with electron imaging confirms the crystallinity and wider scale morphology of the hydroxyapatite is unaffected. Chemical analysis of the coating reveals that the nature of the hydroxyapatite is unchanged, apart from the gallium or zinc which has been attached to the surface. Gallium ionic release is confirmed from inductively coupled plasma spectroscopy analysis of release fluids. X-ray fluorescence data confirms the method is applicable on a wider scale and allows for comparison between the gallium and zinc elemental uptick.

6.2 Materials and Methods

Hydroxyapatite (HA) coatings were deposited onto substrates using a colloidal solution deposition method as described by Murphy et al[56]–[58]. These HA coatings were highly porous and extensive materials characterisation is used to prove that the dopant is present post polymer processing.

6.2.1 Polymer patterning and polymer brush film formation

Polystyrene-*b*-poly(4-vinylpyridine) (PS-*b*-P4VP) block copolymer (BCP) of molecular weight 50-*b*-6 kg mol⁻¹ and hydroxy terminated poly(4-vinylpyridine) (P4VP-OH) polymer brush (PB) of molecular weight 6.5 kg mol⁻¹ were purchased from Polymer Source Inc and were used as received. All other chemicals/solvents were ex-Sigma Aldrich or Fisher Scientific. BCPs were dissolved in solvent mixture comprising 4:1 toluene (99 %): tetrahydrofuran (99 %). BCP solutions were made to 0.5 wt.% concentration and stirred for 24 h. PB was dissolved in a solvent mixture comprising 2:3 tetrahydrofuran (99 %): Isopropyl alcohol (>98 %). BP solutions were made to 0.2 wt.% concentration and stirred for 24 h.

Either a BCP or a PB solution was spin cast at 3000 RPM for 30 seconds onto a hydroxyapatite coated substrate. See **Appendix 6.5** for schematics of the steps involved in these processes. Annealing was then performed on the as spun polymer layer. For PBs, samples were thermally annealed at 200 °C for 5-15 min depending on thickness of the substrate used. For BCPs, samples were solvent vapor annealed by placing the samples into a sealed glass jar with a 7 ml vial of chloroform in a fridge at 4 °C for 2 h. To fully enhance the micro-phase separation of the BCP film, samples were immersed in 100 % ethanol for 15 min afterwards. Inorganic precursor solutions were made up in the range of 1 wt.% to 2 wt.% using gallium (III)nitrate hydrate 99.9 % or zinc nitrate hexahydrate 98 % in anhydrous ethanol (99.8 %). Metal nitrates were used as precursors since they form amorphous metal oxides post photodecomposition.[59] Solutions were stirred for 1 h to ensure full dissolution of the salt. Inorganic solutions were Spin cast over the polymeric layers at 3000 RPM for 30 seconds and placed in a Novascan PSD Pro UV Lamp for 4 hours; this removes the organic polymeric layer and leaves behind inorganic structures in place of the poly(4-vinylpyridine) (P4VP).

6.2.2 Characterisation

Atomic force microscopy (AFM) was performed using an aXE-7, Park Systems AFM with non-contact cantilevers. AFM calculated average roughness values as average roughness (Ra) and peak-to-valley roughness (Rpv). X-ray diffraction (XRD) patterns were acquired using a Bruker Advance Powder Diffractometer (Cu-K α radiation with $\lambda = 1.5406 \text{ \AA}$, operating voltage of 40 kV and current of 40 mA). Measurements were performed in the 2θ range from 10 ° to 60 ° at steps of 0.004 °. Scanning electron microscopy (SEM) data were collected using a Carl Zeiss Ultra Microscope equipped with an in-lens detector. An accelerating voltage of 5 to 10 kV was used. Energy-dispersive X-ray spectroscopy (EDX) spectra were acquired at 15 kV on an Oxford Inca EDX detector. Fourier transform infrared spectroscopy (FTIR) spectra were obtained using a Perkin Elmer's Spotlight 200i benchtop device with attenuated total reflectance (ATR, 4000–500 cm^{-1} , 8 scans, and 4 cm^{-1} resolution diamond crystal). Inductively Coupled Plasma Optical Emission Spectroscopy (ICP-OES) was performed using Agilent Technologies 5110 ICP-OES on Phosphate Buffer Solution (PBS) in which

samples were immersed for various times. X-ray Fluorescence (XRF) mapping was performed using a Bruker S8 Tiger Series 2 with a 170 mA excitation current and 300 μm spot size.

6.3 Results

Post deposition of HA, samples underwent extensive characterisation to assess their chemical and morphological intricacies. Coatings consisted of octacalcium phosphate (OCP) phase with some crystalline HA and amorphous calcium phosphate (ACP). Samples had a clear porous and needle structure with a calcium phosphate ratio in the region of 1.33, **Figure 6.2**. [57], [58]

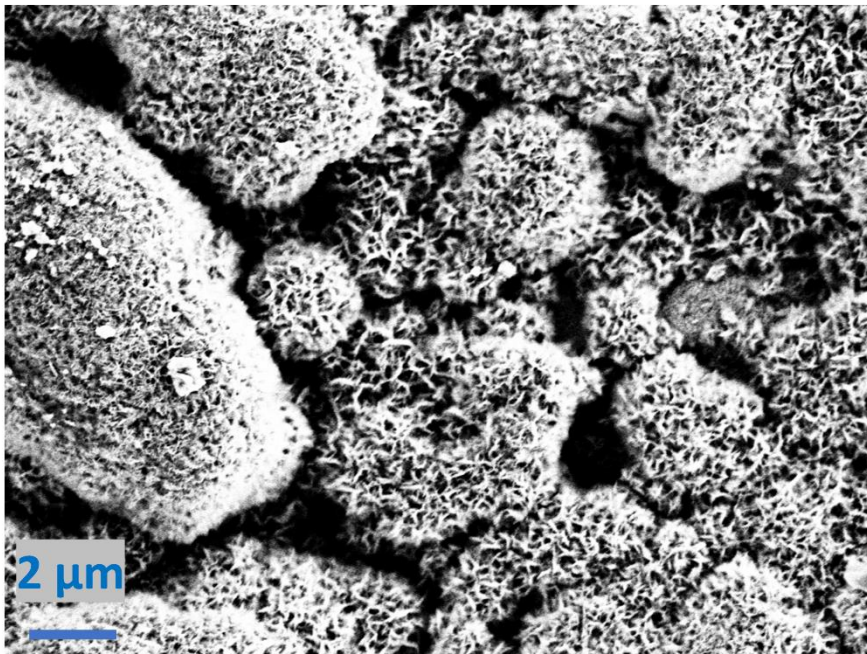


Figure 6.2: Scanning Electron Micrograph of porous hydroxyapatite coating on titanium parts.

6.3.1 Formation of nano gallium coating cast via polymer template over HA films

A selection of HA samples (3 of each sample set) underwent polymer layer deposition, be it BCP pattern or a PB layer. The polymeric layer was infiltrated with gallium at varying concentrations and the polymeric layer removed by UV ozone, results herein characterise the HA layer with a gallium coating on top (the polymer pattern used is identified in sample labels also). This data in this chapter presents 2wt.% gallium unlike **Chapter 5** in which the max was 1wt.% gallium,

this was to account for the non-uniformity of the HA surface compared with silicon-wafer based planar surfaces. Initially we were unsure what the uptick of gallium templated over this HA ceramic would be, therefore, a higher precursor concentration was used along with 1wt.%.

The first analysis undertaken was to examine if the polymer patterning or gallium infiltration of same had an impact on the structural integrity of the hydroxyapatite film. AFM using non-contact cantilevers showed that the needle-like interconnectivity and porous structure of the HA remained intact post polymer and post gallium inclusion, **Figure 6.3**. **Figure 6.3A** shows AFM images of the coating at various stages and **Figure 6.3B** the corresponding topography line profile for each sample. Post HA deposition the roughness is measured at Rpv of 1074 nm with Ra of 130 nm. Post PB deposition over the HA the roughness of the samples increases with Rpv of 1683 and Ra of 257 nm. However, this roughness value diminishes post infiltration of the BCP or PB layer with the inorganic gallium. BCP templated gallium gives Rpv of 1183 nm and Ra of 141 nm whereas PB templated gallium gave Rpv of 1369 nm and Ra of 150 nm. It is clear from these data that the HA only is matched in pore size and topography to the HA which has been gallium doped. The topography line profile shows that all samples have 4-6 pores within 1 μm while depth for all samples is matched from -400 nm to +400 nm.

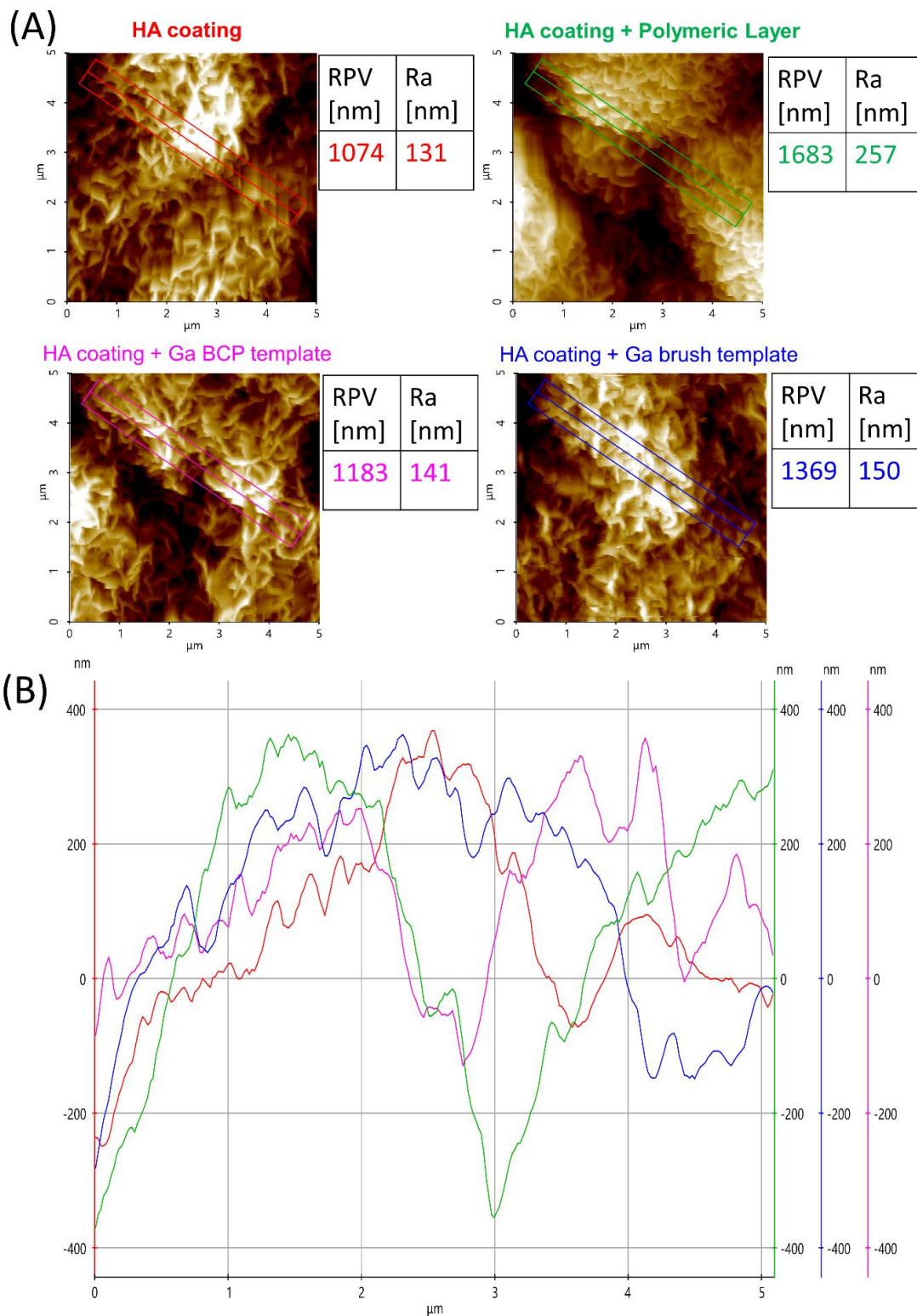


Figure 6.3: (A) Atomic force microscopy (AFM) images of sample of HA coating, HA coating with a polymer layer, HA coating with Ga infiltration of BCP layer and HA coating with Ga infiltration of PB polymer layer and (B) corresponding topography line profile for each sample.

It is not possible to determine self-assembled features on the highly roughened HA surface. However, based on previous work using the same BCP of PS-*b*-P4VP 50-*b*-6 kg mol⁻¹ on smooth substrates, we estimate that the resulting gallium feature size has a diameter between 30 and 40 nm with a feature height of around 10 nm.[47] Similarly at this PB solution concentration used, we estimate a 5 nm thick layer of gallium is deposited.[60] The XRD and SEM analysis reveal that the HA coating has been coated without any structural effects, **Figure 6.4**. **Figure 6.4B** is the SEM image of a BCP cast gallium content and **Figure 6.4C** is the SEM image of the PB cast gallium layer – neither of which show a difference. Comparing **Figure 6.4(B)** with **Figure 6.4(C)** shows no morphological difference between the use of a BCP template and a PB template. Both images reveal that the porosity and needle-like interconnectivity of the HA post gallium doping is perfectly intact.

XRD analysis charts which crystalline phases of HA are present, **Figure 6.4(A)** whereby known HA phases are labelled. One peak which at 33 ° is not labelled since it is a substrate inherent peak, sometimes presents if the X-rays are able to penetrate parts of the HA. The largest HA peaks are OCP indicative [002] at 26 ° and a signature HA triple peak at 32.5 °. [61] The intensity of [002] plane is greater than the intensity of HA triple peak for HA only. This relationship is replicated for the two types of gallium coated samples which both exhibit narrow sharp peaks at 26°, **Figure 6.4(A)**. It can be deduced that the lesser peaks of [210] and [301] had a sharper line shape post Ga coating – this is most likely due to the heating of samples during UV ozone treatment. Overall, this data shows that there is no impact to HA crystallinity from the polymer patterning process. Samples are aligned with uncoated HA and not altered by the polymer method used. The amount of gallium coated onto the HA has not interfered with the HA since no new compounds have arisen at XRD.

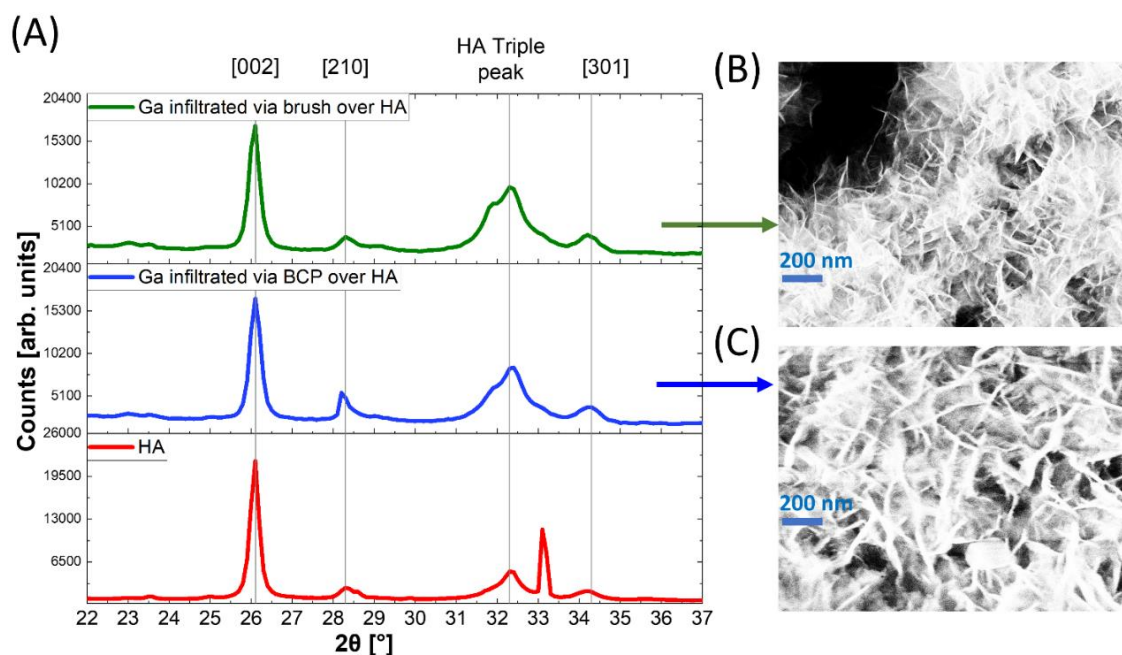


Figure 6.4: (A): X-ray diffraction (XRD) patterns in terms of counts per second versus diffraction angle of 2θ collected for Ti thin film substrate with Ga infiltrated via polymer brush over HA (green), Ga infiltrated via BCP over HA (blue) and solely HA (red), side images are the corresponding scanning electron microscope (SEM) images for the XRD patterns: (B) SEM image of Ga infiltrated via polymer brush HA and (C) SEM image of Ga infiltrated via polymer brush HA.

To confirm the chemical integrity of the film is maintained, FTIR and SEM-EDX data was collected. FTIR data was recorded in the region of 800 to 1600 cm^{-1} wavenumbers for two reasons; (i) this is the region which gives rise to significant phosphate peaks of HA [62], [63] and (ii) within this region there are known P4VP vibrational bands such as pyridine rings or C-H bending. [64]–[66] By cataloguing this FTIR data we know if the HA is chemically intact and if there is any residual polymer remaining. **Figure 6.5A** shows the FTIR spectra for gallium coated HA samples with green dotted lines at the locations of P4VP polymer vibration energies – none of which are present. This confirms the removal of the polymeric material. The blue lines in **Figure 6.5A** are the phosphate vibrational energies. **Figure 6.5A** shows matched traces for HA, Ga -coated HA (via BCP) and Ga-coated HA coated (via PB). The two modes of PO_4^{3-} and the HPO_4^{2-} peak are in the same position and at the same intensity. We can conclude that since the gallium coated traces have the peaks of phosphate region present in the exact

same locations and there is no measurable difference between the polymer methods.

EDX gave elemental data on the HA post gallium inclusion, **Figure 6.5B-C**. Samples were infiltrated by BCP or PB with either 1 wt. % or 2 wt. % solution of gallium. The calcium to phosphate ratio (Ca/P) was calculated from EDX data and per previous studies was in the region at 1.33 ± 0.14 . [56] **Figure 6.5C** shows that all gallium coated samples have a Ca/P within the distribution of samples of solely HA. The samples all have a Ca/P of 1.25 to 1.34 showing no indication of a trend with polymer pattern method used or gallium concentration applied. Since there has been processing applied to the HA layer post deposition, it would imply a slight alteration of the oxygen species at the surface. Previously samples had O at. % of 56 ± 3.5 %. Ga 2wt. % samples have higher O at. % than their Ga 1 wt. % counterparts, this implies that the higher gallium content could give rise to small amount of gallium oxides, however a larger sample size would be required to prove this.

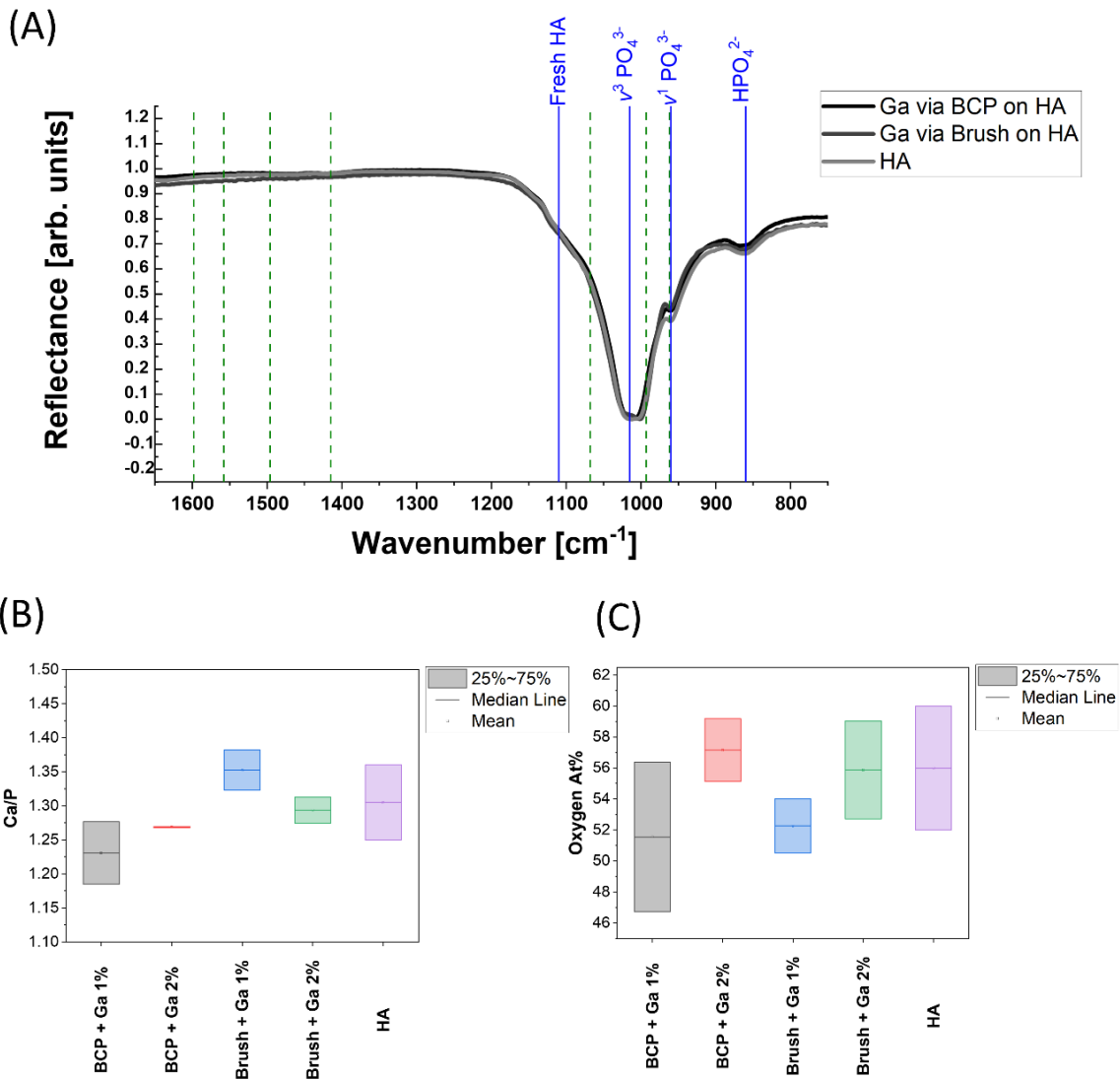


Figure 6.5: (A): Fourier Transform infrared (FTIR) spectra the region of 1600–800 cm⁻¹ for as deposited HA and Ga coated HA (via BCP and Brush) (B): Collated electron-dispersive X-ray data showing the calcium-to-phosphorus atomic ratio (Ca/P) found in the HA film as deposited and after Ga coating from 1 wt% Ga and 2 wt% gallium precursors (via BCP and Brush), (C): Atomic % oxygen (Atomic% O) found in the HA film as deposited and after Ga coating from 1 wt% Ga and 2 wt% gallium precursors (via BCP and Brush).

Thus far the data has shown minor change to the HA film besides expected low concentration levels of gallium present in the film post polymer pattern infiltration and this was confirmed by EDX, **Figure 6.6**. EDX analysis proved that we could target the gallium amount infiltrated through polymer method and the inorganic solution concentration, **Figure 6.6**. BCPs consist of a bcc spherical pattern of P4VP whereas PB consists of a covering of P4VP. After UV-ozone treatment the

P4VP of both is infiltrated with gallium and subsequently removed. The EDX detection of gallium confirms this process since the BCP formed gallium coated HA has less than 0.5 at. %, **Figure 6.6**. The PB formed Ga layer over HA however has higher Ga detection and it is clear for these samples that the increased gallium precursor concentration also affects the gallium content in the final film: Brush + 1wt % Ga is 0.4 at. % Ga and Brush + 2wt % Ga is 0.9 at. % at EDX, **Figure 6.6**.

Since these samples have intended biological applications, it was necessary to detect the level to which gallium would elute from the surface of the HA using ICP-OES. Samples were submerged in phosphate buffer solution (PBS) for 24 hours to replicate *in vivo* conditions. The ICP-OES data is presented in **Figure 6.6**. We consider 0.5ppm the low limit of detection for the ICP device therefore showing that BCP pattern Ga 1wt. % samples have little gallium ionic release. Evidently PB templated samples eluted more gallium than the BCP samples, as expected since the films cover the whole surface. The highest gallium ionic release was the brush templated Ga 2 wt. % samples with 0.15 - 0.2 ppm release into PBS after 24 hours. The Ga levels detected at ICP are low since not all of the gallium will release in 24 hours and some of the gallium will be bonded to active site on the surface of HA so may not dissolve in PBS at all. For the atomic % at EDX you would expect much higher ICP levels however this is a proof-of-concept dataset and the release of ions from HA is difficult to model. This dataset proves however, that the Ga levels detected by both EDX and ICP are tuneable and both methods increase accordingly. At this gallium release level other studies have shown that gallium can diminish osteoclastic proliferations while not affecting osteoblast growth. [67]

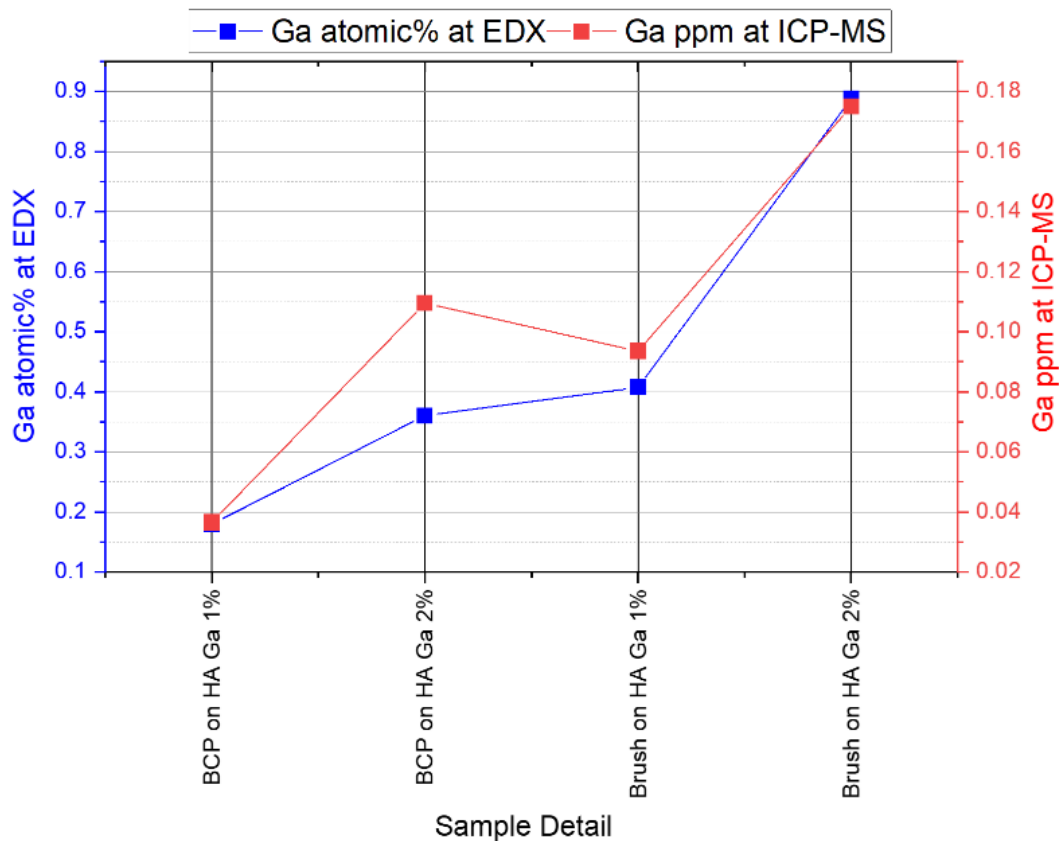


Figure 6.6: Left hand Y-axis: Atomic % Gallium (Atomic% Ga) found in the HA film as deposited and after Ga coating from 1 wt% Ga and 2 wt% gallium precursors (via BCP and Brush) and Right-hand Y-axis Gallium ionic concentration [ppm] as measured by Inductively Coupled Plasma Optical Emission Spectroscopy of phosphate buffer solution (PBS) in which samples were immersed for 24hours, sample were made using BCP or brush polymer template infiltration with either 1 wt. % or 2 wt. % gallium precursor concentrations.

6.3.2 Expansion of polymer brush templating to form zinc and gallium nanocoating on HA films.

These findings so far have confirmed that this patterning process works to coat HA with low levels of gallium without affecting the HA lattice. These gallium levels allow for ionic release into fluid *in vitro*. Since we have now proved the efficacy of the system, we replicated the process with zinc on HA and performed XRF and EDX analysis on a wider scale– this more closely resembles an orthopaedic implant. From the above dataset we chose the PB and dopant 1 wt.% system to replicate. Additionally, we increased the sample size to confirmed reproducibility through increased statistics.

Various samples of HA had a polymer brush (PB) deposited onto them. Half of these samples were infiltrated with Ga 1 wt.% solution and the other half with Zn 1 wt.% solution before EDX data was recorded. **Figure 6.7A** shows that samples have a mean gallium at. % of 0.1 with a very narrow distribution. **Figure 6.7C** shows that the zinc detection is much higher at 0.41 at. %, meaning the uptake of zinc into the PB is quadruple that of gallium. Since both ionic Ga^{3+} and Zn^{2+} are cations, they ought to intercalate in lieu of Ca^{2+} . However, the difference in valency between Ga^{3+} and $\text{Ca}^{2+}/\text{Zn}^{2+}$ probably contributes to the lower uptick of gallium into the calcium lattice positions on the outer layer of the HA coating. This data is supported by the wider scale coverage analysis provided by XRF mapping of 8 mm diameter areas of the samples. **Figure 6.7B** shows that the gallium detection measured by XRF as an intensity range of .0013 to 0.0199 arb.u. The gallium is spread across the full area of the sample albeit is lower in the upper right quadrant. **Figure 6.7D** shows the zinc detection measured by XRF as an intensity range of .0001 to 0.0253 arb.u. The zinc detection is higher in general across the whole sample with some lower areas in the middle. While some of the dopant material is covalently bonded onto the surface of the HA via the polymer, some may also be intercalated into the very top layers of the HA. When intercalation into a HA lattice, dopants take the place of a Ca^{2+} ion, for this reason the Zinc uptick may be higher than the Gallium since Zn^{2+} has the same valency as Ca^{2+} whereas Ga^{3+} does not. This valence would make Zinc intercalation to more readily occur. Comparing the gallium coverage in **Figure 6.7B** to zinc coverage in **Figure 6.7D** much higher levels of zinc are present for the zinc sample with the most homogenous overall coverage.

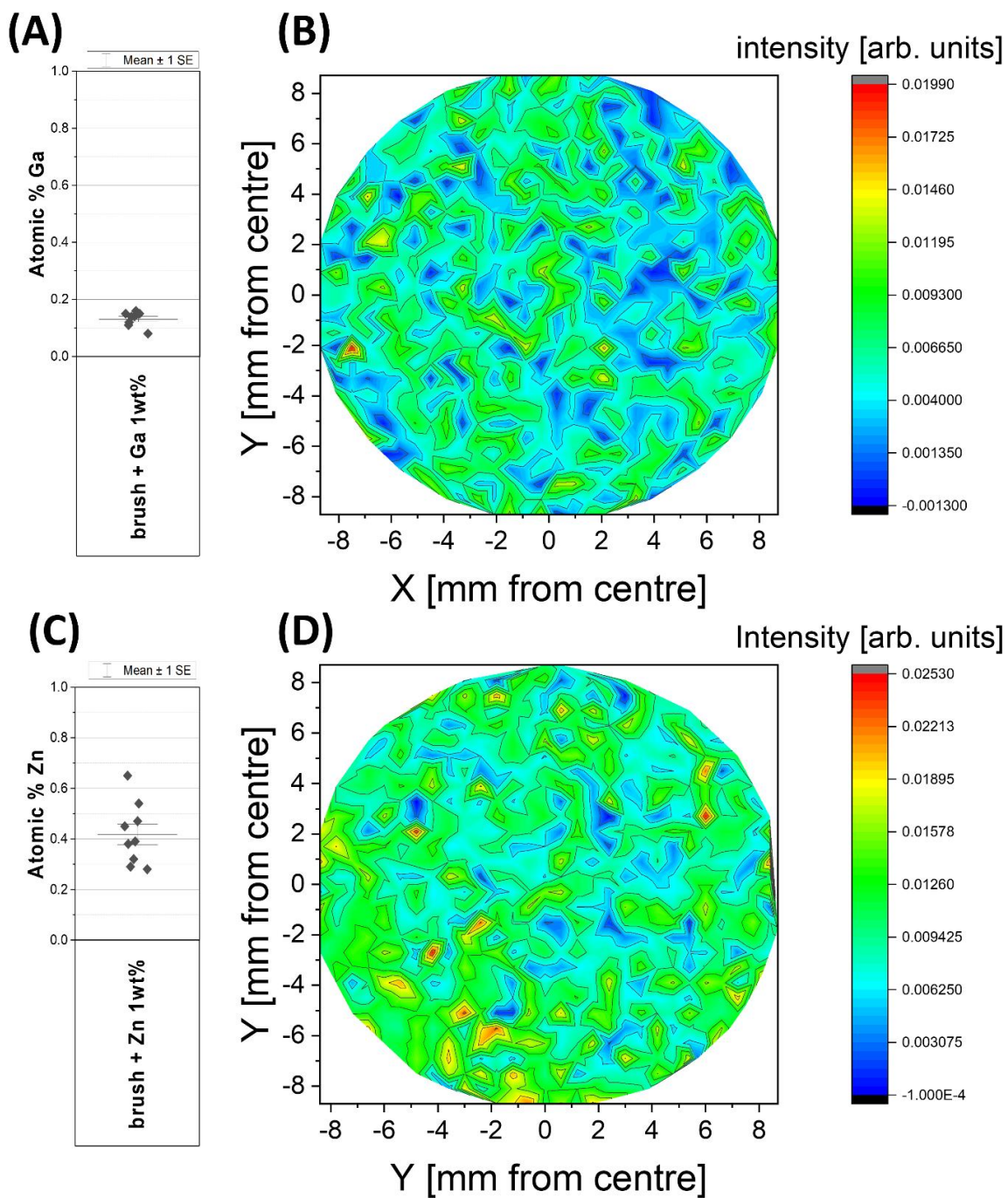


Figure 6.7: (A) Atomic % gallium (Atomic% Ga) found in the HA film after Ga coating from polymer brush and 1 wt% Ga precursor solution, (B) X-ray Fluorescence (XRF) Map of an 8mm diameter circle of gallium coated HA showing the intensity of gallium detection across the area according to the colour scale (C) Atomic % zinc (Atomic% Zn) found in the HA film after Zn coating from polymer brush and 1 wt% Zn precursor solution and (d) XRF Map of an 8mm diameter circle of zinc coated HA showing the intensity of zinc detection across the area according to the colour scale.

6.4 Conclusion

As outlined in the introduction, there is a growing need for the advancement of orthopaedic implant coatings to not just include HA but to include other more osteoinductive and antimicrobial components. Unfortunately, the inclusion of any ions into HA coating affects physiochemical properties which in turn can have an adverse effect on the *in vivo* performance of the coating.

We have proven that we can overcome this issue through selective infiltration of a polymer pattern over HA coatings. We have shown that the polymer pattern can be deposited using a facile spin coating method and subsequently infiltrated with antimicrobial gallium. This is a new technology which could be patent protected and studies could easily model whether it is industrially scalable. We have shown that the structural integrity of the HA remains intact through AFM, XRD and SEM datasets post gallium coating. HA retains its porous interconnected structure on the nanometre scale. The chemical integrity of HA remains aligned to its previously studied composition in terms of phosphate vibrational energies, Ca/P and oxygen atomic %. FTIR data confirms that the polymer itself is fully removed leaving gallium ions (as oxide). In fact, the only indication of gallium being present is a low level EDX detection and a subsequent gallium ionic release measured by ICP-OES. Combined, these data prove that the gallium, at exceptionally low levels, sits atop the HA coating ready to be released into PBS but not having any structural impact on the HA lattice.

Furthermore, we have selected a polymer brush method with 1 wt. % inorganic precursor solution as the optimum settings for coating HA and applied it to the doping of HA with zinc as well as gallium. EDX and XRF data show that for the same process, the uptick of zinc dopant is much higher than gallium. XRF data confirms that the samples have widespread dopant coverage and that this process is highly relevant to larger orthopaedic implants not just lab-scale samples.

This study has revealing opportunities in the advancement of orthopaedic implant coatings. Using sacrificial polymer layers, many different surfaces can be nano coated with an array of advantageous compounds or elements which can reduce negative patient outcomes.

6.5 Appendix Chapter 6

Appendix 6.5.1 Block Copolymer Deposition Technique.

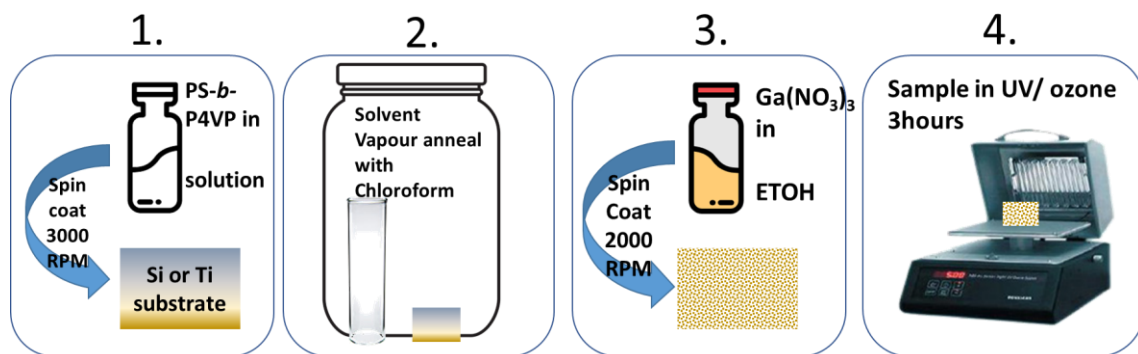


Figure A6.1: Schematic of Block Copolymer deposition over a surface

1. Cast the BCP: Polystyrene-*b*-poly(4)vinyl pyridine in solution onto a substrate.
2. Swell in solvent for micro-phase separation and reveal inherent BCP nano-dot pattern.
3. Infiltrate with inorganic (Ga) solution which has affinity to the P4VP dot.
4. UV-ozone removes polymer and leaves gallium/zinc oxide nano-dots.

Appendix 6.5.2 Polymer Brush Deposition Technique.

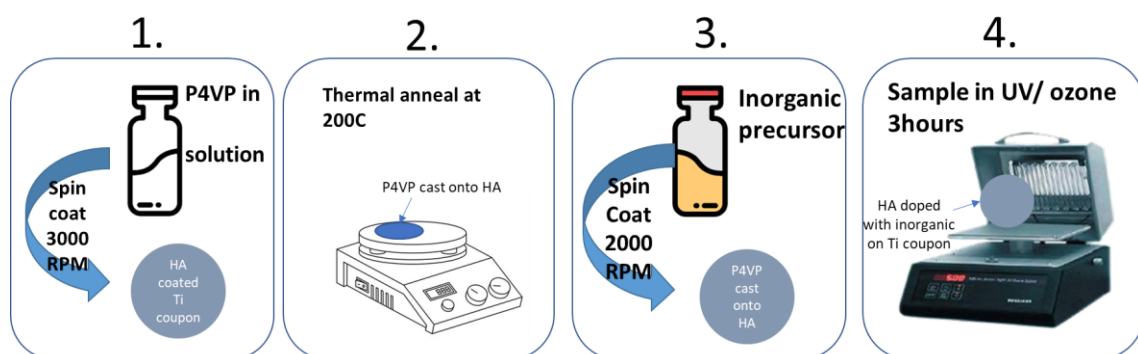


Figure A6.2: Schematic of Polymer Brush deposition over a surface

1. Cast the Polymer Brush (poly(4)vinyl pyridine) in solution onto a substrate.
2. Thermally anneal at 200°C to graft the brush to the substrate
3. Infiltrate with inorganic (Ga) solution which has affinity to the P4VP.
4. UV-ozone removes polymer and leaves gallium/zinc oxide nano-layer.

6.6 References

- [1] Y. Okazaki, "Development trends of custom-made orthopedic implants," *J Artif Organs*, vol. 15, no. 1, pp. 20–25, Mar. 2012, doi: 10.1007/s10047-011-0584-6.
- [2] W. L. Jaffe and D. F. Scott, "Current Concepts Review - Total Hip Arthroplasty with Hydroxyapatite-Coated Prostheses*," *JBJS*, vol. 78, no. 12, p. 1918, Dec. 1996.
- [3] R. G. Geesink and N. H. Hoefnagels, "Six-year results of hydroxyapatite-coated total hip replacement," *The Journal of Bone & Joint Surgery British Volume*, vol. 77-B, no. 4, pp. 534–547, Jul. 1995, doi: 10.1302/0301-620X.77B4.7615595.
- [4] R. G. T. Geesink, "Osteoconductive Coatings for Total Joint Arthroplasty.," *Clinical Orthopaedics and Related Research (1976-2007)*, vol. 395, pp. 53–65, Feb. 2002.
- [5] J. Dumbleton and M. T. Manley, "Hydroxyapatite-Coated Prostheses in Total Hip and Knee Arthroplasty," *JBJS*, vol. 86, no. 11, p. 2526, Nov. 2004.
- [6] Y.-T. Sul, C. Johansson, A. Wennerberg, L.-R. Cho, B.-S. Chang, and T. Albrektsson, "Optimum Surface Properties of Oxidized Implants for Reinforcement of Osseointegration: Surface Chemistry, Oxide Thickness, Porosity, Roughness, and Crystal Structure," vol. 20, no. 3, p. 12, 2005.
- [7] I. H. Arita, V. M. Castano, and D. S. Wilkinson, "Synthesis and processing of hydroxyapatite ceramic tapes with controlled porosity," *J Mater Sci: Mater Med*, vol. 6, no. 1, pp. 19–23, May 1995, doi: 10.1007/BF00121241.
- [8] D. D. Deligianni, N. D. Katsala, P. G. Koutsoukos, and Y. F. Missirlis, "Effect of surface roughness of hydroxyapatite on human bone marrow cell adhesion, proliferation, differentiation and detachment strength," *Biomaterials*, vol. 22, no. 1, pp. 87–96, Jan. 2000, doi: 10.1016/S0142-9612(00)00174-5.
- [9] A. K. Lynn and D. L. DuQuesnay, "Hydroxyapatite-coated Ti–6Al–4V Part 1: the effect of coating thickness on mechanical fatigue behaviour," p. 10, 2002.
- [10] R. Ghosh, S. Das, S. P. Mallick, and Z. Beyene, "A review on the antimicrobial and antibiofilm activity of doped hydroxyapatite and its composites for biomedical applications," *Materials Today Communications*, vol. 31, p. 103311, Jun. 2022, doi: 10.1016/j.mtcomm.2022.103311.
- [11] A. T. Adesoji, J. P. Onuh, I. P. Palang, A. M. Liadi, and S. Musa, "Prevalence of multi-drug resistant *Pseudomonas aeruginosa* isolated from selected residential sewages in Dutsin-Ma, Katsina State, Nigeria," *J Public Health Afr*, vol. 14, no. 2, p. 2152, Mar. 2023, doi: 10.4081/jphia.2023.2152.
- [12] L. Serwecińska, "Antimicrobials and Antibiotic-Resistant Bacteria: A Risk to the Environment and to Public Health," *Water*, vol. 12, no. 12, Art. no. 12, Dec. 2020, doi: 10.3390/w12123313.
- [13] A. Sharma *et al.*, "Globalisation of antibiotic-resistant bacteria at recurring mass gathering events," *The Lancet*, vol. 0, no. 0, Nov. 2022, doi: 10.1016/S0140-6736(22)01995-X.
- [14] J. Pietrzak, H. Common, H. Migaud, G. Pasquier, J. Girard, and S. Putman, "Have the frequency of and reasons for revision total knee arthroplasty changed since 2000? Comparison of two cohorts from the same hospital: 255 cases (2013–2016) and 68 cases (1991–1998)," *Orthopaedics & Traumatology: Surgery & Research*, vol. 105, no. 4, pp. 639–645, Jun. 2019, doi: 10.1016/j.otsr.2019.01.025.

- [15] C. R. Lehman, M. D. Ries, G. D. Paiement, and A. B. Davidson, "Infection after total joint arthroplasty in patients with human immunodeficiency virus or intravenous drug use," *The Journal of Arthroplasty*, vol. 16, no. 3, pp. 330–335, Apr. 2001, doi: 10.1054/arth.2001.21454.
- [16] S. Kessler and W. Käfer, "Overweight and Obesity: Two Predictors for Worse Early Outcome in Total Hip Replacement?," *Obesity*, vol. 15, no. 11, pp. 2840–2845, 2007, doi: 10.1038/oby.2007.337.
- [17] P. O. Zingg, A. Schallberger, H. A. Rüdiger, V. Poutawera, and C. Dora, "Does previous hip arthroscopy negatively influence the short term clinical result of total hip replacement?," *Arch Orthop Trauma Surg*, vol. 132, no. 3, pp. 299–303, Mar. 2012, doi: 10.1007/s00402-011-1352-z.
- [18] M. Akram, R. Ahmed, I. Shakir, W. A. W. Ibrahim, and R. Hussain, "Extracting hydroxyapatite and its precursors from natural resources," *J Mater Sci*, vol. 49, no. 4, pp. 1461–1475, Feb. 2014, doi: 10.1007/s10853-013-7864-x.
- [19] I. Cacciotti, "Cationic and Anionic Substitutions in Hydroxyapatite," in *Handbook of Bioceramics and Biocomposites*, I. V. Antoniac, Ed., Cham: Springer International Publishing, 2015, pp. 1–68. doi: 10.1007/978-3-319-09230-0_7-1.
- [20] I. Ratha, P. Datta, V. K. Balla, S. K. Nandi, and B. Kundu, "Effect of doping in hydroxyapatite as coating material on biomedical implants by plasma spraying method: A review," *Ceramics International*, vol. 47, no. 4, pp. 4426–4445, Feb. 2021, doi: 10.1016/j.ceramint.2020.10.112.
- [21] A. A. White, S. M. Best, and I. A. Kinloch, "Hydroxyapatite–Carbon Nanotube Composites for Biomedical Applications: A Review," *International Journal of Applied Ceramic Technology*, vol. 4, no. 1, pp. 1–13, 2007, doi: 10.1111/j.1744-7402.2007.02113.x.
- [22] H. Shi, Z. Zhou, W. Li, Y. Fan, Z. Li, and J. Wei, "Hydroxyapatite Based Materials for Bone Tissue Engineering: A Brief and Comprehensive Introduction," *Crystals*, vol. 11, no. 2, Art. no. 2, Feb. 2021, doi: 10.3390/cryst11020149.
- [23] L. Chen, Y. Wang, X. Cao, Z. Zhang, and Y. Liu, "Effect of doping cation on the adsorption properties of hydroxyapatite to uranium," *Journal of Solid State Chemistry*, vol. 317, p. 123687, Jan. 2023, doi: 10.1016/j.jssc.2022.123687.
- [24] F. Tosan, N. Rahnama, D. Sakhaei, A. H. Fathi, and A. Yari, "Effects of doping metal nanoparticles in hydroxyapatite in Improving the physical and chemical properties of dental implants," *Nanomedicine Research Journal*, vol. 6, no. 4, pp. 327–336, Nov. 2021, doi: 10.22034/nmrj.2021.04.002.
- [25] A. Fakharzadeh, R. Ebrahimi-Kahrizsangi, B. Nasiri-Tabrizi, and W. Jeffrey Basirun, "Effect of dopant loading on the structural features of silver-doped hydroxyapatite obtained by mechanochemical method," *Ceramics International*, vol. 43, no. 15, pp. 12588–12598, Oct. 2017, doi: 10.1016/j.ceramint.2017.06.136.
- [26] P. Yang, Z. Quan, C. Li, X. Kang, H. Lian, and J. Lin, "Bioactive, luminescent and mesoporous europium-doped hydroxyapatite as a drug carrier," *Biomaterials*, vol. 29, no. 32, pp. 4341–4347, Nov. 2008, doi: 10.1016/j.biomaterials.2008.07.042.
- [27] S. Panda, C. K. Biswas, and S. Paul, "A comprehensive review on the preparation and application of calcium hydroxyapatite: A special focus on atomic doping methods for bone tissue engineering," *Ceramics International*, vol. 47, no. 20, pp. 28122–28144, Oct. 2021, doi: 10.1016/j.ceramint.2021.07.100.
- [28] S. Awasthi, S. K. Pandey, E. Arunan, and C. Srivastava, "A review on hydroxyapatite coatings for the biomedical applications: experimental and theoretical perspectives," *J. Mater. Chem. B*, vol. 9, no. 2, pp. 228–249, Jan. 2021, doi: 10.1039/D0TB02407D.
- [29] D. Arcos and M. Vallet-Regí, "Substituted hydroxyapatite coatings of bone implants," *J. Mater. Chem. B*, vol. 8, no. 9, pp. 1781–1800, Mar. 2020, doi: 10.1039/C9TB02710F.
- [30] N. C. Reger, A. K. Bhargava, I. Ratha, B. Kundu, and V. K. Balla, "Structural and phase analysis of multi-ion doped hydroxyapatite for biomedical applications," *Ceramics International*, vol. 45, no. 1, pp. 252–263, Jan. 2019, doi: 10.1016/j.ceramint.2018.09.160.

- [31] T. Baskaran, N. F. Mohammad, S. S. M. Saleh, N. F. M. Nasir, and F. D. M. Daud, "Synthesis Methods of Doped Hydroxyapatite: A Brief Review," *J. Phys.: Conf. Ser.*, vol. 2071, no. 1, p. 012008, Oct. 2021, doi: 10.1088/1742-6596/2071/1/012008.
- [32] V. Uskoković, "Ion-doped hydroxyapatite: An impasse or the road to follow?," *Ceramics International*, vol. 46, no. 8, Part B, pp. 11443–11465, Jun. 2020, doi: 10.1016/j.ceramint.2020.02.001.
- [33] C. Park, J. Yoon, and E. L. Thomas, "Enabling nanotechnology with self assembled block copolymer patterns," *Polymer*, vol. 44, no. 22, pp. 6725–6760, Oct. 2003, doi: 10.1016/j.polymer.2003.08.011.
- [34] G. O. R. Alberda van Ekenstein, R. Meyboom, G. ten Brinke, and O. Ikkala, "Determination of the Flory–Huggins Interaction Parameter of Styrene and 4-Vinylpyridine Using Copolymer Blends of Poly(styrene-co-4-vinylpyridine) and Polystyrene," *Macromolecules*, vol. 33, no. 10, pp. 3752–3756, May 2000, doi: 10.1021/ma992118+.
- [35] M. A. Morris, "Directed self-assembly of block copolymers for nanocircuitry fabrication," *Microelectronic Engineering*, vol. 132, pp. 207–217, Jan. 2015, doi: 10.1016/j.mee.2014.08.009.
- [36] Y.-H. Kang *et al.*, "Large-Area Uniform 1-nm-Level Amorphous Carbon Layers from 3D Conformal Polymer Brushes. A 'Next-Generation' Cu Diffusion Barrier?," *Advanced Materials*, vol. 34, no. 15, p. 2110454, 2022, doi: 10.1002/adma.202110454.
- [37] J. Y. Bae, H.-J. Lee, and W. S. Choi, "Cube sugar-like sponge/polymer brush composites for portable and user-friendly heavy metal ion adsorbents," *Journal of Hazardous Materials*, vol. 320, pp. 133–142, Dec. 2016, doi: 10.1016/j.jhazmat.2016.07.067.
- [38] G. Gunkel, M. Weinhart, T. Becherer, R. Haag, and W. T. S. Huck, "Effect of Polymer Brush Architecture on Antibiofouling Properties," *Biomacromolecules*, vol. 12, no. 11, pp. 4169–4172, Nov. 2011, doi: 10.1021/bm200943m.
- [39] T. Kreer, "Polymer-brush lubrication: a review of recent theoretical advances," *Soft Matter*, vol. 12, no. 15, pp. 3479–3501, 2016, doi: 10.1039/C5SM02919H.
- [40] C. Cummins and M. A. Morris, "Using block copolymers as infiltration sites for development of future nanoelectronic devices: Achievements, barriers, and opportunities," *Microelectronic Engineering*, vol. 195, pp. 74–85, Aug. 2018, doi: 10.1016/j.mee.2018.04.005.
- [41] W. A. Lopes and H. M. Jaeger, "Hierarchical self-assembly of metal nanostructures on diblock copolymer scaffolds," *Nature*, vol. 414, no. 6865, pp. 735–738, Dec. 2001, doi: 10.1038/414735a.
- [42] M. Krishnamoorthy, S. Hakobyan, M. Ramstedt, and J. E. Gautrot, "Surface-Initiated Polymer Brushes in the Biomedical Field: Applications in Membrane Science, Biosensing, Cell Culture, Regenerative Medicine and Antibacterial Coatings," *Chem. Rev.*, vol. 114, no. 21, pp. 10976–11026, Nov. 2014, doi: 10.1021/cr500252u.
- [43] R. Yang, X. Wang, S. Yan, A. Dong, S. Luan, and J. Yin, "Advances in design and biomedical application of hierarchical polymer brushes," *Progress in Polymer Science*, vol. 118, p. 101409, Jul. 2021, doi: 10.1016/j.progpolymsci.2021.101409.
- [44] D. Li, L. Xu, J. Wang, and J. E. Gautrot, "Responsive Polymer Brush Design and Emerging Applications for Nanotheranostics," *Advanced Healthcare Materials*, vol. 10, no. 5, p. 2000953, 2021, doi: 10.1002/adhm.202000953.
- [45] W. Li, S.-S. Feng, and Y. Guo, "Block copolymer micelles for nanomedicine," *Nanomedicine*, vol. 7, no. 2, pp. 169–172, Feb. 2012, doi: 10.2217/nnm.11.182.
- [46] C. Cummins *et al.*, "Self-assembly of polystyrene-block-poly(4-vinylpyridine) block copolymer on molecularly functionalized silicon substrates: fabrication of inorganic nanostructured etchmask for lithographic use," *J. Mater. Chem. C*, vol. 1, no. 47, p. 7941, 2013, doi: 10.1039/c3tc31498g.
- [47] B. Murphy, C. Martins, M. Maggio, M. A. Morris, and D. A. Hoey, "Nano sized gallium oxide surface features for enhanced antimicrobial and osteo-integrative responses," *Colloids and Surfaces B: Biointerfaces*, vol. 227, p. 113378, Jul. 2023, doi: 10.1016/j.colsurfb.2023.113378.

- [48] G. Nie, G. Li, L. Wang, and X. Zhang, "Nanocomposites of polymer brush and inorganic nanoparticles: preparation, characterization and application," *Polym. Chem.*, vol. 7, no. 4, pp. 753–769, Jan. 2016, doi: 10.1039/C5PY01333J.
- [49] D. Berman and E. Shevchenko, "Design of functional composite and all-inorganic nanostructured materials via infiltration of polymer templates with inorganic precursors," *J. Mater. Chem. C*, vol. 8, no. 31, pp. 10604–10627, Aug. 2020, doi: 10.1039/D0TC00483A.
- [50] M. Shokri, M. Kharaziha, H. A. Tafti, M. B. Eslaminejad, and R. M. Aghdam, "Synergic role of zinc and gallium doping in hydroxyapatite nanoparticles to improve osteogenesis and antibacterial activity," *Biomaterials Advances*, vol. 134, p. 112684, Mar. 2022, doi: 10.1016/j.msec.2022.112684.
- [51] A. Donnadio *et al.*, "Bioinspired Reactive Interfaces Based on Layered Double Hydroxides-Zn Rich Hydroxyapatite with Antibacterial Activity," *ACS Biomater. Sci. Eng.*, vol. 7, no. 4, pp. 1361–1373, Apr. 2021, doi: 10.1021/acsbomaterials.0c01643.
- [52] D. G. Tamay *et al.*, "Corrosion Resistance and Cytocompatibility of Magnesium–Calcium Alloys Modified with Zinc- or Gallium-Doped Calcium Phosphate Coatings," *ACS Appl. Mater. Interfaces*, vol. 14, no. 1, pp. 104–122, Jan. 2022, doi: 10.1021/acsaami.1c16307.
- [53] M. Kurtjak, M. Vukomanović, L. Kramer, and D. Suvorov, "Biocompatible nano-gallium/hydroxyapatite nanocomposite with antimicrobial activity," *J Mater Sci: Mater Med*, vol. 27, no. 11, p. 170, Oct. 2016, doi: 10.1007/s10856-016-5777-3.
- [54] C. Wang and H. Zhao, "Polymer brush-based erasable and rewritable nanostructured particle surfaces," *Mater. Chem. Front.*, vol. 6, no. 13, pp. 1788–1794, Jun. 2022, doi: 10.1039/D2QM00209D.
- [55] M. Zhang, M. Wei, D. Wang, and Y. Duan, "Preparation and characterization of a drug vehicle: Polymer brush immobilized Ag nanoparticles onto titanium nanotubes," *Materials Letters*, vol. 135, pp. 51–54, Nov. 2014, doi: 10.1016/j.matlet.2014.07.138.
- [56] B. Murphy, J. Baez, and M. A. Morris, "Characterizing Hydroxyapatite Deposited from Solution onto Novel Substrates in Terms of Growth Mechanism and Physical Chemical Properties," *Materials Proceedings*, vol. 14, no. 1, Art. no. 1, 2023, doi: 10.3390/IOC2023-14491.
- [57] B. Murphy, M. A. Morris, and J. Baez, "Development of Hydroxyapatite Coatings for Orthopaedic Implants from Colloidal Solutions: Part 1—Effect of Solution Concentration and Deposition Kinetics," *Nanomaterials*, vol. 13, no. 18, Art. no. 18, Jan. 2023, doi: 10.3390/nano13182577.
- [58] B. Murphy, M. A. Morris, and J. Baez, "Development of Hydroxyapatite Coatings for Orthopaedic Implants from Colloidal Solutions: Part 2—Detailed Characterisation of the Coatings and Their Growth Mechanism," *Nanomaterials*, vol. 13, no. 18, Art. no. 18, Jan. 2023, doi: 10.3390/nano13182606.
- [59] J. He *et al.*, "Photodecomposition of Metal Nitrate and Chloride Compounds Yields Amorphous Metal Oxide Films," *J. Am. Chem. Soc.*, vol. 139, no. 50, pp. 18174–18177, Dec. 2017, doi: 10.1021/jacs.7b11064.
- [60] P. Yadav *et al.*, "Fabrication of High- κ Dielectric Metal Oxide Films on Topographically Patterned Substrates: Polymer Brush-Mediated Depositions," *ACS Appl. Mater. Interfaces*, vol. 14, no. 28, pp. 32729–32737, Jul. 2022, doi: 10.1021/acsaami.2c07966.
- [61] P. Ducheyne, W. Van Raemdonck, J. C. Heughebaert, and M. Heughebaert, "Structural analysis of hydroxyapatite coatings on titanium," *Biomaterials*, vol. 7, no. 2, pp. 97–103, Mar. 1986, doi: 10.1016/0142-9612(86)90063-3.
- [62] A. Ślósarczyk, Z. Paszkiewicz, and C. Paluszkiwicz, "FTIR and XRD evaluation of carbonated hydroxyapatite powders synthesized by wet methods," *Journal of Molecular Structure*, vol. 744–747, pp. 657–661, Jun. 2005, doi: 10.1016/j.molstruc.2004.11.078.
- [63] A. Ślósarczyk, C. Paluszkiwicz, M. Gawlicki, and Z. Paszkiewicz, "The FTIR spectroscopy and QXRD studies of calcium phosphate based materials produced from the

powder precursors with different ratios," *Ceramics International*, vol. 23, no. 4, pp. 297–304, Jan. 1997, doi: 10.1016/S0272-8842(96)00016-8.

[64] K. H. Wu, Y. R. Wang, and W. H. Hwu, "FTIR and TGA studies of poly(4-vinylpyridine-co-divinylbenzene)–Cu(II) complex," *Polymer Degradation and Stability*, vol. 79, no. 2, pp. 195–200, Jan. 2003, doi: 10.1016/S0141-3910(02)00261-6.

[65] E. Groppo *et al.*, "Exploring the Chemistry of Electron-Accepting Molecules in the Cavities of the Basic Microporous P4VP Polymer by in situ FTIR Spectroscopy," *J. Phys. Chem. C*, vol. 112, no. 49, pp. 19493–19500, Dec. 2008, doi: 10.1021/jp802368x.

[66] S. Roland, C. Pellerin, C. G. Bazuin, and R. E. Prud'homme, "Evolution of Small Molecule Content and Morphology with Dip-Coating Rate in Supramolecular PS–P4VP Thin Films," *Macromolecules*, vol. 45, no. 19, pp. 7964–7972, Oct. 2012, doi: 10.1021/ma301383v.

[67] E. Verron *et al.*, "Gallium modulates osteoclastic bone resorption *in vitro* without affecting osteoblasts," *British Journal of Pharmacology*, vol. 159, no. 8, pp. 1681–1692, 2010, doi: 10.1111/j.1476-5381.2010.00665.x.

Chapter 7: Conclusions and Future Work

7.1 Perspective

Hydroxyapatite coatings play a significant role in enhancing the osteointegration of specific orthopaedic implants; nevertheless, they do not ensure the complete success of all surgeries. Novel and emerging coating techniques have the potential to enhance the performance of hydroxyapatite coatings, enabling their application on new materials and facilitating the incorporation of bioactive elements into the coating. This thesis has explored a solution-based coating process and demonstrated that, under specific process parameters, repeatable and reproducible hydroxyapatite deposition can be achieved. Furthermore, by strategically functionalising the surfaces, hydroxyapatite films can be successfully replicated on novel substrates. This thesis has shown very promising results for apatite formation on non-Ti substrates using this approach. As parts move from metal implants to materials closer in density to bone (such as plastics), this methodology could be pivotal in developing HA coatings and improving osteointegration.

In addition to coating method development, this thesis has experimented with unconventional polymer methods to create nano-coatings aimed at improving osteointegration and antimicrobial performance, both on flat surfaces and over hydroxyapatite films. The development and analysis presented in this thesis offer potential avenues for enhancing the success rates of hydroxyapatite-coated implants. The following sections provide highlights and results from each chapter, followed by exciting prospects for future work that could pave the way for the next generation of orthopaedic coatings.

7.2 Conclusions

The use of hydroxyapatite coatings on orthopaedic implants is a well-established field of science and while it is proven to improve surgical outcomes, there are still areas where it can be improved upon. Industrial coating techniques are limited by poor porosity, crystallinity and phase control and mostly show the greatest applicability to deposit hydroxyapatite on titanium-based substrates and implants. The solution-based coating method developed here could mimic biological bone growth and produce porous and well adhered hydroxyapatite coatings and

potentially coat novel surfaces. The doping of hydroxyapatite with antimicrobial and osteogenic elements is complex and difficult to achieve without adverse effects on the structure of the hydroxyapatite coating. The use of polymer pattern coatings can be used to evaluate the biological impact of certain elements and in an innovative approach could be applied to hydroxyapatite coatings.

Chapter 2 introduced the solution deposition process and outlined the chemical concentration, particle size and ionic strengths of the process solutions. Through careful control of solutions, agitation, temperature and pH monitoring it was possible to identify a process window in which hydroxyapatite films grew on Ti-6Al-V4 activated parts. By analysing previous studies and from experimental data a chemical pathway was proposed which reveals what species form and nucleate in solution ultimately leading to heterogeneous mineral growth at the solution-surface interface. It was interesting that while sodium chloride is used in relatively high concentrations to increase the ionic strength of the process, it was almost undetectable in the hydroxyapatite films grown. While all process solutions produced hydroxyapatite films, there was a variation in the weight of film formed and its Ca/P molar ratio. Extensive elemental analysis showed that some solutions were too dilute to produce coherent hydroxyapatite films whereas some were too concentrated and gave rise to less desirable physiochemical properties (i.e., too dense, lower adhesion, high carbonates and cracks in the films). Despite this, above a certain concentration all solutions gave rise to amorphous calcium phosphate, some pure hydroxyapatite and a large signal for octacalcium phosphate phases within the coating. An ideal process solution which had optimum solution kinetics was identified based off the film characteristics such as morphology, coverage, porosity and phase composition.

Chapter 3 focussed on hydroxyapatite film formation from the ideal solutions defined in Chapter 2. Hydroxyapatite was analysed in two forms; in removed powder and as an in-situ film. Thermal analysis revealed that there was both absorbed water which dehydrated initially below 200 °C and interstitial water which was lost up to 400 °C. 2D heteronuclear correlation data recorded by solid state nuclear magnetic resonance added to the picture by proving that the hydroxyapatite had two distinct molecular packing orders identified by different proton pair correlations. Some of the material was crystalline well-formed

hydroxyapatite, while the rest was less formed amorphous calcium phosphate, hydrogen phosphate and confirmed a water content. X-ray diffraction analysis of the hydroxyapatite films at various stages of the process shows how the crystalline phases emerged and proved how the presence of a substrate drives crystallinity over amorphous growth. Initially tricalcium phosphate and some pure hydroxyapatite phases were detected but as the process continued the mineral grew preferentially along the [002] with a high indication of the octacalcium phase of hydroxyapatite. Transmission electron microscopy showed again that the hydroxyapatite film was an amorphous matrix with crystalline pockets. Of these crystalline pockets, fast Fourier transform data showed that they had d-spacings corresponding mainly to the octacalcium phosphate phase with some pure hydroxyapatite again.

Chapter 4 compared the growth of hydroxyapatite from the colloidal solution deposition process again but added in novel substrates to understand whether the film grows in the same manner on them. Planer silicon was used as a novel substrate and a subset of samples were coated using e-beam with 100nm titanium thin films. The first study was to understand the chemistry of the substrates after basic activation and through water contact angle analysis, elemental analysis and roughness analysis. Sufficient hydrophilicity and roughness were achieved, with available hydroxyl to entice calcium ions to bond. To further analyse the growth mechanism of hydroxyapatite relative to substrate chemistry a batch of titanium thin film samples were activated at varying times, analysed and then subjected to hydroxyapatite solution deposition. Post deposition the films were analysed using X-ray photoelectron spectroscopy which gave detailed chemical bond states for elements at the very top nanometres of film attachment.

Further analysis of the various substrates showed that hydroxyapatite grew identically in terms of morphology, coverage, composition and crystallinity for the Ti thin film samples and bulk Ti samples. Silicon gave rise to less material and of the hydroxyapatite that formed it was less well developed. This chapter proved that a nanoscopic layer of titanium is sufficient to seed and support the growth of a medical grade hydroxyapatite film and this paves the way for future opportunities in changing the underlying bulk material of an orthopaedic implant.

Chapter 5 is a standalone study proving the efficacy of: 1. The use of block copolymer patterns to create nano coatings for biomedical testing and usage and 2. The efficacy of nano-gallium to promote osteoblasts, i.e., Bone growth stem cells. Block copolymer bcc spherical arrays were formed on silicon and titanium substrates proving that nanodots of poly(4-vinylpyridine) could be formed at differing radii and coverage by altering the molecular weight of the block copolymer. These polymer dots were infiltrated with gallium and the geometry of the dot was retained as shown by atomic force and electron microscopy. It was possible to confirm the subsequent ionic release of the gallium into phosphate buffer solution was dependant on gallium precursor solution and time. One key feature of this work was understanding the bio-properties of these surfaces and their mechanism for possible osteointegrative enhancement. A collaborative study performed in the Trinity Centre for Biomedical Engineering showed that these gallium coating surfaces had no widespread cell cytotoxicity. Further tests showed that the proliferation of bone promoting cells (osteoblasts) was unchanged while the proliferation of bone resorbing cells (osteoclasts) was almost fully ceased in a dose dependant manner. However further direct contact tests would complement these findings. This chapter showed that polymer templating could work as a means to deliver bioactive elements to a biological fluid and also encouraged the use of nano gallium for orthopaedic recovery.

Chapter 6 represents the culmination of all the work. Knowledge of hydroxyapatite films from **Chapters 2, 3 and 4** was used as a starting point to refer to after coating the films with polymer patterns. The findings of **Chapter 5** were used to apply gallium nanodots to the hydroxyapatite film. The experimental work proved that applying a polymer pattern to hydroxyapatite does not affect the physiochemical properties of the film. Due to constraints regarding the porosity of the hydroxyapatite films, a brush type of poly(4-vinylpyridine) film was the preferred method since the detection and identification of a bcc spherical array was impossible over the hydroxyapatite film. Gallium was capable of infiltrating into the polymer, which allowed for the inclusion of it onto the coating to be detected, with the gallium subsequently released into phosphate buffer solution. The advantage of this system was such that it was easily replicated for the inclusion of zinc (also an osteoinductive antimicrobial element) over

hydroxyapatite. X-ray fluorescence data showed that the doping of the hydroxyapatite was successful across a millimetre scale, not just in nanoscopic pockets, and this would thoroughly support the use of this method for large orthopaedic coatings.

In summary the work outlined in this thesis provides a clear pathway by which solution deposition of hydroxyapatite could be implemented on an industrial scale to produce coatings which match and improve upon existing methods. The industry co-funding partner has recently commissioned an industrial scale system based on this method and initial results look promising. Experimental results show that the process could also be easily applied to other substrates. The most exciting thing about this body of work has been the invention of a polymer patterning method for doping hydroxyapatite without compromising on any chemical or structural integrity of the coating which is paramount to its success. All of the aims and objective outlines in the introduction have been met and achieved while also being peer reviewed in four different first authored publications.

7.3 Future Work

It is a challenge to write this section. It is hard to believe deeply in the approach developed and studied, become excited by future possibilities and yet must identify future work by other students and researchers. Alas, the project was only four years so let me now outline some extremely exciting future work that could continue from this PhD project.

Statistical Analyses

To bridge the gap between laboratory apparatus and industrial scale up, there would be a huge benefit gained from collating all the process data. Process data could be gathered for implementation of applied process controls to support automated controls such as temperature and pH and solution top-ups. Process data should also be joined to the characterisation data to allow for extensive multivariate analysis. I did some initial research on this and am sure that there are endless possibilities from extended data analysis. There are various research papers outlining how more heat and different pH values within a system can alter

the Gibbs free energy of the system and change the thermodynamic driving force towards different phases of hydroxyapatite if preferred. [1]–[3]

Applying 100nm Ti Layers to Polymers

I believe that the data shown in this thesis could be valuable for realising HA functionalised bulk polymeric implants. For various reasons such as surface energies or roughness, polymeric implants are difficult to coat with HA. [4]–[6] If a 100nm titanium film could be deposited onto a polymer I am confident that this would facilitate the deposition of hydroxyapatite using this colloidal solution system.

Applying solution deposition to resorbable Magnesium Implants

It became clear during literature research over the years that the field of absorbable magnesium implants is gaining attention. [7]–[13] These implants are beneficial for younger patients as they hold bone together and, while the patients are still developing their skeletal structure, the new bone can grow and reabsorb the Mg implants. Applying hydroxyapatite to these implants is complicated by the fact that they cannot be sealed from the body entirely to allow the magnesium to reabsorb. I believe this colloidal deposition system would enable the formation of nano layers of porous hydroxyapatite on these implants. It would be beneficial to run experiments and compare the results as per **Chapter 4** of this thesis.

***In situ* film growth monitoring.**

I performed initial studies of monitoring film growth using a quartz crystal microbalance (QCM). [14]–[21] The QCM sensor was coated with titanium, activated as if the coated sensor was a normal substrate and submerged in the deposition chamber where HA was deposited. A QCM will monitor film growth on the surface of the sensor based off resonance frequency and dissipation of a piezo electric crystal. The data I collected was promising but requires further analysis. The Sauerbrey equation used to correlate mass of film to the frequency when used in its most basic form is only valid for rigid layers in air. Therefore, more complicated permutations of the frequency – mass relationship need to be considered. Similarly, the dissipation data showed phase changes within the HA

on the sensor post deposition and it would be exciting to dig deeper into the data to identify the very first crystal nucleation within the process.

Further gallium studies

It would be informative to expand on the findings presented in **Chapter 5**. The results in this chapter only focus on a 24 hour gallium release into media. ICP data however, had shown that the gallium release was much higher at 5 days and plateaued at 10days. It would have been scientifically significant to apply the same biological testing to cultured media that was left for 5 days, 10 days (or even longer).

Further to this idea is would have been scientifically valuable to conduce direct contact culture tests since these gallium-templated surfaces are designed to be used as implant coatings. Direct contact tests would closely compare to an implant *in vivo* as blood and bodily fluids would be in contact with the surface of any gallium modified surface if it were to be implanted.

The doping of hydroxyapatite using polymer templates.

The data in **Chapter 6** prove how polymer patterns can apply nano amounts of a dopant to the surface of hydroxyapatite without affecting it. It is difficult to understate just how complicated the doping of hydroxyapatite is and virtually every method of doing so incurs changes to the crystal lattice.[22]–[27] It would be fantastic to widen this study to different dopant elements and polymers and undertake more analysis of how the polymer templated dopant attached to the hydroxyl groups on the surface of the hydroxyapatite. Also, it would be extremely exciting to then run biological comparison of the coatings and prove that the desired effects of improving osteointegration and antimicrobial performance are achieved.

7.4 References

- [1] S. Jebri, I. Khattech, and M. Jemal, "Standard enthalpy, entropy and Gibbs free energy of formation of «A» type carbonate phosphocalcium hydroxyapatites," *The Journal of Chemical Thermodynamics*, vol. 106, Nov. 2016, doi: 10.1016/j.jct.2016.10.035.
- [2] N. Sahai and M. A. Schoonen, "Accuracy of Thermodynamic Databases for Hydroxyapatite Dissolution Constant," *Astrobiology*, vol. 20, no. 1, pp. 157–160, Jan. 2020, doi: 10.1089/ast.2019.2158.

- [3] Y. Zhu *et al.*, "Characterization, dissolution and solubility of the hydroxypyromorphite–hydroxyapatite solid solution [(PbxCa1-x)5(PO4)3OH] at 25 °C and pH 2–9," *Geochem Trans*, vol. 17, p. 2, May 2016, doi: 10.1186/s12932-016-0034-8.
- [4] F. D. Al-Shalawi *et al.*, "Biodegradable synthetic polymer in orthopaedic application: A review," *Materials Today: Proceedings*, vol. 74, pp. 540–546, Jan. 2023, doi: 10.1016/j.matpr.2022.12.254.
- [5] S. Krishnakumar and T. Senthilvelan, "Polymer composites in dentistry and orthopedic applications-a review," *Materials Today: Proceedings*, vol. 46, pp. 9707–9713, Jan. 2021, doi: 10.1016/j.matpr.2020.08.463.
- [6] S. Cometa, M. A. Bonifacio, M. Mattioli-Belmonte, L. Sabbatini, and E. De Giglio, "Electrochemical Strategies for Titanium Implant Polymeric Coatings: The Why and How," *Coatings*, vol. 9, no. 4, Art. no. 4, Apr. 2019, doi: 10.3390/coatings9040268.
- [7] D. Bairagi and S. Mandal, "A comprehensive review on biocompatible Mg-based alloys as temporary orthopaedic implants: Current status, challenges, and future prospects," *Journal of Magnesium and Alloys*, vol. 10, no. 3, pp. 627–669, Mar. 2022, doi: 10.1016/j.jma.2021.09.005.
- [8] J. Chen *et al.*, "Recent Advances on Development of Hydroxyapatite Coating on Biodegradable Magnesium Alloys: A Review," *Materials*, vol. 14, no. 19, Art. no. 19, Jan. 2021, doi: 10.3390/ma14195550.
- [9] S. Mahmud, M. Rahman, M. Kamruzzaman, H. Khatun, M. O. Ali, and M. M. Haque, "Recent developments in hydroxyapatite coating on magnesium alloys for clinical applications," *Results in Engineering*, vol. 17, p. 101002, Mar. 2023, doi: 10.1016/j.rineng.2023.101002.
- [10] D. G. Tamay *et al.*, "Corrosion Resistance and Cytocompatibility of Magnesium–Calcium Alloys Modified with Zinc- or Gallium-Doped Calcium Phosphate Coatings," *ACS Appl. Mater. Interfaces*, vol. 14, no. 1, pp. 104–122, Jan. 2022, doi: 10.1021/acsami.1c16307.
- [11] V. Tsakiris, C. Tardei, and F. M. Clicinschi, "Biodegradable Mg alloys for orthopedic implants – A review," *Journal of Magnesium and Alloys*, vol. 9, no. 6, pp. 1884–1905, Nov. 2021, doi: 10.1016/j.jma.2021.06.024.
- [12] F. Xing *et al.*, "Recent progress in Mg-based alloys as a novel bioabsorbable biomaterials for orthopedic applications," *Journal of Magnesium and Alloys*, vol. 10, no. 6, pp. 1428–1456, Jun. 2022, doi: 10.1016/j.jma.2022.02.013.
- [13] A.-M. Zhang, P. Lenin, R.-C. Zeng, and M. B. Kannan, "Advances in hydroxyapatite coatings on biodegradable magnesium and its alloys," *Journal of Magnesium and Alloys*, vol. 10, no. 5, pp. 1154–1170, May 2022, doi: 10.1016/j.jma.2022.01.001.
- [14] J. Auge, P. Hauptmann, F. Eichelbaum, and S. Rösler, "Quartz crystal microbalance sensor in liquids," *Sensors and Actuators B: Chemical*, vol. 19, no. 1–3, pp. 518–522, Apr. 1994, doi: 10.1016/0925-4005(93)00983-6.
- [15] B. Becker and M. A. Cooper, "A survey of the 2006–2009 quartz crystal microbalance biosensor literature," *Journal of Molecular Recognition*, vol. 24, no. 5, pp. 754–787, 2011, doi: 10.1002/jmr.1117.
- [16] Y. Chao, O. Horner, F. Hui, J. Lédion, and H. Perrot, "Direct detection of calcium carbonate scaling via a pre-calcified sensitive area of a quartz crystal microbalance," *Desalination*, vol. 352, pp. 103–108, Nov. 2014, doi: 10.1016/j.desal.2014.08.004.
- [17] A. D. Easley, T. Ma, C. I. Eneh, J. Yun, R. M. Thakur, and J. L. Lutkenhaus, "A practical guide to quartz crystal microbalance with dissipation monitoring of thin polymer films," *Journal of Polymer Science*, vol. 60, no. 7, pp. 1090–1107, 2022, doi: 10.1002/pol.20210324.
- [18] T. Ikoma *et al.*, "The Surface Property of Hydroxyapatite: Sensing with Quartz Crystal Microbalance," *KEM*, vol. 396–398, pp. 89–92, Oct. 2008, doi: 10.4028/www.scientific.net/KEM.396-398.89.
- [19] J. Kankare, "Sauerbrey Equation of Quartz Crystal Microbalance in Liquid Medium," *Langmuir*, vol. 18, no. 18, pp. 7092–7094, Sep. 2002, doi: 10.1021/la025911w.

- [20] K. A. Marx, "Quartz Crystal Microbalance: A Useful Tool for Studying Thin Polymer Films and Complex Biomolecular Systems at the Solution–Surface Interface," *Biomacromolecules*, vol. 4, no. 5, pp. 1099–1120, Sep. 2003, doi: 10.1021/bm020116i.
- [21] A. Sarkar *et al.*, "Monitoring Organic Thin Film Growth In Aqueous Solution *In-situ* With A Combined Quartz Crystal Microbalance and Ellipsometry," *MRS Proc.*, vol. 1146, pp. 1146-NN09-02, 2008, doi: 10.1557/PROC-1146-NN09-02.
- [22] L. Chen, Y. Wang, X. Cao, Z. Zhang, and Y. Liu, "Effect of doping cation on the adsorption properties of hydroxyapatite to uranium," *Journal of Solid State Chemistry*, vol. 317, p. 123687, Jan. 2023, doi: 10.1016/j.jssc.2022.123687.
- [23] S. Panda, C. K. Biswas, and S. Paul, "A comprehensive review on the preparation and application of calcium hydroxyapatite: A special focus on atomic doping methods for bone tissue engineering," *Ceramics International*, vol. 47, no. 20, pp. 28122–28144, Oct. 2021, doi: 10.1016/j.ceramint.2021.07.100.
- [24] I. Ratha, P. Datta, V. K. Balla, S. K. Nandi, and B. Kundu, "Effect of doping in hydroxyapatite as coating material on biomedical implants by plasma spraying method: A review," *Ceramics International*, vol. 47, no. 4, pp. 4426–4445, Feb. 2021, doi: 10.1016/j.ceramint.2020.10.112.
- [25] M. Shokri, M. Kharaziha, H. A. Tafti, M. B. Eslaminejad, and R. M. Aghdam, "Synergic role of zinc and gallium doping in hydroxyapatite nanoparticles to improve osteogenesis and antibacterial activity," *Biomaterials Advances*, vol. 134, p. 112684, Mar. 2022, doi: 10.1016/j.msec.2022.112684.
- [26] F. Tosan, N. Rahnama, D. Sakhaei, A. H. Fathi, and A. Yari, "Effects of doping metal nanoparticles in hydroxyapatite in Improving the physical and chemical properties of dental implants," *Nanomedicine Research Journal*, vol. 6, no. 4, pp. 327–336, Nov. 2021, doi: 10.22034/nmrj.2021.04.002.
- [27] A. Fakharzadeh, R. Ebrahimi-Kahrizsangi, B. Nasiri-Tabrizi, and W. Jeffrey Basirun, "Effect of dopant loading on the structural features of silver-doped hydroxyapatite obtained by mechanochemical method," *Ceramics International*, vol. 43, no. 15, pp. 12588–12598, Oct. 2017, doi: 10.1016/j.ceramint.2017.06.136.

List of Publications

Journal Articles Published

- [1] Yadav, P.; Gatensby, R.; Prochukhan, N.; C. Padmanabhan, S.; Davó-Quiñonero, A.; Darragh, P.; Senthamaraikannan, R.; **Murphy, B.**; Snelgrove, M.; McFeely, C.; Singh, S.; Conway, J.; O'Connor, R.; McGlynn, E.; Lundy, R.; Morris, M. A., "Fabrication of High- κ Dielectric Metal Oxide Films on Topographically Patterned Substrates: Polymer Brush-Mediated Depositions," *ACS Appl. Mater. Interfaces*, vol. 14, no. 28, pp. 32729–32737, Jul. 2022, doi: 10.1021/acsami.2c07966.
- [2] **B. Murphy**, J. Baez, and M. A. Morris, "Characterizing Hydroxyapatite Deposited from Solution onto Novel Substrates in Terms of Growth Mechanism and Physical Chemical Properties," *Materials Proceedings*, vol. 14, no. 1, Art. no. 1, 2023, doi: 10.3390/IOCN2023-14491.
- [3] **B. Murphy**, C. Martins, M. Maggio, M. A. Morris, and D. A. Hoey, "Nano sized gallium oxide surface features for enhanced antimicrobial and osteo-integrative responses," *Colloids and Surfaces B: Biointerfaces*, vol. 227, p. 113378, Jul. 2023, doi: 10.1016/j.colsurfb.2023.113378.
- [4] **B. Murphy**, J. Baez, and M. A. Morris, "Characterising Hydroxyapatite Deposited from Solution onto Novel Substrates: Growth Mechanism and Physical Properties," *Nanomaterials*, vol. 13, no. 17, Art. no. 17, Jan. 2023, doi: 10.3390/nano13172483.
- [5] **B. Murphy**, M. A. Morris, and J. Baez, "Development of Hydroxyapatite Coatings for Orthopaedic Implants from Colloidal Solutions: Part 1—Effect of Solution Concentration and Deposition Kinetics," *Nanomaterials*, vol. 13, no. 18, Art. no. 18, Jan. 2023, doi: 10.3390/nano13182577.
- [6] **B. Murphy**, M. A. Morris, and J. Baez, "Development of Hydroxyapatite Coatings for Orthopaedic Implants from Colloidal Solutions: Part 2—Detailed Characterisation of the Coatings and Their Growth Mechanism," *Nanomaterials*, vol. 13, no. 18, Art. no. 18, Jan. 2023, doi: 10.3390/nano13182606.

Conferences

2020:

- “SODHA Coating Process: Rationalisation of coating route and functionalisation of coating additives.” Poster Presentation, AMBER International Conference 2020, Portlaoise, Ireland
- “SODHA Coating Process: Rationalisation of coating route and functionalisation of coating additives.” Poster Presentation, DePuy Synthes Ireland Academic Research Partner Symposium, Cork, Ireland

2022:

- “Block Copolymer Assisted Fabrication of Gallium Nanofilms for Orthopaedic Implant Coatings.” Poster Presentation, European Materials Research Society (eMRS) Conference, Spring 2022, Virtual Conference.
- “Enabling Applied Process Control of Solution Deposition of Hydroxyapatite Using JMP® Software.” Poster Presentation, Materials Research Society (MRS) Fall Meeting and Exhibit 2022, Virtual Conference

2023:

- “Nano Sized Gallium Oxide Surface Features for Enhanced Antimicrobial and Osteo-Integrative Responses.” Poster Presentation, AMBER International Conference 2023, Limerick, Ireland.
- “Characterizing Hydroxyapatite Deposited from Solution onto Novel Substrates in Terms of Growth Mechanism and Physical Chemical Properties.” Proceedings Paper, The 4th International Online Conference on Nanomaterials 2023 (IOCN 2023), Virtual Conference
- “Development of a Surface-Modified Quartz Crystal Microbalance Technique to monitor Hydroxyapatite Film Growth in situ.” Poster Presentation, European Materials Research Society (eMRS) Conference, Spring 2023, Strasbourg, France